Professor Yanenko Oleksey Pylypovych, Doctor of Technical Sciences, is an expert in the field of biomedical devices and systems, methods for measuring low-intensity microwave signals, metrological support for biomedical equipment and radiometric measurements ;. For about 10 years he worked in a medical research center, developing microwave medical equipment and radiometric systems for measuring weak electromagnetic fields and radiation from physical and biological objects. Professor O Yanenko is the author and co-author of 15 monographs and textbooks, he has more than 350 scientific articles and 105 patents for inventions devoted to these issues. For more than 20 years, combines research activities with teaching at the Faculty o Radio Engineering at the National Technical University of Ukraine “Igor Sikorsky Kyiv Polytechnic Institute”.

Shevchenko Konstantin. Doctor of Technical Sciences. Professor, Department of Information and Measuring Technologies, National Technical University of Ukraine "Igor Sikorsky Kyiv Polytechnic Institute". Specialist in the field of information measurement technology. Full member of the Academy of Metrology of Ukraine. Member of TC13 Technical Committee - Measurement in Biology and Medicine of the International Confederation for Measurement Technology IMEKO. The results of scientific activity are published in 5 monographs, 1 study guide, in more than 100 scientific articles and 64 patents.

Kychak Vasyl Martynovych. Honored Worker of Education of Ukraine, Doctor of Technical Sciences, Professor, Head of the Department of Telecommunication Systems and Television of Vinnytsia National Technical University, Academician of the International Academy of Applied Radio Electronics, the author of over 400 scientific works, 15 monographs and 3 textbooks.

METHODS AND MEANS OF FORMATION, PROCESSING AND USE OF LOW-INTENSITY ELECTROMAGNETIC SIGNALS

Yanenko O.P., Shevchenko K.L., Kychak V.M.

METHODS AND MEANS OF FORMATION, PROCESSING AND USE OF LOW-INTENSITY ELECTROMAGNETIC SIGNALS

Yanenko O. P., Shevchenko K. L., Kychak V. M.

Dedicated to the
memory
of Professor
Yuri Skrypnik

METHODS AND MEANS OF FORMATION, PROCESSING AND USE OF LOW-INTENSITY ELECTROMAGNETIC SIGNALS

Vinnytsia
VNTU
2020

UDC 621.317: 621.371: 615.849

Recommended for publication by the Academic Council of Vinnytsia National Technical University of the Ministry of Education and Science of Ukraine (minutes № 11 of 28.05.2020)

The publication is recommended by the Academic Council of the Radio Engineering Faculty of the National Technical University of Ukraine «Kiev Polytechnic Institute» named after Igor Sikorsky (Minutes No. 06/2020 of 25.06.2020)

Reviewers:

Doctor of Engineering, Prof. **Burmistenkov Oleksandr Petrovych**, Professor of the Department of Computer Engineering and Electromechanics at Kyiv National University of Technologies and Design;

Doctor of Engineering, Prof. **Boiko Juliy Mykolayovych**, Professor of the Department of Telecommunications and Radio Engineering at Khmelnytskyi National University;

Doctor of Engineering, Prof. **Krizhanovski Volodymyr Grygorovych**, Head of the Department of Radio Physics and Cybersecurity at Vasyl' Stus Donetsk National University

Yanenko, O.

Methods and means of formation, processing and use of low-intensity electromagnetic signals : monograph / O. P. Yanenko, K. L. Shevchenko, V. M. Kychak – Vinnytsya : VNTU, 2020. – 268 p.

ISBN 978-966-641-812-1

The monograph summarizes scientific and technical experience gained by the authors in the field of formation, selection, conversion, and processing of weak signal parameters. Authors consider features of commutation and modulation transformations, and circuits of highly sensitive radiometers of microwave and optical range, as well as methods and means of formation of low-intensity signals with the use of Josephson junctions. The monograph may be useful for students and postgraduates, as well as for specialists in the sphere of development and use of low-signal equipment in telecommunications and radio communications, physics, biology, medicine, materials science, and other applied fields of science and technology related to using low-intensity signals.

UDC 621.317: 621.371: 615.849

ISBN 978-966-641-812-1

CONTENTS

Introduction 6
Section 1 Low-intensity microwave signals and their application in biology, medicine and scientific research 10
Preliminary remarks 10
1.1 Classification of means for measuring the parameters of low-intensity radio frequency signals 10
1.2 Therapeutic equipment and specialized sources of low-intensity microwave signals of the mm-range 13
1.3 Metrologic apparatus software and technologies of low-intensive microwave therapy 16
1.4 Technologies of therapy with low-intensive microwave signals. Peculiarities and appliance fields of millimeter therapy 18
1.5 Scientific directions of low-intensity electromagnetic fields and radiation of millimeter range researches 22
1.6 Natural sources of the mm-range irradiation and using peculiarities in physiotherapy 27
1.6.1 Research EMR natural treatment formula for physio procedures 28
1.6.2 Research EMR minerals and precious stones 30
1.6.3 Determination of the human body's reaction to external microwave low-intensity irradiation 33
1.6.4 The study of electromagnetic parameters of textile and leather for clothes and shoes manufacturing 35
1.7 Future areas of research intensive low signals in biology and medicine 39
Section 2 Low-intensity optical signals and their use in medical equipment for biological purposes 41
Preliminary remarks 41
2.1 Interaction of low-intensity optical signals with biological tissue and device for irradiation of acupuncture points .. 41
2.2 Automated system for irradiation of biologically active points of the human body 48
2.3 Radiometric modulation meter of low intensity of optical radiation 54

2.4 Photometric spectrum analyzer of the absorption capacity of poorly transparent biomaterials 58
2.5 Optoelectronic system with automated determination of maximum absorption frequencies 67
2.6 Features of metrological support for measuring the low-intensity optical signal parameters 76
Section 3 Radiometric modulation methods and means for parameters of low-intensity microwave signals measuring 80
Preliminary remarks 80
3.1 Features of high-sensitivity modulation radiometers constructions 81
3.2 A radiometric system of a direct conversion with a regenerative feedback 89
3.3 A modulation radiometric system with the compensation for a fluctuating noise of combination frequencies 95
3.4 A one-port dual-channel radiometer with the cancellation of a correlation noise 100
3.5 A dual-channel differential radiometric system for recording the difference values of radiation intensities 108
3.6 A multifunctional RS for measuring energy and correlation characteristics of signals 113
3.7 A radiometric system for measuring the power of electromagnetic radiation of EHF by the zero method 120
3.8 A radiometric system for assessing the emission properties of tissues of biological objects 127
3.9 Radiometric system with advanced measuring functions 130
3.10 A radiometric system for measuring phase shift of reflected microwave oscillations 135
3.11 RS for detection and registration of natural resonant frequencies of BAP bioobjects 141
3.12 Radiometric system for measuring reflective and absorbing properties of bio objects 150
3.13 Feedback radiometric system using the object own radiation level 162
3.14 Radiometric system with automatic regulation of irradiation power 168

3.15 Measurement assurance of high-sensitivity microwave radiometric systems 174
Section 4 Devices for the formation, reception and processing of low-intensity signals based on Josephson junctions 182
Introduction to section 4 182
4.1 Mathematical model of Josephson transition 184
4.2 A Josephson junction-based superconducting quantum interferometers 191
4.3 Microwave low-intensity signal generators based on Josephson junctions 197
4.4 The estimation of the oscillator frequency instability of low-intensity signals based on Josephson junction 207
4.5 Frequency converters for the processing of low-intensity signals 218
4.6 Superconducting digital radio engineering devices for processing low-intensity signals 230
4.7 Development of a device for converting a pulse-potential code into frequency-pulse code using Josephson junctions 235
4.8 Generator of tactical impulses on Josephson junction 241
4.9 Pulse-code modulator for processing of low-intensity signals in the terahertz frequency range 249
List of references 256

INTRODUCTION

The intensive development of modern science and technology, radio engineering and radio electronics, the gradual exploration of the entire spectrum of electromagnetic waves contribute to the spread and implementation of the latest achievements in the field of signals generation, transformation and amplification in telecommunication, radio communication, radiolocation, radio navigation, radio astronomy and meteorology systems, in physics, medicine and biology, and in industrial-technological control systems. Such technological advance is almost always associated with the expansion of the measurement area and the use of low-intensity signals. In full, this applies not only to radio engineering signals but also to low-intensity signals of the optical, acoustic, and magnetic spectra.

The processes of generating, processing, and using weak signals are closely connected to the necessity of developing new methods and means of their implementation to guarantee the highlighting of the information against background noises that are often compared to the level of these signals. More and more attention has been paid lately to the radiometric measurement methods and study of the information about the state of various objects, and for this purpose high-sensitivity radiometers of both radio and optical spectra are used [1–4, 28]. With new elements of electronic technology and the use of computing tools and software packages, the lack of specialized literature in the field of radiometric equipment does not contribute to its development and practical implementation in various areas of science and technology.

The purpose of this monograph is to summarize the scientific and technical experience gained by the authors in the field of formation and transformation of weak signals, separation, processing and radiometric measurements of the parameters of these signals, based on switching modulation transformations, the formation of low-intensity signals using Josephson junctions and practical use of developed methods and structural schemes.

The first section deals with low-intensity signals of the millimeter spectrum wavelengths and examples of their use in biology and medicine. Measuring radio engineering systems are classified by their purpose and by the level of measuring power. It is noted that standard measuring receivers are

used for measuring weak coherent and quasi-coherent signals with a power of 10^{-6}…10^{-12}W, and radiometric systems (RS) are used for measuring low-intensity noise signals with a power of less than 10^{-12} W. There are examples of low-signal generating equipment in the spectrum of 30…78 GHz, its parameters and examples of use in microwave therapy technologies. The section addresses the issues of metrological support using certified non-standardized RS of the millimeter spectrum with a sensitivity of 10^{-14} W. The section shows options for the possible use of highly sensitive RS in biomedical research and the results of experimental studies of low-intensity electromagnetic fields and radiation of physical and biological objects that interact with the human body.

The second section deals with the structures of formation, transformation, and possible use of low-intensity signals of the optical spectrum. There is a promising use of low-intensity optical therapy of a wide spectrum from 250 nm to 700 nm for medical and biological research [20, 22, 28]. The section examines the interaction of low-intensity signals of the optical spectrum with biological human tissue. It also shows the original functional schemes of devices for the formation and radiation of the human body developed by the authors, and the research results of the interaction of luminous fluxes with organic materials. The section examines dynamic radiation systems with modulation and determination of maximum absorption frequency. The section shows the possibility of using switching modulation transformation of optical signals for original schemes of highly-sensitive optical radiometers creation, and for measuring the parameters of absorption, reflection, and light flux transit. The results of experimental research of the interaction between modulated light fluxes of different wavelengths and biotissue samples are presented. The section considers metrological support of the optical equipment of low-intensity signals. It is shown that the measurement of optical power at a level of less than 10^{-9} W is possible using non-standard optical radiometer systems.

The third section of the monograph addresses the physical basics and features of switching modulation transformation of low-intensity signals to provide high-sensitivity and accuracy of the power measurement by radiometric systems.

The classification scheme of modulation RS of short and contact action of the microwave band (30…112 GHz) is developed. It is shown that, in addition to measuring the power of low-intensity monochromatic and

broadband (noise) signals, such systems also provide an estimation of other parameters – absorption coefficients, reflection, measurement of frequency and time parameters and correlation function, conducting a spectral analysis of the signal structure, which is not typical for long-range radio systems.

The section shows methods of sensitivity control, developed by the authors, through the use of positive and negative feedback communication, which allows reducing the fluctuation threshold of sensitivity of such RS to $10^{-22}…10^{-23}$ W / Hz. The section presents the original single and dual-pass measuring RS and systems with advanced functions. The section addresses the sources of errors of highly sensitive RS and gives recommendations to reduce them. The analysis of the metrological support of the RS developed by the authors at 37…53 GHz and 53…78 GHz frequency range is conducted. It is shown that such systems can be tested using a substitution method or using reference noise generators (NG). The section shows results of the RS verification using certified NG developed by the authors, which provides a higher (2…2,5 times higher) accuracy of the check. The section addresses the methods and means of the construction of highly sensitive radiometric systems of the receiving and radar type, shows the original authors' schemes of the RS for the use in both the biomedical research field and other fields of science and technology. The patents of Ukraine protect most of the developed schemes of the modulation radiometers of the radio and optical spectrum, presented in the monograph.

The fourth section of the monograph focuses on methods and means of formation, processing, and application of low-intensity signals using Josephson junctions. The mathematical model of Josephson junctions is considered. The section shows the possibility of the construction of digital devices for receiving and processing low-intensity microwave signals based on Josephson junctions, including analog-to-digital converter, clock pulse generators, superconducting quantum interferometers, balance comparators. The section shows the results of using Josephson junction for the construction of the devices for receiving and processing of low-intensity microwave signals on the examples of microwave filters, frequency mixers, pulse-steady to frequency-pulse signals converters. The section considers the possibility and perspectives of using highly sensitive superconducting quantum interferometers for the study of biomedical signals.

Expert's awareness of the results of prospective research and development presented in the monograph will contribute to further development and improvement of the use of weak signaling equipment in telecommunication, radio communication systems, physics, biology, medicine, materials science, and other applied fields of science and technology.

The authors express their appreciation and to the reviewers: Prof. Burmistenkov O. P., Prof. Boiko J. M., Prof. Krizhanovski V. G. for participating in the discussion of the monograph and their valuable comments on improving the structure and content of the book.

The authors note (posthumously) the great contribution of Professor Skrypnyk Y. O. and his active participation in the development of highly sensitive switching and modulation radiometric systems for measuring the parameters of low-intensity microwave signals and medical devices.

The authors are also grateful to their colleagues: Prof. Sytko S. P., As. Prof. Peregudov S. N., As. Prof. Golovchanska A. D., med. practitioner Fedotova I. V., As. Prof. Semenova O. A., As. Prof. Shtofel D. Kh., As. Prof. Zozulia I. Ye. for their participation in our projects, rendering qualified assistance in the practical implementation of the developed particular technical devices and their use, conducting experiments and measurements, translating and organizing the text of the monograph.

The authors will be grateful to readers for criticisms and suggestions regarding the content of the book sent by e-mail:

op291@meta.ua

vmkychak@gmail.com

SECTION 1 LOW-INTENSITY MICROWAVE SIGNALS AND THEIR APPLICATION IN BIOLOGY, MEDICINE AND SCIENTIFIC RESEARCH

Preliminary remarks

The intensive development of radio-frequency engineering, radio electronics, optoelectronics, nanotechnics and other scientific and technical directions contribute to the widespread distribution and implementation of the latest radio-frequency engineering and optoelectronic achievements in processes of generation, transformating and amplifying signals in devices and systems of telecommunication, radio astronomy and meteorology, physics, biology and medicine. The list of fields of science and technology is closely linked to application of low-intensity signals from a wide frequency range. It was facilitated by the emergence of new semiconductor elements of electronic technology, namely IMPATT diodes, Gunn diodes, Schottky diodes, Josephson junction elements, and so on.

These achievements promoted to the gradual exploitation of the wider frequency bandwidth of electromagnetic waves in the radio and optical range, acoustic waves in the ultrasonic range, magnetic fields and radiation. All of these achievements are fully utilized to create new medical equipment, enhance its capabilities and functions. Most of the characteristics of such equipment are related to application and measurement of energy parameters of low-intensity signals.

1.1 Classification of means for measuring the parameters of low-intensity radio frequency signals

In modern conditions the rapid development of science and technology stimulates the widespread use of low-intensity signals, as well as means and systems for their generation and amplification, reception, selection and conversion of signals, processing and evaluation of final information.

The classification of the radio systems (Fig. 1.1) using low-intensity information signals is primarily determined by their purpose:

information transmission systems (radio telemetry, radio communication, radio control, etc.);

information allocation systems (radiometry of physical and biological objects, radio astronomy, radar, etc.);

radio counteraction systems, etc. [1–4].

The received RTS signals can be divided by type into two large classes: for reception of quasi-coherent signals and incoherent ones, mainly radio thermal radiation, these are radiometric systems. The first larger class includes RTS for transmission and destruction of information, active radar and radio navigation systems. The second class of RTS includes RS, which are used in remote and contact control of composition and properties of physical and biological objects, radiolocation, radio astronomy, for object detection on background surfaces, etc.

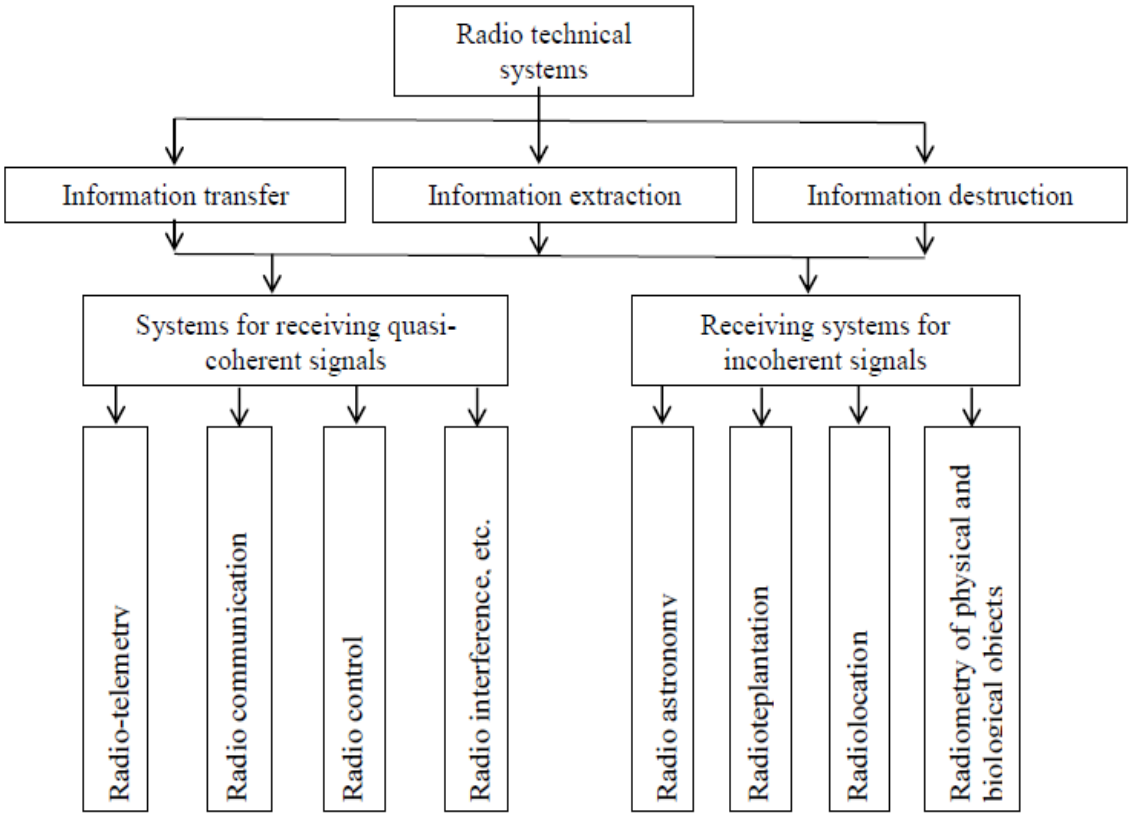

Figure 1.1 – Classification of radio engineering systems by their purpose

Evaluation of the attenuation coefficient, absorption and reflection coefficient, full impedance of high frequency circuits, determination of the standing wave coefficient, transmission coefficient or gain of high frequency nodes and other parameters are closely related to direct measurement of energy parameters and indirect determination of corresponding coefficients and characteristics of microwave devices [5].

Depending on the level of the estimated power, the meters can be divided into several groups (Fig. 1.2).

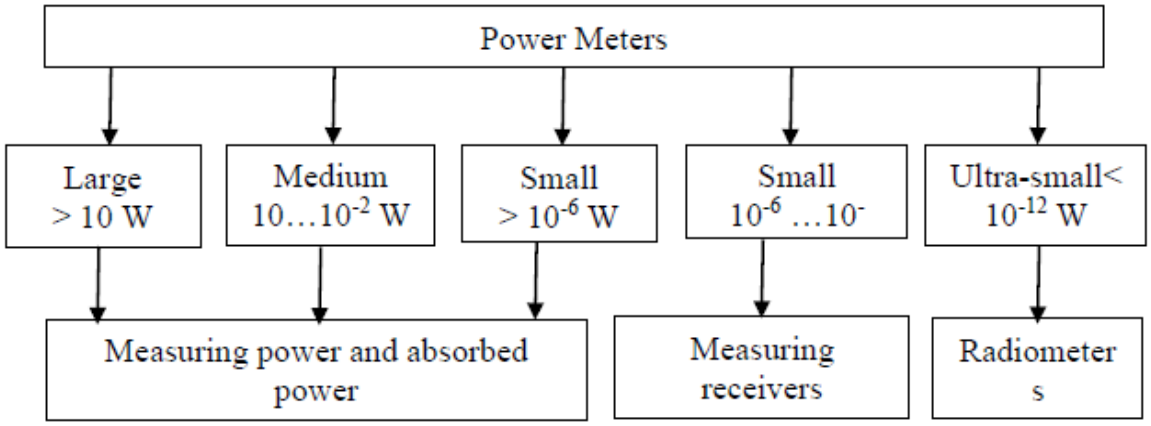

Figure 1.2 – Classification of power meters for radio frequency signals

In this case, the average value of the power level is used for measuring the energy parameters of monochromatic signals, while the total and spectral value of the power level are used for measuring the energy parameters of noise signals. The average power of a monochromatic signal during the oscillation period can be determined using the well-known formula [6]:

$$P_C = \frac{1}{T}\int_0^T U(t)\cdot i(t)dt = \frac{1}{T}\int_0^T U^2(t)/R_n dt, \qquad (1.1)$$

where T – is the harmonic signal oscillation period; $U(t)$, $i(t)$ – are voltage and current of harmonic oscillations respectively; R_n is the load resistance.

Using a quadratic diode converter it is possible to obtain on its output load the average value of the total signal power:

$$P_i = U_g^2 / R_n, \qquad (1.2)$$

where U_g is the effective voltage of the signal.

Measuring the energy parameters of random (noise) signals is associated with determining the power spectral density of the signal or total power. The power spectral density of noise electromagnetic radiation (EMR) is determined by the expression:

$$G_f = P_C / \Delta f, \qquad (1.3)$$

taking into account (2.2) we obtain:

$$G_f = U_g^2 / \Delta f. \qquad (1.4)$$

The total noise power is determined by the expression:

$$P_i = \sum_1^n G_f(f)/n, \tag{1.5}$$

where n – 1, 2, 3... is a number the noise power spectral density measurements in the radiometer's operating frequency range.

The product of voltages of two noise signals (U_1,U_2) and the cross-correlation coefficient (ρ) determines the power level for the correlated signals:

$$P_K = \rho U_1 U_2. \tag{1.6}$$

Measuring the energy parameters of signals with total power of 10^{-5} W or more is provided by standard means of transmitting and absorbing power. However, it should be mentioned that when analyzing the interaction of objects with electromagnetic radiation of the microwave range, it is often necessary to measure signals whose total power is less than 10^{-12} W, for example, when studying physical or biological objects according to the level of their own thermal radiation [4]. To solve this problem, non-standard radiometric equipment must be developed and utilized applying new methods and means of converting, extracting and measuring the power of extremely weak microwave signals, which intensity is less than the intrinsic noise level in radiometers. Moreover, such equipment should provide high sensitivity and measurement accuracy in a wide range of operating frequencies. These requirements were especially acute during exploiting the microwave range (mm waves) and its use for construction and operation of medical equipment.

1.2 Therapeutic equipment and specialized sources of low-intensity microwave signals of the mm-range

Currently, therapy with mm-range signals use about 25–30 types of specialized medical equipment [7].

Creation of the mm-wave band generators with low output associated with the solution of a number of complex technical problems. The main ways of obtaining low-intensity signals from devices for practical medicine are [7]:

– create generators for tens mW with subsequent reduction of power via attenuators;

– use second harmonic generator with resetting output by applying on its output high pass filter;

– use the frequency multipliers for the formation and allocation *n*-th harmonic signal;

– use of heat and spark generators.

There are several developed apparatus generating mm-range waves for medical purposes [7]:

– sets of harmonic signals with fixed operating frequencies, «Явь-1» («Yav-1»), «Электроника-КВЧ» («Electronics-UHF»), «РАМЕД-ЭКСПЕРТ» («RAMED-Expert»);

– «broadband generators» of the harmonic signals, «AMPT-01»(«AMRT-01»), «AMPT-02»(«AMRT-02»), later types of devices «Електроніка» («Electronics»), «АМТ-Коверт-04» («AMT-Covert-04»), «ARIA-SC»;

– «broadband devices» of noise signals «Поріг-1» («Porig – 1»), «Поріг-3» («Porig -3»), «Поріг-3М» («Porig -3M»), «Арцах» («Artsakh»), «Шлем»(«Shlem (Helmet)");

– combined devices generating as noise so harmonic signals, «AMPT-01»(«AMRT-01»), «Арцах»(«Artsakh»);

– devices with additional modes of quasi noise signals formatting due to «spill» the spectrum of harmonic signals, frequency sweeping within the operating frequency range «АМТ-Коверт-04» («AMT-04 Covert «), «ARIA-SC». This mode is easily implemented in new devices with embedded microprocessor (microcomputer).

The main types of such devices and their parameters are given in Table 1.1.

By operating frequency range of equipment located mainly in the 37 to 78 GHz, some devices (mainly noise signals generators) cover bands up to 90 GHz and 118 GHz even.

Apparatus for millimeter therapy

There are attempts to create devices designed at more high frequency, which work even in the range of terahertz waves. The level of power generated also varies widely and covers the area from 10 mW to 1 nW for monochromatic and $1 \cdot 10^{-8}$ to $1 \cdot 10^{-20}$ W/Hz for noise signals.

Table 1.1

Name of the device	Country of origin	Type of signal	Operating range, GHz	Output power, W
«AMRT-01»	Ukraine, Kharkiv	harmonic, noise	58…62 53…78	$3 \cdot 10^{-3}$
«Electronics-UHF»-101» (2 modification)	Ukraine, Kyiv	– // –	59…63 57…65	$5 \cdot 10^{-3}$ $5 \cdot 10^{-5}$
«Artsakh» (4 modification)	Armenia, YRFE NAS	– // –	59…61, 42…95	5 mW/c^2 10^{-19} W /Hz
«AMRT-02»	Ukraine, Kharkiv	harmonic, quasinoise	52...62	$1 \cdot 10^{-4}$
«ARIA-SC»	Ukraine, Kharkiv	– // –	53...64	$5 \cdot 10^{-5}$
LDK «Sharm», «Yav-1»),	Russia,	– // –	42,2; 53,5	$1 \cdot 10^{-2}$
«Stela- 2»	Russia, Tomsk	– // –	59...63	$1 \cdot 10^{-4}$
(«Porog -3» (4 modification)	Ukraine, Kyiv	noise	53...78	$10^{-17} - 10^{-19}$ W /Hz
«Covert -01»	Russia, Moscow	– // –	53...78	10^{-20} W /Hz
MU-2001	Switzerland	– // –	42...78	$1 \cdot 10^{-21}$ W /Hz
«Electronics-UHF -011, 013» (2 modification)	Ukraine, Kyiv	quasinoise	57...65	$5 \cdot 10^{-5}$

Fig. 1.3 shows the distribution of power and frequency range of devices for millimeter therapy.

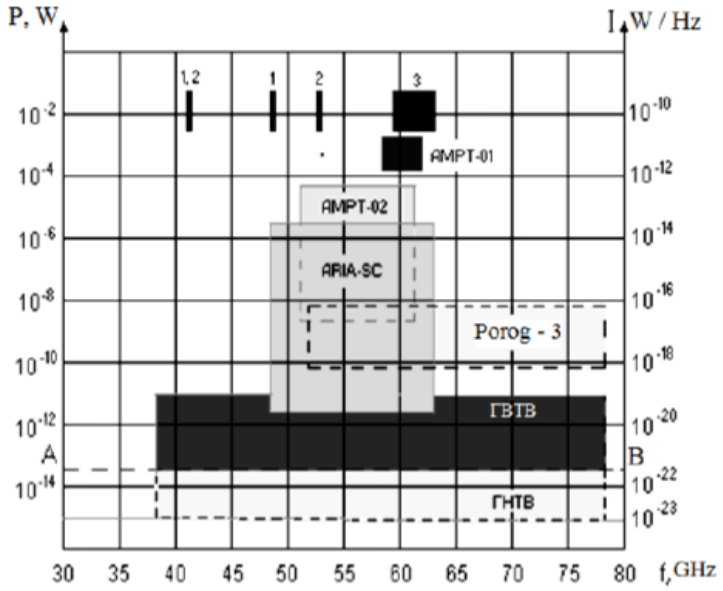

Figure 1.3 – Distribution of power and frequency range of devices Microwave resonance therapy: 1 – «Yav-1»), 2 – «Alenushka», (Ukraine), 3 –«Electronics-UHF»), (Ukraine); ГНТВ – «Porog-NT» (Ukraine); ГВТВ – «Porog-VT»(Ukraine); the line AB – power level natural human radiation

The information about the feasibility of the submillimeter range signals usage in practice of medicine has appeared recently.

Fig. 1.4 shows two types of noise generators with low-intensive output signals, positive flow «Porog-VT» and negative flow «Porog-NT.

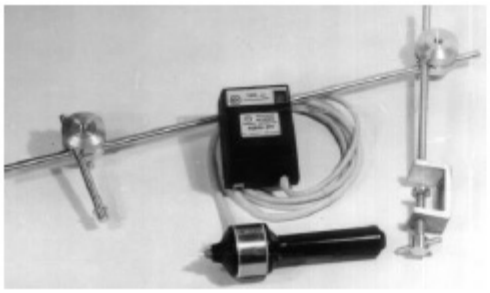

«Porog-VT» Patent of Ukraine № 265
(Bullet № 2 from 25.07.1994)

«Porog-NT» Patent of Ukraine № 53743
(Bullet № 2
from 7.02.2003)

Figure 1.4 – Noise generators with low-intensive output signals, positive flow «Porog-VT» and negative flow «Porog-NT»

1.3 Metrologic apparatus software and technologies of low-intensive microwave therapy

One of the problems to be solved in quantum medicine technologies are providing metrology and inspection of the equipment attribution during its operation. It should be noted that the lack of standard tools for measuring such small capacities does not allow to provide metrological support the equipment for quantum medicine and for biomedical research in the millimeter wavelength range [7]. Radiation of the ultra-low levels is monochromatic so noise signals are used in the new microwave technologies. The minimum values of integral power of monochromatic signals can be 10^{-10}–10^{-12}Wt (eg, ,ARIA-SC, AMPT-02), and the power spectral density of the noise signal is 10^{-16}-10^{-21}Wt/Gz («Порог3», «ПорогВТ», «ПорогНТ», «Коверт-01» («Porog3», «Porog-VT» , «Porog-NT» «Covert-01»). To measure such power levels, it is necessary to radiometric sensitivity setting was at least an order of magnitude higher,

and the measurement accuracy is not worse than the standard equipment of the same long-range power, ie 10…15 % [8, 9].

To solve this problem have been developed and certified by Standards Committee of Ukraine two highly sensitive radiometric systems (RMS) with a modulation transportation of the signal in frequency bands 37…53 GHz and 53…78 GHz, which provided Metrology maintenance and measurement of specialized medical mm range equipment in Ukraine [7, 10].

The radiometric measuring (on frequency bands 37…53 GHz) arrangement provides the following technical characteristics, which are verified by metrological certification:

– power measurement diapason, W …… $0.3 \cdot 10^{-13}$ … $0.5 \cdot 10^{-5}$;
– relative error tolerance, as maximum, dB …… $\pm$ 3.0;
– relative frequency error tolerance, as maximum, %..$\pm$ 2.5;
– sensitivity threshold, as maximum, W …..……... $3 \cdot 10^{-14}$;
– frequency band, as maximum, MHz …….. 100;
– operating frequency diapason, as minimum, GHz …. 37–53.

Figure 1.5 – Appearance of the radiometric unit
on frequency bands 37…53 GHz

1.4 Technologies of therapy with low-intensive microwave signals. Peculiarities and appliance fields of millimeter therapy

The use of mm-range signals in the practical medicine stimulated the emergence of several types of medical technologies that practically used [7]. Classification of the main technological directions of mm-range signals treatment is shown in Fig. 1.6.

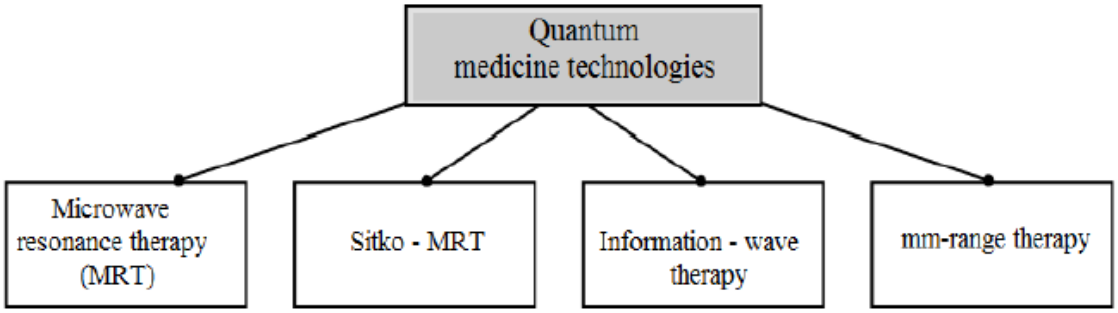

Figure 1.6 – Classification of main technologies of quantum – medicine

Despite the different names, these technologies have in common is that their use of millimeter wave signals using low intensity level reaches 10^{-20}–10^{-21} W/Hz*cm^2 [8].

The most common among these technology areas is microwave resonance therapy (MRT), which by order of the Ministry of Health of Ukraine № 136 from 06.22.1989, is officially recommended for implementation in the hospitals of the country in separate MRT-cabinets [10]. The use of MRT is characterized by a general positive impact on the functional systems of the human body, and therefore used in various areas of practical medicine fig. 1.7 [11].

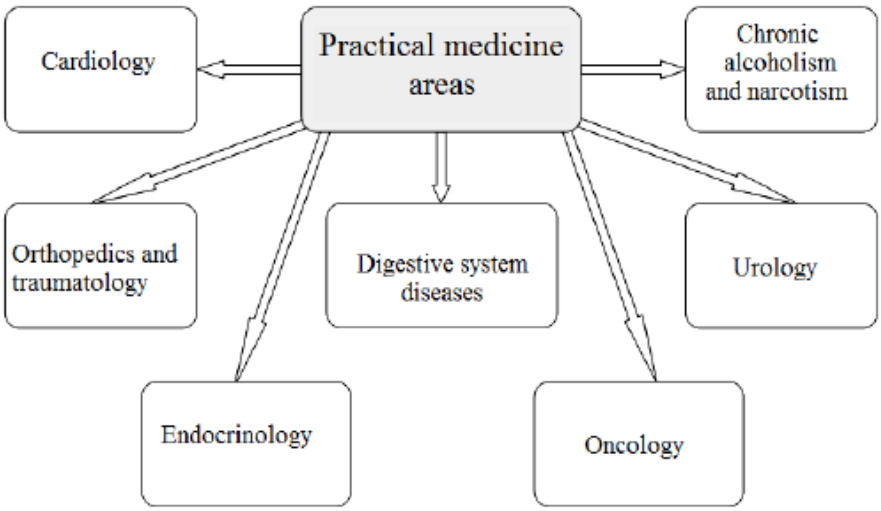

Figure 1.7 – Applications areas of Quantum Medicine

The most practical checking of the effectiveness of MRT was conducted in such areas of the medical practice: orthopedics and traumatology, gastroenterology, hematology, oncology. Promising is the use of MRI in cardiology in acute coronary disease – heart attacks, strokes and other diseases of the cardiovascular system. The experience of the Ambulance and infarction branch Department of the National Medical Academy for Advanced Training on over 100 patients in which MRT was used, along with the use of pharmacological agents significantly improves patient's state: decreases blood pressure, decreases tachycardia, stroke and minute cardiac output, as peripheral vascular resistance normalizes [11]. The use of MRT dramatically increases the effectiveness of pharmaceuticals.

The use of MRT in endocrinology at stages I-II of diabetes mellitus and insulin-independent diabetes with manifestations of diabetic macro-and micro angiopathies, polyneuropathy normalizes hemodynamic parameters in the lower extremities, increased pulse blood current, improves the conduction of nerve impulses in peripheral nerves.

MRT is effective in treatment of pain and paraesthetic syndromes in Dentistry. We have experience of good effect of MRT using in treatment of glossodynia (burning mouth syndrome) and in neuropathy of inferior alveolar nerve.

In addition, MRT gives a therapeutic effect without the deductive use of drugs, which reduces the load side and a negative impact on the patient of pharmatheutical therapy. The method can be widely used in the hospital and in the outpatient treatment of diabetes. The course of treatment is 10…15 sessions duration of 30…50 minutes of MRT.

MRT provides high efficiency in the treatment of stomach ulcers, enshrined on clinical examination in more than 6000 patients [11]. The results of MRT show favorably high therapeutic effect – complete healing of gastric ulcers by gastroduodenoscopy observed in 80…85 % of patients.

The process of treatment (10…15 sessions) accompanied by relief of pain syndromes, the normalization of the secretory and motor functions of the stomach, decreasing the concentration of hydrochloric acid and the volume of gastric juice. Concentration of the adrenaline and cortisol in the blood decreases, and levels of prolactin and aldosterone increases, which ensures normalization of fluid and electrolyte metabolism.

Promising is the use of MRI technology and Sitko-MRT in the treatment of cancer patients in stage III–IV, who received standard treatment [10, 11]. If the cancer disease is characterized by significant pain,

which is facilitated by the use or docked pharmaceuticals containing narcotic substances with following violations. The use of MRT allows decrease the dose of narcotic medicines.

Quantum medicine technologies can be a good alternative to pharmacological methods of pain relief, with a significant improvement in the «quality» of life. The example, of more than 40 cancer patients in stage III-IV who received standard treatment and were treated at the Center of quantum medicine «Feedback» [10, 11] shows that Sitko-MRT provides quick anesthetic effect, even for a few minutes, common state of patients improves; after treatment with MRT course of 10…20 sessions 85 % of cancer patients report decrease of pain during 10 and more days [10]. After using of MRT immune-modulating effect was received: the amount and subpopulation correlation of immunocompetent cells normalized, their functional activity increased. In fact, MRT technologies effectiveness does not yield to traditional medicinal preparations.

At the last time diseases of bronchopulmonary system become widespread. MRT can be a good assistant in the treatment of nonspecific lung diseases with bronchial obstructive syndrome because bronchodilator medicines usage in great quantity can lead complications.

MRT technologies allow receive positive effect without complications in acute and chronic bronchitis, pneumonia, asthma, in breath insufficiency I-II stages. In these cases use of MRT improve health in more than 80 % patients simultaneously to abolition of pharmaceutical medicines.

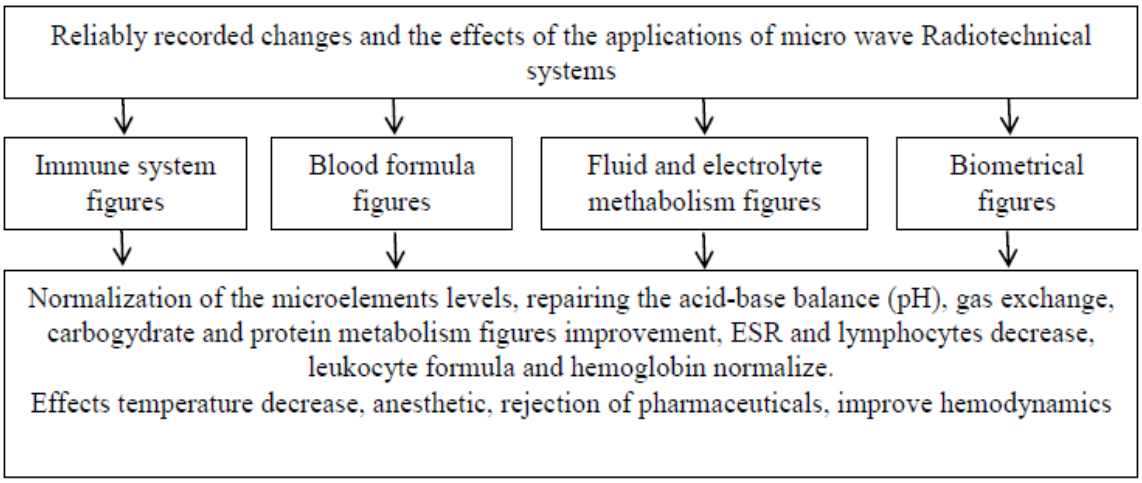

Figure 1.8 – Effects of Quantum Medicine

The results of the use of MRT in some diseases listed in the table. 1.2 [12].

Table 1.2

Diseases	Improvement (%)	Recovery (%)
Alcoholism	90	40
A septic necrosis of the femoral head	98	60
Bronchial asthma	85	60
Bronchial obstructive syndromes	90	82
Vegetative and vascular dystonia	85	70
Gastritis, gastroduodenitis	95	89
Kids cerebral palsy	100	60
Osteochondrosis	94	70
Polyarthritis	80	67
Diabetes	80	63
Sores	92	68
Ulcer of stomach and duodenum	98	90
Other pathologies	60–95	35–90

It proved that the use of the MRT is quite promising in the treatment of a wide range of diseases and helpful in most of them.

Microwave therapy is widely used in various fields of practical medicine as a separate type of treatment, or in combination with other methods of influence on the patient.

Medical apparatus for microwave therapy is characterized by low output power (10^{-6}…10^{-13} W) and use mostly 37,5…78,3 GHz frequency range and is sufficiently safe for both the patient and for staff.

Further development of the considered therapeutic areas is possible through the creation of a new generation of equipment that would provide feedback to the patient and self-adjusting output parameters, as well as mastery of higher frequency millimeter range waves.

1.5 Scientific directions of low-intensity electromagnetic fields and radiation of millimeter range researches

Thus, the development and deepening of biomedical researches and technologies require the creation of highly sensitive radiometric equipment using new achievements of microwave technologies and element base and exploring possible directions for its use.

Promising is the use of radiometric instrumentation for early diagnosis of diseases associated with the presence thermal irregularities in humans, as well as for the study of electromagnetic fields and radiation (EMR) of the biological objects and of the human body characterizing the exchange of information both within the living organism and with the external environment.

Early diagnosis and measurement of thermal irregularities within the human body (at the (50…80) mm of depth) is possible with the radiometer operating at low frequencies, (0,9…1,5) GHz, and the sensitivity of such equipment should be at the level of (10^{-15}…10^{-16}) W.

The research of natural electromagnetic fields and radiation and their interaction with the environment also requires the development of radiometric equipment with the sensitivity of the order of (10^{-14}…10^{-16}) W, depending on the range of operating frequencies.

Given the above, a classification of medical and biological problems that can be solved with the use of microwave radiometry equipment was developed fig. 1.9**.**

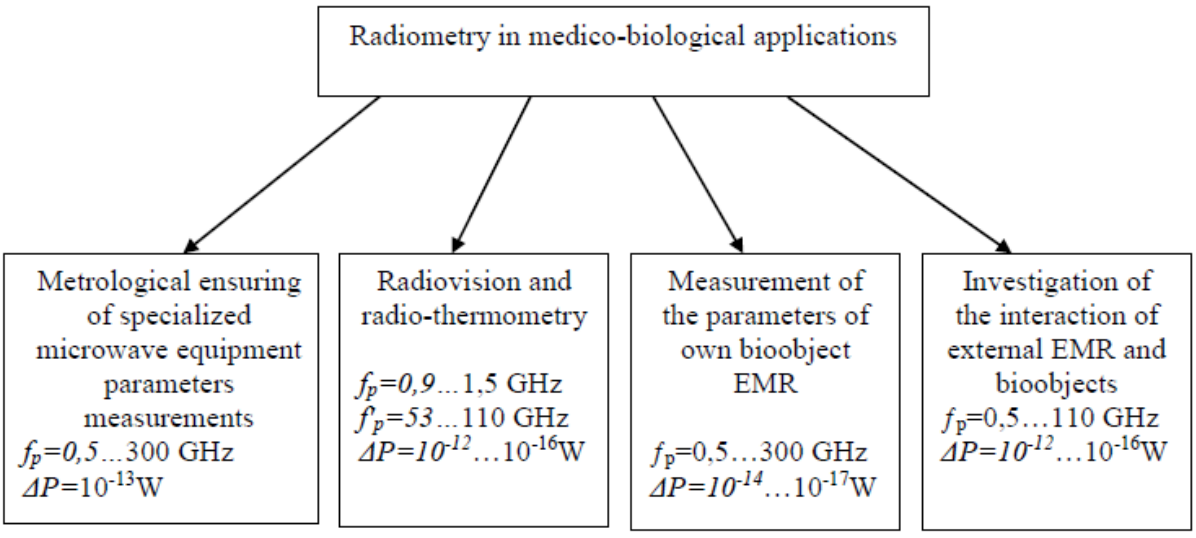

Figure 1.9 – Classification of radiometric problems in the medical and biological applications

Analysis of the Figure 1.9 data shows that, depending on the task of the biomedical applications, operating frequency range of radiometric equipment can vary from a few to hundreds of gigahertz, and the sensitivity – from 10^{-13} to 10^{-17} Watts.

Implementation of structural schemes of radiometric equipment such sensitivity is usually performed using the compensation, correlation or modulation method of transformation of input signals [8, 9].

Promising direction to use the microwave radiometric equipment is studying the parameters of own electromagnetic radiation (EMR) of living organisms.

Figure 1.10 shows the classification of the possible parameters of bio object own EMR, measurement of which can be performed using radiometric equipment.

For reliable signal recording the sensitivity of such circuits, operating on the difference signals, should be at the level (10^{-15}…10^{-16}) W.

Another area to use radiometric equipment when examining biological objects own EMR is to measure the correlation characteristics of the radiation

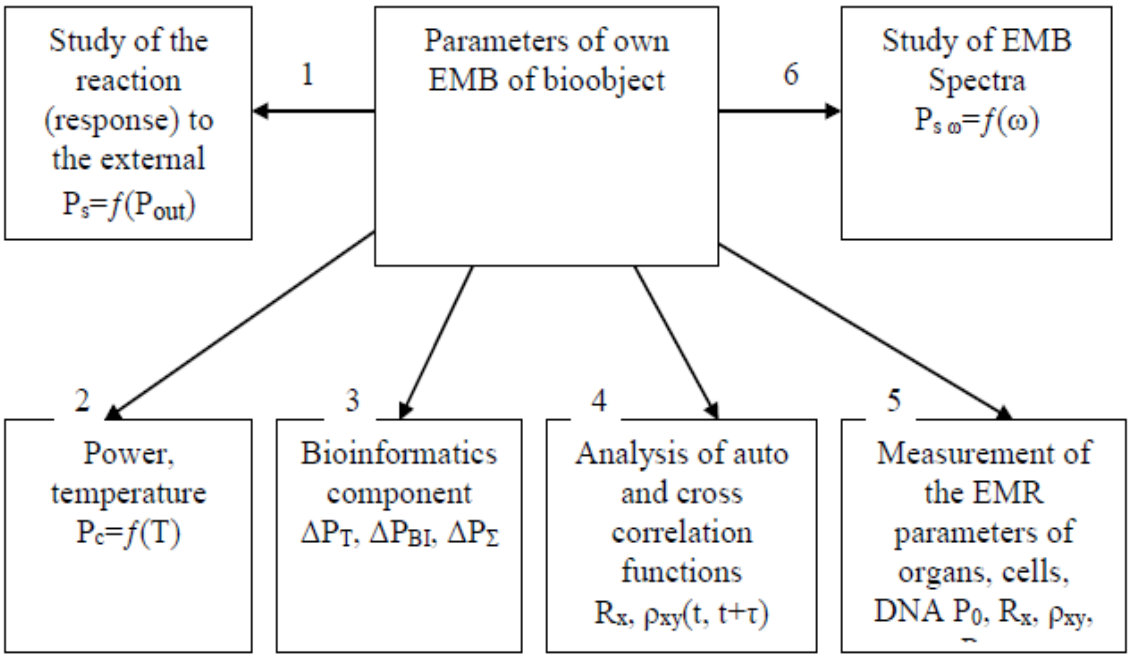

Figure 1.10 – Classification of radiometric problems
in the medical and biological applications Classification
of measuring tasks in the study of the bioobject own EMR

Radiothermal radiation, which is formed in equilibrium processes has a noise character, and its intensity is proportional to the temperature of the object *T*. Bioinformatic (non-thermal) radiation at the cellular level, which is determined by the non-equilibrium processes and provides synchronization of the body is deterministic. Due to the small size of the cell the energy density EMR already at a short distance from the biological object is reduced in many times, besides this reduction is accompanied by stochastization of the radiation. The total radiation of a living organism can be represented as a superposition of a deterministic and noise signal

$$U_{\Sigma}(t) = U_{\omega}(t) + U_{T}(t). \qquad (1.7)$$

Registration of the deterministic weak signal $U_{\omega}(t)$ against a background of strong noise signal $U_{T}(t)$ is a difficult technical problem, the solution of which is possible only with the use of specialized highly sensitive radiometric system that measures the autocorrelation function.

Register autocorrelation function opens the possibility of identifying deterministic processes that can be masked by noise and thus to identify the source of bioinformatic radiation of the living organism.

An important parameter may be the cross-correlation characteristics of the two signals, providing registration of distribution (location) of the deterministic signal on those or other bio object areas.

Measurement of inter-correlation function allows exploring the gradients of temperature fields in the presence of selected sources in the bio object body (local thermal irregularities). Sensitivity of such RMS must be on the level of (10^{-16}…10^{-17}) Watts.

Temperature anomalies in alive organism arising from tumors, trauma, inflammation, etc. strongly influenced the frequency features of EMR. Localization of the thermal irregularities sources may be at different depths from the body surface. Emission wavelength varies depending on the depth of its occurrence. Therefore, recording the frequency dependences of the intensity of EMR can detect and localize thermal irregularities sources in the human body.

Shape of the curve in the coordinates of frequency-voltage $U = f(\omega)$ provides information on the nature of the thermal irregularities and temperature gradient inside the object. Intensity on the frequency coordinate allows determining the depth of the source of thermal radiation.

One example of the use high-sensitive radiometric system is conducted by the authors [13, 20] studies the electromagnetic characteristics of dental materials, in order to determine the parameter which would provide a more accurate identification (compatibility, matching) with the natural tooth material.

These dental materials were studied: Sample № 1 – based on resorcin-formalin mix material «Foredent» (SPOFA, Slovenia); sample № 2 – glass-ionomer cement Endion (VOCO, Germany); sample № 3 – Zinc-oxide-eugenol material «Endomethazone» (Septodont, France); sample № 4 – polymer cement AH Plus(Dentsply, USA); sample № 5 – light-cured composite «Spectrum» (Dentsply, USA) (shade A3,5); sample № 6 – self-cured composite «Compolux» (Septodont, France); sample № 7 – glass ionomer cement «Cavitan – plus» (SPOFA, Slovenia); sample № 8 – natural tooth material (enamel); № 9 – natural tooth material (dentine); № 10 – porous osseous tissue (cross section).

Samples № № 1–4 represent materials used for root canals sealing, thus received in study data were compared to the similar data for dentine (sample № 9), which they contact with. Samples of materials № № 5-7 use for tooth surfaces restorations so their properties were compared with dental enamel (sample № 8), too.

During the experiment, the intensity of each material radiation was tested at a temperature of 37^{o} C, the level of which was recorded by approved measuring setting НУ-2 with sensitivity of $1 \cdot 10^{-14}$ W at a frequency of 52 GHz.

According to the conducted measurements, the radiation power of the considered number of dental materials was concentrated in the range of $(1{,}8 \ldots 3{,}1)10^{-13}$ W/cm^2. Identification was carried out by comparing the greyness coefficient of materials, which is calculated according to the formula

$$\beta = I_T / I_{A\text{ЧТ}}, \tag{1.8}$$

where I_T – measured power of the studied material, $I_{A\text{ЧТ}}$ – the intensity of blackbody radiation at the same temperature, calculated by the formula Rayleigh-Jeans

$$I_{A\text{ЧТ}} = \beta \left(f / c \right)^2 kT, \tag{1.9}$$

where k – Boltzmann constant; T – temperature; β – physical body grayness ratio; f – radiation frequency; c – speed of light.

The results of the measurement and the calculation of the gr ayness coefficient of the material are presented in the on Fig. 1.11.

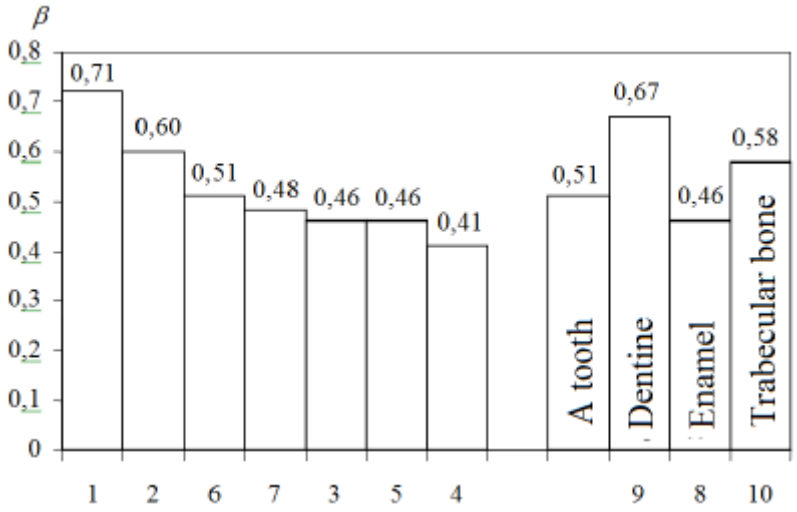

Figure 1.11 – The factor β of dental materials samples 1–10

Identification of the grayness coefficient values gives deviation 38.0 % of the materials paired № № 4 and 9, and 7.6 % in the pair № № 1 and 9 used in root canals sealing, and from 0 % in the materials paired № № 5 and 8 to 10.8 % in a pair № № 6 and 8 – in the materials are used to filling the tooth surface.

Therefore, the preference should be given to matching materials. In addition, such verification is promising in the development of new dental materials.

Conducted studies allow to make some conclusions: 1. Alive organisms are characterized by large set of parameters of their own microwave EMR; its measurement and study contributes not only to deepen the knowledge of living objects, but also the development of new diagnostic and treatment methods.

Radiometric methods and tools have great potential for solving of practical and research problems in biology and medicine – metrological provision of specialized equipment, diagnosis of the state of alive organism, the study of the own microwave EMR parameters and their relationship with the environment.

Radiometry use in biomedical applications due to the need for fluctuation sensitivity to the level (10^{-15}…10^{-17}) Wt, which is a complicated

technical task requiring its decision to create new options for highly sensitive radiometric equipment.

The proposed technical solutions, while providing the required sensitivity, extend the functionality of radiometric equipment, in relation to the objects of wildlife and humans.

1.6 Natural sources of the mm-range irradiation and using peculiarities in physiotherapy

Using low- intensive signals of the mm-range is effective enough in many areas of practical medicine – orthopedics, neurology, endocrinology pulmonology and other branches and technologies of physiotherapy. At the same time, along with specialized medical equipment, the materials and objects of natural origin are widely used in different technologies of the physiotherapy. First of all, these materials include primarily mineral wax, mud, paraffin, salt and a wide range of minerals used in lithotherapy [14].

The study of electromagnetic microwave fields and irradiations (EMR) of the minerals conducted by authors [8, 15, 16] confirmed the presence in the spectrum signal components of the millimeter range, which can be used as a therapeutic component when minerals are heated to therapeutically acceptable temperatures (40–50) ^{0}C. In the course of the studies were selected minerals with high emissivity which include jade, agate, onyx. When the human body temperature is 36 ^{0}C the radiation level of these minerals is greater than the level of human body emission that promotes positive flow of EMR. Also were found minerals that at this temperature have less radiation level, thus in this case negative flow of EMR forms.

For the first time negative flows of the mm-range waves were recorded and studied by group of authors [17].

Considering these features authors [18] proposed a heat generator with reversible temperature control and appropriate formation of various streams EMR. Effective enough action of the negative flows confirm laboratory and clinical researches conducted at the R.E. Kavetsky Institute of Oncology (NAS of Ukraine) and Research Center of Quantum Medicine (Ministry of Health of Ukraine), as reflected in treatment technology, approved with patent [18]. In vitro studies showthe inhibition (for 27.4 %) of model «Sarcomas C-37» in laboratory animals when they were irradiated with negative flows. The positive flow accelerates (for 13,5 %) tumor growth.

The effectiveness of natural materials using for Physiotherapy is explained mainly by heat and warming the respective areas of the patient's body. They don't take into account that during heating these materials emit a wide range of radio-frequency signals [8, 15, 16]. The therapeutic total effect will consist of thermal and microwave components, and therefore more in-depth study of the structure of natural materials signals for Physiotherapy is an urgent task.

1.6.1 Research EMR natural treatment formula for physio procedures

To study EMR properties of the natural mixed materials were chosen commonly used for the Physiotherapy materials – ozokerite (Borislav deposit, Lviv region), mud (Mykulyntsi, Ternopil region) crystalline salt (Artemivsk) and paraffin as a component of therapeutic compounds [16].

Emissivity of the slice of wood (ash) and a fragment of bone were also examined for comparison records. Ozokerite has a high heat capacity and low thermal conductivity with the possible temperature to use in thermal applications 40…50^0 C. It includes paraffin, ceresin, as well as in the composition of the curative mud – biologically active substances. As a result of measuring in the frequency $f = 45ГГц$ the following values of the irradiation samples were obtained. They are presented in table 1.3.

The process of measuring the values of irradiation power was conducted using certified radiometric system with sensitivity, which makes it possible to confidently talk about the accuracy and reliability of the results.

Table 1.3 shows that the radiation level of the areas of the palm of the person, even at a temperature (31^0C), significantly lower than the temperature of the heated material (40^0C), is greater in 2 times compared to pure wax and in 4 times in relation to the treatment mix mud and paraffin.

Analysis of the results shows that along with warming ozokerite and mud applications (creation of positive flows) a microwave component is formed which creates «negative flow» in relation to the patient's body that can reduce pain syndromes with excess temperature. Paraffin, which added to the ozokerite and mud in the preparation of therapeutic mixture to stabilize it, reduces the emissivity of the mixture in the microwave range, the value of which depends on the percentage of components. This ratio can adjust the «negative» flow, adding to the mixture a higher percentage of paraffin, and therefore the effectiveness of pain syndromes treatment increases. The same ability has salt and solutions based on it (salt

applications, baths, etc.), in opposite to wood and bone that have a higher level of radiation than the human body and form towards it EMR positive flows.

Table 1.3 – EMR properties of the natural mixed materials

Studied sample	The value of power (W/cm^2)	β
Ozokerite(pure)	$1{,}8\cdot10^{-13}$	0,1
Themud (pure)	$1{,}6\cdot10^{-13}$	0,08
Paraffin (pure)	$1{,}05\cdot10^{-14}$	0,05
Paraffin+ mud (used)	$0{,}5\cdot10^{-13}$	0,02
Wood	$6\cdot10^{-13}$	0,3
Salt	$2{,}2\cdot10^{-13}$	0,11
Manhand (t_r=31^{0}C)	$4\cdot10^{-13}$	0,21
Bone	$6{,}8\cdot10^{-13}$	0,35

The dynamics of change of the material proper EMR when it cooled from the maximum heating temperature used during the procedure (50^0 C) to body temperature (controlled palm point) was also investigated. The graph showing the integrated power change is presented in Fig.1.12.

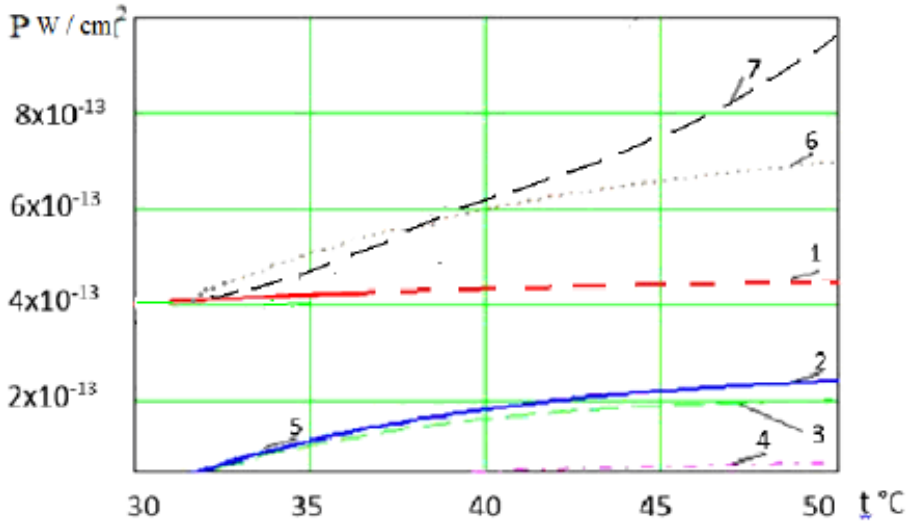

Figure 1.12 – The graph of the integrated power changes:
1 – human body; 2 – ozocerite mix; 3 – mud with added paraffine; 4 – paraffine; 5 – mud (pure); 6 – wood; 7 – bone

The level of the human body emission for the temperature control points 31°C, 40°C and 50°C was calculated using the Nyquist formula

$$P = kT\Delta f\ , \qquad (1.10)$$

where $\Delta f = 10^8$ Hz – analysis band of highly sensitive radiometric system.

For point 31^0C the calculated value is 4.18 10^{-13} W/cm^2 which is different from the measured less than for 5 percent, which is suitable for microwave measurements and verifies measurements certainty well. The human body radiation levels were calculated for temperature 40^o C and 50^o C similarly.

From the studies of the EMR of medical materials using for physio procedures the following conclusions may be done:

Effective use of natural materials in the thermal physiotherapy should be associated not only with the presence of infrared components, but as studies have shown with the presence of microwave component, which has a significant impact on treatment outcome.

Microwave EMR of the studied therapeutic materials has negative flow in relation to the human body, which creates the effect of «selection» of energy at local inflammatory processes.

Using a material with low radiating ability (paraffin) mixed with the main component (ozokerite or mud) can not only stabilize the therapeutic mix, but also adjust the power of the negative flow.

It should be noted also that human bones have higher levels of microwave radiation component, compared with soft tissue and are a kind of microwave generators that stimulate the cells of our body.

1.6.2 Research EMR minerals and precious stones

In folk medicine for the treatment of certain diseases different gems and minerals are using, too.

The research results presented in [8, 15] confirm the difference of the electromagnetic activity of gems and minerals from other bodies creating in this way the possibility of their use for medical purposes. Measuring the level of EMR of the gems and minerals was performed at the frequency of 60 GHz and the temperature of 37°C, which corresponds to the upper boundary of the normal human body temperature.

Fig. 1.13 shows the intensity distribution of various minerals.

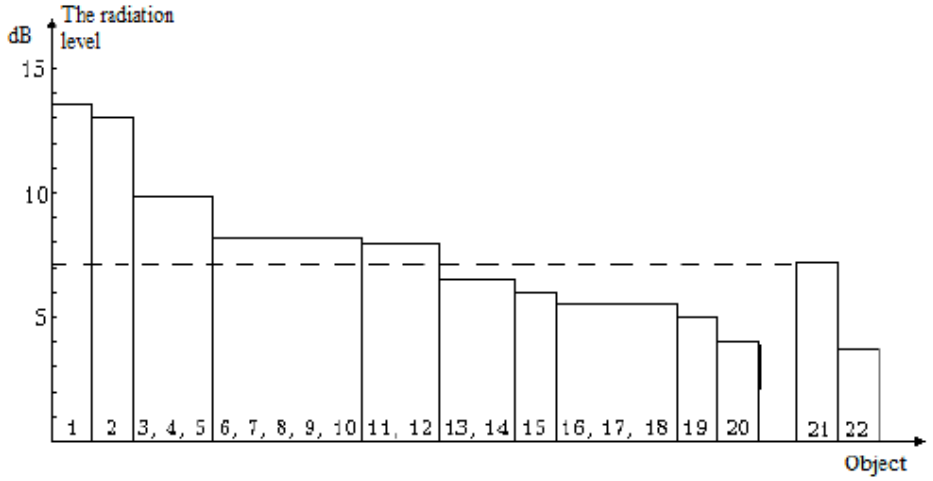

Figure 1.13 – Distribution of emissivity of minerals and other materials

The radiation level of minerals is given in columns diagram. Minerals were assigned to the following digital indexing: jade – 1, onyx – 2, agate – 3, coquina (shell rock)- 4, big femoral bone – 5, amethyst – 6, amber – 7, jasper – 8, pyrite – 9, small bones – 10, quartz (single crystal) – 11, chalk – 12, sulfur – 13, fluorite – 14, flint – 15, amazonite – 16, rhinestone – 17, calcite (feldspar) – 18, topaz – 19, morion (quartz) – 20. Under number 21 denotes the level of human palm radiation and column under number 22 characterizes the position of the electromagnetic properties of the water at a temperature of 37°C.

The listed minerals can be divided into two groups according to their microwave EMR levels – greater or less than proper human body EMR at the normal temperature (36…37°C). It reflected on the Fig. 1.13 with a dotted line. Minerals with a larger radiation are jade, onyx, agate, amethyst, amber, jasper. In the thermal contact with a human body these minerals generate a microwave signal, which is redundant to human skin, and it is completely absorbed. Thus, these minerals provide «recharging» the energy in the case of continuous wear them on the human body.

The second group of objects contains minerals such as sulfur, fluorite, silicon, amazonite, rock crystal, calcite, topaz, morion. When these minerals are heated to the body temperature the radiation level is below the person's own radiation and they provide the absorption of the human microwave energy in thermal contact with the human body. In some minerals, such as chalk and a single crystal of quartz, almost the same with the person’s level of radiation was recorded, so they are balanced (neutral) in electromagnetic respect.

It should be noted also that the electromagnetic activity of «big» and «small» human bones is significantly higher than radiation intensity of the skin, as well as water as a main component of a living organism. A similar situation is with coquina (shell rock), which is mineral residue of biological objects – its EMR intensity is also higher than the body, especially the human palm. At the same time the structure of coquina and of the bone is different. If seashells are formed by deposition of calcium flat layers, some human bones have pipe shape. This provides the effect of some kind of resonance. The presence of calcium in the bones and coquina, despite structural difference, provides a high level of EMR. The positive effect of calcium on the radio- and thermal activity is also confirmed by the analysis of the chemical composition of minerals – jade and onyx, in which fixed the maximum intensity of the radiation and which contain a significant percentage of calcium.

Thus, living beings bones provide significantly greater level of radiation compared with surrounding soft tissues, obviously performing the function of thermal generators of the mm-range microwaves and play an important role in the external electromagnetic fields (EMF) influence on living organism.

Based on the results of experimental radiometric studies of physical bodies in mm-wave band it can be stated that in the simulated temperature gradients that actually occur in the natural environment, electromagnetic fields and radiation of mm-radiation are generated. The sources of these emissions are the various physical bodies and the environment (water, soil, stones). Similar EMFs are formed around human and living beings.

As can be seen from Fig.1.13, nephritis has significantly higher levels of radiation (13,5 dB) than human skin (7 dB), and quartz (morion) EMR level is slightly below the water data. A possible cause of increased level of radiation in the past three objects is the presence calcium salts in the human bones, shell rock and nephritis (for example, in bones – calcium phosphate $Ca_3 (PO4)_2$. It is known that Ca atoms are responsive actively to thermal impacts. The mean square displacement of Ca atoms during thermal oscillations is equal to 0,114 $\mathring{A}$ [17]. By the reaction on thermal influence Ca takes place among such active elements as Li, Na, K, Rb and Cs, some of which (K, Na, Ca) are commonly used in biological objects during their life support. Obviously the raising of the radiation levels of the considered elements (bones, jade and shell rock) is associated with an increased rate of theirs greyness coefficient. Human bones are the kind of generator and a

waveguide of the microwave oscillations and provide irradiation and transmitting the electromagnetic waves inside a biological object, in contrast to the human skin, which absorbs low-intensity mm range signals.

Considered the listed above, the reaction of the human body on the external low intensity microwave radiation was studied.

1.6.3 Determination of the human body's reaction to external microwave low-intensity irradiation

Figure 1.14 is a diagram showing the distribution of relative absorbance ability of the biological object according to the irradiating signal level and the level of the object own radiation at a resonant frequency

$$K_{\text{П}} = 10 \lg \frac{I_C}{I_0}, \tag{1.11}$$

where $I_0 = I_0' + I_0''$; I_0' – the level of the object own radiation; I_0'' – the level of the reflected signal.

Considering meaning I_o equation can be written as

$$K_{\text{П}} = 10 \lg \frac{I_C}{I_0' + I_0''}. \tag{1.12}$$

Increasing capacity of the irradiating generators within $1 \cdot 10^{-21} < I_C < 1 \cdot 10^{-19}$ W/Hz at selected frequencies leads to full absorption of the acting signal (AB portion of Fig. 1.14).

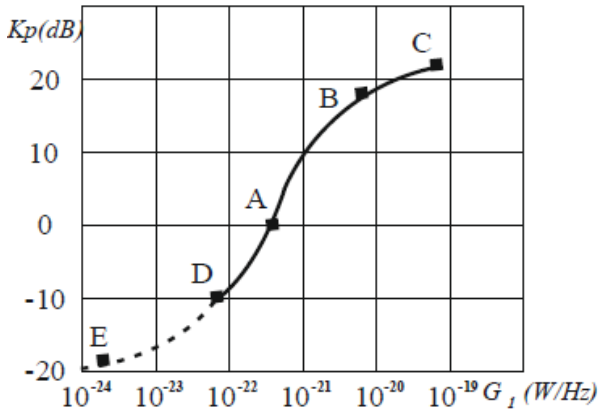

Figure 1.14 – Distribution of absorptivity of the human palm in interaction with positive and negative EMI fluxes

At further increase in capacity $I_C > 1 \cdot 10^{-20}$ W/Hz the reflected signal appears, which characterizes the saturation effect of the treated area (BC in Fig. 1.14) of the skin. In this case, the reflection component I_0'' increases,

and the resulting bioobject radiation I_0 is relatively increased with the coefficient K_{Π} decreasing (Fig. 1.14).

Physical reduction of absorption, in our opinion, is connected to the saturation of the upper energy levels of biomolecules and the lack of free carriers that can absorb EMR photons. A further increase in the irradiation power (up to the appearance of thermal effects) favors a slight increase in absorption. Thus, living beings show the dosage ability to absorb mm-band EMR [8].

Note that the slope of increase of the reflected power exceeds the rising slope of the irradiation power. As a result the saturation occurs with the characteristics curvature on the section BC (Fig. 1.14). Based on the experimental data [8] and the distribution illustrated in fig. 1.14, it can be concluded that the dynamic range of the bio object absorptive capacity in levels that exceed its own level of radiation, is 15-20 dB. By the way, about the same level of microwave radiation has a wormwood cigarette, which is used in Chinese moxibustion. Levels of capacity placed on the intensities axis at the right of the point A, create a positive flow of EMR comparing to own biological object radiation, and placed on the left – negative flow [8, 17].

In studies [11, 12] the results of experiments on the effects of positive flows of EMR, which are used for the construction of the ABC distribution area (Fig. 1.14) are listed. Experimental verification of the negative EMR flows impact was carried with power levels about 10…15 dB lower than the power level of self-radiation (AD site). A further power reduction of the negative flows source (generator), and experimental verification of distribution represent a significant technical challenge that requires further additional research.

At the same time, as shown by laboratory and clinical studies [18] medical devices on the negative flows are very effective method for use in a variety diseases with the manifestation of «syndrome of excess», especially with pain syndromes – dystrophic lesions of the joints and spine: arthrosis, arthritis, osteochondrosis. Positive changes in patients with bronchial asthma and chronic obstructive bronchitis, in some number of cancer patients were noted also. From the above we can conclude:

- using a RMS to assess the objects absorbance abilities allow significantly reduce the levels of irradiating signals that reliably analyzed and are 10^{-12}…10^{-14} W/Hz for monochromatic and 10^{-20}…10^{-22} W/Hz for noise signals;

- the absorbance and reflection abilities of living organisms has a pronounced non-linearity with respect to the level of exposure;

- analysis of experimental data of the biological objects absorbance ability shows that the human body responds to the signal level, which differs in 2…5 times from its own radiation;

- substantial (in 10…100 times) increase in intensity leads to reflection of the illuminating signal power which indicates the protective properties of living organisms.

1.6.4 The study of electromagnetic parameters of textile and leather for clothes and shoes manufacturing

Measurement of weak EMF via RMS opens up the possibility of studying the interaction of human own field with textile and leather materials which are used for clothing and footwear manufacturing [8].

The model fig. 1.15 presented in [8] describes all physical processes that run in the boundaries between researched materials and the human body. These processes are necessary to consider in research of materials compatibility with human organism. The materials are considered to reduce as the environmental EMR (flow A– EMR of external environment) so the EMR generated by the human body (flows H and I – thermal and biological radiation of the human body). Besides, material heated by the human body is the source of additional EMR (flow D – thermal EMR of the material) interacting with human organism.

The reflective and absorbing properties of materials are mainly determined by their structure and raw material composition. For the instance, structure parameters (linear density of threads, direction and degree of twisting, through porosity, etc.) and also chemical composition of threads and fibres are important for textile materials. In relation to EMR these materials are represented as heterogeneous absorbing and dispersing medium which has the average refractive index higher than air does. Therefore, in the boundary between material and air the part of EMR is reflected (flow C– reflected EMR) and another part penetrates into the material (flow B – absorbed EMR).

Due to absorption and dispersion the flow B is decreasing while passing through the material. The flow F (EMR transmission), which has passed through the material, influences on the skin. Part of the flow G (EMR entering the human body) penetrates into biological tissues of the human body and interacts with molecules (dissociation, electronic interaction, oscillating and rotating motion).

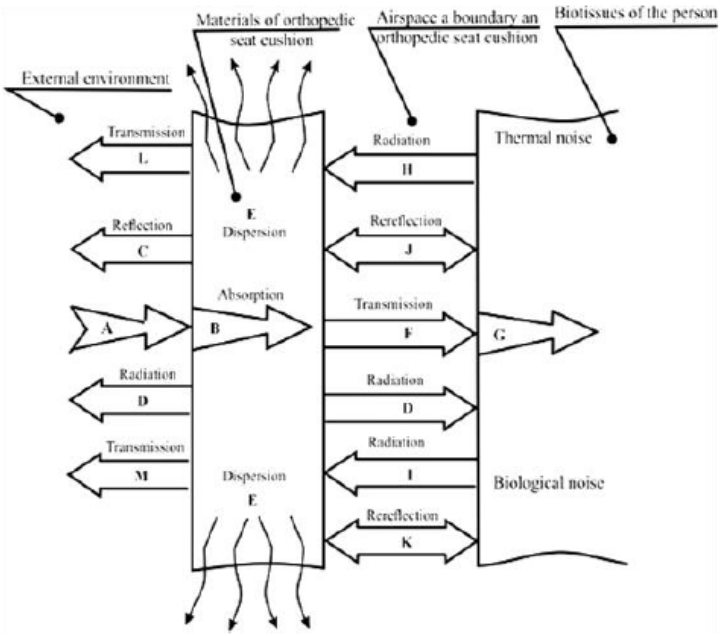

Figure 1.15 – The model of EMR flows interaction with materials and human

Figure 1.15 also shows: dispersion flows E; thermal and biological EMR multiple reflections from the material and the skin J and K; thermal and biological EMR of the human body transmitting thorough material L and M.

For experimental studies of the materials, a radiometric system was used integral sensitivity of which was $3 \cdot 10^{-14}$ W/cm^2 as well as a technological device for heating materials. The experimental studies were performedat frequency of 52 GHz. The scheme of technological equipment for experimental studies using the microwave RS is presented in Fig. 1.16.

Conventional notations in Fig.1.16 are as follows: 1 – the power supply; 2 – the thermostat; 3 – the attenuator; 4 – the radiometric system; 5 – the measuring device; 6 – the test material; 7 – the contact antenna; 8 – the thermostat plate; 9 – the temperature controller.

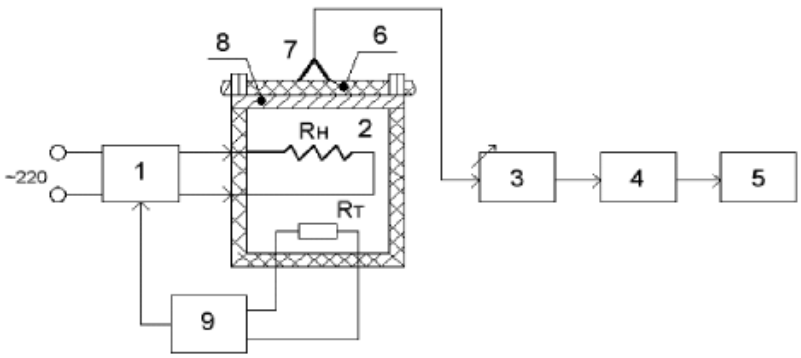

Figure 1.16 – Scheme for study radio emission of material samples

Methodology of the experiment: the studied materials were heated in an oven at a temperature of 36,0±0,5°C, which corresponds to the average human body temperature at the comfortable climatic conditions, and then their radiation was measured. Evaluation of the emissivity was carried out using the RMS at a frequency of 52 GHz. The results of experimental research textile materials are shown in Fig. 1.17.).

Because of the intensity distribution (I_ω), it is clear that natural materials (fur, cotton, linen) are closest to the emissivity of the human body. Synthetic or mixed materials have significantly lower emissivity and, in fact, are the source of electromagnetic negative flow, leading to increased energy extraction from the human body surface. At the same time, natural fibers help maintain the body temperature, and are more compatible with the human microwave field; they weakened it less.

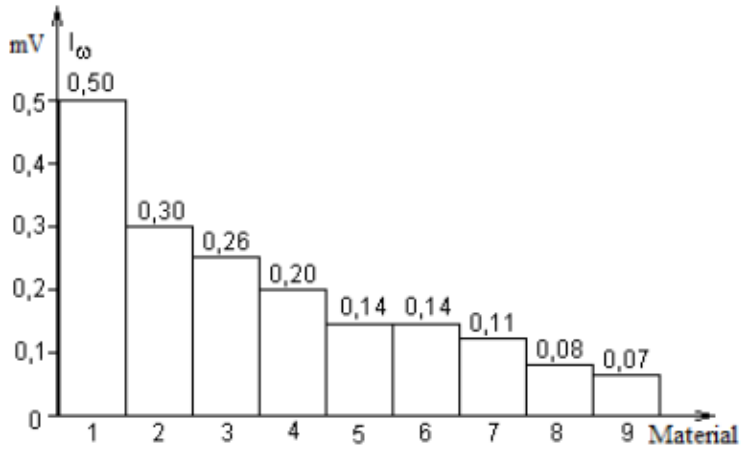

Figure 1.17 – Distribution emissivity of textile materials for clothes: 2 – nutria fur, 3 – fox fur, 4 – linen, 5 – sheepskin, 6 – cotton, 7 – glsin (35 % polyester, 65 % cotton), 8 – glzel (65 % polyester, 35 % cotton), 9 – 100 % polyester; the column 1 – show the mean data of the human body irradiation

Separate studies were carried out to assess irradiative abilities of the leather. During experimental studies of leather samples checked: the proper microwave irradiation at 36^{o}C and radio transparency by two figures – delay and bypass of the probing signal, which are difficult to define in the technological cycle of leather.

Heating the leather sample to the temperature of the human body, as seen from the formula (1.10), lead to the formation of extremely low signal with intensity within 10^{-13} W. To register this signal RMS with a sensitivity of 10^{-14} Watts was used. The measurement results are shown in Figure 1.18.

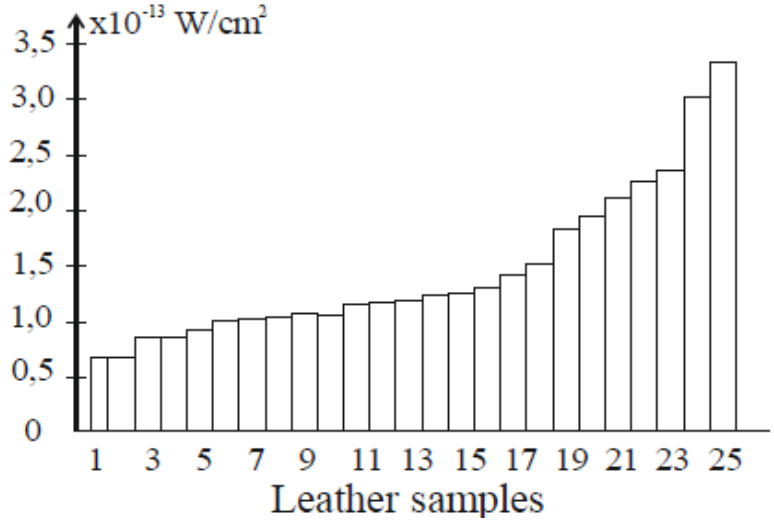

Figure 1.18 – Distribution of own radiation of skin samples

Name of the leather samples: 1- goby; 2 – as; 3 – shark; 4 – crocodile; 5 – goats glazed kid leather (black); 6 – sheep (brown); 7 – pig leather; 8 – pork leather; 9 – goats; 10 – sheep chevron; 11 – white sheepskin; 12 – half- sheepskin; 13 – black sheepskin; 14 – blue shark; 15- goats glazed kid leather (brown); 16 – sheepskin (gray); 17- bull; 18- «fish» dressed pork leather; 19 – bull; 20 – OPOEK elastic; 21- bullok; 22- horse leather; 23- vymitka; 24 – Elastic grown-up; 25 – Elastic lot.

There are follow groups of leather samples for theirs proper irradiation: with low intensity at the level $0{,}5 \cdot 10^{-13}$ W/cm^2 (samples 1-4); with intensity about $1 \cdot 10^{-13}$ W/cm^2 (samples 5-16); samples with emissivity banding 1,5…2,5 W/cm^2 (17-23); and samples of leather with elastic dressing which have radiation intensity more than $3 \cdot 10^{-13}$ W/cm^2 (samples 24, 25).

Considering the compatibility of the leather samples with the human body skin, which has the radiation level about $3{,}5 \cdot 10^{-13}$ W/cm^2, materials with higher level of irradiation have the benefits.

Measuring procedure of the radio transparency (Fig. 1.19) was performed as follows. At the beginning signal from the approved reference oscillator of low intensity noise G (10^{-12}…10^{-13} W/cm^2) by transmitting X_1 and X_2 receiving antenna was directly measured by RMS.).

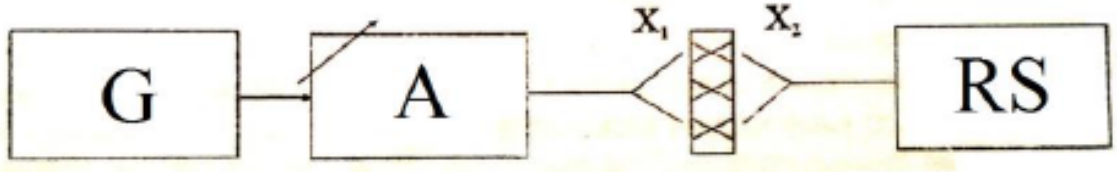

Figure 1.19 – Scheme to study radio transparency of leather samples

Then the leather sample was placed between antennas and power that passes through it was measured – P_{in}.

Power that delay or reflect by the leather sample determined with ratio

$$P_{abs} = P_{out} - P_{in}, \tag{1.13}$$

where P_{out} – power on the output of the transmitting antenna X_1; $P_{in.}$ – power on the inlet of the receiving antenna X_2.

For skin thickness in the range of 0.1 to 3 mm the absorption and radio transparency is almost at the same level, despite the low level of the probe signal ($1 \cdot 10^{-13}$ W/cm^2). Dispersion of the figures of absorption and radio transparency does not exceed 15 %.

Thus, the study of microwave properties of leather samples for light industry showed the possibility to evaluate some of its parameters with radiometric control method. It's enough to assess its suitability for quality manufacturing a particular type of footwear and clothing for the population.

In addition, the devices of high sensitivity are necessary to measure the thickness and density of the leather, its moisture and the presence of hidden defects.

1.7 Future areas of research intensive low signals in biology and medicine

Creating radiometric systems with sensitivity of 10^{-13} to 10^{-17} Watts enhances the research of weak fields and radiation from alive and inanimate objects. The main directions of promising scientific research using highly sensitive radiometric systems are:

- study the dynamics of natural radiation the human body during his life;
- evaluation of correlations between the various parameters of the human body;
- study the electromagnetic properties of water and aqueous solutions as key components of the human body;
- measuring proper electromagnetic radiation of bio objects, materials and substances that come into contact or are close to human and can affect it.

Application problems that can be solved by using highly sensitive RMS include:

- measuring the level of radiation of bone and tooth tissue and it substitutes for the identification and assessment of electromagnetic compatibility with the human body;

- assessing the compatibility of textiles with the human body and their comfort considering electromagnetic properties;

- measuring the emissivity of precious minerals and stones so as products with them;

- assessing the possibility of the registration of impurities in dielectric materials for their emissivity;

- carry out the flaw of dielectric materials and establishing correlation between radiation and the presence of defects (cracks, irregularities included).

During radiometric studies a number of features associated with the body and properties of some materials were revealed:

- the proper radiation of the human body is within $10^{-21}…10^{-22}$ W/Hz см^2;

- the level of radiation an individual organism is constant, which is determined by the intensity of its cell metabolism and skin temperature. In fact, this level describes «electromagnetic homeostasis» of the living organism that is disturbed in diseases, stress conditions, which can be used as diagnostic sign;

- the correlation coefficient between the level of radiation and temperature of the body part is situated in the limits 0,85…0,87;

- registered experimentally sensitivity of the human body to external EMR ~ 10^{-20} W/Hz. About this level of radiation has wormwood cigarette (moxa) used in Chinese medicine;

- the level radiation of the osseous tissue (bones, teeth) more than the radiation level of the soft tissues at the same temperature, and in fact, the bones are natural generators of microwaves, tanning surrounding cells of living tissues;

- testing the interaction of various bone and dental implants, garments items, jewelry and other materials and comparing it with the human body showed that the most consistent are the physical bodies with radiation close to the human body emission.

SECTION 2 LOW-INTENSITY OPTICAL SIGNALS AND THEIR USE IN MEDICAL EQUIPMENT FOR BIOLOGICAL PURPOSES

Preliminary remarks

The optoelectronics elemental base development, the emergence of semiconductor lasers, light diodes of a wide optical range, high-sensitivity photodiodes and photo-transistors, fiber optic lines and light guides, light-emitting diode and photodiode arrays, ultra-bright miniature light sources and other new optoelectronic devices stimulate their active use and implementation in various branches of science and engineering. High miniaturization of the optoelectronic elemental base facilitates creating compact devices and systems with high functional capabilities.

Optoelectronic technology is widely used in medical equipment, especially in medical, diagnostic and laboratory technologies.

Phototherapy and color therapy, blood photophoresis, optical tomography, photo plethysmography and oximetry, photometric laboratory analyzers-colorimeters, spectrophotometers, fluorimeter, titrometers (for measuring mass or volume of reagents) is an incomplete list of applications of photometric equipment in medical and biological technologies and researches. Using the photometric equipment is mostly connected with formatting measuring and processing low intensity optical signals. Some variants of construction and use of such equipment are offered by the authors in this section.

2.1 Interaction of low-intensity optical signals with biological tissue and device for irradiation of acupuncture points

Light is understood as a electromagnetic radiation flow in range, visible for a human eye and located within 0,4…0,7 nm. The light flux can affect a human body in two ways – through sight or through skin. When light affects the skin one may observe usual optical effects that occur when light passes through a heterogeneous medium as well as a biological response of a human body. Visible light is a regulator of human biorhythms, it affects the skin, subcutaneous cells complex, blood components and a nervous system (mind and emotional state) [20].

Since the skin has an inhomogeneous and multilayer structure, processes of reflection, dispersion and absorption of light fallen on its surface proceed very difficult, taking into account also the diverse influence of light of different wavelengths.

Some part of the light fallen on a skin reflects from its surface. Penetrating into the tissue optical radiation undergoes multiple scattering and absorption by various biological structures. The light in the substance is absorbed by ions, atoms, molecules and their complexes, and less complex biological structures, such as cell nuclei, mitochondria, cells themselves, etc. [21].

Light fluxes of different wavelengths are known to have different depths of penetration and absorption capacity. The depth of optical radiation penetration is determined by both the structure and characteristics of a tissue, and by a wavelength of radiation [22]. The human skin in different ways passes electromagnetic waves of the visible range. In the range of wavelengths greater (400…700 nm) there is a change in the light absorption with wavelength increasing. In this case, a greater penetrating ability is the radiation of the red range (630…700 nm); penetration depth can reach 15…20 mm. For a purple range of waves from 400 to 440 nm, the depth of penetration of optical radiation is about 2…3 mm, and for UV (400…250 nm) it is a fraction of millimeters [21].

With the constant development of science and technology, optoelectronic treatment with the use of low intensity light signals becomes increasingly important. The level of power of these signals can thus reach the unit – tens of milliwatts [20, 22]. Practical medicine puts forward new high requirements for investigating the effects of optical radiation on the human body, in particular, to study the interaction of light at biologically active points (BAP) as one of the sensitive structures of the human body. Unfortunately, the state of the art equipment and known technical solutions are not always fully in line with the problems posed.

The task of modern researchers is to create cheaper, more economical, safe and effective devices for the treatment of the human body. Such devices can be optical devices that emit light in the visible, ultraviolet and infrared ranges.

Under the action of light on the skin are observed, as usual, optical effects that occur when light passes through a heterogeneous medium, and the biological response of the human body. Optical radiation is a regulator of human metabolism and biorhythms through the effects on the skin, the subcutaneous complex of cells, on the components of the blood and the nervous system (on the psyche and emotional state). Since the skin has an inhomogeneous and multilayer structure, the processes of reflection, dispersion and absorption of the incident on its surface of light proceed

very difficult, taking into account also the versatile influence of light of different wavelengths. The nature of the photodiode of light radiation on a biological tissue is determined by its composition and absorption coefficient at the wavelengths of radiation.

Light flux is better to irradiate acupuncture points, because in acupuncture points resistance of the skin and the thickness of the skin itself is less, and their reaction to external irritation is more active. In this case, the light will be much less reflected and penetrate more and more in depth to the human body. It should also be taken into account that acupuncture points are known to be related to individual organs of the human body, which will also be more responsive to such light effects. The equipment for light therapy covers the entire visible range and, depending on the design features, provide external therapy (for the needs of dermatology and cosmetology: fungal skin diseases and eczema, trophic ulcers, etc.), intracavity therapy (in otolaryngology inflammatory diseases, in dentistry – periodontal disease, catarrhal gingivitis, stomatitis, etc., in the urology – prostatitis, cystitis, etc., in proctology – cracking of the rectum, hemorrhoids, anal itching, etc., and in gynecology – diseases of the cervix, appendages, etc.) and percutaneous irradiation of blood, which is used to eliminate the effects of internal diseases, pathology, musculoskeletal system, skin lesions, lesions of the peripheral nervous system, diseases of the genitourinary system, and so on. [22]. The disadvantages of known devices for light therapy include scattering of light flux over the surface of the skin, which reduces the effectiveness of therapeutic procedures.

Figure 2.1 shows the proposed scheme of the device for the irradiation of acupuncture points by two diffused light sources – blue and red [23].

As a G1 generator, a multivibrator is used that generates control pulses for both light sources of different wavelengths (U_{m1} and U_{m2} fig. 2.2). LEDs are located at the same angle of incidence of light flux on human skin $\alpha_1 = \alpha_2 = 20^0$. Thus, two LEDs alternately illuminate the same point on the body, this may be BAP or other sensitive areas. With the attenuator, you can change the amplitude of the signal that comes to the LED, that is, you can change the brightness of the radiation of the LEDs.The power of each LED is less than $E_0 = 10mW$, and the normalized power of radiation per square millimeter:

$$E = \frac{E_0}{S} = \frac{10}{21.2} = 0.47(mW / mm^2). \qquad (2.1)$$

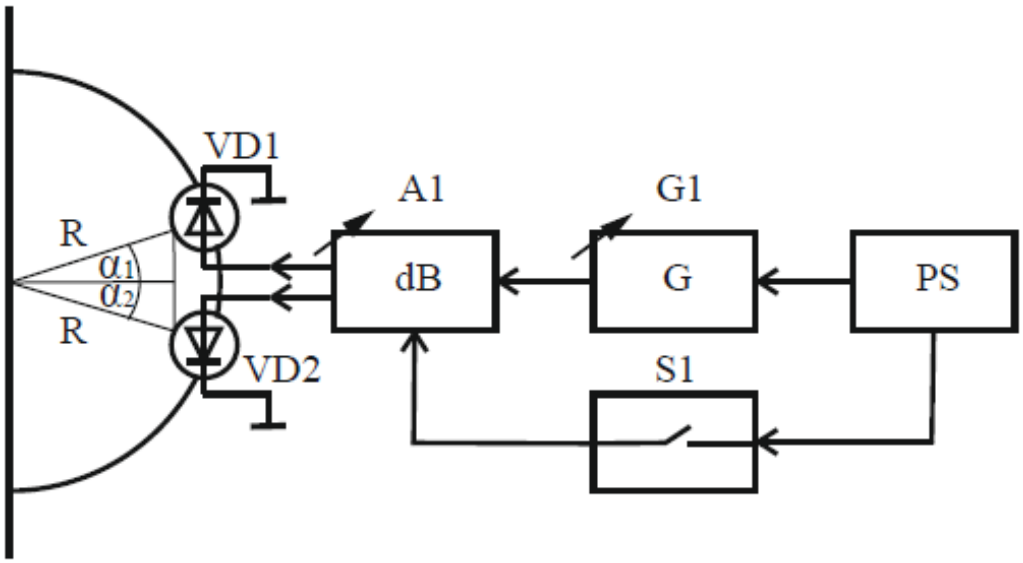

Figure 2.1 – Scheme of device for acupuncture therapy with two LEDs of different wavelengths

Due to different wavelengths, we receive frequency-modulated U_{FM} (Fig. 2.2) pulsed stimulation of the surface layer of the skin (blue and red) and impulse amplitude-modulated U_{IAM} deep (red light).

During the study, a simulation of the attenuation of light radiation from two light diodes aimed at the human skin was carried out.

Figure 2.2 shows the input and output forms of control impulses, on LEDs. As can be seen from the graphic, the LEDs work in turn, at the same time when one LED lights up, the other does not glow, and the switching is performed with the frequency of human rhythms ($f_{\min} = 1/T_{\min}, f_{\max} = 1/T_{\max}$). This property of the alternating irradiation of the acupuncture point provides the possibility of better absorption by the human body of the light flux.

Pulse alternating switching mode (in the experimentally verified frequency range 10…150 Hz) provides the possibility of using LEDs of different wavelengths.

As can be seen from the graph in Fig. 2.2, the depth of light penetration depends on the length of the light wave, and therefore when using LEDs with different wavelengths, it is possible to influence the different depth of the skin.

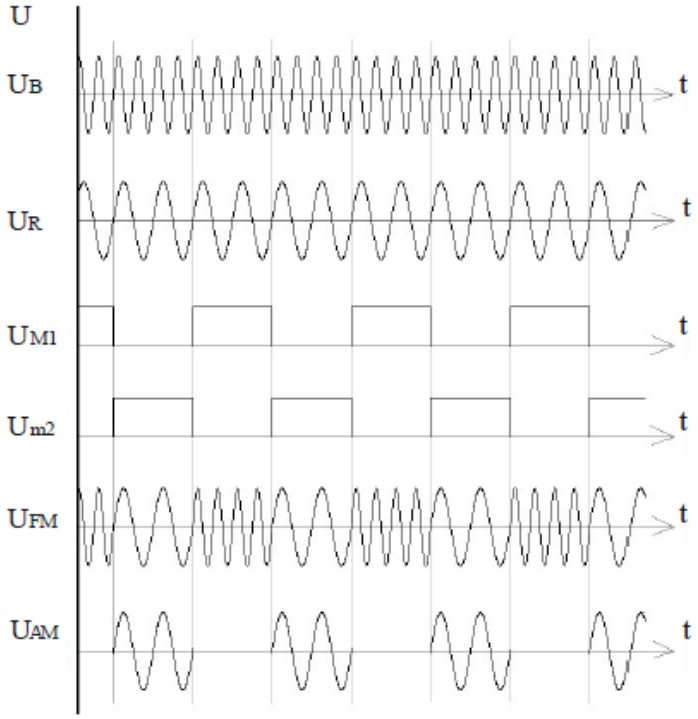

Figure 2.2 – The form of pulse control of each LED

For the example given, when the first pulse is connected, a light stream that has a weak absorption penetrates deep into the skin (red) and is absorbed there, while at the second pulse, the light flux is completely absorbed on the skin surface (blue). The periodic repetition of this process leads to deep modulation of BAT and increases the effectiveness of therapy.

For the proposed scheme, the authors carried out a simulation of the passage and distribution of light streams in biological tissue using the «Mathcad» program. The results of numerical simulation of the attenuation in the bio radiation of a beam of light radiation from each LED in a three-dimensional space is depicted in Fig. 2. 3.

A three-dimensional image provides an opportunity to see the distribution of the intensity of the light flux around and inside the BAP. Fig. 2.3 shows the distribution of the intensity of the light flux in the depth of the fabric, taking into account the distance from the point of falling light to the skin horizontally in the plane x, y (the radius of the light beam changes).

For blue light (Fig. 2.3 a) it is seen that the distribution is narrowed, since blue light is absorbed in the upper layers of the skin and penetrates to a small depth.

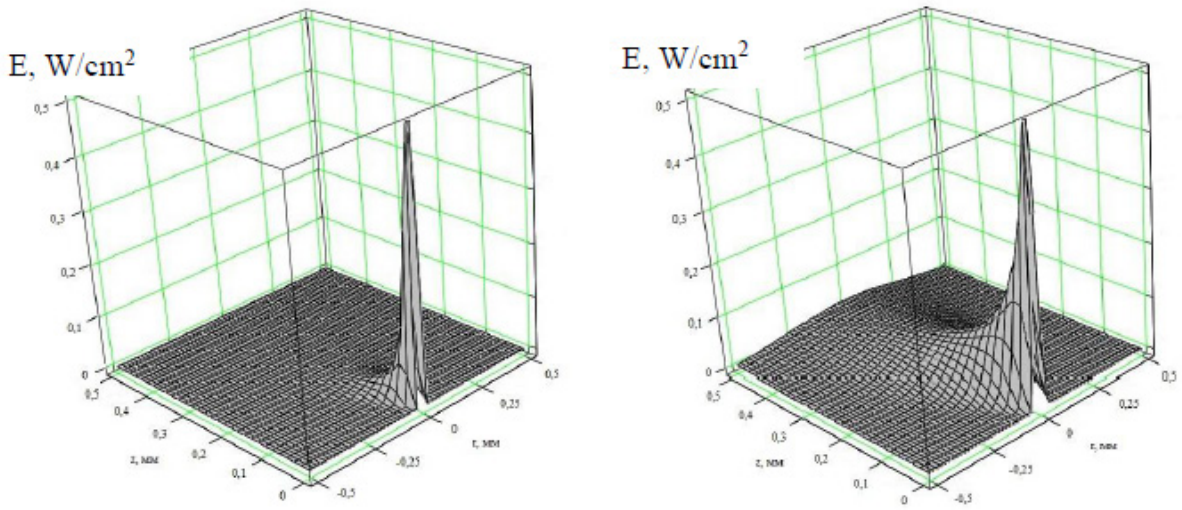

a) *b)*

Figure 2.3 – Attenuation of the light beam at the wavelength: a) 470 nm; b) 660 nm

For red light (Fig. 2.3 b), the deep absorption effect is observed quite clearly. Due to scattering in the skin, the light flux extends within a radius with an increase in penetration depth. From the results of the simulation, it follows that the light flux in the bite due to the refraction and dispersion in the skin takes a drop form.

The greatest effectiveness of the light therapy is manifested in the irradiation of muscle tissue, blood vessels and vascular system capillaries. The grease tissue is less responsive to the effect of light. Therefore, an experimental study of light passing through samples of such tissue is relevant. The scheme of the measuring unit is shown in Fig. 2.4.

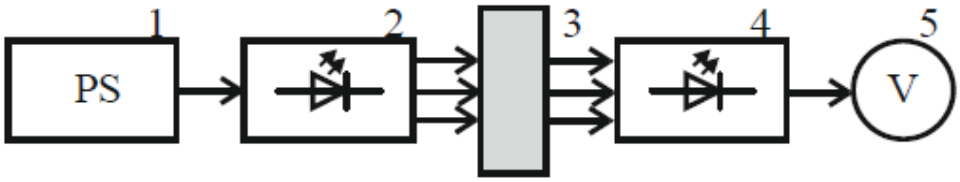

Figure 2.4 – Scheme of conducting the experimental study of light propagation through a sample of bioassay tissue: 1 is a power supply unit; 2 is a light source (light diode); 3 is a sample; 4 is a photodiode; 5 is a voltmeter

The sample's thickness in the experiment varied from 0 to 25 mm. The sample consisted of a skin with 2 mm thickness, and a grease tissue. Passing through the tissue, the light was repeatedly reflected, dissipated, absorbed, therefore the light intensity of at the sample output fell. The

impact of these effects can be reduced due to the concentrated formation of the light beam. Before the measurement, a calibration was performed, at which the same values (maximum) of the output voltage were obtained at the photodetector output when using light streams of red and blue colors. The measurement results are shown in Fig. 2.5.

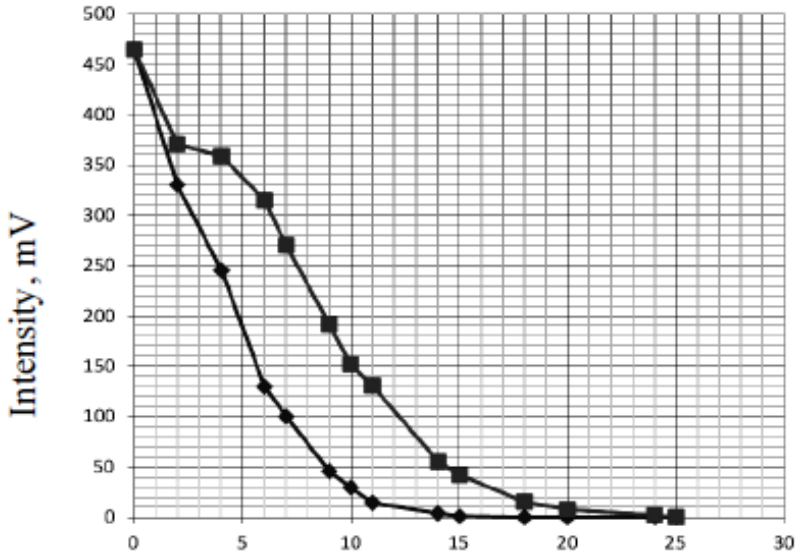

Figure 2.5 – Distribution of the light flux intensity when passing through bio fabric: the upper graph corresponds to red light, the lower graph corresponds to blue light

One may see in Fig. 2.5 that both blue and red light diminishes significantly when the thickness of the sample increases. Moreover, red light penetrates to the depths of 24 mm and blue light penetrates to the depths of 15 mm.

The distribution of intensity for the light passing through the sample has an exponential dependence.

So considering the proposed device can be stated as follows:

- the proposed device for irradiation of acupuncture points using LEDs of different lengths and impulse mode of operation can significantly increase the efficiency of light therapy;

-using a light flux concentrator (reflectometer) provides a point increase in power in the BAT zone and the best absorption of light flux by the human body;

- developed device for laser light therapy has a significant prospect for use in medical technologies of practical medicine.

2.2 Automated system for irradiation of biologically active points of the human body

In connection with the growth of the use of optical signals in practical medicine, new and increased requirements for deepening research on the effects of radiation on the human body, in particular, to the study of the propagation of similar signals at biologically active points (BAP), are put forward. Unfortunately, the current state of the equipment and known technical solutions are not always fully in line with the tasks set, namely:

- the possibility of using a variety of light sources in the range of frequencies in one device;

-a availability of control over the radiation dose and energy absorption of light flux;

-the possibility of modulation of light flux frequencies of human biorhythms;

- the presence of automated control of operating modes of equipment using microprocessor technology and a combination of diagnostic capabilities with feedback, etc.

The analysis of known research results showed the following: the use of light therapy (laser therapy) in the form of low-intensity laser radiation of different wavelengths – infrared, visible and ultraviolet in such areas of medicine as orthopedics and traumatology, dermatology, urology, ophthalmology, dentistry and others [20].

Light therapy has proven itself well in treating trophic ulcers, various erosions and pain points. It is effective to use light therapy for irradiation of biologically active points or human body areas characterized by the presence of a conglomerate of extremely sensitive cells that also have special electrophysical and electromagnetic parameters and characteristics [24].

Important in laser therapy is the choice of the intensity of the irradiation signal, the frequency of radiation and the frequency of modulation of the light flux. Typically, the frequency of the carrier signal is determined by the type of source (laser), and the modulation frequency can vary widely from Hz to 1 kHz. The intensity of radiation from low-energy laser radiation (NELB) used in laser specialist devices, for example, for laser therapy BAP: «Ellada 7», «Orion», «Mustang» and others, according to [25], is 1…30 mW/cm^2.

At the same time, the effectiveness of treatment depends not only on the intensity of the source of radiation, but on the absorbed dose, which is proportional to the biological effect, but virtually no therapeutic devices that provide measurement of the absorbed dose of laser radiation. The dose of the incident signal energy is mainly measured to protect the patient from harmful effects (eg, burns) of laser radiation.

In [26], a device is described in which the control of the absorption intensity is performed by measuring the temperature of the area of the patient being irradiated. The disadvantages of this device include the impossibility of directly assessing the intensity of the absorbed dose and, accordingly, assessing the biological effect and the low accuracy of the measurement due to the double transformation of the intensity of the light flux, first in the heat, and then in the voltage. It should also be noted that the measurement process is low.

The authors [23] proposed a device that allows measuring the absorption dose at a single fixed modulation frequency, but the presence of a selective switching amplifier and the lack of automation elements greatly reduce the capabilities of the device when used in light therapy technologies.

Measurement of the intensity of the absorbed energy is especially important when modulating the light flux with human biorhythm frequencies (F_{mod} up to 200 Hz) and irradiation of biologically active points during reflexotherapy. At different absorption frequencies may vary considerably, resonance absorption is possible and the maximum effect of the treatment will be observed (shown) at these frequencies, and the types of modulation may be varied, but the advantage is given to amplitude modulation [7]. By the results of experimental studies on the influence of electromagnetic signals on human and animal acupuncture points, the author noted [27]:

- the biologically active band of pulse modulation frequencies is in the range of 0,1…100 Hz, with the maximum sensitivity for brain tissue in the range of 6…20 Hz;

- low frequency pulse modulation leads to the appearance of clear biological effects, confirmed experimentally;

- modulation provides the possibility of a significant reduction in the level of electromagnetic signal while maintaining the effectiveness of the effect.

Therefore, the introduction of pulse modulation and automated determination of frequency modulation with maximum absorption is an urgent task for the developers of medical equipment and thus will contribute to the expansion of the possibilities of light therapy.

The purpose of this work is to develop and research an automated system for light therapy by influencing biologically active points or areas of the human body, which would provide control of the direct dose of the energy absorbed by laser radiation, in the range of modulation frequencies. In addition, the possibility of choosing radiation frequencies, with the maximum absorption of light flux in the biologically active area of the patient's skin, was provided, which would increase the effectiveness of treatment.

Thus, as it follows from the analysis, it was found that none of the existing devices for light therapy provides the necessary control of the received dose of laser irradiation. At the same time, the complexity of ensuring the automation of the system for irradiation of biologically active points of the human body is the reason for the inadequate application of photomedical technologies, which raises the problem of applying new technical solutions, transformation algorithms and electronic elements. Therefore, the development of an automated system, with the possibility of low-frequency modulation of light emitting flux and simultaneous measurement of the dose of energy absorbed, is an urgent task, the solution of which the authors present in this paper.

The authors propose automated systems for irradiation of biologically active points or zones of the human body using radar irradiation regime, in which the source of light energy is modulated. In the calibration and diagnostics mode, measurements of the power of light streams are performed, and the radiation dose receiver with switching-modulation signal transduction provides accurate measurement and fixation of the BAP response to laser irradiation.

Further processing of the results of two-stage measurement and construction of the absorption charts BAP, depending on the modulation frequency is carried out using the software of the microcontroller and personal computer.

In the drawing Fig. 2.6 a functional structure diagram of an automated system for irradiation of biologically active points of a human organism is presented [23].

The system comprises connected in series a standalone power supply 1, 2 modulator, attenuator 3 and 4 laser emitter installed in a reflex reflector 5 at an angle α_1. The radiation dose receiver has in its composition a photodiode 6, set at an angle α_2, with $\alpha_1 = \alpha_2$. The output of the photodiode is connected to the input amplifier connected in series 7, 8 quadratic detector, amplifier, frequency modulation 9, the synchronous detector 10 and lowpass filter (LPF) 11. The output of LPF 12 via the ADC input connected to the output of the microcontroller 13.

Two outputs of the microcontroller 13 are connected to the switching inputs of the modulator 2 and synchronous detector 10, one output of the microcontroller 13 is connected to the input of the PC 14, and modulation frequency amplifier 9 made broadband. The proposed system for light therapy works in several stages as follows. Initially, the first stage of a calibration device, which in point A (focus reflector) mirror set, which is a perfect reflector, while the distance is selected according to the plan selected BAP exposure. Since the microcontroller 13 in the «calibration» is held scanning frequency modulation (F) from 0 to 200 Hz with selected step, for example, *ΔF=10 Hz*. Impulse voltage of the microcontroller 13 is fed to the modulator 2, which provides a periodic modulation of the laser emitter voltage 4.

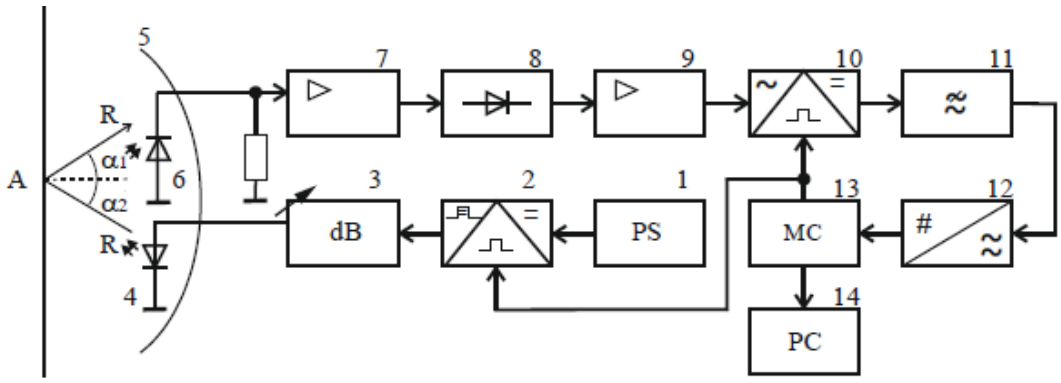

Figure 2.6 – The block diagram of the automated system for irradiation of BAP

The reflected light flux from the mirror in the «calibration» or BAP, in the «diagnostics» perceived photodiode 6 and converted into measuring channel receiver.

As a result, of switching-modulation transformation at the output of the low-pass filter 11 receiver, in the «calibration» mode, for example, we obtain the voltage for one of the frequencies:

$$U_k = S_0 \frac{I_{F1}}{2} R_H \equiv N_{F1}, \qquad (2.2)$$

where I_{F1} – photocurrent in the load chain R_H during the calibration process at the frequency *F1*; S_0 – total conversion factor of the measuring channel of the receiver.

At the same time, the voltage U_k is proportional to the code N_{F1} at the output of the ADC 12. At the output of the receiver, for each step of the modulation frequency band, we obtain a constant voltage proportional to the incident power of the laser 4, which converts the ADC 12 into the code N_i and is fixed to the PC 14.

Its own noise is compensated by the use of switching modulation transformation.

The voltage values for all points (for the selected value, for example, 20 measurements) are converted into codes and fixed in the computer 14 in the form of a reflection graph in the «calibration» mode.

At the second stage, measurements of the absorption dose are performed at the patient's irradiation in the mode of the microcontroller «diagnostics». The skin area (or BAP) is placed in the focus of the reflector 5 at the distance of the mirror. Similarly, a voltage measurement of the reflected signal in the «diagnostics» mode for frequency *F1* and a number of frequencies is performed

$$U_d = S_0 \frac{I'_{F1}}{2} R_H \equiv N'_{F1}. \tag{2.3}$$

Using the computer program 14, the BAP absorption calculation is calculated for each step of the frequency range, which is defined as the difference between equations 2.2 and 2.3, and for the frequency *F1* we obtain

$$U_{BAP} = U_k - U_d = \frac{1}{2} S_0 R_н (I_{F1} - I'_{F1}). \tag{2.4}$$

From equation 2.4 the absorption level of BAP is determined by the difference in the intensity of the signals in the mode of «calibration» and «diagnostics». Equation 2.4 can be written in the form of code differences, for example for frequency F_1

$$N_{BAP} = N_{F1} - N'_{F1}. \tag{2.5}$$

As a result, on the computer screen or on a paper carrier, a summary chart of the absorption capacity of BAP is displayed in the frequency range of human biorhythms.

On Fig. 2.7 one of the distribution options (illustrative) of the output voltage of the automated system is presented in the process of preparation for treatment.

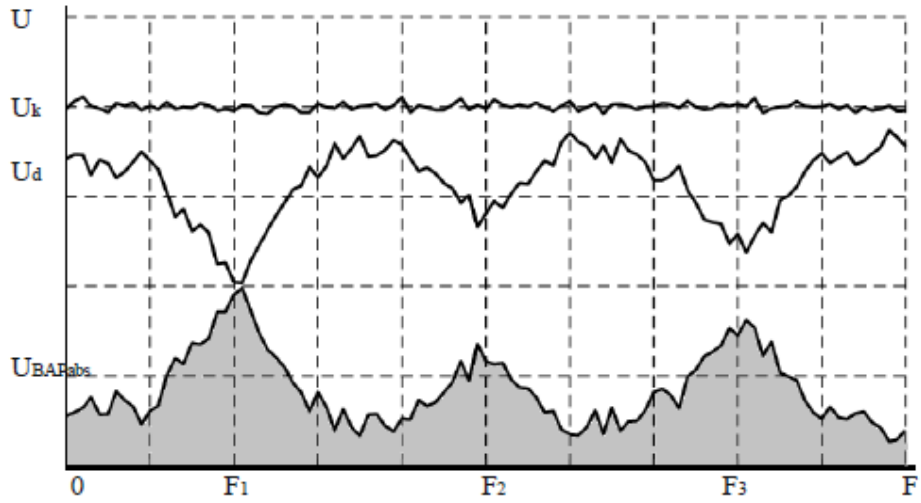

Figure 2.7 – The variant of the distribution of the output voltage of the system in the process of calibration and diagnostics, depending on the frequency of modulation

The upper line characterizes the voltage distribution of the calibration when the modulation frequency changes, usually within the range of 0…200 Hz. This range can be changed (reduced or enlarged), and also extended, for example, within the heart rate, and so on. The voltage formed during reflection from the mirror has the maximum value and uniform distribution. The middle line describes the distribution of the output voltage in the diagnostic mode. The value of this voltage is somewhat less than at the calibration through absorption in the selected range of modulation frequencies. However, this absorption is uneven, at the frequencies F_1, F_2 and F_3, a sharp decrease in the reflected signal characterizing the resonance absorption is observed. The distribution of absorption voltage U_{BAP}, as a difference $U_k - U_d$, represented by the lower line and the shaded area.

Checked absorption across the range of modulating frequencies resonant frequencies but it significantly increased, and in this case, should be preferred especially radiation at a frequency F_1, then F_3, and finally at the frequency F_2. It should be noted that the distribution charts for each treatment case and the selected point (irradiation zone) are original and valid for this patient and the selected BAP.

The frequency of maximum energy absorption luminous flux has an advantage because the devoured biological effect is proportional to dose and enhance the effectiveness of light therapy. Additionally, information about the measurement results of certain BAPs is stored in the computer and can be used to treat the patient in subsequent sessions of light therapy without additional testing. Changes in the readings of the absorption capacity of BAP can also serve as a statistical diagnostic parameter for functional changes in the body of a sick person.

Research results**.** Thus, the proposed automated system for light therapy provides control immediate dose of energy absorption luminous flux in the frequency range of modulation, and provides a choice of frequency modulation with maximum (resonance) absorption irradiation of biologically active points, which certainly increases the efficiency of the treatment process. Also, monitor the level of absorption of the optical radiation during therapeutic procedure allows assessment of biological effect and create predictions about the reaction of the patient to radiation.

The proposed automated system for light simplifies the installation process treatment options and increases their objectivity and provides the ability to determine the level of correlation between the absorption and effectiveness of light therapy. When applying this system it is also possible to use the spaced-apart frequency of light sources in one device. The presence of control over the dose of irradiation and absorption of energy of light flux while also optimizing the light source.

Realization luminous flux modulation frequencies of biorhythms human body through the automated management modes equipment using microprocessor technology and a combination of diagnostic capabilities may be an element of feedback the medical device and the patient.

2.3 Radiometric modulation meter of low intensity of optical radiation

Radiometric methods are increasingly used to measure, control and evaluate the parameters of weak signals in various fields of science and technology – in radio astronomy, physics and plasma physics, medicine and biology [1]. Radiometry is less used in optics, despite its significant potential capabilities. This is mainly due to the complexity of the radiometric apparatus, the microwave range features, lack of serial samples and its significant cost. However, development of theoretical foundations and emergence of new circuit design solutions for the radiometric

equipment construction contribute to its proliferation, including in optical measurements [1, 28].

In [28], schemes for measuring the energy parameters of light streams are considered, in which transformation of the measured stream intensity and the standard electric signal into heat with a subsequent comparison is used. The disadvantage of this device is the lack of measurement sensitivity and accuracy due to the non-identity of channels for heterogeneous physical quantities conversion (light to current or voltage).

Also, the scheme for measuring the intensity of light streams is known [29], based on a comparison of the intensity of light fluxes from two sources: measured and reference ones. The intensities Φ_1 and Φ_2 of these sources are compared with each other using a differential amplifier. The disadvantages of this scheme include the lack of sensitivity, since the amplification is possible only with a direct current, the complexity of ensuring the identity of conversion channels and the low accuracy of measurement, due to different sensitivity of photocells γ_1, γ_2, the amplification factor of the differential amplifier channels K_1, K_2, and, consequently, significant inequalities of the product

$$\Phi_1 \gamma_1 K_1 \neq \Phi_2 \gamma_2 K_2. \tag{2.6}$$

To align the components of equation (2.6) into one of the channels, the absorber is additionally introduced, which also reduces the measurement sensitivity and accuracy.

The patent [30] provides a means of measuring the intensity of light streams using an opto-mechanical modulator and a photosensor. The disadvantages of such a measurer include the complexity of the opto-mechanical converter and the lack of accuracy of measuring the light flux.

A device for photometric measurements [31] is also known as part of the measuring photodiode connected to the resistive load and to the photodetector input. The disadvantages of this device include the lack of sensitivity, which is limited by the presence of a dark photodiode current and impossibility of significant amplification in the photodetector, in selection of both alternating and direct current due to the presence of photodetector self-noises. In addition, the device does not provide the required precision due to the lack of comparison with a well-known normalized base or standard.

Therefore, creating the optical radiation intensity measurer, which would simplify the circuit and increase the sensitivity and accuracy of measuring the light flux parameter, is an urgent task. The authors have proposed a structural diagram of the optical radiation measurer using the modulation transformation of an input signal, having improved metrological characteristics.

Figure 2.8 shows a block diagram of a modulation-type optical radiation intensity meter [32]. The designed device contains the measuring photodiode 1, connected to the first input of the switch 4, the reference photodiode 2 in the light protection shell 3, connected to the second input of the switch 4, which output is connected to the input of the photodetector amplifier 6 and the matched load 5. The amplifier output is connected to the indicator 12 through the serially coupled amplitude detector 7, selective switching amplifier 9, synchronous detector 10 and low-pass filter 11. The switching frequency generator output 8 is connected to the control inputs of the switch 4 and the synchronous detector 10. In addition, the supply voltage is applied to the measuring and reference photodiodes to support them in closed position.

Modulation-type optical radiation intensity meter intensity operates at two positions of the switch 4 in the following way. In the presence of the light flux that falling on the measuring diode 1 in position 1 of the switch 4, the photodiode connects to the circuit, consisting of the photodiode 1 and the coordinated load 5, in which the photocurrent I_1 flows.

This current is identical to the light flux intensity.

$$I_1 \equiv P_1 \tag{2.7}$$

Under the action of the pulses of the generator 8, the switch 4 periodically switches from position 1 to 2 and vice versa.

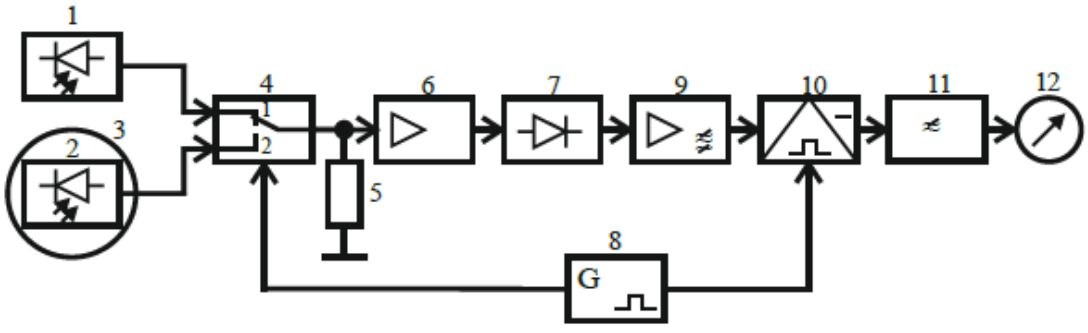

Figure 2.8 – Modulation-type optical radiation intensity meter

At the coordination load 5 in the switch position 1 the voltage is formed

$$U_1 = (I_1 + I_1^{'})R_н = I_\Sigma R_н, \tag{2.8}$$

where $I_1^{'}$ – is a dark current of the measuring photodiode.

When the switch turns to position 2, the dimmed photodiode 2 connects to the load 5 and the voltage proportional to the dark current I^r of the reference photodiode appears

$$U_2 = I_2^{'}R_н, \tag{2.9}$$

As result of feeding the voltage (2.8) and (2.9) on the input of the amplifier 6, the voltages appears at its output in the switching period

$$U_3 = K_1 I_\Sigma R_н = K_1\left(U_1 + U_n\right), \tag{2.10}$$

$$U_4 = K_1\left(U_2 + U_n\right), \tag{2.11}$$

where K_1 – is a transmission factor of the amplifier 6; U_n – is a voltage of the measuring stage noises, calculated in reference to the amplifier's input 6.

Voltages 2.10 and 2.11 are fed to the amplitude detector 7. The switch 4 is controlled by the rectangular voltage of the generator 8, therefore an alternating component of the switching frequency Ω and the noise voltage of the measuring channel are presented on the output of the amplitude detector 7 during the switching period.

As a result of work of the switch 4 operating continuously, the selective amplifier 9 separates a variable component with an envelope of the form:

$$U_5 = K_1 K_2 S_1 \frac{(U_3 - U_4)}{2} sign \sin \Omega t, \tag{2.12}$$

where $sign \sin \Omega t$ is a periodic process sign envelope; S_1 is a steepness of the amplitude detector 7 transformation; K_2 – is a gain factor of the selective amplifier 9.

The voltage is fed (2.12) to the commutator detector 10, and on its output the low-pass filter 11 separates a direct component, proportional to the light flux intensity.

$$U_6 = K_1 K_2 K_3 S_1 S_2 \frac{(U_3 - U_4)}{2} \tag{2.13}$$

where K_3 − is a transmission factor of the low-pass filter 11; S_2 − is a steepness of the commutator detector 10 transformation.

Considering equation 2.8 and 2.9, we get

$$U_6 = K_1 K_2 K_3 S_1 S_2 \frac{[(I_1 + I_1^{'})R_н + U_n - I_2^{'} R_н - U_n]}{2} \qquad (2.14)$$

Having simplified the equation 2.14 and taking into account that the voltage U_6 is identical to the light flux intensity Φ_1 we may write

$$P_1 = S_0 \frac{(I_1 + \Delta I)}{2} R_н, \qquad (2.15)$$

where $S_0 = K_1 K_2 S_1 S_2$ is a total conversion ratio of the measuring channel, $\Delta I = I_1^{'} - I_2^{'}$ – is a noise differences in the dark currents of photodiodes.

As follows from the obtained equation, light flux intensity is proportional to the sum of the measuring diode output current and the remain of the difference in dark currents of the measuring and reference diodes.

Thus, as one may see from (2.15), the photodetector self-noise does not affect the measurement result, and also the dark current effect for the photodiodes decreases almost to zero if they are chosen equal by this parameter, it increases significantly the sensitivity and accuracy of the optical radiation intensity measurement. In addition, the scheme and design of the photometric measurer is greatly simplified due to exclusion of the optical modulator and the introduction of the electronic one.

2.4 Photometric spectrum analyzer of the absorption capacity of poorly transparent biomaterials

Measurement of the optic irradiation parameters, first of all the intensity of the light flux passing through the biological tissue or other slightly transparent (cloudy) materials and environments is actual task due to the development of the new sources of the light with different wavelengths and their usage in different fields of human activity [28, 32].

Effectiveness of the laser and diode sources of the tanning signals used in the technologies of the practice medicine, food industry, in laboratory studies of the various solutions in medicine, chemistry is closely linked to the definition of the penetrating power of light fluxes into objects of study.

It’s important to provide the high sensitivity and measurement accuracy of the output parameters of the light fluxes passing through the studied materials – depth of penetration, coefficient of attenuation or absorption. Indicated in the [33] methods and devices do not provide the necessary sensitivity and measurement accuracy of the light fluxes parameters.

Photometric spectrum analyzers considered in [34,36] provide better metrological data, but the presence of the special optic means (photometric ball and light-measuring bench, the system of the protection from the extraneous light sources etc.) so as complicated optical mechanical communications and use the mechanical modulators of the light flux make the process of the measurement more complicated at all. Meanwhile, the necessary sensitivity and accuracy of measurement parameters of weak optical signals of different wavelengths is not provided.

Described at [36] photometer used modulation (electronic) method of converting the intensity of the light flux, somewhat simplifies and enhances the sensitivity of the measurement parameters of flux, but it lacks the ability to assess absorbance capacity of the materials and liquids, the penetration depth of the light flux through biological tissues and determine the attenuation coefficient. At the same time, measurement and assessment of these parameters can be used to predict, for example, the effectiveness of treatment with light therapy.

The presence of the discussed disadvantages of the known photometers and photometric spectrum analyzers more or less hinder their practical use. The design of the simple construction but high metrological characteristics optic spectrum absorbance analyzer of slightly transparent materials and liquids would help its more widespread use in various fields of science and technology. Especially important parameter of measuring devices is increased sensitivity when light flux passing through slightly transparent analyzing material. This allows more deeply evaluate the interaction of light fluxes and biomaterials samples, for example, in biology and medicine, and to predict their impact on the level of the whole organism. Thus, considering the identified deficiencies of these devices for measurement light fluxes – the complexity, lack of sensitivity and precision, the aim of this study is to develop photometric spectrum analyzer, in which, along with the simplification of the scheme and increasing sensitivity and measurement accuracy, the score of penetration depth of light flux into biological or other slightly transparent material, the

determination of the attenuation coefficient and the spectrogram construction on the analysis of two signals, separated by wavelength light sources, is ensured.

One of the directions to increase the sensitivity and accuracy of the measurement devices is use the modulating method of the output signals transformation [1, 39]. Realization of this method use provides significant reducing of the proper noises of the transformation signal path. It fully concerns to optical measurements of the slightly transparent substances and materials properties.

Figure 2.9 shows a functional diagram to realize the measurement of the absorbance ability of the slightly transparent materials with use of the modulating transformation of the optic signal [40].

Explication: 1- microcontroller, whose outputs are connected under the control inputs of the modulator 2, key 3 and synchronous detector 11; 4, 5- emitting diodes, which are connected to the inputs outputs key 3, and outputs irradiate object of study 6; 7- moving carriage with a photocell 8, its outputs connected to an amplifier 9 and through selective switching frequency filter 10 connected with the alarm input synchronous detector 11.

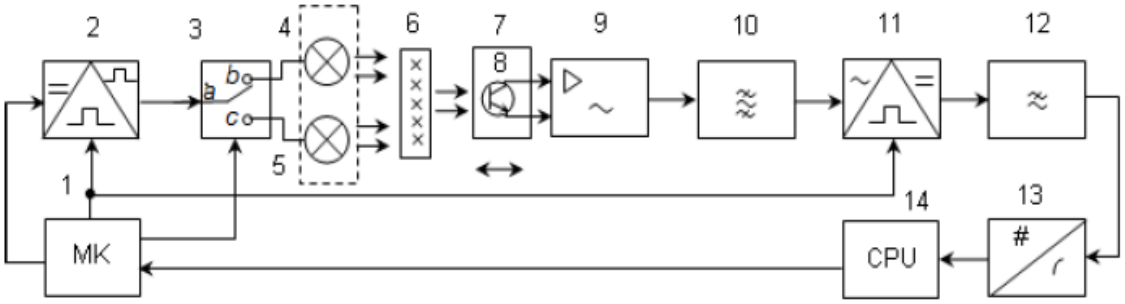

Figure 2.9 – Functional diagram of the photometric absorbance spectrum analyzer of the slightly transparent biomaterials

The output of the synchronous detector 11 through a low frequencies filter 12 and analog-to-digital converter 13 is connected to the computer input 14 and the output of a computer connected to the input of the microcontroller.

Photometric measuring device of the materials absorbance properties works in several stages as follows. Under the program, which is installed in the computer 14, the device calibration is conducted in the beginning of the work. For this the work signal mode is fed from the computer 14 to microcontroller 1 and on its outputs are set: on the first output – voltage of

the emitting diodes, on the second – pulse voltage switching frequency Ω; on the third entry is set the key position, such as *ab* and to the pulsed power is connected, for example, light diode 4 with a wavelength λ_1. The carriage 7 with photocell 8 is installed at a distance corresponding to the thickness of the studying material. Under the influence of a switching rectangular signal type (2.16) by modulator 2 is held periodically (with a frequency Ω) power supply for light diode 4:

$$U_1(t) = F_1(t) + F_2(t), \qquad (2.16)$$

where $F_1(t) = \left[\frac{1}{2} + \frac{2}{\pi}\sum_{n=1}^{\infty}\frac{\sin(2n-1)\Omega t}{2n-1}\right]$; and $F_2(t) = \left[\frac{1}{2} - \frac{2}{\pi}\sum_{n=1}^{\infty}\frac{\sin(2n-1)\Omega t}{2n-1}\right]$,

Accordingly, the alternate light flux emission with power Φ_1 is carried. It should be noted that the power supply to the light emitting diodes is provided by feeding the modulator with the positive half-wave modulating signal $F_1(t)$. On the output of the photocell 8, by the periodical work of the modulator 2, the pulse voltage, which amplitude is proportional to the power of light flux $U_{P_1} \equiv P_1$, is formed.

Figure 2.10 shows a block conversion spectrum analyzer.

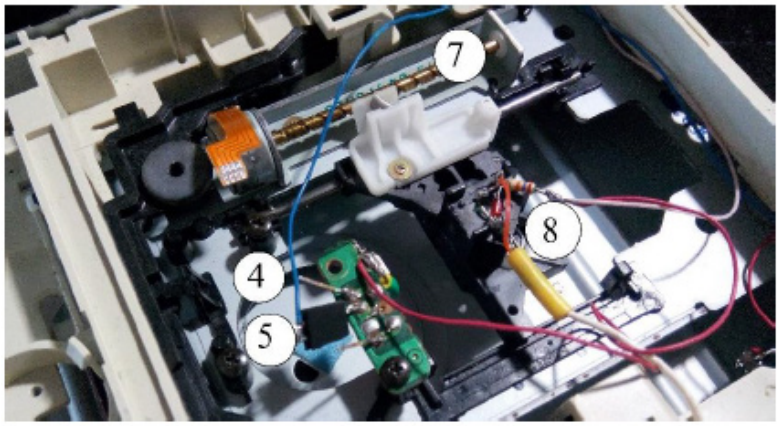

Figure 2.10 – The design of optoelectronic transducer and measure channel spectrum analyzer (designation according to fig.2.9)

The received pulse voltage is increased to the desired value with the amplifier 9 and, as a result, on the output of the frequency selective filter 10 the switching signal is released

$$U_2(t) = U_{P_1} S_1 K_1 K_2 F_1(t) = U_{P_1} S_1 K_1 K_2 sign \sin \Omega t, \qquad (2.17)$$

where S_1 – slope conversion of the photocell 8; K_2 – transmission coefficient of the selective filter 10; $F_1(t) = sign \sin \Omega t$ – signum function (bypass of the periodic process sign).

Power (2.17) is fed to the signal input of the synchronous detector 11, on its managing input the rectangular reference voltage of the same frequency $F_0(t)$ is fed. As a result of multiplying the measuring U_2 *(t)* and reference signals U_1 *(t),* for each of the half switching period, taking into account the properties of switching functions, that $F_0(t) = F_1(t)$, and the [$F_1(t)$]$^2 = F_1(t)$, receive signal

$$U_3(t) = U_{P_1} U_0 S_1 S_2 K_1 K_2 F_1(t) = U_{P_1} U_0 K_1 K_2 S_1 S_2 \left[\frac{1}{2} + \frac{2}{\pi} \sum_{n=1}^{\infty} \frac{\sin(2n-1)\Omega t}{2n-1} \right], \tag{2.18}$$

where S_2 – slope conversion of the synchronous detector, U_0 – reference voltage amplitude.

On the output of the low frequencies filter 12 the constant component of voltage equation (2.18) is released, and the variable is delayed

$$U_4 = \frac{U_{P_1} U_0}{2} S_1 S_2 K_1 K_2 K_3 = \frac{U_{P_1} U_0}{2} K_\Sigma, \tag{2.19}$$

where K_3 – transfer coefficient of the low frequencies filter, and $K_\Sigma = S_1 S_2 K_1 K_2 K_3$.

Power (2.19) turns by ADC in the calibration code N_1 for light diode 4 and computer 14 remember it.

A similar transformation algorithm implemented with the second light diode 5 signal, with the wavelength λ_2, at the key position *ac* to receive the code value N_2.

After calibration completion they place studied material and carry out the same algorithm for measuring the level of the sample output signal receiving the code for light diode 4 – N_3, and the light diode 5 – N_4.

Correlation

$$\alpha_1 = N_3 / N_1 \tag{2.20}$$

characterizes the ability of the material to absorb the light flux from emitting diode 4 with a wavelength λ_1, and

$$\alpha_2 = N_4 / N_2 \ , \tag{2.21}$$

the same data for light diode 5 with a wavelength λ_2.

Observed values defined parameters, for example, of separated light diodes (λ_1=400 nm – purple and λ_2=700 nm – red) allow to construct with computer program predicted diagram of the absorption of other wavelengths light fluxes.

Value for the first variant of radiation

$$\beta_1 = (N_1 - N_3) / d_1 \qquad (2.22)$$

provides a definition of the linear absorption values, which allow to count the weakening for similar material of other thickness d_x without additional measurements.

The use of the optical spectrum analyzer is closely related to the definition of light streams' ability to penetrate into the objects of research and measurement of the low intensity signal, whose attenuation can be determined by the Bouguer-Lambert-Beer formula. The intensity of the light flux passing through the material at a different thickness of the material is determined by the expression:

$$J_2 = J_1^{-\alpha d} \ , \qquad (2.23)$$

where J_1, J_2 – is a light flux intensity at the material input and output respectively; α –is an absorbtion coefficient for the material; d – is a density of the material.

In this case it is important to provide a high sensitivity and accuracy of measuring initial parameters of light streams with low intensity passing through the investigated materials, these parameters are depth of penetration, coefficient of weakening or absorption. The main element influencing these parameters is an optoelectronic converter (OEC) of the spectrum analyzer, its simplified scheme is shown in Fig. 2.11.

The optoelectronic converter includes: power supply 1, modulator 2, light source 3, photodetector with a conversion channel and an indicator 4, generator of modulating frequency 5.

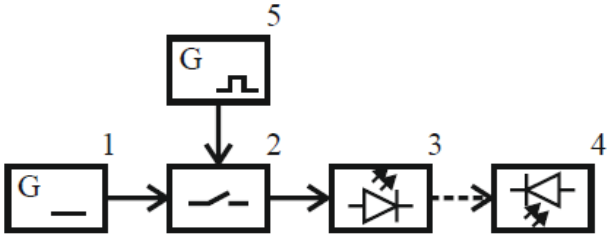

Figure 2.11 – Simplified structure diagram of OEC

The light source 3 and the photocell 4 provide a proportional transformation of the light flux into electrical signals.

The main components of the optoelectronic converter are the light source, which uses the led matrix PLCC-6 with embedded emitters of blue (λ = 460 nm), green (λ = 520 nm) and red light (λ = 630 nm), and a transistor photocell of BPX 43–5 type for the wavelength range from 450 nm to 1100 nm.

Taking into account the importance of the OEC and its influence on the spectrum analyzer output parameters and the ability to convert low-intensity signals under action of noise, the authors have researched the influence of switching frequency on the conversion factor and sensitivity of the developed block, the result is presented in Fig. 2.12.

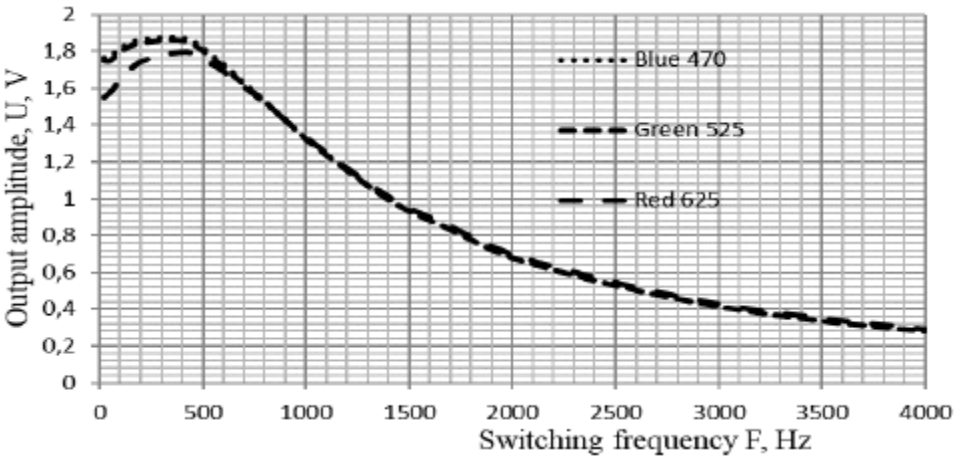

Figure 2.12 – Dependence of the OEC output amplitude on the switching frequency

The light flux modulation was performed with a pulsed interruption of the light diode supply at frequencies from 20 Hz to 2.0 kHz on each of the light sources. In this case, the output voltage of the optoelectronic converter in the range of modulation frequencies was measured. One may see in Fig 2.12 , that the level of output signal practically does not depend on the type of a switched light.

The maximum transmission coefficient of the optoelectronic converter and, accordingly, the highest sensitivity of the spectroanalyzer is in the range of switching frequencies from 100 Hz to 500 Hz. The switching frequency increase from 500 Hz to 2.0 kHz results in a transmission factor reduction for almost an order. Thus, implementing the optical radiometer as a spectrum analyzer and providing the relevant sensitivity are tied with necessity to take into account the optoelectronic converter parameters.

The developed highly sensitive modulating optical spectroanalyzer has allowed to conduct a series of experimental researches of some poorly transparent biomaterials.

The samples of biomaterials have divided into three groups:

- the first group included samples of animal origin – fatty tissue, fatty tissue with skin, as well as muscle tissue, living tissue of a person (point Hegu);

- the second group included biological samples of plants contacting with solar radiation during the growth process;

- the third group includes samples of vegetables, having no contact with sunrays during the growth process.

There were several options for installation of the samples with respect to the probe light flux during the research Fig. 2.13.

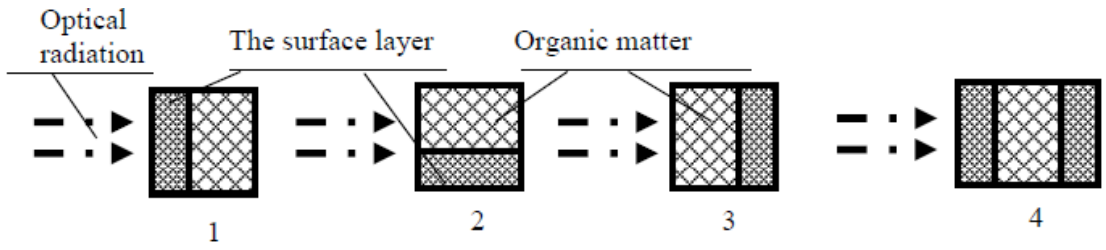

Figure 2.13 – Options of the sample installation

In the figure 1 is an irradiation of the sample from the surface layer (peel, skin), 2 is an irradiation of the sample from the side (without peel), 3 is an irradiation of the sample in the opposite direction with respect to position 1, 4 is the light stream passing through the surface layer, organic matter and another surface layer.

The first to be considered is the light streams passing through the living soft tissue of a human body (point Hegu) and samples of animal origin. Fig. 2.14a illustrates the spectrogram of the light attenuation coefficient in the sample of the human body living soft tissue. As shown in Fig. 2.14a, in a living tissue, the red light flux attenuation is about 1dB/mm, and the attenuation of the green and blue light fluxes of is about 5dB/mm. Fig. 2.14 b shows the spectrogram of the light attenuation distribution in samples of animal origin.

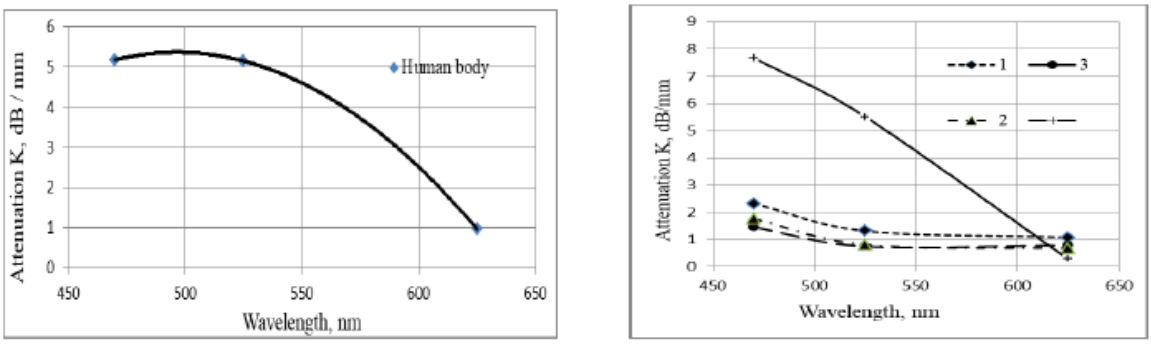

a b

Figure 2.14 – Spectrograms of the light streams passing through the biological tissue samples

Lines 1,2,3 in Fig. 2.14b characterize light passing through a fat tissue, as described above, and a solid line is an attenuation distribution in a muscle tissue, it coincides with the graph of Fig. 2.14a in shape and in attenuation level.

The light flux attenuation in the fatty tissue is within the range of 1…2,2 dB at different variants of irradiation. Light streams free penetrating through the fatty tissue is a positive factor to perform the light therapy for patients with excessive weight.

Fig. 2.15 shows the spectrogram of the light attenuation distribution in samples of vegetable origin, aloe and beet.

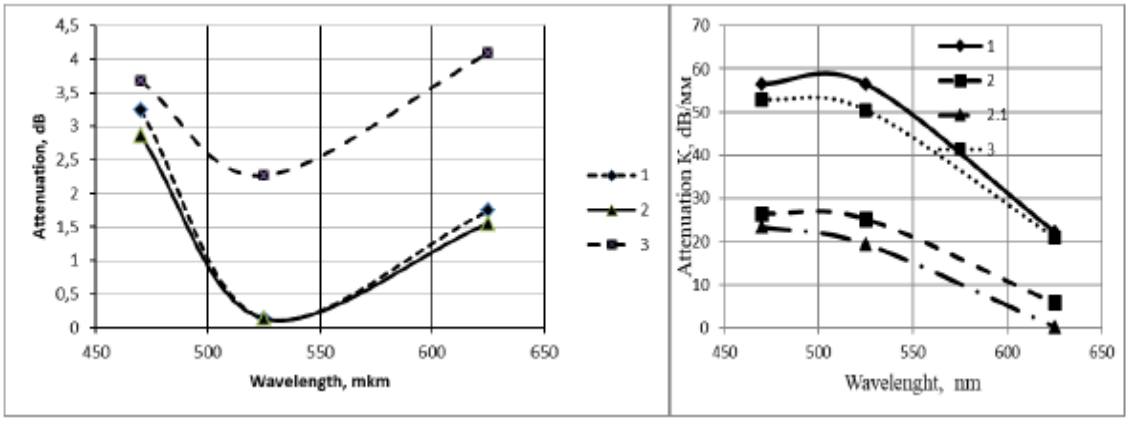

а б

Figure 2.15 – Spectrograms showing distribution of the light streams passing in tissue samples of aloe (a) and beet (b)

The method of studying the aloe samples is shown in Fig. 2.15 a, where 1, 2 is the radiation through the surface layer and a soft tissue and vice versa, 3 is the radiation through a leaf. From the spectrograms charts one may see that the green light flux has the least damping attenuation. The spectrogram of the light streams passing into a kalanchue leaf has an analogous form and similar absorption coefficients throughout the wavelength range, it is a peculiarity of green leaves. Method of studying the beet samples is shown in Fig. 2.15 b, where 1 is the radiation through the surface layer and a soft cloth of dark color, 3 is the radiation through the surface layer and a soft cloth of light color. The presence of a dense red pigment in the beet tissue figure line 2 results in a sharp decay of light streams, and the illumination of the tissue figure line 2.1 results in its significant reduction. The form of the spectrogram in Fig. 2.15 b coincides with the graph in Fig. 2.15a, that is explained by the presence of hemoglobin in the blood. This effect may serve for constructing a non-invasive method for diagnosing hemoglobin levels in a human body.

Considered possibilities greatly simplify the measurement process. The use of the modulating transformation of the light flux provides increase in sensitivity almost an order and provides increase the measurement accuracy, because such transformation compensates the intrinsic noise level and noise of the measurement channel. As the light source semiconductor matrix is used. It provides accommodation of two crystals at one point of light diodes with the most spaced wavelengths, allowing them to be placed on the same axis with photocell and excludes collateral scattering of the light flux.

2.5 Optoelectronic system with automated determination of maximum absorption frequencies

Optoelectronic systems are widely used in various fields of science and technology, including the transfer of large volumes of information signals in telecommunication equipment, military affairs, technological processes, biology and medicine.

Both powerful and weak signals are used in such systems, for example, in the devices for light therapy with low-intensity optical signals in physiotherapy technologies. Therapy is based on the influence of light energy of the corresponding intensity (usually low intensity) and wavelength on certain areas of the patient's body [22]. Usually it may be active zones or biologically active points of the human body

The choice of the modulation frequency of the light flux, which according to [27] is within the range of 0.1…100 Hz, is an important element in the technologies of light therapy. The specified frequency range of the light flux modulation is biologically active, with a maximum sensitivity for brain in the interval of 6…20 Hz. In addition, impulsed modulation leads to clear biological effects appearance which are confirmed experimentally. This allows to reduce the level of electromagnetic influence while its effectiveness is preserved.

The maximum effect of light therapy arises from the largest (or resonance) absorption of the energy of the illuminating signal. At the same time, devices for light therapy, in which the assessment of the absorption capacity of the irradiated area of the patient's body, depending on the frequency of modulation of the light f practically are absent. For example, in widely known apparatus for light therapy, which are currently used in the physiotherapy – Mustang, MILTA-F-01, Orion, impulsed modulation

modes with fixed frequency (Orion -1500 Hz), or discrete change of these frequencies are used (MILTA-F-01 from 0.5 to 1500Hz, 5 frequencies), or with a smooth selection of frequencies in the range (Mustang from 0.5 to 3000 Hz) [25]. However, in the considered devices, there is no objective choice of modulation frequency to ensure the high efficiency of light procedure and this parameter is not related to the power of irradiation and absorption in no way. In fact, the choice of parameters of light therapy depends on the qualifications of the doctor and his, accumulated in the process of work, practical experience.

In [13, 32] the variants of continuous irradiation of the selected body region at the fixed frequency without determining the level of absorption are considered. The main photo biological methods of the optical radiation of the ultraviolet wavelength range (250…400 nm) influence, which are used to irradiate the affected skin were analyzed by the authors

Whereas the ultraviolet range, whose signals cause a mostly superficial effect, is considered, the task of the work was to achieve an even distribution of power, which was achieved through the use of LED matrices. A similar solution is used in the range of visible light in matrices and devices «Barva» Korobova [25], using light streams with the other wavelengths that penetrate more deeply into the biological tissue. Despite the use of modulation in these devices, the choice of frequency is performed empirically, which reduces the effectiveness of light therapy and is one of the major shortcomings of such equipment.

The authors of works [35, 37] developed devices for light therapy, which have expanded functionality and allow to determinate the absorption at the therapeutic frequency. Structural construction of the schemes of the considered devices is performed with switching modulation transformation of probing and receiving signals. The need for selective allocation of the switching frequency signal in the conversion channels limits such a measurement with a band of sample elements.

The indicated disadvantage significantly affects the possibilities and effectiveness of these schemes of light therapy.

The most successful options for improving the effectiveness of light therapy with the use of modulation capabilities are presented in the authors' work [35, 38]. The developed automated systems allow to measure the level of absorption of the irradiated body area at the switching frequency (modulation) of the light flux, but is rather complex and expensive, which is a disadvantage of these technical solutions.

The purpose of the proposed work is to create optoelectronic microprocessor system for light therapy, which in the automated mode provides the possibility of modulation frequencies range scanning, whith simultaneous determination of the optimal (with maximum absorption) frequencies for light therapy in the selected area of the patient's skin. The presence of the optoelectronic converter and the developed software reduces its cost and greatly simplifies its use.

The automated system for light therapy, which provides the ability to automatically reconfigurate the frequency of modulation in the range close to the frequencies of human biorhythms with a synchronous measurement of the level of absorbed light flux by the biological object is presented in Fig. 2.16. The scheme has in its composition elements of generation of light flux, its modulation, an optoelectronic transformer consisting of two lenses, measuring sensor (photocell) and a control unit (microcontroller).

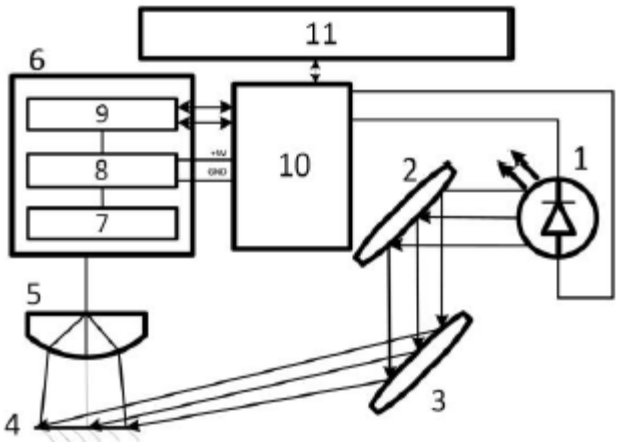

Figure 2.16 – The block diagram of the automated system for light therapy

The explication to the figure: 1 is a red LED (wavelength ~ 660 nm), because it provides penetration into human body tissues to a depth of about 8 – 10 mm; 2, 3 – a system of focusing lenses; 4 – a biological object; 5 – collecting lens, 6 – optical sensor, 10 – microcontroller, 11 – PC.

In turn, the optical sensor 6 contains of the three main blocks: Image Processor 7, Image Control System 7, Voltage Regulator and Power Control 8 and Data Transer System Serial Port 9.

The model of the developed optoelectronic converter of the automated system consisting of the optical sensor and microcontroller is presented in fig. 2.17.

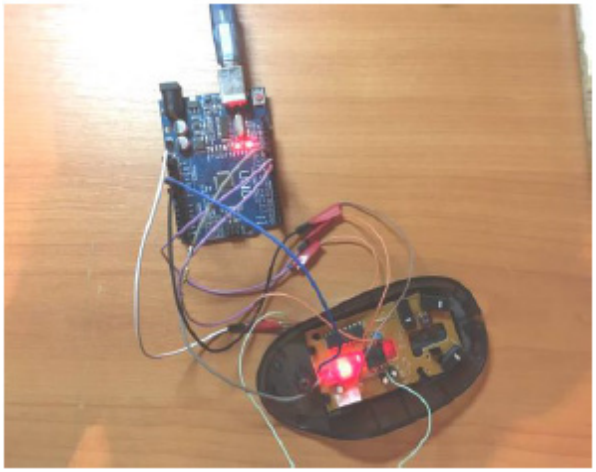

Figure 2.17 – The model of optoelectronic converter consisted of optical sensor and microcontroller

The work of the system and the processes coming about in this case, can be described as follows. The selected light radiation can be represented as a monochrome signal, which is described by the expression:

$$I_0(t) = I_0 \sin(\omega_0 t + \varphi_0), \tag{2.24}$$

where I_0 – optical signal amplitude, ω – signal frequency.

If there is an own noise in the automated system, the full signal at the output of the channel of the transformation will be presented in the following formula:

$$I_1(t) = I_0(t) + I_N(t), \tag{2.25}$$

where $I_0(t)$ – useful signal, $I_N(t)$ – own noises at the system input.

For the signals formation in the automated system, the switching-modulation method is used [63]. The light flux represented by the formula (2.24, 2.25) is modulated (switched) by a low frequency signal (meander) with human biorhythm frequencies in the range of 1…100 Hz by changing the supply voltage of the red light of the diode 1 and using a sufficiently accessible microcontroller Arduino Uno 10.

Switching rectangular voltage (signal switching function) $F_0(t)$ is written as:

$$F_0(t) = F_1(t) + F_2(t), \tag{2.26}$$

where $F_1(t)$ – the state of the signal «logical unit» – the switching on the optical signal, $F_2(t)$ — the level of the «logical zero» when the signal is off.

The compounding parts of the formula (2.26) can be written in the form:

$$F_1(t) = \frac{1}{2} + \frac{2}{\pi}\sum_{n=1}^{\infty}\frac{\sin(2n-1)\Omega t}{2n-1}, \qquad 2.27)$$

$$F_2(t) = \frac{1}{2} - \frac{2}{\pi}\sum_{n=1}^{\infty}\frac{\sin(2n-1)\Omega t}{2n-1}, \qquad (2.28)$$

where Ω – frequency of switching (modulation) of signals.

Thus, during the switching period (at $F_1(t)$ and $F_2(t)$), two signals alternately act, which occupy exactly the halves of the period of the modulation frequency:

$$\begin{cases} I_1(t) = I_0(t) + I_N(t), \\ I_2(t) = I_N(t). \end{cases}.$$

Modulated light flux, for the switching period, can be represented as follows:

$$I(t) = \left[I_0(t) + I_N(t)\right]F_1 + I_N(t)F_2. \qquad (2.29)$$

Substituting the value of the commuting function (2.27, 2.28) in equation (2.29), we obtain the equation of the total signal:

$$I(t) = I_0\sin(\omega t + \varphi)\left(\frac{1}{2} + \frac{2}{\pi}\sum_{n=1}^{\infty}\frac{\sin(2n-1)\Omega t}{2n-1}\right) + I_N(t)F_1 + I_N(t)F_2. \qquad (2.30)$$

Taking into account that we neglect the noise that arise in the zero state of the commuting function under F_2, and which almost do not affect the original image and equating $\varphi = 0$, we receive a useful signal in the form:

$$I(t) = \frac{1}{2}I_0\sin\omega t + \frac{2I_0}{\pi}\sum_{n=1}^{\infty}\frac{\sin(2n-1)\Omega t}{2n-1}\sin\omega t. \qquad (2.31)$$

The output spectrum of the signal of the type «meander» has in its composition only odd harmonics. The largest intensity of the modulated optical signal is determined mainly by the influence of the first and third harmonics. Considering the written above, equation (2.31) can be represented in the form:

$$I(t) = \frac{1}{2}I_0\sin\omega t + \frac{2I_0}{\pi}\left(\sin\Omega t\sin\omega t + \frac{\sin 5\Omega t\sin\omega t}{5}\right). \qquad (2.32)$$

Having expanded and simplified formula (2.32), we obtain a modulated optical signal that irradiates a definite area of the patient's body:

$$I(t) = 0,5I_0 \sin \omega t + 0,32I_0[\cos(\Omega + \omega)t - \cos(\Omega - \omega)t] + \\ +0,06I_0[\cos(5\Omega + \omega)t - \cos(5\Omega - \omega)t] \quad . \quad (2.33)$$

As can be seen from the result of the calculation of formula 2.33, in the spectrum of the light flux in addition to the fundamental harmonic, both the upper and lower side components of the modulation frequencies are present, however, the intensity of these components is much smaller. The modulated light flux 2.33 through the system of focusing lenses 2, 3 directs and irradiates a specific area or BAP of the patient's skin 4. The part of the light flux is absorbed by the bioobject, and the part of it is reflected.

The reflected light with the help of a collecting lens 5 enters the optical sensor 6. In turn, the optical sensor 6 with a high frequency (kHz) scans and shoots the area of the body surface that is irradiated and independently process them, since it contains three main blocks: the image processing and image processing system Image Processor 7, the power control system Voltage Regulator and Power Control 8 and data transfer system Serial Port 9.

Based on the analysis of the received sequential images (representing a square matrix of pixels of different brightness in grey gradations (from 0 – «*complete black*» till 63 – «*complete white*») the integrated DSP processor 7 calculates the resulting values, that is, the brightness value of the entire matrix at certain points in time.

As an optical sensor, the ADNS-2610 chip, with a resolution of up to 400 cpi (counts per inch), and an image capture rate of 1500 frames per second is used.

Although the sensor «see» the black and white image, the sensitivity of the matrix depends on the wavelength, so the LED with the largest wavelength (660 nm) was selected. The sensor summarizes the brightness of all 324 pixels in the current frame. The calculation of the average brightness value is made according to the formula:

$$A = X \times 128 / 324 , \quad (2.34)$$

where: A – the average brightness of the pixels, X – the current value of the register (multiplied by 128 because of the current shift of the number relative to the register on 2^7).

Following the development of the scheme and layout of the device, experimental studies have been conducted with various biological objects *in vivo*. As a biological object were selected, the reverse side of the palm – the results on Fig 2.18, soft tissue of the hand – the results on Fig. 2.19, and soft tissue of the hip – the results on Fig. 2.20. The research was conducted at a frequency change of 1 to 100 Hz, which corresponds to the most biological rhythms of the human body.

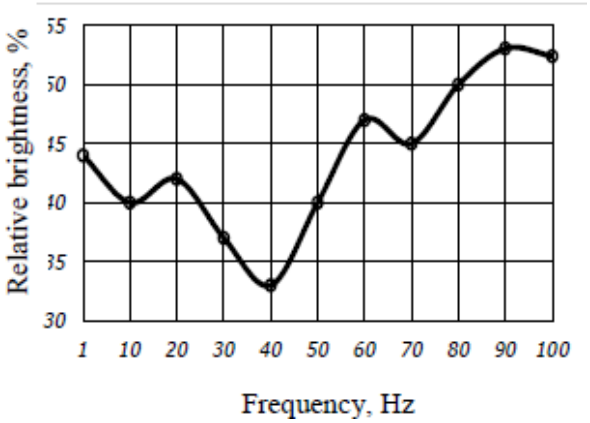

Figure 2.18 – The results of the experimental studies
of the reverse side of the palm

Experimental measurements were performed on the indicated parts of body in the young healthy respondents without significant fatty layer of skin.

From Fig. 2.18. it is evident that the maximum absorption of the reverse side of the palm in the area of 25...45 Hz and the frequency of 40 Hz is the most suitable for the process of light therapy. Absorption at these frequencies is at least 1.5 times better than at other frequencies.

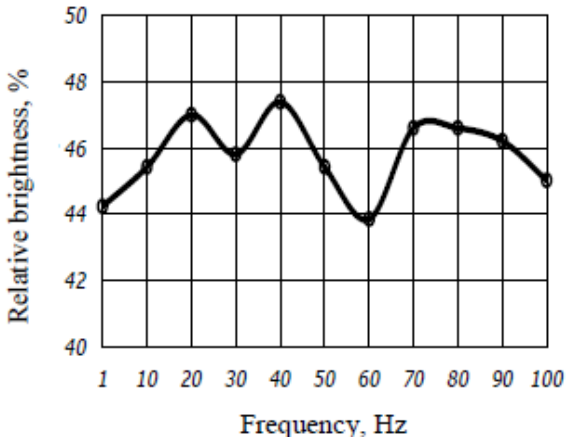

Figure 2.19 – The results of the experimental studies of the soft tissue
of the hand (acupoint GI 4 – He-Gu)

Possible options for light therapy, as follows from Fig. 2.19., for low frequency modulation (1 Hz). It is also acceptable the absorbtion of the soft tissues of the hand in the area of 45…65 Hz, and the frequency of 60 Hz, with maximum absorption, is most appropriate for this respondent.

The next graph of Fig. 2.20 describes the response of the hip soft tissues, in essence, the muscle tissue of the young respondent, to the light irradiation frequency. From the figure it is clear that the maximum absorption for the soft tissue of the hip is located at a section of 35…55 Hz, and the frequency 50 Hz is the most acceptable.

From the given Figures from 5 to 7 it's clear that the greatest absorption capacity of human body biological tissues is within 35…65 Hz. Increasing the modulation frequency to 100 Hz results in a smooth growth of the reflecting component.

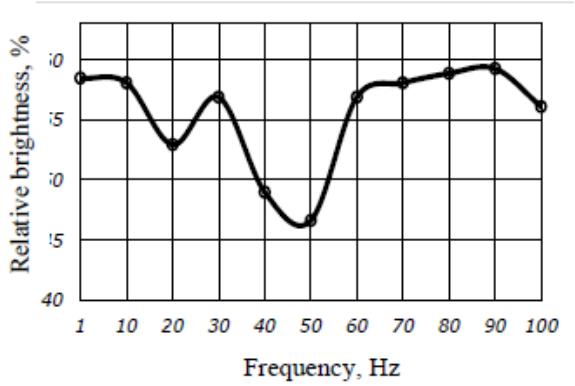

Figure 2.20 – The results of the experimental studies of the soft tissue of the hip

The conducted studies of absorption capacity of a sample of adipose tissue of pig *in vitro* (Fig. 2.21.) showed that in addition to the first maximum absorption (resonance), there is still a similar absorption area in the frequency range of 75...85 Hz, but there is also a frequency range of modulation in the range of 60...75 Hz where the maximum reflection of the light flux occurs.

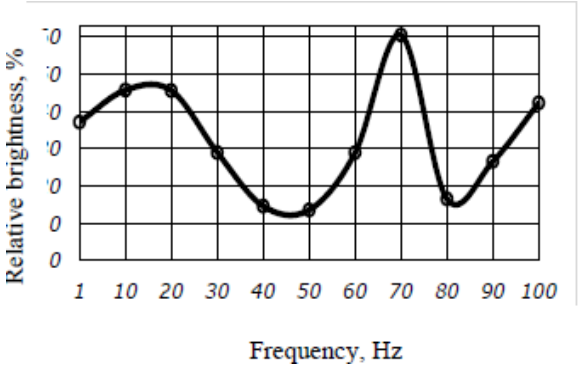

Figure 2.21 – The results of the experimental studies of the adipose tissue of pig

It was also decided to check the absorption capacity of a sample of organic leave of the Linden tree, Fig. 2.22.

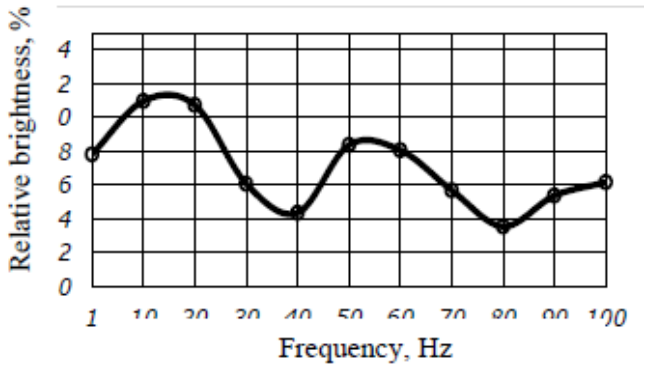

Figure 2.22 – The results of the experimental studies of the Linden tree leave

The graph shows that the sample has a good absorbtion capacity across the entire frequency interval, but there are two maxima at frequencies 35...45 Hz and 75...85 Hz.

For comparison, an experimental study and measurement were conducted in the absence of modulation of the light flux and full illumination of the irradiation area. As a biological object, the reverse side of the palm is selected (as in Fig. 2.18.). The result of this study is shown in Fig. 2.23.

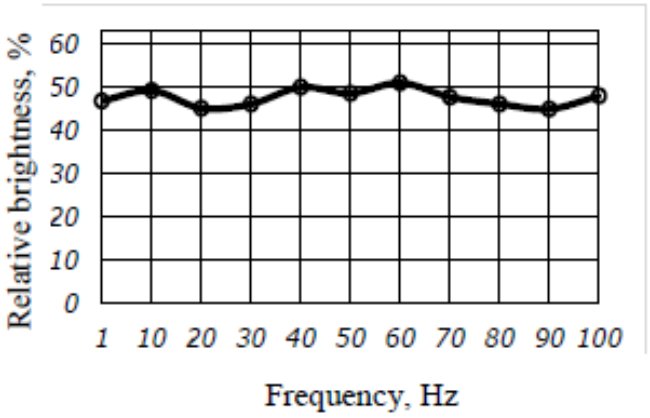

Figure 2.23 – The results of the experimental studies of the reverse side of the palm without modulation of the light flux

When using modulation for this human body area, the maximum absorption was at frequencies 25...45 Hz. However, we do not observe this tendency without modulation, and we have almost monotonous data that show the advisability of using modulation, because the values of the relative brightness without modulation are 1.5 times worse than with using modulation at certain intervals. At the selected area, almost the maximum

reflection of the light flux is recorded, and therefore, it is possible to predict the minimum benefit from this mode of illumination exposure.

Experiments with different areas of the human body and different biological objects were conducted and the frequencies with maximum absorption of light were determined:

- these experiments confirmed the differences in light flux absorption with modulation and without it, and the possibility of using such technique and systems in the technologies of light therapy;

- the developed system allows practically in real time regimen to determine the frequency of maximum absorption of the selected area of the patient's body. The time taken for the measurement and construction of the absorption schedule is 2…3 minutes;

- experimental verification showed that the maximum absorption of light flux is at frequencies close to 30…60 Hz, which corresponds to the smallest value of relative brightness (0 is completely black, 63 is completely white) on the sensor, since reflected beams at these frequencies are the smallest;

- experimental study of the sample of the animal biological tissue have shown that the presence of fatty layer can lead to the appearance and shift of the maximum absorption frequencies, which should be considered when conducting light therapy.

2.6 Features of metrological support for measuring the low-intensity optical signal parameters

The power measurements in the optical range can be performed using a standard optical power measurer such as MKZ-18A (λ=0,4…3,5 μm, P=10^{-4}…10^{-2}W), M3-49 (λ=0,4…11 μm, P=10^{-3}…10^{-1} W). It is also possible to use specialized equipment for measuring the parameters of fiber optic lines OMZ-65 (λ = 0,8…1,0 μm, P=10^{-9}…10^{-2} W) and OMCK-76B (λ=1,0…1,3 μm, P=10^{-6}…10^{-4} W for low-frequency signals, 10^{-8}…10^{-5} W for modulated signals) [28].

The disadvantages of such apparatus should include a limited range of power measuring and, for the majority of cases, another frequency range and fixation of these frequencies, due to the specifics of optical generators for fiber optic communication lines. The following remarks should also be entirely attributed to the specialized equipment of foreign firms FPM-600, TEMPO 522-HP, TOPAZ 3200, devices of Grandway series, and others.

Thus, the classification scheme of the optical modulation radiometric systems, taking into account the above mentioned information, has the form presented in fig. 2.24.

As one may see in fig. 2.24, values of low and extremely low power is measured using measuring receivers.

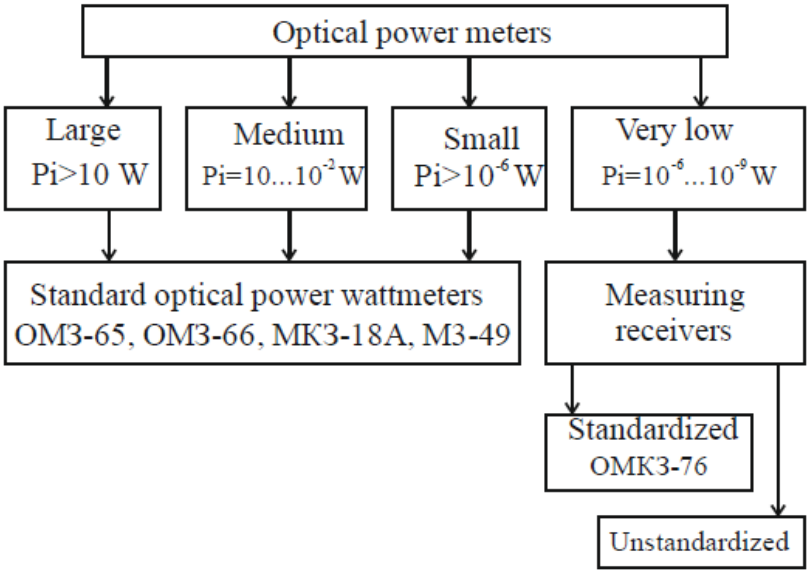

Figure 2.24 – Classification of the optical power measurers

Limitations in the optical range (400…730 nm) of specialized standardized measuring devices at 10^{-9}…10^{-12} W restrain the measurements and research in various fields of science and technology, including biology and medicine.

At the same time, in radio astronomy, radiolocation, medicine at frequencies > 30 GHz, as well as in the optical range, there are tasks of measuring the powers with values of 10^{-9}…10^{-12} W, which are several orders smaller than those achieved by standard measuring instruments (10^{-2}…10^{-9} W).

Measurement of such low-intensity radiation can be carried out only using non-standardized special measuring devices, whose base unit is a high-sensitivity measuring receiver – a radiometer, and for optics – an optical radiometer [1].

The limit sensitivity of this measuring receiver is determined by the expression [2]:

$$P_{ls.} = kT_0 \Delta f K_n = 4 \cdot 10^{-21} \Delta f K_n, \qquad (2.35)$$

where $k-$ is the Boltzmann constant ($k = 1{,}37 \cdot 10^{-23}\,\mathrm{J \cdot K^{-1}}$); T_0 – is thermodynamic temperature ($T_0 =$ 290°K); K_n – is the noise factor of the receiver path; Δf is the bandwidth of the receiver.

Thus, the marginal sensitivity is proportional to the noise factor and the bandwidth of the measuring receiver. Development of such high-sensitive measuring receivers and creation of measuring devices on their basis are possible using the modulation method of converting weak signals, which provide compensation of the measuring channel intrinsic noises [1,2].

The theory and practice of short-range radio systems is somewhat different from systems working with objects that are removed far from signal receivers. By criteria [41], a radiometer can be classified as near-action provided:

$$R_0 \le \frac{2(S_{hp} + S_o)^2}{\lambda}, \qquad (2.36)$$

where R_0 – is the distance from the receiving photocell to the object; S_{hp} – is the area of the photoreceiver; S_o – is the area of the reflection object; λ – is the wave length.

Short range and contact action radiometric systems, in addition to measuring the power of low-intensity monochromatic laser and broadband (noise) signals, can also provide evaluation of parameters, such as absorption and reflection coefficients, correlation function, measurement of frequency-time parameters, and fulfillment of spectral analysis of a signal structure that is not characteristic for long-range optical radio systems, such as light-range meters. At the same time, in radio astronomy, radiolocation, medicine at frequencies > 30 GHz, as well as in the optical range, there are tasks of measuring the powers, whose values are several orders of magnitude smaller than the values achieved by standard measuring devices.

Measurement of such low-intensity radiation can be carried out only using non-standardized special measuring devices, whose base unit is a high-sensitivity measuring receiver – a radiometer, and for optics – an optical radiometer [4,28].

Thus, utilization of the switching modulation transformation for constructing modulation optical radiometers and options of their

application in medicine, biological research and materials technology provide:

- significant simplification of the structural diagrams and the process of optical signals intensity measuring, due to using optoelectronic elements and missing optical-mechanical components of the measuring path;
- measurement of the low-intensity optical signal power of $10^{-9}…10^{-12}$ W, due to instrument noise compensation for the optoelectronic converter and the measuring channel OP;
- ability to constructe modern devices for light therapy with measuring the dose of energy absorbed by selection of reflected and scattered energy, which enhances prediction and treatment efficacy;
- ability to choose modulation frequencies with maximum light flux absorption and constructing automated systems with irradiation signal frequency scanning;
- enhancing the ability of medical-biological research, using low-intensity optical signals, to detect new effects and construct more modern medical and diagnostic equipment.

SECTION 3 RADIOMETRIC MODULATION METHODS AND MEANS FOR PARAMETERS OF LOW-INTENSITY MICROWAVE SIGNALS MEASURING

Preliminary remarks

For measuring the parameters of weak and super-weak random (noise) signals absorbing are used highly sensitive radiometric receivers – radiometers (R).

The inclusion of an antenna and an information processing device (computer) with an information display indicator into the radiometric receiver allows to construct a radiometric system (RS). Radio thermal noise signal, which can be represented as a narrowband signal [1, 3]

$$u_0(t) = U_0(t)\sin\left[\omega_0 t + \phi(t)\right], \qquad (3.1)$$

contains curve – $U_0(t)$, phase – $\varphi(t)$ and center circular frequency ω in the analysis band – $\Delta\omega$.

The random nature of changes in the parameters of wideband signals – amplitude, frequency, and phase shift leads to the absence of regular components and necessitates the measurement of such parameters and characteristics of these signals as noise power spectral density and integrated power, polarization coefficients, and autocorrelation function.

The task of measuring these parameters is complicated by the fact that the level of input signals is mostly comparable to or less than the level of RS self-noise. For the most part, the radiometer can measure the power of not only noise, but also weak sinusoidal signals. The main characteristics of the RS include:

- operating frequency range;
- fluctuation threshold of sensitivity; sensitivity;
- the upper limit of measuring the power of signals;
- error of signal power measurement;
- bandwidth of the radiometric channel to the quadratic detector.

The range of operating frequencies is determined by the frequency band between the minimum and maximum operating frequencies (in wideband RSs, it is limited by the waveguide cross section). The fluctuation threshold of sensitivity is the minimum value of the input signal that can be detected and measured, i.e. the ratio of the signal and the self-noise at the output of the RS is equal to one.

Sensitivity is the ratio of the output RS value to the measured (input) value. The dynamic range is determined by the ratio of the upper limit of the measured power to the fluctuation threshold of sensitivity.

Ensuring the metrological characteristics of the RS with weak and super-weak levels of input signals is possible through the use of compensation, correlation and modulation methods for converting input signals.

A compensation radiometer has a fairly simple implementation scheme, which includes antennas connected in series, a high frequency amplifier, a quadratic detector, a DC amplifier, a low-pass filter, a comparator, a compensating voltage source, and an indicator that measures the differential voltage. At the same time, due to the need to ensure a large gain when measuring the power of radio thermal signals (10^{-12}…10^{-15} W/cm^2), fluctuations of the transmission coefficient of the radiometric channel increase significantly, which leads to an increase in the DC component at the detector output, its compensation impossibility, and therefore, to an increase of the sensitivity threshold. Flicker noise at the detector output, whose intensity increases in the region of low frequencies (in the passband of the output low-pass filter), has a special influence on the sensitivity threshold of a compensation radiometer.

The correlation radiometer includes one or two antennas, depending on the type of allocable correlation function and the number of signals, two identical channels that are isolated between themselves, a multiplying device, a low-pass filter (LPF) and an indicator. Frequency components having auto and correlation coupling form a constant component at the output of the low-pass filter, the level of which characterizes the magnitude of this relationship. However, correlation radiometers also have drawbacks that increase the threshold of its sensitivity and consist in passing the intrinsic noise from one channel to another and the appearance of an additional constant component, as well as the difficulty of ensuring the identity of the phase-frequency characteristics of the channels. Modulation-switching methods for the conversion of ultra-weak signals and modulation radiometers made on this basis have received wider application in radiometry.

3.1 Features of high-sensitivity modulation radiometers constructions

Radiometric systems are widely used in various fields of science and technology for measuring extremely weak signals, the level of which may be below the level of intrinsic noise of these systems. This is what contributed to their widespread introduction into the practice of weak signals measuring.

Typically, radiometric equipment is used to measure signals from radiation sources located at considerable distances from receiving devices, for example, in radio astronomy, radar, and radio navigation.

The use of RS in such areas as physics, living physics, biology, and medicine involves measurement procedures that are implemented at close distances or in contact with a radiation source – a physical body or a biological object. In this case, RS antennas are placed directly on the object of study, are coordinated with its surface and provide both the reception of radio signals and their transmission upon irradiation of the object.

The use of a radiometric system in contact with the object of measurement (physical body or biological object) allows us to consider this case as the limit transition of the electromagnetic field from one medium to another with the same (consistent) or different dielectric constant.

Considering the fact that in the mm-range (30…300 GHz) there are practically no standardized means of measuring for extremely low power densities (10^{-12}…10^{-15} W/cm^2), in the future we will consider possible variants for building of highly-sensitive non-standardized radiometric modulation systems. An analysis of the classical schemes possibilities for constructing highly sensitive RSs has shown the perspective for using modulation transformations, taking into account the characteristics of the mm-wave range [39, 43]. Broadband modulation radiometric systems without conversion of the input frequency (direct conversion) are mainly used in the frequency range up to 30 GHz [1, 44], and in the mm-wave range the more common are narrow-band schemes with single or double conversion of the input frequency, because the use of wideband amplification for input signals is very difficult, especially by means of solid-state amplifiers. The considered radiometric systems of the near and the contact action of the microwave band, in addition to measuring the power of low-intensity monochromatic and broadband (noise) signals, also provide an assessment of other parameters – absorption, reflection and correlation coefficients, measurement of frequency-time parameters, and spectral analysis of the signal structure that is not typical for long-range radio systems.

Thus, the classification scheme of modulation radiometric systems of the microwave range, taking into account the above considerations, can be presented as follows (Fig. 3.1). The proposed scheme on Fig. 3.1 allows us to choose the structure of the RS, depending on the measurement target. Later we will consider the possible variants for building high-sensitivity non-standardized (specialized) systems. The analysis of the possibilities of

classical schemes for the construction of high-sensitivity RS showed the perspective for using modulation radiometers taking into account the features of the range of mm-waves [1, 44, 45]. In order to investigate the direct transformation broadband modulation RSs, we will analyze the basic relations that arise in the structural scheme of this device.

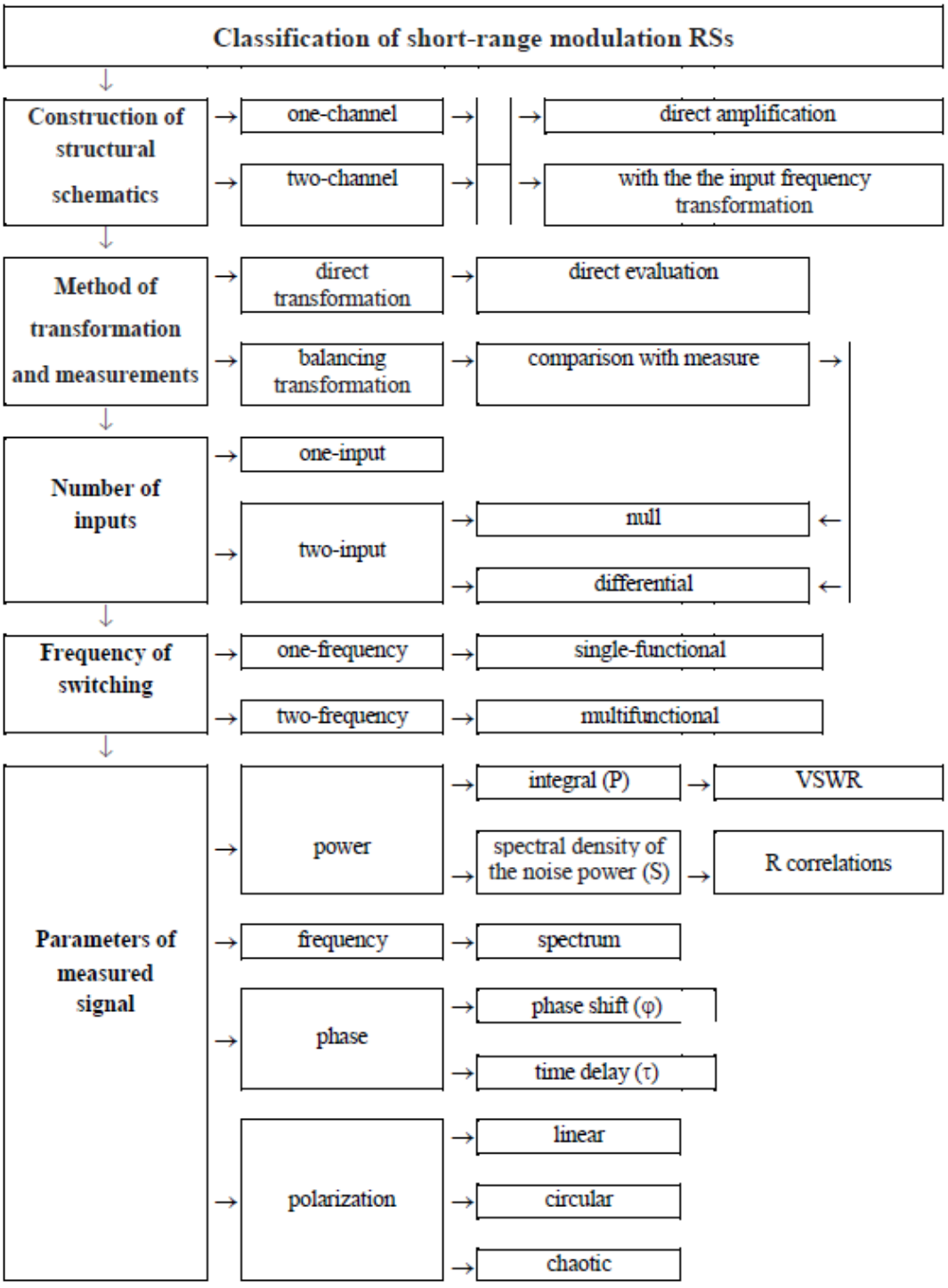

Figure 3.1 – Classification scheme of modulation radiometric systems

In order to investigate the direct transformation broadband modulation RSs, we will analyze the basic relations that arise in the structural scheme of this device.

To simplify the analysis, let us consider the processes occurring in the direct conversion radiometer circuit with linear amplification before the detector (Fig. 3.2) when a monochromatic signal is fed to its receiving antenna X1

$$u_0(t) = U_0 \sin\left[\omega_0 t + \phi\right].$$

Switching S1 to position 1 allows the signal to pass through the wideband linear amplifier A1 to the square detector U1. Due to the presence of self-noise in the radiometric system, the full signal at the detector input is

$$u_1(t) = u_o(t) + u_w(t), \tag{3.2}$$

where $u_w(t)$ – intrinsic noise at the radiometric system input.

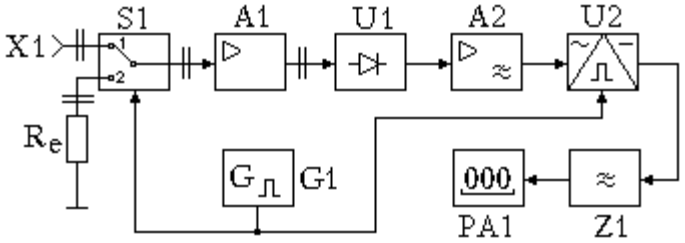

Figure 3.2 – Broadband modulation direct conversion RS

The commuting of the rectangular voltage (switching function) is [80]:

$$F_0(t) = F_1(t) + F_2(t),$$

where:

$$F_1(t) = \frac{1}{2} + \frac{2}{\pi}\sum_{n=1}^{\infty}\frac{sin(2n-1)\Omega t}{2n-1};$$

$$F_2(t) = \frac{1}{2} - \frac{2}{\pi}\sum_{n=1}^{\infty}\frac{sin(2n-1)\Omega t}{2n-1}, \tag{3.3}$$

and its properties can be described by such equations:

$$F_1(t) + F_2(t) = 1; \qquad F_1(t)\cdot F_2(t) = 0;$$

$$\left[F_1(t)\right]^2 = F_1(t); \qquad \left[F_2(t)\right]^2 = F_2(t), \tag{3.4}$$

where Ω – switching signals circular frequency.

Switching the switch S1 to position 2 causes the signal $u_o(t)$ to turn off, but the intrinsic noises $u_w(t)$ continue to act at the input of the quadratic detector. Thus, after the switching period $T_K = \frac{2\pi}{\Omega}$ at the input of a quadratic detector, two signals alternately act:

$$\begin{cases} u_1(t) = u_o(t) + u_w(t); & 0 < t < \frac{\pi}{\Omega}; \\ u_2(t) = u_w(t); & \frac{\pi}{\Omega} < t < \frac{2\pi}{\Omega}. \end{cases} \tag{3.5}$$

As a result of switching, the modulated voltage is generated at the output of the switch S1

$$u_{S1}(t) = \left[u_o(t) + u_w(t)\right]F_1 + u_w(t)F_2, \tag{3.6}$$

which after amplification is fed to the square detector U1.

Considering that the characteristic of a quadratic detector has the form $u_3 = au^2$, output signal can be written as

$$\begin{aligned} u_{U1}(t) &= aK_1\left\{\left[u_o(t) + u_w(t)\right]F_1 + u_w(t)F_2\right\}^2 = \\ &= aK_1\left\{\left[u_o^2(t) + 2u_o(t)u_w(t) + u_w^2(t)\right]F_1 + u_w^2(t)F_2\right\}, \end{aligned} \tag{3.7}$$

where K_1– amplifier gain of A1; u_w^2 – dispersion (intensity) of the noise signal.

Substituting the value (3.3) at $\varphi_o = 0$ within (3.7) and performing mathematical transformations, we get

$$\begin{aligned} u_{U1}(t) &= \frac{aK_1^2U_o^2}{2}\left[(1 - \cos 2\omega_o t)F_1 + 2U_o \sin\omega_o t\ u_w(t)F_1 + u_w^2(t)F_1 + u_w^2(t)F_2\right] = \\ &= aK_1\frac{U_o^2}{2}\left[\frac{1}{2} + \frac{2}{\pi}\sum_{n=1}^{\infty}\frac{\sin(2n-1)\Omega t}{2n-1}\right] - \frac{aK_1U_o^2}{2}\cos 2\omega_o t\left[\frac{1}{2} + \frac{2}{\pi}\sum_{n=1}^{\infty}\frac{\sin(2n-1)\Omega t}{2n-1}\right] + \\ &+ 2aK_1U_o \sin\omega_o t\ u_w(t)\left[\frac{1}{2} + \frac{2}{\pi}\sum_{n=1}^{\infty}\frac{\sin(2n-1)\Omega t}{2n-1}\right] + aK_1u_w^2(t)\left[\frac{1}{2} + \frac{2}{\pi}\sum_{n=1}^{\infty}\frac{\sin(2n-1)\Omega t}{2n-1}\right] + \\ &+ aK_1u_w^2(t)\left[\frac{1}{2} - \frac{2}{\pi}\sum_{n=1}^{\infty}\frac{\sin(2n-1)\Omega t}{2n-1}\right]. \end{aligned} \tag{3.8}$$

Excluding the signal components (3.8), which are delayed by the selective filter of the A2 amplifier, we can write

$$u_{A2}(t) = aK_1^2 K_2 \frac{U_o^2}{\pi} \sum_{n=1}^{\infty} \frac{\sin(2n-1)\Omega t}{2n-1} + aK_1^2 K_2 \Delta u_w^2(t), \qquad (3.9)$$

where K_2 – the gain of the amplifier A2; $\Delta u_w^2(t)$ – noise dispersion, which fall into the bandwidth of the selective amplifier.

The selected voltage (3.9) is fed to a synchronous detector, the second input of which receives the reference signal with commutation frequency Ω

$$u_2(t) = U_2\left(F_1 - F_2\right) = \left\{\left[\frac{1}{2} + \frac{2}{\pi}\sum_{n=1}^{\infty}\frac{\sin(2n-1)\Omega t}{2n-1}\right] - \left[\frac{1}{2} - \frac{2}{\pi}\sum_{n=1}^{\infty}\frac{\sin(2n-1)\Omega t}{2n-1}\right]\right\}U_2 =$$
$$= \frac{4U_2}{\pi}\sum_{n=1}^{\infty}\frac{\sin(2n-1)\Omega t}{2n-1}, \qquad (3.10)$$

where U_2 – voltage reference amplitude.

As a result of multiplying the signal (3.9) by the reference switching voltage (3.10) at the output of the synchronous detector U2, we get

$$u_{U2}(t) = u_{A2}(t)u_2(t) =$$
$$= aK_1^2 K_2\left[\frac{U_o^2}{\pi}\sum_{n=1}^{\infty}\frac{\sin(2n-1)\Omega t}{2n-1} + \Delta u_w^2(t)\right]\frac{4U_2}{\pi}\sum_{n=1}^{\infty}\frac{\sin(2n-1)\Omega t}{2n-1} =$$
$$= aK_1^2 K_2 K_3\left\{\frac{2U_2U_o^2}{\pi^2}\left[\sum_{n=1}^{\infty}\frac{1}{2n-1} - \sum_{n=1}^{\infty}\frac{\cos(2n-1)2\Omega t}{2n-1}\right] + \frac{4U_2}{\pi}\Delta u_w^2(t)\sum_{n=1}^{\infty}\frac{\sin(2n-1)\Omega t}{2n-1}\right\}, \qquad (3.11)$$

where K_3 – transmission coefficient of synchronous detector.

The low-pass filter Z1 highlights the constant component of the signal (3.11) and the harmonic components formed from the voltage of the signal and the frequency components of the noise transmitted to the synchronous detector, while the voltage with $2\Omega t$ frequency is delayed by the filter Z1

$$u_{Z1} = \frac{2aK_\Sigma U_2 U_o^2}{\pi^2} + 4K_\Sigma a\frac{U_2}{\pi}\Delta U_w^2(f)\sum_{i=1}^{K}(\Omega - \Omega_i), \qquad (3.12)$$

where K_Σ – total transmission coefficient of the radiometric channel.

A significant disadvantage of the RS structural scheme (Fig. 3.2) is the impossibility of providing a wide band of operating frequencies in the mm-wave range and a significant gain of input signals, which limits the circuit's capabilities as a metrological signal system of extremely low power.

In addition, as can be seen from (3.12), low-frequency components from the components close to the switching frequency ($\Omega_i \approx \Omega$) and falling into the pass-band of the low-pass filter pass through the radiometric channel, leading to an increase in the fluctuation threshold.

For the mm-wave range, a radiometric system with a single or double conversion of the input frequency is more promising. Such a construction of the RS structural scheme provides a significant increase in the system gain due to the large gain of the intermediate frequency amplifier and the possibility of band operation at frequencies f>30 GHz by tuning the local oscillator frequency.

The source of radiometric devices self-noise are shot and thermal noise, with a uniform distribution of power in a wide range of frequencies (type of «white noise»), as well as low-frequency noise whose intensity varies according to the law $1/f$ (flicker-noise). Usually the frequency at which the intensity of the flicker-noise corresponds to the intensity of thermal noise is in the frequency range from zero to hundreds of hertz.

The spectral power density of thermal noise, taking into account the temperature T=293 K, is determined by the value $I_T = kT = 4{,}04 \cdot 10^{-21}$ W/Hz.

Fig. 3.3 shows noise power distribution $1/f$ in the frequency range up to 1 kHz taking into account the calculations, as well as the frequency spectrum of thermal noise, which passes to the output of the selective switching frequency amplifier A2.

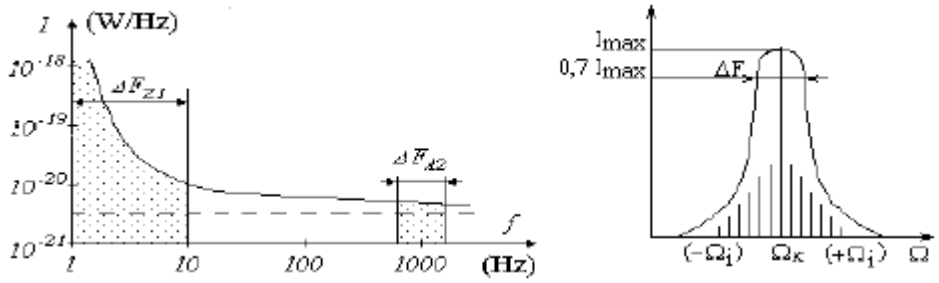

a) b)

Figure 3.3 – The intensity distribution of flicker noise (a) and thermal noise components close to the switching frequency (b) at the output of a quadratic detector

As you can see, the power level of flicker noise significantly exceeds the thermal noise power. Flicker noise is weakly suppressed by low pass filter (zone ΔF_{Z1} from 1 to 10 Hz). Therefore, in the radiometers of the compensation and correlation type, flicker-noise increases their sensitivity threshold by increasing the level of indicator fluctuations.

In a modulation radiometer (Fig. 3.2), the signal received by antenna X1, before entering the amplifier of receiver A1, is modulated in intensity by switch S1 with a low frequency of generator G1. The low voltage of the modulation envelope frequency, formed at the output of the quadratic detector U1, stands out from the fluctuation background of the noise of the quadratic detector by a narrow-band low-frequency filter. The last one is most often performed according to the following scheme: the selective amplifier of low-frequency modulation A2 – a synchronous detector U2, which is controlled by the modulation frequency voltage. The amplitude of the low-frequency envelope, allocated by the synchronous detector, is proportional to the signal power received by the X1 antenna.

The switching frequency and bandwidth ΔF_{A2} of the filter of A2 amplifier are chosen in such a way as to ensure a significant suppression of the influence of the low-frequency components of the flicker-noise and the high-frequency components of the thermal noise. The latest provides an advantage and explains the wider use of modulation radiometers.

Radiometric modulation systems that use the comparison method, when the measured value is compared with the reference one and the zero or close to zero difference of these signals is established by the RS indicator, seem very promising. Such RS are quite simply implemented using a modulation scheme, and the comparison is carried out using a compensating microwave signal from the input of the additional channel. The block diagram of the compensation-modulation system (Fig. 3.4) includes: antenna X1, radiometric channel, indicator P1, input waveguide switch S1, attenuator A1, generator of reference noise G1, waveguide switch S2, standard power meter P2.

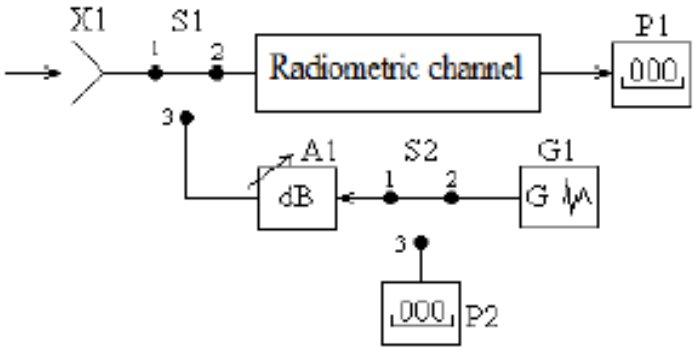

Figure 3.4 – Compensation-modulation RS of balancing transformation

The measurement process is implemented in two stages. At the beginning, the signal from the antenna is connected (switch S1 in position 1–2) and indicator P1 is marked. Then the switch S1 is set to position 2–3 and the same indicator reading corresponding to the input signal is set by attenuator A1. Next, the switch S2 is set to position 2–3 and the output signal of the generator G1 is fixed with a standard power meter P2. The value of the input signal power of the antenna (without taking into account the error) is determined by the expression $P_X = P_{G1}/\alpha$, where α – attenuator transfer ratio in relative units; P_{G1} – reference generator output power.

The considered scheme of implementation of the compensation modulation method allows to measure the power of weak and super-weak signals of physical and biological objects (10^{-12}…10^{-15} W/cm^2) in the presence of standard generator of monochromatic or noise signals and a power meter with a measurement limit of 10^{-3}...10^{-6} W. The automatic operation of the switch S1 implements the algorithm of operation of the zero modulation radiometer [46], when the output signal of the radiometric channel controls the power of the generator G1 or transmission coefficient A1.

3.2 A radiometric system of a direct conversion with a regenerative feedback

Switching radiometers are used to measure the intrinsic emission of biological objects. They were first used in radio astronomy measurements of weak radiation of spatial objects, where the noise power integral or spectral density of a researchable object is an informative parameter.

However, the sensibility and responsivity of direct conversion schemes were insufficient to measure the electromagnetic emission of biological objects. Therefore, it became necessary to convert the frequency of an input signal and additional gain at an intermediate frequency.

It is necessary to increase the modulation depth of a converted signal to sensitize further RS sensibility. It is possible to achieve if an additional noise signal is added to a received noise signal, the power of which is proportional to a measuring signal [47, 48].

A switching radiometer with automatic modulation deepening (Fig. 3.5) consists of series-connected antennas X1, an adder unit A1, a commutation switch S1, a high-frequency amplifier (HFA) A2 and a mixer U1, a local oscillator G1, an intermediate-frequency amplifier (IFA) A3, a

quadratic detector U2, a low-frequency amplifier (LFA) A4, a synchronous detector U3, a low-pass filter (LPF) Z1 and an indicator P1 are connected to the second input. Moreover, the radiometer contains a voltage divisor A5, the input of which is connected to the output of the low-pass filter Z1. The output is connected to the first input of a controlled attenuator A6. An additional noise generator G3 is connected to the second input of the controlled attenuator A6, and the output is connected to the second input of the adder A1.The circuit also has a modulating frequency switching generator G2, which is connected to the controlled inputs of switch S1 and synchronous detector U3.

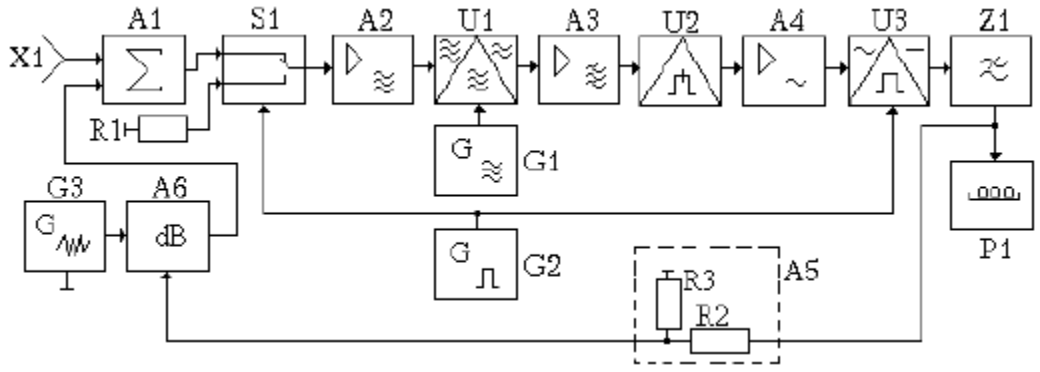

Figure 3.5 – RS direct conversion with a regenerative feedback

A switching radiometer works in the following way. Radio-frequency emission from a researchable biological object is fed to the input of the antenna X1, at the output of which a microwave noise signal U1 (t) is formed. Its dispersion can be represented as follows:

$$\overline{U}_1^2 = ST, \tag{3.13}$$

where S – an antenna sensitivity; T – temperature of a scanned area of an biological object.

The noise signals of an antenna X1 are added together with a part of the noise signal $U_{15}(t)$ of a generator G3 in an adder A1, which passed through a controlled attenuator A6. Since summed signals are not correlated, the dispersion of a combined signal has the following form:

$$\overline{U}_2^2 = \overline{U}_1^2 + K_{14}\overline{U}_{15}^2, \tag{3.14}$$

where K_{14} – an attenuator transmission coefficient A6 to the power; $\overline{U}_{15}^2$ – the dispersion of a noise signal of a generator G3.

The combined signal $U_2(t)$ is amplified by HFA A2 in a shown position of the key S1 in Fig. 3.5. Taking into account the intrinsic noise of a broadband amplifier A2, the voltage value at its output can be represented as dispersion:

$$\overline{U}'^2_4 = K_4^2\left(\overline{U}_1^2 + K_{14}\overline{U}_{15}^2 + \overline{U}_{31}^2\right), \tag{3.15}$$

where K_4 – a coefficient of amplification of HFA A2; $\overline{U}_{31}^2$ – the dispersion of intrinsic noises of an HF amplifier A2 at the first position of a switch S1.

The high-frequency noise voltage $U_4(t)$ is converted into an intermediate frequency voltage with the help of a mixer U1 and a local oscillator G2, increased by an amplifier A3 in a frequency band of its transmission.

A constant voltage component is formed at its output in a result of a quadratic transformation in a detector U2:

$$U'_8 = K_4^2 S_5^2 K_7^2 S_8 \overline{U}'^2_4, \tag{3.16}$$

where S_5 is a conversion conductance of a mixer U1; K_7 – a transfer constant of an amplifier A3; S_8 is the sensibility of a quadratic detector U2.

A load in the form of a resistance R_1 is connected to an input of HFA A2 in the opposite position of a switch S1, which is chosen equal to the output resistance of an adder A1. Therewith, the value of a noise voltage of an amplifier A2 does not change:

$$\overline{U}''^2_4 = K_4^2\overline{U}_{32}^2 = K_4^2\overline{U}_{31}^2, \tag{3.17}$$

and a constant component at an output has the following form:

$$U''_8 = K_4^2 S_5^2 K_7^2 S_8 \overline{U}''^2_4. \tag{3.18}$$

As a result of the continuous operation of a switch S1, which is controlled by the voltage of a low-frequency switching generator G2, an alternating voltage of the modulation frequency is formed at an input of LFA A4, which is amplified to a value:

$$U_9 = K_9 \frac{U'_8 - U''_8}{2} sign\, sin\,\Omega t, \tag{3.19}$$

where K_9 – a coefficient of the amplification of LFA A4; Ω – a circular switching frequency.

The alternating voltage U_9 is rectified by a synchronous detector U3 controlled by the same voltage as a switch S1. The output voltage of a low-pass filter Z1 is:

$$U_{11} = \frac{1}{2} K_9 K_{10} K_{11} \left(U_8' - U_8'' \right) = \alpha_0 \left(\overline{U}_1^2 + K_{14} \overline{U}_{15}^2 \right), \qquad (3.20)$$

where $\alpha_0 = \frac{1}{2} K_4^2 S_5^2 K_7^2 S_8 K_9 K_{10} K_{11}$ – RS direct conversion coefficient.

The transfer coefficient of a controlled attenuator A6 is set proportionally to the output voltage of a low-pass filter Z1. Denoting by β the transfer coefficient of a voltage divider A5 in the inverse transformation circuit, we get the transfer coefficient of a controlled attenuator A6 with the power output:

$$K_{14} = \beta U_{11}. \qquad (3.21)$$

Substituting the value of K_{14} from the expression (3.21) in (3.20), we get:

$$U_{11} = \alpha_0 \left(\overline{U}_1^2 + \beta U_{11} \overline{U}_{15}^2 \right). \qquad (3.22)$$

Solving equation (3.22) regarding the output voltage U_{11} RS, we finally get:

$$U_{11} = \frac{\alpha_0}{1 - \alpha_0 \beta \overline{U}_{15}^2} \overline{U}_1^2. \qquad (3.23)$$

Taking into account the expression (3.13), measured by the indicator P1 voltage takes the following form:

$$U_{12} = \frac{\alpha_0 S}{1 - \alpha_0 \beta \overline{U}_{15}^2} T. \qquad (3.24)$$

Thus, the measured voltage is proportional to the power of the received radiation or the temperature of a scanned area of a researchable object. RS output voltage has the following form in the absence of an additional noise signal from the G3 generator ($\beta = 0$):

$$U_{12}' = \alpha_0 S T. \qquad (3.25)$$

If an additional noise signal from the G3 generator is present ($\beta > 0$), then the radiometer sensitivity increases by a number of times:

$$\frac{U_{12}}{U_{12}'} = \frac{1}{1 - \alpha_0 \beta \overline{U}_{15}^2}. \qquad (3.26)$$

For example, when executing the denominator of an expression (3.26) as $\left(1-\alpha_0\beta\overline{U}_{15}^2=0{,}1\right)$, the radiometer sensitivity will increase by 10 times in comparison with an open circuit. In practice, the increase in the sensitivity is limited by the possibility of self-oscillations in an isolated system of a measuring transducer.

Assuming that self-oscillations occur under the condition:

$$1-\alpha_0\beta\overline{U}_{15}^2=0, \tag{3.27}$$

a transfer constant of a voltage divisor which consists of R_2 and R_3 and should equal:

$$\beta=\frac{R_3}{R_2+R_3}<\frac{1}{\alpha_0\overline{U}_{15}^2}. \tag{3.28}$$

Fig. 3.6 (1) shows the distribution of the gain in the sensitivity in the case of different values of regenerative feedback parameters, and Fig. 3.6 (2) represents distribution waveform of signals in a switching radiometer circuit. It is seen from Fig. 3.6 (1) that when a transmission factor of a voltage divider A5 (supports R_2 and R_3) β changes from 0 to 0.9, the sensitivity increases by almost an order of magnitude.

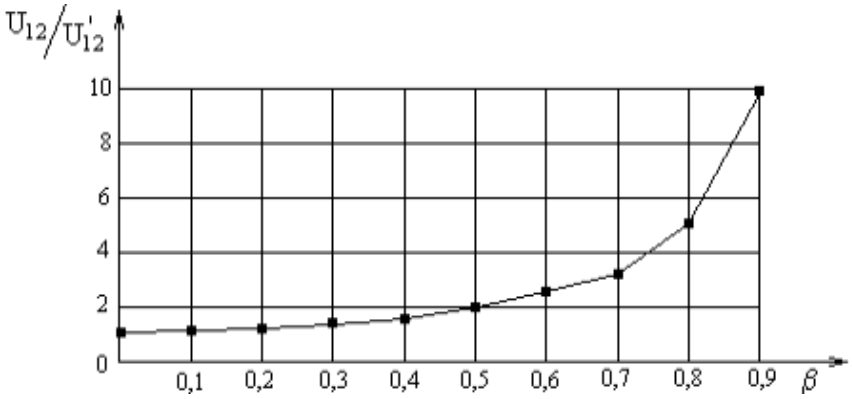

Figure 3.6 (1) – Distribution of a gain in the sensitivity with a regenerative feedback

The diagrams of signals are shown in Fig. 3.6 (2) that are characteristic of the radiometer circuit in Fig. 3.2 (diagrams a, b, c, d), Fig. 3.5 (diagrams a, b, c, e, f). Diagrams (a, b, c, e, g) in Fig. 3.6 (2) describe the processes that occur in the circuit of a negative feedback radiometer. The depth of modulation with a negative feedback (diagram g) decreases.

The diagram of Fig. 3.6 (2) (fig. f) shows that the modulation depth increases by value:

$$\Delta U' - \Delta U = U_{G3}. \tag{3.29}$$

An increase in U_{G3} causes the increase in the modulation depth, a change in the ratio (3.26) and an equivalent increase in the sensitivity of a radiometric system.

Thus, the amplitude modulation is deepened by adding a proportional part of a reference noise signal to a measured signal at the input of a quadratic detector, which increases the sensitivity of a switching radiometer.

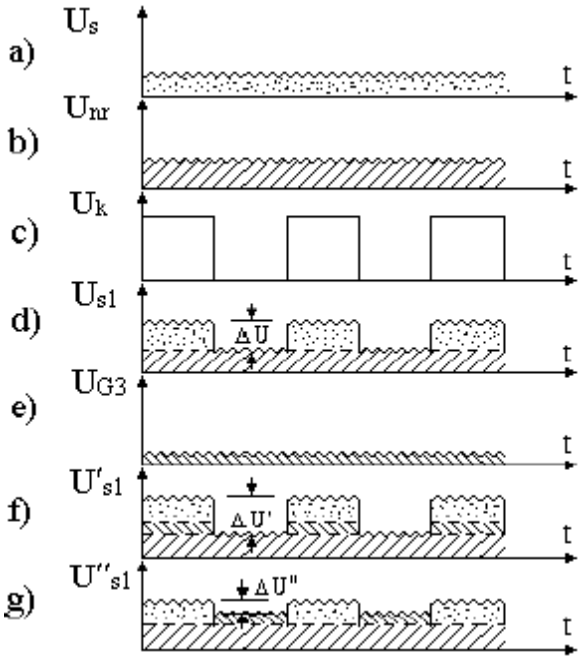

Figure 3.6 (2) – Waveform when adjusting the sensitivity of a switching radiometer

U_s – signal voltage; U_{nr} – radiometer noise voltage; U_k – switching frequency voltage; $U_{s1} = U_k (U_s + U_{nr})$ – voltage at the output of a radiometer switch S1; U_{G3} – noise generator voltage G3; $U'_{s1} = U_k (U_{G3} + U_s + U_{nr})$; $U''_{s1} = U_k (U_s + U_{nr} – U_{G3})$ –voltage at the output of the switching switch and detector of the radiometer with positive and negative connection.

Theoretically, radiometer sensitivity can be increased in a closed structure tens or hundreds of times, bringing the left side of equation (3.27) closer to zero. Practically, the sensitivity of a switching radiometer can be increased by two orders of magnitude and reach the sensitivity that is adequate to the density of $10^{-22}...10^{-23}$W/Hz of a power spectral, which is equal to the fluctuating temperature rating of an object's sensitivity of 10^5 K.

A further increase in sensitivity can be achieved by introducing special corrective links and flexible feedbacks into the RS circuit to ensure the stability of a closed system.

3.3 A modulation radiometric system with the compensation for a fluctuating noise of combination frequencies

Reduction of the level of fluctuations can be achieved by different methods, the main of which is the use of a narrow-band filter tuned to the switching frequency at the output of a quadratic detector and buildup of the constant time of a low-pass filter at the output of a synchronous detector, which reduces RS speed.

We review the RS schema beneath in which the introduction of a voltage feedback of combination frequencies provides the suppression of spectral components of the voltage in a bandpass amplifier that are close to its center frequency [49, 50].

This allows reducing its fluctuation threshold and thereby increasing the sensitivity without increasing the time to neutralization of an output signal (Fig. 3.7).

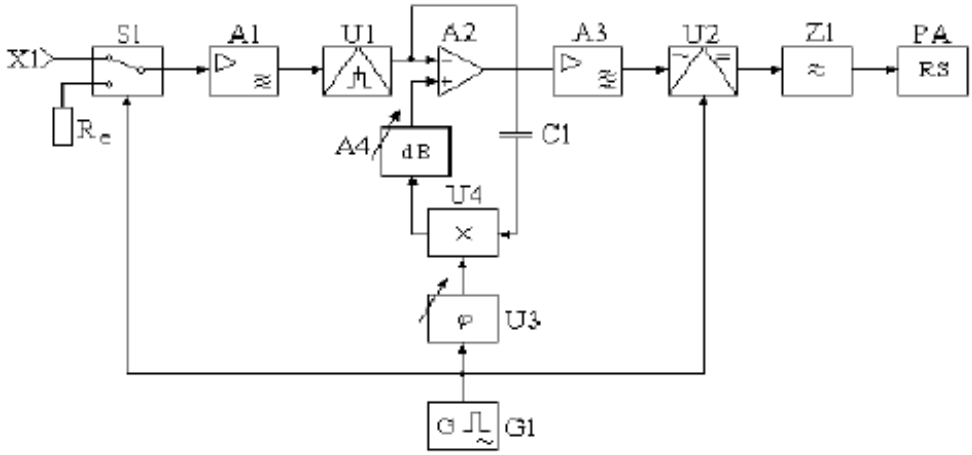

Figure 3.7 – A modulation radiometric system with the compensation for fluctuating noise

A RS consists of an antenna X1, to which a series-connected commutation switch S1 with an equivalent load R_e at the other input, a high-frequency amplifier A1, an amplitude detector U1, a differential amplifier A2, a low-frequency band amplifier A3, a synchronous detector U2, a low-pass filter Z1 and a recorder PA are connected.

The low-frequency generator G1 is connected to control inputs of a commutation switch S1, a synchronous detector U2 and a variable phase shifter U3, the output of which is connected to one input of a multiplying unit U4. Its other input is connected through a capacitor C1 to the output of a differential amplifier A2. The other input of the amplifier is connected to the output of a multiplying unit U4 through a variable attenuator A4.

The thermal radio radiation, received by an antenna X1 through a commutation switch S1, is fed to the input of the HFA. The noise level of the HFA A1 will be determined by the output resistance of an antenna X1, bypassing the input of the HFA, at the indicated position of a commutation switch S1.The dispersion of the received signal is the following one:

$$\overline{U}_1^2 = S_1 T_i \Delta f\,, \tag{3.30}$$

where S_1 – is the antenna sensitivity; T_i – temperature of emission source; Δf – frequency band of HFA A1.

HFA intrinsic noise intensity at its input is

$$\overline{U}_2^2 = R(F-1)T_o \Delta f\,, \tag{3.31}$$

where R is the input resistance of the HFA; F – HFA noise figure; T_o = 273 K is the temperature corresponding to zero degrees Celsius.

In RS a received signal is much weaker than the amplifier own noise $\left(\overline{U}_1^2 << \overline{U}_2^2\right)$. Therefore, the HFA A1 amplifies the mixture of noise signals that are further detected with the amplitude detector U1 with a quadratic characteristic. Since the amplified signals are not correlated with each other, the output voltage of the detector has the form:

$$U_3' = S_2 K_1^2 \left(\overline{U}_1^2 + \overline{U}_2^2\right), \tag{3.32}$$

where: S_2 –conversion conductance of a amplitude detector; K_1 – HFA gain.

The resistance R_e is connected to the input of the HFA A1 in the opposite position of the switch S1, equivalent to output resistance of the antenna X1 and a temperature equal to an antenna temperature. Therefore, the output voltage of the detector in this case takes the value:

$$U_3'' = S_2 K_1^2 \overline{U}_2^2\,. \tag{3.33}$$

A commutation switch S1 is controlled by the rectangular voltage of a low frequency generator G1. Therefore, a variable composite of switching frequency Ω and a noise signal from the presence of intrinsic noises of the HFA detector and the fluctuation of the HFA gain will be present at the output of the amplitude detector U1 for the switching period:

$$U_4(t) = \frac{U_3' - U_3''}{2} sign\, sin\, \Omega t + V_w(t), \qquad (3.34)$$

where $V_w(t)$ – voltage of low-frequency noise.

The low-frequency signal (3.34) is amplified by differential amplifier A2 and fed to the input of narrow-band amplifier A3, the center frequency of which is chosen equal to a switching frequency $\Omega = \Omega_K$. Spectral noise components close to the switching frequency $(\Omega_i \approx \Omega_K)$ also enter the gain band along with a valid signal. Amplified voltage is a mixture of a deterministic frequency signal Ω and a narrowband signal consisting of spectral components $\pm\sum_{i=1}^{K}\Omega_i$ (Fig.3.3b).

Entering the synchronous detector U2, controlled by the voltage of the low-frequency generator G1, the alternating voltage of the switching frequency Ω is rectified. The spectral components of the noise voltage create a low-frequency fluctuation voltage of combination frequencies. Therefore, the result of synchronous detection is the signal:

$$U_5 = \frac{K_2}{2}(U_3' - U_3'') + K_2 V_1\, sin \sum_{i=1}^{K}(\Omega \pm \Omega_i)\cdot t, \qquad (3.35)$$

where K_2 – narrowband amplifier gain; $V_1\, sin \sum_{i=1}^{K}(\Omega \pm \Omega_i)\cdot t$ – low-frequency noise of combination frequencies Ω и Ω_i.

The first component of voltage (3.35) is a constant component, which, taking into account expressions (3.32) and (3.33), has the following form:

$$U_6 = 0{,}5 S_2 K_2 K_1^2 \overline{U_1}^2 = 0{,}5 S_1 S_2 K_2 K_1^2 T_D \Delta f. \qquad (3.36)$$

The second component

$$U_7 = K_2 V_1\, sin \sum_{i=1}^{K}(\Omega \pm \Omega_i)\cdot t \qquad (3.37)$$

is narrowband noise with a maximum power spectral density close by a zero point $(\Delta\Omega_i << \Omega)$.

The constant component of the voltage (3.36) is a valid signal, which is allocated by the low-pass filter Z1 and registered by the output recorder PA.

The level of suppression of low-frequency noise $\Sigma(\Omega \pm \Omega_i)$ is greater, the larger the time constant of a filter Z1, which determines the averaging time of an output signal. Low-frequency noise intensity $V(\Omega_i)$ is determined by the spectral power density of the noise signal $V_w(t)$ in the area of switching frequency Ω. Since the density distribution of low-frequency noise is inversely proportional to the frequency $\left(1/\Omega\right)$, then the intensity of the nearby part of the low-frequency noise $V(\Omega_i)$ decreases with increasing switching frequency Ω. It determines the gain of a modulation radiometer in comparison with the compensation one. However, an increase in the switching frequency of more than 1000 Hz does not give a significant gain in reducing the noise of $V(\Omega \pm \Omega_i)$, since high-frequency noise is thermal and has an equilibrium distribution up to high frequencies.

To suppress the spectral components of noise in the area of the switching frequency Ω, the output voltage of the quadratic detector U1 is supplied through an isolation capacitor C1 to one input of the multiplying unit U4, to the other input of which a low-frequency voltage Ω is supplied from the generator G1 through a phase shifter U3.

As a result of multiplying a frequency signal with low-frequency components of the noise voltage $V_w(t)$, spectral components with frequencies of the form are formed at the output of block U4

$$\sum_{i=1}^{K} \Omega \pm \Delta\Omega_i ,$$

where $\Delta\Omega_i$ – the frequencies of the spectral components of noise close to zero.

A switching frequency component Ω is absent in the output voltage, since the isolation capacitor C1 does not pass the constant component of the detector U1.

A voltage component (3.34) the switching frequency is multiplied with the voltage of a generator G1 and forms an alternating voltage of a doubled switching frequency (2Ω) at the output of the block U4.

Thus, the output voltage of a multiplying unit U4 has the following form:

$$U_7(t) = V_2 \sin\Sigma\left[\left(\Omega + \Delta\Omega_i\right) + \varphi\right] + K_3 U_m \operatorname{sign} \sin 2\left(\Omega t + \varphi\right), \qquad (3.38)$$

where φ – a phase shift introduced by a phase shifter U3; U_m– voltage amplitude of a generator G1; K_3 – gear ratio that takes into account the transfer properties of a phase shifter U3 and a multiplying unit U4.

Phase relationships of spectral components $\sum_{i=1}^{K}(\Omega \pm \Delta\Omega_i)$ are determined by a phase shift φ, introduced by a phase shifter U3.

Voltage (3.38) is supplied to the other input of a differential amplifier A2. The differential voltage is formed at the output of the differential amplifier:

$$U_8 = K_4\left[U_4(t) - U_7(t)\right], \tag{3.39}$$

where K_4 – a differential amplifier gain.

The differential voltage (3.39) is amplified by a narrow-band amplifier A3 with a gain K_2 in a transmission band.

Taking into account the voltage values (3.34) and (3.38), the reinforced voltage has the following form:

$$\begin{aligned} U_9 &= 0{,}5S_1S_2K_1^2K_2K_4T_i\Delta f \cdot sign\, sin\,\Omega t + \\ &+ K_2K_4\left\{V_1\, sin\sum_{i=1}^{K}\Omega_i t - K_5V_2\left[sin\sum_{i=1}^{K}\left[(\Omega \pm \Delta\Omega_i)t \pm \varphi\right]\right]\right\} + \\ &+ K_3K_4U_m\, sign\, sin\, 2(\Omega t + \varphi), \end{aligned} \tag{3.40}$$

where $V_1(\Omega_i)$ – a part of noise voltage $V_w(t)$, supplied to a transmission band of an amplifier A3; K_5 – gain of an adjustable attenuator A4; $\Delta\Omega_i$ – flicker noise frequencies at the detector output.

Taking into account that the spectral components of noise $\sum_{i=1}^{K}(\Omega \pm \Delta\Omega_i)$ are close to the switching frequency, we can assume:

$$\sum_{i=1}^{K}(\Omega \pm \Delta\Omega_i) = \sum_{i=1}^{K}\Omega_i \approx \Omega. \tag{3.41}$$

Then the other component of the expression (3.40) can be minimized and brought closer to zero:

$$V_1(\Omega_i) \cong K_5V_2(\Omega_i, \varphi). \tag{3.42}$$

To achieve condition (3.42), the phase φ and transfer coefficient K_5 are adjusted in such a way that the level of the combination components $\sum_{i=1}^{K}(\Omega \pm \Omega_i)$ at the output of the synchronous detector U2 will be minimal. The phase and amplitude of the compensating voltage $K_5 V_2(\Omega_i, \varphi)$ are regulated by the minimum value of oscillations of a pointer of the PA registrar.

The third component in expression (3.40) is not a constant component at the output of the synchronous detector U2, since components with combination frequencies Ω and 2Ω are suppressed by the low-pass filter Z1.

The first voltage component (3.40) is rectified by a synchronous detector U2 and smoothed by a low-pass filter Z1. As a result, only the valid voltage is recorded:

$$U_{10} = 0{,}5 S_1 S_2 K_1^2 K_2 K_4 T_i \Delta f \,. \qquad (3.43)$$

Considering that narrow-band noise with spectral components in the passband of amplifier A3 is attenuated by the compensating voltage from the output of attenuator A4, the time constant of the low-pass filter Z1 can be significantly reduced, which contributes to the radiometer speed. While maintaining an acceptable lag effect of a filter, the fluctuation threshold of the RS sensitivity is significantly reduced.

The experimental verification was carried out on an experimental model of a single-channel modulation radiometer with a time constant of an output filter of30 s and a switching frequency of 1000 Hz, which threshold of sensitivity to noise signals was 10^{-19} W/Hz. After introducing of a single-channel radiometer of a compensating unit with an adjustable attenuator and a phase shifter with the same sensitivity into the circuit, the time constant was reduced by 10 times (3 s). The sensitivity threshold is reduced to 10^{-21} W/Hz with the same inertia of the filter (30 s).

3.4 A one-port dual-channel radiometer with the cancellation of a correlation noise

The superheterodyne detection of a thermal and bioinformation radiation from a human body, animals, plants and other objects can significantly increase the sensitivity of radiometers without using low-noise

input HF amplifiers band L and M. Since the input signal of a radiometer has a wide spectrum, which differs little from the spectra of intrinsic noise signals of RS input elements (mixers, local oscillators, etc.), it becomes necessary to separate a valid noise signal received by the antenna and the instrument noise. This problem is most easily solved in dual-channel superheterodyne radiometers, consisting of two identical channels with mixers and a common local oscillator. The measuring circuit is constructed in such a way that the constant components of currents or voltages, caused by intrinsic noise, are taken away at the channel outputs. As a result, valid signals are summed.

In Fig. 3.8, a functional diagram of a dual-channel superheterodyne radiometer developed by authors [51] is given, which has a significantly simplified microwave part (block I) and a more complex block of intermediate (II) and low (III) frequency, as well as a block for recording measurement results (IV).

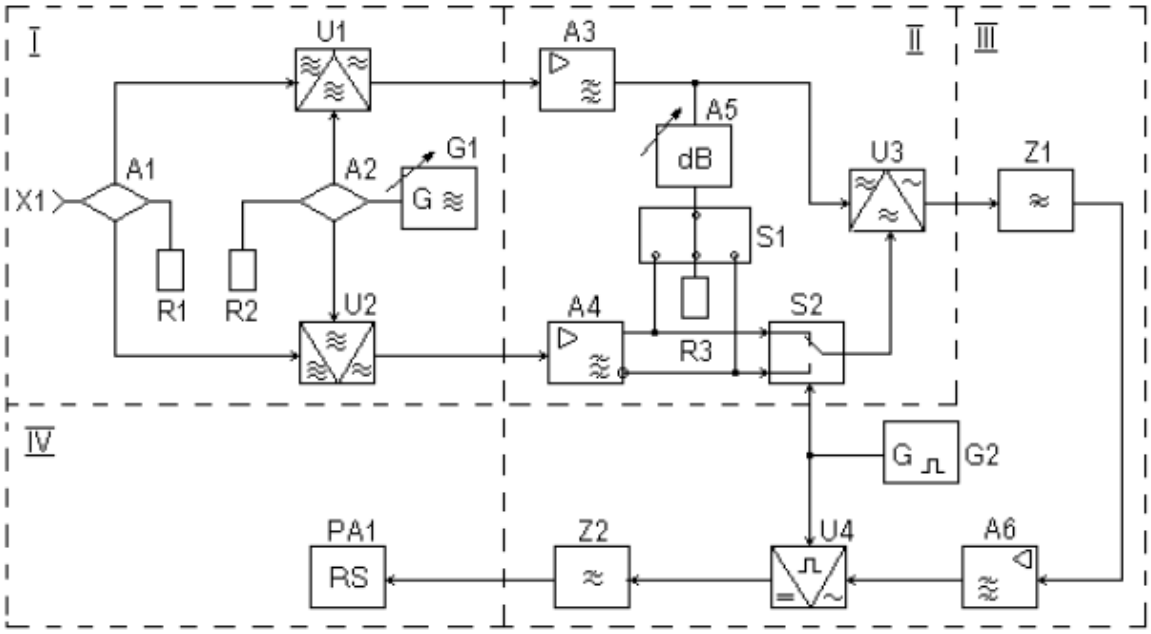

Figure 3.8 – The one-port dual-channel radiometer with the cancellation of a correlation noise

A dual-channel superheterodyne radiometer operates in the following way. The signal $U_1(t)$ received by the X1 antenna has a wide spectrum, which can be represented as a complex quantity $\dot{U}_1$, the modulus and argument of which vary randomly. Since the load of the hybrid waveguide

tee A1 is the equivalent of the antenna R1, two identical complex signals with the opposite sign are formed at the outputs of the hybrid tee: $\dot{U}_2 = \dot{U}_1$ and $\dot{U}_3 = -\dot{U}_1$. The signals $\dot{U}_2$ and $\dot{U}_3$ are fed to the inputs of the mixers U1 and U2 of the receiver channels, to the other inputs of which the signal of the common local oscillator G1 passes through the shoulders of the hybrid tee A2. The intensities of the input signals of the mixers U1 and U2 are the identical and can be represented as:

$$\overline{U}_2^2 = \overline{U}_3^2 = \frac{1}{2} S_1 K_1 T_X \Delta f_1 = \frac{1}{2} \overline{U}_1^2, \tag{3.44}$$

where S_1 – the antenna sensitivity; T_X – a temperature of a radiation object; Δf_1 – a band of the received frequency; K_1 – a coefficient, determined by the constants of electromagnetic radiation of an object.

The noise of a dual-channel super heterodyne receiver is determined by the noise received at the inputs of a receiver, that is, to the inputs of the mixers U1 and U2, as well as the noise of the mixers, the local oscillator and the intermediate frequency amplifiers. The noise intensity at the inputs of the mixers is determined by the noise properties of the receiver:

$$\overline{U}_4^2 = \overline{U}_5^2 = k(F-1)T_0 \Delta f_2, \tag{3.45}$$

where k – Boltzmann's constant; F – receiver noise factor; T_0 – ambient temperature $(T_0 = 293K)$; Δf_2 – a transition band of intermediate frequency amplifiers.

The received signal in the radiometer is of the same order with the intrinsic noise of the receiver. Therefore, the signals at the inputs of the mixers can be represented as the sum of complex quantities:

$$\dot{U}_4 = \frac{1}{2} \dot{U}_1 + \dot{U}_4, \tag{3.46}$$

$$\dot{U}_5 = -\frac{1}{2} \dot{U}_1 + \dot{U}_5. \tag{3.47}$$

The signal $\dot{U}_1$ is received both through the main and image channels of the radiometer receiver and are equivalent in relation to each other. Therefore, the signals at the outputs of amplifiers A3 and A4 of intermediate frequency can be represented as follows:

$$\dot{U}_6 = 2S_4K_6\left(\frac{1}{2}\dot{U}_1 + \dot{U}_4\right)\dot{U}_8, \tag{3.48}$$

$$\dot{U}_7 = 2S_5K_7\left(-\frac{1}{2}\dot{U}_1 + \dot{U}_5\right)\left(-\dot{U}_8\right) = 2S_5K_7\left(\frac{1}{2}\dot{U}_1 - \dot{U}_5\right)\dot{U}_8, \tag{3.49}$$

where S_4 и S_5 – the conversion conductance of mixers U1 и U2; K_6 и K_7 – a gain factor of amplifiers A3 и A4; $\dot{U}_8$ – heterodyne G1 complex voltage.

A signal is generated at the output of the intermediate frequency amplifier A4 (at its inverse output):

$$\dot{U}_9 = -\dot{U}_7 = 2S_5K_7\left(-\frac{1}{2}\dot{U}_1 + \dot{U}_5\right)\dot{U}_8. \tag{3.50}$$

The automatic switch S2 is controlled by the rectangular voltage of a generator G2 of the low frequency F_{G2}. Therefore, the signal $\dot{U}_7$ passes through its output at one position of the switch; and the signal $\dot{U}_9$ passes at the other position. In this case, the switch S1 is installed in the closed center position and its output is connected to the load R3. In conditions of continuous operation of the switch with a frequency F_{G2}, packets of noise signals with a half-period switching are formed at its output $\left(\frac{1}{F_{\text{П}}}\right)$:

$$\dot{U}'_{10} = 2S_5K_7\left(\frac{1}{2}\dot{U}_1 - \dot{U}_5\right)\dot{U}_8,, 0 < t < \frac{1}{2F_{G2}}, \tag{3.51}$$

$$\dot{U}''_{10} = 2S_5K_7\left(-\frac{1}{2}\dot{U}_1 + \dot{U}_5\right)\dot{U}_8, \frac{1}{2F_{G2}} < t < \frac{1}{F_{G2}}. \tag{3.52}$$

The intermediate frequency signals are multiplied in the balanced mixer U3. The following signal is generated at the output of the balanced mixer U3 for one half-cycle of the switch S2 operation:

$$\dot{U}'_{11} = S_{11}\dot{U}_6\dot{U}'_{10} = 4S_{11}S_4S_5K_6K_7\left(\frac{1}{4}\dot{U}_1^2 - \frac{1}{2}\dot{U}_1\dot{U}_5 + \frac{1}{2}\dot{U}_1\dot{U}_4 - \dot{U}_4\dot{U}_5\right)\dot{U}_8^2, \tag{3.53}$$

where S_{11} – conversion conductance of the balanced mixer U3.

The following signal is generated during the second half-cycle of the switch S2 operation:

$$\dot{U}''_{11} = S_{11}\dot{U}_6\dot{U}''_{10} = 4S_{11}S_4S_5K_6K_7\left(-\frac{1}{4}\dot{U}_1^2 + \frac{1}{2}\dot{U}_1\dot{U}_5 - \frac{1}{2}\dot{U}_1\dot{U}_4 + \dot{U}_4\dot{U}_5\right)\dot{U}_8^2. \quad (3.54)$$

Noises of two independent channels of RS receivers in the presence of a good isolation are not correlated between themselves. Therefore, the product of noise signals $\dot{U}_4\dot{U}_5$ does not give a constant component, but only expands the spectrum of the result signaling tone.

The signal $\dot{U}_1$ received by the antenna is also not correlated with noise $\dot{U}_4$ and $\dot{U}_5$. Products of noise signals $\dot{U}_1\dot{U}_5$ and $\dot{U}_1\dot{U}_4$ do not form a constant voltage component. At the same time, the block of the noise signal $\dot{U}_1^2$ gives a constant component that is proportional to its dispersion, i.e. intensity (3.44).In this case, the sign of the constant component of the signal $\dot{U}_1^2$ (3.53) и (3.54) reverses when switching signals, which means the formation of an alternating component of the output voltage of the balanced mixer U3 with a switching frequency F_{G2}.

The high-pass filter Z1 extracts the desired signal of alternating voltage and the voltage of the high-frequency part of the noise, which were created as a result of the balanced mixing of uncorrelated noise signals. The filter suppresses low-frequency (the most intense one) noise.

The voltage at the filter Z1 output can be represented as:

$$U_{12}(t) = K_{12}\left[\alpha\overline{U}_1^2\overline{U}_8^2 \, sign \, sin\,\Omega t + U_{11}(t)\right], \quad (3.55)$$

where K_{12} – high pass filter Z1 coefficient; $\alpha = S_{11}S_4S_5K_6K_7$ – conversion factor of the dual-channel part of the radiometer; $U_{11}(t)$ – voltage of high-frequency noise falling into the filter band Z1; $\Omega = 2\pi F_{G2}$ – switching circular frequency.

The voltage $U_{12}(t)$ is allocated by a low-frequency selective amplifier A6, tuned to the frequency F_{G2} of the generator G2:

$$U_{13}(t) = K_{12}K_{13}\left[\alpha\overline{U}_1^2\overline{U}_8^2 \, sin\,\Omega t + U_{12}(t)\right], \quad (3.56)$$

where K_{13} – amplifier gain A6; $U_{12}(t)$ – part of high-frequency noise, falling into the transition band of the selective amplifier A6.

The amplified voltage is rectified by a synchronous detector U4, controlled synchronously with switch S2 by the rectangular voltage of generator G2. The converted voltage takes the following form, as a result

of multiplication in a synchronous detector with a control voltage of the frequency F_{G2}:

$$U_{14}(t) = K_{12}K_{13}K_{14}\left[\alpha\overline{U}_1^2\overline{U}_8^2 + U_{13}\left(\sum_{i=1}^{K} sin(\Omega \pm \Omega_i)\cdot t\right)\right], \quad (3.57)$$

where K_{14} – a gain of synchronous detector U4; $U_{13}\left(\sum_{i=1}^{K} sin(\Omega \pm \Omega_i)\cdot t\right)$ – voltage of combination frequencies; Ω_i – frequencies close to the switching frequency Ω, falling into the bandwidth of the amplifier A6.

The voltage (3.57) emitted by the low-pass filter Z2 is supplied to the recorder PA1. Intermodulation components of summation frequencies $\sum_{i=1}^{K} sin(\Omega \pm \Omega_i)\cdot t$ are almost completely suppressed at the time constant τ of the filter, significantly exceeding the rectified voltage period $\left(\tau \geq \frac{100}{F_{G2}}\right)$. The recorder receives only constant voltage and low-frequency noises of beats $\sum_{i=1}^{K}(\Omega - \Omega_i)$, which amplitude is reduced by a factor of τ:

$$U_{15}(t) = K_{12}K_{13}K_{14}K_{15}\alpha\overline{U}_1^2\overline{U}_8^2 + \frac{1}{\tau}U_{14}\left(\sum_{i=1}^{n} sin(\Omega - \Omega_i)\cdot t\right), \quad (3.58)$$

where K_{15} – the filter Z2 gain of low frequencies; $U_{14}\left(\sum_{i=1}^{n} sin(\Omega - \Omega_i)\cdot t\right)$ spectrum of combination frequencies, in which the maximum number n is determined by the working band of the registrar.

The recorded voltage has the following form with a sufficiently large value of the time constant τ of the filter Z2, taking into account the value of the intensity (3.44) of the received signal:

$$U_{16} = S_0(T_X + \Delta T), \quad (3.59)$$

where $S_0 = S_1K_1S_4S_5K_6K_7S_{11}K_{12}K_{13}K_{14}K_{15}$ – the resulting sensitivity of a dual-channel radiometer with a phase switching of intermediate frequency signals; ΔT – a pointing error of a radiometer.

A pointing error ΔT of a radiometer emerges due to the presence of a correlated noise in radiometer channels, arising from the incomplete isolation of receiver channels by the hybrid tees A1 and A2, as well as the thermodynamic inadequacy of an antenna X1 and the equivalent of an antenna R1.

The antenna X1 is shielded before measuring to compensate for the pointing error ΔT. A switch S1 is moved to one of the full distance positions. A correlated noise begins to arrive at both inputs of a balanced mixer U3 in a corresponding switching half-period when connecting the output of an intermediate frequency amplifier A3 through an attenuator A5 to one of the inputs of an automatic switch S2.An additional pulse of constant voltage appears at the output of the mixer U3 from the product of these correlated noises. The intensity of such a pulse is controlled by the A5 attenuator. An additional noise signal is not supplied to the second input of a balanced mixer U3 and the additional pulse at the output of a mixer U3 is absent in the opposite position of a switch S2.

If a switch S1 is moved to the second full distance position, then the correlated noise will enter the next half-cycle switching to a balanced mixer U3.

The corresponding constant voltage pulse will appear precisely in this half-cycle at the output of a balanced mixer. Since the DC voltage pulses appear in different half-cycles of signal switching in accordance with the position of a switch S1, the initial phase of an additional variable component changes by 180° at the output of a high-pass filter Z1.

Therefore, the output voltage of the filter Z1 can be represented as follows if there is an additional connection between the channels of the radiometer through the attenuator A5:

$$\begin{aligned} U'_{12}(t) = K_{12}\Big[&\alpha\overline{U}_0^2\overline{U}_8^2 \operatorname{sign}\sin\Omega t \pm \\ &\pm 4S_{11}S_4^2K_6^2K_{19}\overline{U}_4^2\overline{U}_8^2 \operatorname{sign}\sin\Omega t + U_{11}(t)\Big], \end{aligned} \tag{3.60}$$

where $\overline{U}_0^2$ – intensity of correlated noises that are entailed to inputs of mixers A3 and A4; K_{19} – attenuator gain A5.

The position of the switch S1 is chosen in such a way that the variable components in the formula (3.60) are in the reversed phase. In this case, the voltage value $U'_{12}(t)$ is set equal to zero by adjusting the attenuator A5, and

after amplifying it A6 and rectifying it with the synchronous detector U4, the zero value is fixed by the recorder PA1.

We determine the necessary attenuator gain A5

$$K_{19} = \frac{S_5 K_7}{S_4 K_6} \cdot \frac{\overline{U}_0^2}{4\overline{U}_4^2}. \tag{3.62}$$

from the equation

$$\alpha \overline{U}_0^2 = 4 S_{11} S_4^2 K_6^2 K_{19} \overline{U}_4^2, \tag{3.61}$$

taking into account the value α (3.55).

The parameters of the receiver channels are chosen the same in dual-channel radiometer $\left(S_4 = S_5,\ K_6 = K_7\right)$. Then a transfer constant is:

$$K_{19} = \frac{\overline{U}_0^2}{4\overline{U}_4^2}. \tag{3.63}$$

If the intensity of the correlated noise $\overline{U}_0^2$ is expressed taking into account the pointing error ΔT of the radiometer, then we obtain similarly to expression (3.44):

$$\overline{U}_0^2 = S_1 K_1 \Delta f_1 \Delta T. \tag{3.64}$$

Substituting into the expression (3.63) $\overline{U}_0^2$ from (3.64) and $\overline{U}_4^2$ from (3.45) taking into consideration that both noise signals are amplified in the same bandwidth of amplifiers of intermediate frequency, we obtain:

$$K_{19} = \frac{S_1 K_1}{4k\left(F-1\right)T_0} \Delta T. \tag{3.65}$$

Thus, the transfer coefficient of the attenuator A5 is uniquely determined by the pointing error ΔT and does not depend on the instability of the parameters of the RS converter circuits. The latter increases the stability of RS zero, and therefore provides an increase in its accuracy and sensitivity.

As follows from expressions (3.51), (3.52) and (3.55), the inevitable inequality of the transfer constants of the switch S2 arms does not cause a pointer centering error that is inherent in the known circuits of radiometers.

This inequality causes only a slight change in the constant components in expressions (3.53) and (3.54) and a slight decrease in the sensitivity of

the RS, which is easily compensated by an increase in the gain of the low-frequency amplifier U4. If we take into account that the automatic switch operates in circuits of a relatively low intermediate frequency, then a significant reduction is achieved in pointing errors from spurious connections through the closed arms of the switch.

The demands are significantly reduced for the speed of the switch and the uniformity of its frequency response at an intermediate frequency. The simplified circuit of the microwave unit (I) allows it to be implemented as a replaceable converter unit for one or other section of the waveguide. The operability of the radiometric system in the entire range of mm waves (30-300 GHz) can be ensured through changes in the input microwave unit.

3.5 A dual-channel differential radiometric system for recording the difference values of radiation intensities

To study the gradients of the electromagnetic field of biological objects, you can use differential radiometers that measure the difference in radiation intensities from neighboring or remote biologically active points (BAP), as well as various (for example, symmetrical) parts of a patient's body to compare the radiation of two patients.

To increase the sensitivity of differential radiometers, it is reasonably to use power feedback to small difference intensities, which provides a deep modulation. In Fig. 3.9, a functional diagram of a differential RS positive feedback [52] is presented, which consists of two microwave antennas X1 and X2, attached to matching elements A1 and A2 that are connected to two inputs of the microwave switch S1. A hybrid tee A4 is connected to the output of a microwave switch, and the matched load R1 and the controlled attenuator A3 are connected to its inputs, too. A microwave amplifier A5, a microwave mixer U1, an intermediate frequency amplifier (IFA) with a filter Z1, a quadratic detector U2, a low-frequency amplifier (LFA) A7, a synchronous detector U3, and a recorder P1 are connected tandem to the output of a hybrid tee A4.

The switching generator G2 is connected to the control inputs of the microwave switch S1 and the synchronous detector U3. A noise generator G1 is connected to the first input of the controlled attenuator A3. A control unit A6 is connected to the second input, the control module of which is connected to the output of the low-frequency amplifier A7.

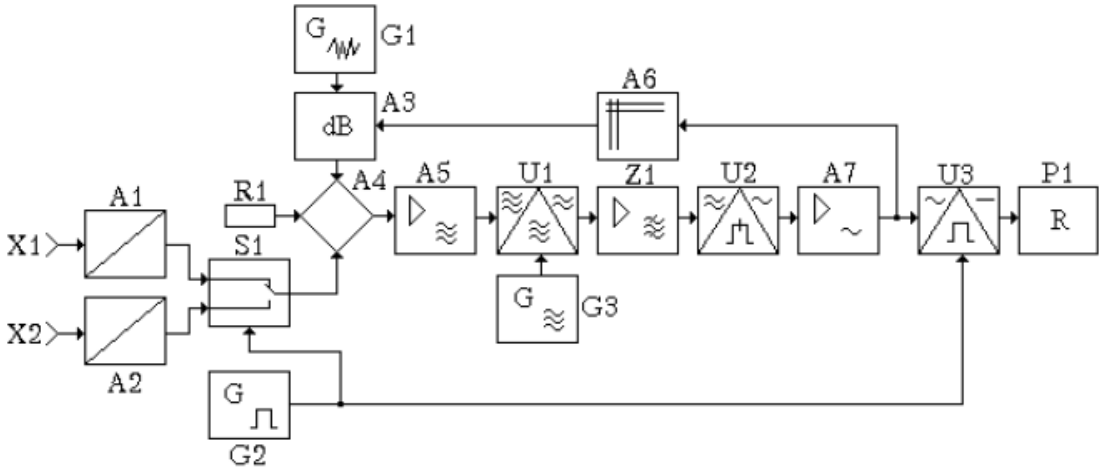

Figure 3.9 – Differential RS for recording the difference in radiation intensities

Microwave antennas X1 and X2 receive the thermal radiation from the surface of an object. The output signals of an antenna can be represented as dispersions of random signals:

$$\overline{U}_1^2 = ST_1, \tag{3.66}$$

$$\overline{U}_2^2 = ST_2, \tag{3.67}$$

where S – the antennas sensitivity; T_1 and T_2 – a temperature of controlled areas of an object surface.

The signals $U_1(t)$ and $U_2(t)$ through matching elements A1 and A2, for example, flexible dielectric (fluoroplastic) waveguides, and the arms of the microwave switch S1 periodically arrive at one input of a hybrid tee A4.

The signal from the noise generator G1 is fed to the second input of the tee through the attenuator A3, controlled by an electrical voltage of only one polarity – negative or positive one.

Since the controlled input of the attenuator is connected through the control unit A6, which is a rectangular voltage generator and a power amplifier that is connected to the output of the LF- amplifier A7, the attenuator opens for a time equal to the half-period of a low-frequency voltage, which is the envelope of the modulated microwave signal. In this case, the half-cycle of the low frequency is equal to the half-cycle of the switching frequency of the microwave switch S1.

In the first switching half-period, when a signal $U_1(t)>U_2(t)$ is fed to the input of the microwave switch, the attenuator A3 opens.

Independent noise signals are summed in a hybrid tee, the sum dispersion of which can be represented in the following way:

$$\overline{U}_4'^2 = K_1\left(\overline{U}_1^2 + K_2\overline{U}_3^2 + \overline{U}_5^2\right), \quad (3.68)$$

where K_1 – the power transmission coefficient of the hybrid tee A4; K_2 – the attenuator power transfer coefficient A3; $U_3(t)$ – the noise generator G1; $U_5(t)$ –the intrinsic noise of a one-link path of a differential radiometer, brought to the input of the amplifier A5.

In the second switching half-cycle, the signal $U_2(t)<U_1(t)$ is supplied to the input of the microwave switch S1, the attenuator A3 is closed by a low-frequency voltage of the opposite polarity (K_2 =0). Therefore, the total noise signal can be represented by the dispersion:

$$\overline{U}''^2_4 = K_1\left(\overline{U}_2^2 + \overline{U}_5^2\right). \quad (3.69)$$

Signals $U_4'(t)$ and $U_4''(t)$, that create one modulated signal, are periodically fed to mixer U1. An amplifier with a filter Z1 selects a signal of difference frequency, the spectrum of which is determined by the passband of the filter.

The quadratic detector U2 receives packets of noise signals of an intermediate frequency, which can be represented as a dispersion:

$$\overline{U}'^2_6 = K_3K_1\left(\overline{U}_1^2 + K_2\overline{U}_3^2 + \overline{U}_5^2\right), \quad (3.70)$$

$$\overline{U}''^2_6 = K_3K_1\left(\overline{U}_2^2 + \overline{U}_5^2\right), \quad (3.71)$$

where K_3 – a gain of the amplifier Z1 in the filter bandpass.

The voltage of the envelope of the switching frequency with the amplitude is allocated at the output of the quadratic detector U2:

$$U_7 = K_1K_3K_4\left(\overline{U}_1^2 + K_2\overline{U}_3^2 - \overline{U}_2^2\right), \quad (3.72)$$

where K_4 – a conversion coefficient of the quadratic detector U2.

An alternating voltage with an amplitude $U_7(t)$ controls the operation of an attenuator A3 and is simultaneously rectified by a synchronous detector U3. The rectified voltage, which is fixed by a indicator P1, can be written as follows:

$$U_8 = K_1K_3K_5K_6\left(\overline{U}_1^2 - \overline{U}_2^2 + K_2\overline{U}_3^2\right) = \alpha\left(\overline{U}_1^2 - \overline{U}_2^2 + K_2\overline{U}_3^2\right), \quad (3.73)$$

where K_5 – the gain of amplifier A7; K_6 – a conversion coefficient of asynchronous detector U3; $\alpha = K_1 K_3 K_5 K_6$ – a resulting coefficient of a direct conversion of RS.

The gain of the controlled attenuator A3 is proportional to the amplitude of the low-frequency voltage $U_7(t)$:

$$K_2 = K_7 U_7, \tag{3.74}$$

where K_7 – the gear ratio of a control unit A6.

If a control voltage $U_7(t)$ is expressed through the output voltage $U_8(t)$, then:

$$K_2 = \frac{K_7}{K_6} U_8 = \beta U_8, \tag{3.75}$$

where $\beta = \frac{K_7}{K_6}$ – a coefficient of the inverse transformation of a RS output voltage.

Substituting the value a transmission coefficient K_2 of the controlled attenuator A3 from expression (3.75) into the expression (3.73), we get:

$$U_8 = \frac{\alpha}{1 - \alpha\beta\overline{U}_3^2}\left(\overline{U}_1^2 - \overline{U}_2^2\right). \tag{3.76}$$

Using expressions (3.76), (3.66) and (3.67), which take into account the temperature of controlled areas of an object, we finally get:

$$U_8' = \frac{\alpha S}{1 - \alpha\beta\overline{U}_3^2}\left(T_1 - T_2\right). \tag{3.77}$$

A change in the sign of the measured temperature difference $\left(T_1 < T_2\right)$ leads to a change in the phase of the low-frequency voltage at the output of the A7 amplifier by 180°.

As a result, the switching half-period changes, in which the controlled attenuator A3 opens, and the noise signal from the generator G1 is summed not with the signal $U_1(t)$, but with the signal $U_2(t)$ (with higher power). Thus, the operation of differential RS is not disturbed, and its indications will be equal to:

$$U_8'' = \frac{\alpha S}{1 - \alpha\beta\overline{U}_3^2}\left(T_2 - T_1\right). \tag{3.78}$$

The rectified voltage can be written in the following form because when the phase of the voltage of a switching frequency changes by 180°, the polarity of a rectified voltage changes at the output of a synchronous detector U3:

$$U_8 = \pm \frac{\alpha S}{1 - \alpha\beta\overline{U}_3^2}(T_1 - T_2). \tag{3.79}$$

Thus, the considered differential RS works consistently at any temperature ratio of the controlled object ($T_1 < T_2$ or $T_1 > T_2$), and the polarity of the measured voltage determines the sign of the controlled temperature difference. If the feedback coupling is absent in differential RS ($\beta = 0$), then the output voltage has the form:

$$U_9 = \alpha S(T_1 - T_2). \tag{3.80}$$

The introduction of positive feedback ($\beta > 0$) leads to the appearance of an output voltage, which is described by expression (3.79), and an increase in the sensitivity of the differential radiometer by a factor equal to:

$$\gamma = \frac{U_8}{U_9} = \frac{1}{1 - \alpha\beta\overline{U}_3^2}. \tag{3.81}$$

If a denominator of expression (3.81), for example, is equal to 0.01, then the sensitivity of differential RS will increase 100 times due to the feedback coupling.

The maximum gain in sensitivity with the condition $\left(\left[1 - \alpha\beta\overline{U}_3^2\right] \to 0\right)$ is limited by the possibility of auto-oscillations in the positive feedback circuit. Phase compensation chains and amplitude limiting elements are introduced to suppress auto-oscillations in control unit A6.

In practice, the fluctuation threshold of sensitivity of a differential radiometer can be reduced to $10^{-22}...10^{-23}$W/Hz by introducing feedback coupling, which corresponds to sensitivity by temperature difference $10^{-4}...10^{-5}$ K.

The usage of the considered differential RS allows to study the gradients of the temperature fields of biological objects in the range of their electromagnetic radiation and to compare the field intensities in biological active points of these objects.

3.6 A multifunctional RS for measuring energy and correlation characteristics of signals

Researching complex biological objects, we experience tasks, associated with measuring the intensity of radiation as well as the study of the structure of emitted signals. It can be achieved by simultaneous measuring the power and correlation function of the signal. However, difficulties arise regarding the multiplication of current signals of different time during alternate periodic signal conversion in RS one-link path.

The use of two switching frequencies in a modulation RS circuit allows this problem to be solved. Multifunctional RS [8] is made in the form of a one-channel circuit with time division of signals (Fig. 3.10).

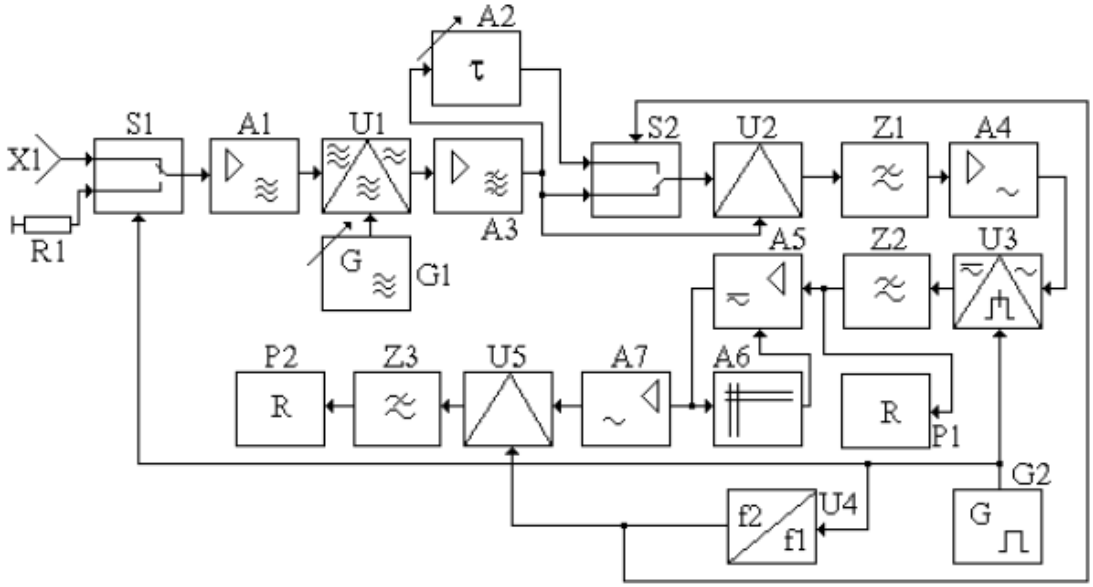

Figure 3.10 – A multifunctional RS for measuring energy and correlation characteristics of signals

The circuit consists of a connected in sequence antenna X1, the first switch S1 with a load R1 that is equivalent to an antenna, a microwave amplifier A1, a mixer U1 with a tunable local oscillator G1, and an intermediate frequency amplifier (IFA) A3. It is followed by a correlation processing unit, which includes a time delay unit A2, the second switch S2, the first multiplier U2, the first low-pass filter Z1 and the first LFA A4. The second multiplier U3, the second low-pass filter Z2 with the first recording unit P1, the controlled broadband amplifier A5 with an automatic gain control unit A6, the second low-frequency amplifier A7, the third multiplier U5, the third low-pass filter Z3 and the second recording unit P2 are connected in series to this block. In addition, the multifunctional RS

contains a series-connected switching generator G2 and a frequency divider U4. Moreover, the output of the switching generator is also connected to the controlled inputs of the first switch S1 and the second multiplier U3. The output of the frequency divider U4 is connected to the controlled input of the second switch S2 and the second input of the third multiplier U5.

The first input of the second switch S2 is connected to the output of the intermediate-frequency amplifier A3 through the time delay link A2, and the second input of the switch S2 is connected directly to the amplifier A3. The second input of the first multiplier U2 is also connected to the output of the intermediate-frequency amplifier A3.

The electromagnetic radiation of a researchable object in the range of super-high frequencies is received by an antenna X1, to the output of which a microwave amplifier A1 is connected through the switch S1.

Switching generator G2 forms a low frequency rectangular voltage («square wave») f_1, which controls the operation of switch S1. The output rectangular voltage of the frequency divider U4 controls the operation of switch S2 with a lower frequency:

$$f_2 = \frac{f_1}{2n}, \tag{3.82}$$

where n – integral number 1, 2, 3...

Since the phases of the controlled voltages are synchronized and the switching frequencies are interconnected by the relation (3.82), the radiometer has four repetitive clock cycles due to different states of the switches S1 and S2. Since the switching frequency $f_1 > f_2$, first, we will consider the operation of a one link path with the position of the switch S2, shown in Fig. 3.10, and periodic switching of the switch S1.

The output signal of the antenna X1 can be represented as dispersion according to (3.13)

$$\overline{U_1}^2 = S_1 T_X, \tag{3.83}$$

where S_1 – antenna sensitivity in the microwave range; T_x – radiation temperature of the researchable object.

The input of the microwave amplifier A1 is switched periodically with a frequency f_1 from the output of the antenna X1 to the equivalent load R1 that is equal to the output resistance of the antenna X1.

The output signal of the microwave amplifier A1 can be represented as a dispersion taking into account the intrinsic noise when connected to the antenna:

$$\overline{U}_{31}^2 = K_1\left(\overline{U}_1^2 + \overline{U}_2^2\right), \tag{3.84}$$

where U_2 – intrinsic noise of the amplifier coming to its input; K_1 – power amplification coefficient of the microwave amplifier.

When the switch S1 is switched to the equivalent load R1, the input resistance of the microwave amplifier A1 does not change. Therefore, only the intrinsic noise of the amplifier is amplified without spurious modulation, and the output signal can be represented as dispersion:

$$\overline{U}_{32}^2 = K_1\overline{U}_2^2. \tag{3.85}$$

Packets of noise voltage with dispersion (3.84) and (3.85) are converted into the area of lower intermediate frequencies in the frequency spectrum with a mixer U1 and a local oscillator G1. Packets of noise signals are formed alternately at the output of the band-pass amplifier of intermediate frequency A3, the dispersion of which can be represented as:

$$\overline{U}_4^2 = S_2 K_2 \overline{U}_{31}^2 = S_2 K_2 K_1\left(\overline{U}_1^2 + \overline{U}_2^2\right), \tag{3.86}$$

$$\overline{U}_5^2 = S_2 K_2 \overline{U}_{32}^2 = S_2 K_2 K_1 \overline{U}_2^2, \tag{3.87}$$

where S_2 – frequency conversion conductance; K_2 – amplification gain factor of intermediate-frequency amplifier in the transition band.

The resolved and amplified signals are multiplied among themselves in the first multiplier U2. As a result, video pulses with amplitudes appear at the output of the first low-pass filter Z1, which are proportional to the power of microwave noise signals:

$$U_6 = S_3 K_3 \overline{U}_4^2, \tag{3.88}$$

$$U_7 = S_3 K_3 \overline{U}_5^2, \tag{3.89}$$

where S_3 –U2 multiplier conversion conductance; K_3 –the transmission coefficient of the low-pass filter Z1in constant voltage mode.

The first LFA A4 isolates and amplifies the frequency envelope*f1*voltage from a sequence of video pulses with amplitudes (3.88) and (3.89)

$$U_8 = K_4\left(\frac{U_6 - U_7}{2}\right) sign\, sin\, 2\pi f_1 t\,, \tag{3.90}$$

where K_4 – amplifier gain A4; $sign\, sin\, 2\pi f_1 t$ – rectangular envelope of video pulses.

An alternating voltage (3.90) is supplied to the first input of the second multiplier U3, to the second input of which a meander of the comparison voltage of the frequency f_1 is supplied. We get a constant voltage of the following form at the output of the second low-pass filter Z2:

$$U_9 = S_4 K_4\left(\frac{U_6 - U_7}{2}\right)(sign\, sin\, 2\pi f_1 t)^2\,, \tag{3.91}$$

where S_3 – U3 multiplier conversion conductance; K_5 – the transmission coefficient of the low-pass filter Z2.

Substituting the amplitude value of the video pulses (3.88) and (3.89) in the expression (3.91), we obtain:

$$U_9 = \frac{K_5 S_4 K_4 S_3 K_3 S_2 K_2 K_1}{2}\overline{U}_1^2 = S_0 \overline{U}_1^2\,, \tag{3.92}$$

where $S_o = \frac{K_5 S_4 K_4 S_3 K_3 S_2 K_2 K_1}{2}$ – the summarized conversion conductance of one-link path (from the block X1 to the output Z2) of RS.

As follows from expression (3.92), the voltage U9 is proportional to the power of electromagnetic radiation of the researchable object in the microwave range. This voltage is measured and recorded in the first recording unit P1. The one-channel conversion conductance S_1 determined during RS calibration.

We will consider the operation of the one-channel RS path with the opposite position of switch S2 and the periodic operation of switch S1. In this case, the conversion processes to switch S2 are similar to the processes described above. Packets of noise signals with dispersion (3.86) and (3.87) alternately arrive after the switch S2 to one input of the multiplier U2. The same signal packets, but delayed by the dead time element A2 for time τ, go to the second input. Therefore, video pulses with amplitudes, which are proportional to the correlation moments, are formed at the output of the first low-pass filter Z1:

$$R_1(\tau) = S_3 K_3 \overline{U}_4^2 \rho_{12}(\tau), \tag{3.93}$$

$$R_2(\tau) = S_3 K_3 \overline{U}_5^2 \rho_2(\tau), \tag{3.94}$$

where $\rho_{12}(\tau)$ – the normalized function of correlation of signals mixture of the antenna X1 and noise of the microwave amplifier A1; $\rho_2(\tau)$ – the normalized function of correlation of intrinsic noise of a microwave amplifier A1.

The amplifier A4 isolates and amplifies the voltage of the envelope of video pulses with the frequency f_1:

$$U_{10} = K_4\left[\frac{R_1(\tau) - R_2(\tau)}{2}\right] sign \sin 2\pi f_1 t\,. \qquad (3.95)$$

The noise signal from the antenna X1 does not depend on the intrinsic noise of the amplifier A1, so the constant voltage has the following form at the output of the low-pass filter Z2:

$$U_{11} = S_o \overline{U_1^2}\,\rho_1(\tau), \qquad (3.96)$$

where $\rho_1(\tau)$ – the normalized function of correlation of the antenna X1 signals.

When there is no delay in link A2 ($\tau = 0$), the normalized function of correlation takes a value of 1 ($\rho_1(0) = 1$). Therefore, the previously obtained constant component of the voltage (3.92) corresponds to the maximum value of the correlation moment, i.e. signal power.

The correlation moment decreases with the introduction of a time delay by link A2 and, as a result, the value of the correlation function decreases ($\rho_1(\tau) < \rho_1(0)$). Therefore voltage U_{11} is always less than the voltage U_9 at $\tau > 0$ ($U_{11} < U_9$).

As a result of periodic commutations of switch S2 with a frequency $f_1 > f_2$, voltage constants U_9 and U_{11} are alternately generated in the time interval $\Delta t = 1/2f_2$ at the output of the second low-pass filter Z2. The pulses of these voltages with a duration Δt are alternately amplified by the broadband amplifier A5, the control circuit of which includes an automatic gain control unit (AGC) A6. The amplitudes of the output pulses get the following value, taking into consideration the value of the gain K_6, which is set by the AGC block:

$$U_{12} = K_6 U_9; \qquad 0 < T < \frac{1}{2f_2}, \qquad (3.97)$$

$$U_{13} = K_6 U_{11}; \qquad \frac{1}{2f_2} < T < \frac{1}{f_2}. \qquad (3.98)$$

The second amplifier A7 isolates and amplifies the alternating voltage component of the second switching frequency f_2:

$$U_{14} = K_7\left(\frac{U_{12} - U_{13}}{2}\right) sign \sin 2\pi\ f_2, \qquad (3.99)$$

where K_7 – ULF gain A7.

The alternating voltage (3.99) is supplied to one input of the third multiplier U5, to the second input of which the meander of the reference voltage of the frequency f_2 is supplied. A constant voltage is generated at the output of the third low-pass filter Z3 after smoothing:

$$U_{15} = S_5 K_7 K_8\left(\frac{U_{12} - U_{13}}{2}\right)(sign\ sin\ 2\pi f_2 t)^2, \qquad (3.100)$$

where S_5 – the multiplier sensitivity U5; K_8 – the filter Z3 gain.

After substituting the voltages U_{12} and U_{13} with (3.97) and (3.98) into expression (3.100), taking into account their previous values (3.83) ... (3.96), we get:

$$U_{16} = S_0 S_5 K_6 K_7 K_8\left[1 - \rho_1(\tau)\right]\overline{U}_1^2. \qquad (3.101)$$

The gain K_6 is determined by the action of the AGC block A6 on the control input of amplifier A5. When the AGC block A6 works with a peak detector (fast response and slow recovery), the gain will be determined by larger amplitude in the sequence of voltage pulses U_{11} and U_9. Since voltage $U_9 = S_o\overline{U}_1^2\rho_1(\tau)$ at $\rho_1(0) = 1$ is always bigger than voltage $U_{11} = S_o\overline{U}_1^2\rho_1(\tau)$, then:

$$K_6 = \frac{U_0}{U_9} = \frac{U_0}{S_o\overline{U}_1^2\rho_1(0)}, \qquad (3.102)$$

where U_o – the amplifier output voltage A5 in limiting mode ($U_o = const$).

Substituting the value of the gain K_6 from the expression (3.102) in the proportion (3.101), we obtain:

$$U_{17} = \frac{S_5 K_6 K_7 K_8\left[1 - \rho_1(\tau)\right]U_0}{\rho_1(0)} = \frac{\alpha\left[1 - \rho_1(\tau)\right]U_0}{\rho_1(0)}, \qquad (3.103)$$

where $\alpha = S_5 K_6 K_7 K_8$ – a low-frequency voltage conversion factor.

The voltage U_{17} is detected by the second registration unit P2.

Thus, changing the time delay τ in link A2 from 0 to τ_{max}, we can record the relative change in the correlation function $\rho_1(\tau)$ of the received microwave signal.

In this case, the measurement result is not affected by the level of both the received signal $\left(\overline{U}_1^2\right)$ as well as the level of the intrinsic noise of the microwave amplifier $\left(\overline{U}_2^2\right)$, the mixer and other elements of the one-channel path. The inconstancy of the resulting conversion coefficient of a one-channel radiometer path does not affect the registration $\left(K_1 K_2 S_2 K_3 S_3 K_4 S_4 K_5\right)$. The conversion coefficient α is stable and is determined during the RS calibration.

The considered scheme of multifunctional RS allows us to register its autocorrelation function along with the power of measuring electromagnetic radiation in the microwave range.

The latter makes it possible to analyze the structure of electromagnetic radiation and, therefore, to identify the source of thermal and bioinformation radiation in the microwave range. In particular, it is possible to determine heat sources in the depth of the researchable object with determining the distance to the source. Using the autocorrelation function, we can get the information on the spectral composition of radiation and on the emissivity of the researchable surface.

The autocorrelation function of the physical process (a signal) allows us to predict the degree of influence of the value of the current process (t_1) on the value of the process at some point in time in the future ($t_1+\tau$).

The autocorrelation function of a harmonic signal repeats its shape in time, and the function of a random signal tends to zero at $\tau\to\infty$. Therefore, it is a good tool for detecting, for example, no nequilibrium, in particular, harmonic processes on the back of noise interference in physics and plasma physics, biology and medicine. Thermal inhomogeneities have a significant effect on the nature of the frequency dependence of radiation, i.e. on the shape of the envelope of the radiation spectrum. These inhomogeneities arise as a result of inflammatory processes, injuries, tumors and other disorders in the state of tissues and organs of a living organism.

Thermal heterogeneities located at different depths (for example, d muscle tissue) have an expressed extreme character. In this case, maximum radiation wavelength depends on the depth and gradient of thermal heterogeneity. Thus, recording of the frequency dependences of the

intensity of microwave radiation or its spectral density at various points on the surface of a body allows us to identify temperature anomalies that are associated with pathological processes.

Radiometers, which are broadband receivers of the centimeter or decimeter range with a temperature resolution of 0,1°*K*, are used for radiothermometry of deep organs and tissues of biological objects. Various antennas or segments of waveguides filled with dielectric material are commonly used as radiation sensors.

3.7 A radiometric system for measuring the power of electromagnetic radiation of EHF by the zero method

The radiation power from biological objects is extremely small (10^{-13}… 10^{-16} W), which is significantly less than the power of the intrinsic noise of electronic measuring equipment. In this regard, the task of developing methods and measuring systems that make it possible to determine and analyze the field and radiation data with high reliability is very important.

Hereunder, we analyze a method for measuring the power of electromagnetic radiation of extremely high frequencies, which ensures the exclusion of the influence of both antenna noise, noise of the radiometer itself, and the instability of the RS parameters on the value of the received signal due to the multi-operation signal processing algorithm. In this case, only the modulator key is used instead of the microwave switch, which should work in set with the antenna equivalent and which is difficult to implement in the mm-range. It is achieved by introducing the operation of attenuating the signal from received radiation by the antenna, the variable attenuator, changing the gain of the attenuator to a value α_1, at which the antenna output signal and antenna noise are compensated by the input noise of the radiometer. Further, the radiation is received from a completely black body. The compensation of the received signal from a source of the known radiation together with the antenna noise and the radiometer input noise is provided by changing the attenuator gain to the value α_2.

The antenna noise is compensated directly by the input noise of the radiometer by shielding the antenna from external radiation and changing the attenuator gain to a value α_3. The power of the measured radiation is calculated from the three values of the transfer coefficient (α_1, α_2, α_3) of the attenuator without using RS parameters.

In fig. 3.11, a circuit for measuring the power of electromagnetic radiation of extremely high frequencies [54] is presented, which contains a horn antenna 1, a variable attenuator 2, a modulator key 3, a balanced mixer 4, a frequency tunable local oscillator 5, an amplifier 6 of an intermediate frequency, a quadratic detector 7, a selective low-frequency amplifier 8, a synchronous detector 9, low-pass filter 10, an indicator 11, a low-frequency generator 12, a researchable object 13 and a reference power source in the form of a heated absolutely black body 14. Converting links 3–12 belong to a modulating heterodyne radiometer. A horn antenna of 1 mm band is directed to a measured radiation source whose power is comparable to or less than the noise power of the antenna itself. The dispersion of the output signal of the antenna is presented in the form:

$$\overline{U}_1^2 = S_1 P_X + \overline{U}_2^2, \qquad (3.104)$$

where S_1 – the antenna sensitivity; P_X – the power efficiency of received radiation; $\overline{U}_2^2$ – dispersion of antenna noise.

The output signal of the antenna 1 through the variable attenuator 2 and the modulator key 3 is fed to one input of the balanced mixer 4, the other input of which is affected by a frequency-tunable local oscillator.

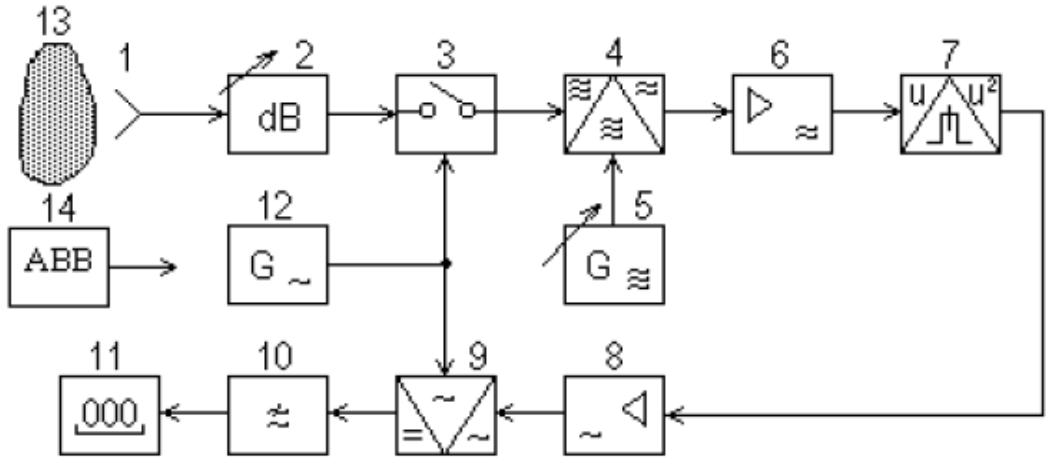

Figure 3.11 – RS for measuring the power of electromagnetic radiation of EHF by the zero method

We will present the dispersion of the input signal of the balanced mixer 4, taking into account its input noise, with the closed state of the modulator key 3 as follows:

$$\overline{U}_4^2 = \alpha\left(S_1 P_X + \overline{U}_2^2\right) + \overline{U}_{31}^2, \qquad (3.105)$$

where α – the attenuator 2 power transfer coefficient; $\overline{U}_{31}^2$ – the dispersion of input noise of a balanced mixer, taking into account the noise of the local oscillator with a closed modulator key.

As a result of mixing the monochromatic signal of the frequency local oscillator ω_Γ and the sum noise signal (3.105) with a wide spectrum, two signals of difference (intermediate) frequency ω_P are formed from spectral components with frequencies ω'_C and ω''_C and symmetric with respect to ω_Γ :

$$\begin{cases} \omega'_C = \omega_\Gamma + \omega_P, \\ \omega''_C = \omega_\Gamma - \omega_P. \end{cases} \qquad (3.106)$$

All frequency-converted signal components (3.105) fall into the amplifier bandwidth $\Delta\omega_P$ of the intermediate-frequency amplifier 6 with a central frequency ω_P. They are displaced from the local oscillator frequency ω_Γ by the value of the intermediate frequency ω_P up and down the frequency axis, taking into account the pass band width:

$$\sum_{i=1}^{n} \omega'_{Ci} = \omega_\Gamma + \omega_P \pm \Delta\omega_P, \qquad (3.107)$$

$$\sum_{i=1}^{n} \omega''_{Ci} = \omega_\Gamma - \omega_P \pm \Delta\omega_P, \qquad (3.108)$$

where the sign «±» means the symmetric frequency of the converted frequencies of the signal (3.104) relative to the displaced frequencies of the local oscillator $\left(\omega_\Gamma + \omega_P\right)$.

As a result of mixing the components (3.107) and (3.108) with the local oscillator signal, low-frequency difference frequency signals are formed:

$$\sum_{i=1}^{n} \omega_{Pi} = \omega_P \pm \Delta\omega_P. \qquad (3.109)$$

The components of the difference frequency (3.109) are intensified by an amplifier 6 of an intermediate frequency and fed to a quadratic detector 7.

As a result of a quadratic transformation of the components of the spectrum of the bands $\Delta\omega'_{Ci}$ and $\Delta\omega''_{Ci}$ and neutralization by the detector filter, a voltage is formed:

$$U_5 = \frac{2K_1S_2}{\Delta\omega_P} \int_0^{\Delta\omega_p} U_4^2(\omega_i) U_3^2 d\omega, \qquad (3.110)$$

where K_1 – gain of the intermediate frequency power amplifier; S_2 – conversion conductance of a balanced mixer; U_3^2 – local oscillator signal power.

When the key-modulator 3 is open, the dispersion of the signal at the input of the balanced mixer is determined only by its intrinsic noise.

$$\overline{U}_6^2 = \overline{U}_{32}^2, \qquad (3.111)$$

where $\overline{U}_{32}^2$ – dispersion of input noise of a balanced mixer, taking into account the noise of the local oscillator with an open key modulator.

The noise level at the input of the balanced modulator 4 depends on the resistance value to which its input is closed. When the modulator 3 key is closed, the input of the balanced mixer 4 is closed to the low-resistance output impedance of the attenuator 2.The input resistance increases in the open state of the modulator key and is determined by the input resistance of the balanced modulator itself. Therefore,

$$\overline{U}_{32}^2 >> \overline{U}_{31}^2. \qquad (3.112)$$

Accordingly, the output voltage of the quadratic detector is

$$U_7 = \frac{2K_1S_2}{\Delta\omega_P} \int_0^{\Delta\omega_p} U_6^2(\omega_i) U_3^2 d\omega. \qquad (3.113)$$

In a modulating heterodyne radiometer, the key 3 is controlled by the voltage of the low-frequency generator 12, which causes the key opening and closing periodically.

A sequence of video pulses with amplitudes (3.110) and (3.113) is formed in accordance with this at the output of the quadratic detector 7. The average amplitudes of the video pulses will take the form, taking into account the dispersion of the signals $\overline{U}_4^2(\omega_i)$ and $\overline{U}_6^2(\omega_i)$:

$$U_5 = 2K_1S_2S_3\left[\alpha\left(S_1P_X + \overline{U}_2^2\right) + \overline{U}_{31}^2\right]\cdot U_3^2, \qquad (3.114)$$

$$U_7 = \left(2K_1S_2S_3\overline{U}_{31}^2\right)U_3^2, \qquad (3.115)$$

where S_3 – the quadratic detector sensitivity.

A modulated sequence of video pulses with amplitudes (3.114) and (3.115) is formed at the output of the quadratic detector 7 during periodic operation of the modulator key 3. A selective low-frequency amplifier 8 that is tuned to the frequency of the generator 12 isolates and amplifies the voltage of the fundamental harmonic of the modulation envelope of the video pulses:

$$U_8 = K_2\frac{U_7 - U_5}{2}cos\left(\Omega t + \Phi\right), \qquad (3.116)$$

where K_2 – low frequency selective amplifier gain; Ω –circular switching frequency of the modulator key; Φ – the initial phase of the envelope voltage of the video pulses.

The amplified voltage (3.116) is rectified by a synchronous detector 9, which is controlled by the frequency Ω voltage of the low-frequency generator 12.

Rectified voltage in terms of expressions (3.114) and (3.115) is

$$U_9 = K_1S_2S_3K_2K_3\left[\overline{U}_{32}^2 - \overline{U}_{31}^2 - \alpha\left(\overline{U}_2^2 + S_1P_X\right)\right]U_3^2, \qquad (3.117)$$

where K_3 – the rectification factor of the synchronous demodulator.

The rectified voltage (3.117) is smoothed by the low-pass filter 10 and is supplied to the indicator 11:

$$U_{10} = S_0\left[\overline{U}_{32}^2 - \overline{U}_{31}^2 - \alpha\left(\overline{U}_2^2 + S_1P_X\right)\right]U_3^2, \qquad (3.118)$$

where $S_0 = K_1S_2S_3K_2K_3K_4$ – the resulting sensitivity of modulation RS; K_4 – the low pass filter gain.

The transfer coefficient of the attenuator 2 is changed until a zero rendering of indicator 11 is obtained, which corresponds to the fulfillment of the condition:

$$\alpha_1\left(\overline{U}_2^2 + S_1P_X\right) = \overline{U}_{32}^2 - \overline{U}_{31}^2, \qquad (3.119)$$

where α_1 – attenuator transfer coefficient, which corresponds to a zero reading of the indicator.

The value of the gain of the attenuator 2 is fixed. After that, the antenna 1 is sent to the reference radiation source 14, which presents the radiation of a completely black body in a known temperature range. In this case, the reading of the modulation RS takes on the following value:

$$U_{11} = S_0\left[\overline{U}_{32}^2 - \overline{U}_{31}^2 - \alpha_1\left(\overline{U}_2^2 + S_1P_0\right)\right]\cdot U_3^2, \qquad (3.120)$$

where P_0 – the radiation power of a completely black body at a known temperature.

The gain of the attenuator 2 is changed until the indicator 11 reaches zero reading. At the same time, the following condition is satisfied:

$$\alpha_2\left(\overline{U}_2^2 + S_1P_0\right) = \overline{U}_{32}^2 - \overline{U}_{31}^2, \qquad (3.121)$$

where α_2 – the second value of the gain of the attenuator, corresponding to the zero reading of the indicator.

The value of the attenuator gain 2 is fixed. Then the antenna 1 is shielded from external radiation, after which the reading of the modulation RS becomes equal:

$$U_{12} = S_0\left(\overline{U}_{32}^2 - \overline{U}_{31}^2 - \alpha_2\overline{U}_2^2\right)\cdot U_3^2. \qquad (3.122)$$

The gain of the attenuator 2 is changed to a third value α_3, at which the zero reading of indicator 11 is again achieved. It meets the condition:

$$\alpha_3\overline{U}_2^2 = \overline{U}_{32}^2 - \overline{U}_{31}^2. \qquad (3.123)$$

The value α_3 of the attenuator gain 2 is fixed. Equating the left sides of equations (3.123) and (3.121), we get:

$$\alpha_3\overline{U}_2^2 = \alpha_2\left(\overline{U}_2^2 + S_1P_0\right). \qquad (3.124)$$

The dispersion of the antenna noise is determined from equation (3.124):

$$\overline{U}_2^2 = \frac{\alpha_2}{\alpha_3 - \alpha_2}S_1P_0. \qquad (3.125)$$

Equating the left-hand sides of equations (3.121) and (3.119), we get:

$$\alpha_2\left(\overline{U}_2^2 + S_1P_0\right) = \alpha_1\left(\overline{U}_2^2 + S_1P_X\right). \qquad (3.126)$$

Substituting the value of the noise variance of the antenna (3.125) into the equation (3.126), we finally get the value of the measured power of the researchable radiation:

$$P_X = \frac{\alpha_2(\alpha_3 - \alpha_1)}{\alpha_1(\alpha_3 - \alpha_2)} P_0 . \qquad (3.127)$$

The radiation power of a completely black body P_0 can be easily determined by calculation of the known temperature T_0 of the radiating body:

$$P_0 = 4K\Delta f T_0 , \qquad (3.128)$$

where K – Boltzmann constant; Δf – the reception bandwidth of the modulation RS.

It can be seen from the obtained expression (3.127) that the antenna noise ($\overline{U}_2^2$), radiometer noise ($\overline{U}_{31}^2, \overline{U}_{32}^2$), instability of radiometer parameters ($K_1, K_2, K_3, K_4, S_2, S_3$), instability of antenna sensitivity (S_1), and local oscillator power variations in adjustment process (U_5^2).

The measurement error depends only on the calibration error of the attenuator, which does not exceed ± 0,1 dB for measuring attenuators of the EHF range. By tuning the local oscillator frequency, we can determine the spectral power density of the researchable object in a wide range of extremely high frequencies.

Human electromagnetic radiation was experimentally studied in the range of extremely high frequencies 53…78 GHz. It was done using a modulating heterodyne RS, which had a fluctuation sensitivity threshold for power no worse than 10^{-15} W or 10^{-22} W/Hz with a reception bandwidth of 100 MHz. A standard waveguide modulator of the M347 type, which is made on varactor diodes, is used as a modulator key.

The losses for the conversion of EHF signals in a diode-balanced mixer ranged from 6 to 8 dB at the lower and upper frequencies of the operating range. The isolation of the signal and local oscillator inputs was ~20 dB and SWR amounted to ≤ 2,0. Noise suppression of the local oscillator was ~25 dB and the local oscillator power was 10^{-15} mW.

The intermediate frequency amplifier is made on field-effect transistors with a Schottky barrier (FTS) with a gain of up to 80 dB and with a noise figure of no more than 2 dB. The quadratic detector contains a tunnel diode of the GI401A type and operates on the reverse branch of the current-

voltage characteristic without additional bias. Radiation is received by a horn antenna with a sensitivity of 10^{-15} W/cm^2.

Studies and power calculations showed that the human body emits electromagnetic waves of millimeter range of different intensity from different parts of the body. A small radiation power is inherent in the palms, parts of the chest and abdomen of a person. In relation to the radiation of a completely blackbody with the temperature of the palms of the human body it is $(P_X/P_0) = 6-8$ dB, and in the forehead is only 3…5 dB.

The level of radiation significantly depends on the state of the person. So stressful conditions significantly reduce the level of radiation (for 2…3 dB), and inflammatory processes increase the level of radiation (for 7…9 dB). The spectral density of radiation power is (1…5)*10^{-21} W/Hz·cm^2. Therapeutic fasting for 24 or 36 hours leads to a decrease in the level of radiation by 1, 5…2 times. Eating (after the hour interval after fasting) raises the level of radiation to an average level that is the characteristic of this person.

A depletion of the level of radiation in patients with chronic diseases is observed, for example, of the gastrointestinal tract, by 7…8 dB. Thus, exceeding the level of human radiation in logarithmic units $[lg(P_X/P_0)]$ can be used as a diagnostic parameter in medicine.

3.8 A radiometric system for assessing the emission properties of tissues of biological objects

In Fig. 3.12, the RS scheme for evaluating the emission properties of biological tissues is shown [55], proposed by the authors:

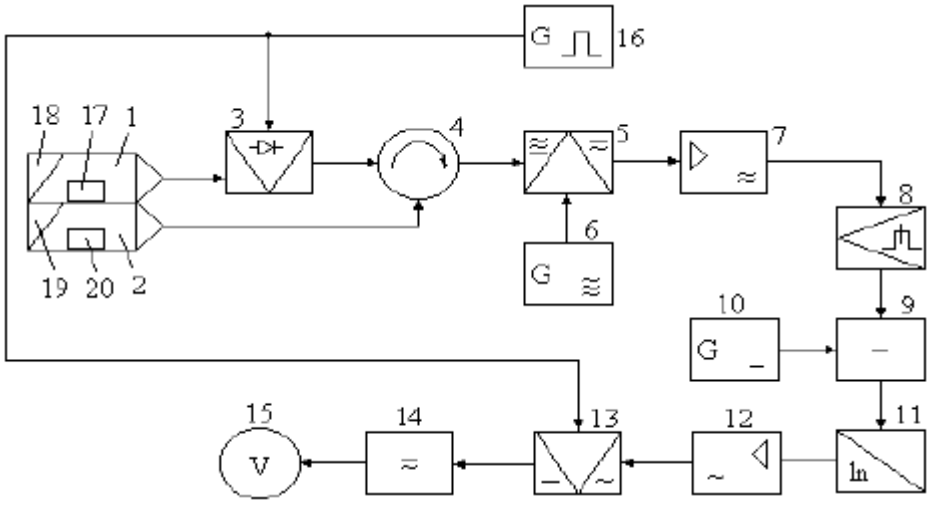

Figure 3.12 – RS for assessing the emission properties of tissues of biological objects

The circuit contains: 1 and 2 – working and reference waveguide sensors; 3 – a controlled modulator-reflector; 4 – a circulator; 5 – a mixer; 6 – a local oscillator; 7 – an intermediate frequency amplifier; 8 – an amplitude detector; 9 – a subtractor; 10 – a constant voltage source; 11 – logarithm; 12 – a low frequency amplifier; 13 – a synchronous detector; 14 – a low-pass filter; 15 – a voltmeter; 16 – a low-frequency generator; 17 and 20 – analyzed and simulation samples; 18 and 19 – absorbers.

The working and reference sensors are made in the form of segments of waveguides that are mechanically connected to each other. Radiation from the working and reference sensors arrives at the inputs of the circulator. The working sensor is connected to the circulator through a modulator-reflector that is controlled by a low-frequency multivibrator oscillator. Noise signals with dispersions arrive at the input of the mixer in different half-periods of the control voltage, with the open and closed modulator-reflector 3.

$$\overline{U}_{11}^2 = K_1\left(\overline{U}_{21}^2 + \overline{U}_3^2 + \overline{U}_4^2\right), \tag{3.129}$$

$$\overline{U}_{12}^2 = K_1\left(\overline{U}_{22}^2 + \overline{U}_4^2\right), \tag{3.123}$$

where $\overline{U}_{21}^2$, $\overline{U}_3^2$, $\overline{U}_4^2$ – the dispersion, respectively, of thermal radio, bioinformation radiation of the analyzed sample and the intrinsic noise of the mixer; K_1 – a waveguide transmission coefficient; $\overline{U}_{22}^2$ – the dispersion of thermal radiation of a simulation sample, which is a «dead» tissue.

The amplitude-modulated signal is generated during periodic operation of the modulator-reflector 3 with a multivibrator oscillator frequency Ω at the output of the mixer 5:

$$M_1 = \frac{\overline{U}_{11}^2 - \overline{U}_{12}^2}{\overline{U}_{11}^2 + \overline{U}_{12}^2} = \frac{\overline{U}_3^2}{2\left(\overline{U}_4^2 + \overline{U}_{21}^2\right)}. \tag{3.131}$$

Using the EHF signal of the local oscillator 6, the EMR spectrum is transferred to the intermediate resonant frequency ω_0, to which the selective amplifier 7 is tuned.

Video pulses are formed after heterodyne conversion and amplitude detection by the detector 8 in different half-periods of the control voltage, the amplitudes of which take the following form after the functional conversion in the subtractor 9 and the logarithm 11:

$$U_{51} = S_3 \, ln\left\{K_1^2 S_1^2 K_2^2 S_2 K_3 \left[\overline{U}_{21}^2(\omega_0) + \overline{U}_3^2(\omega_0)\right]\right\}, \quad (3.132)$$

$$U_{52} = S_3 \, ln\left[K_1^2 S_1^2 K_2^2 S_2 K_3 \overline{U}_{22}^2(\omega_0)\right], \quad (3.133)$$

where S_1, S_2, S_3 – conversion conductance of the heterodyne, quadratic and logarithmic transforms, respectively; K_2 – the intermediate frequency amplifier gain; K_3 – the subtractor transmission coefficient.

When expanding the alternating component of the sequence of video pulses (3.132) and (3.133) in exponential series, it is easy to see that the readings of the voltmeter α are proportional to the ratio of the bio information and radio thermal radiation powers:

$$\eta = \frac{K_0 \overline{U}_3^2(\omega_0)}{\overline{U}_{21}^2(\omega_0)}, \quad (3.134)$$

where K_0 is a proportionality constant.

The resulting ratio is the desired measure of the emission properties of biological tissues. The measured power ratio does not depend on the transfer properties of the sensors and joining waveguides, the inconsistency of the heterodyne conversion conductance of the compared signals, the instability of the gain of the selective amplifier, the sensitivity of the amplitude detector and the gain of the subtractor.

The proportionality coefficient K_0 depends only on the stability of the low-frequency blocks of the circuit and is determined during the calibration process using samples of microorganisms, the emissivity of which is estimated by the results of biochemical studies. A simulation sample is prepared from a biological tissue of the same mass as the researchable sample. Protein preparation in a simulation sample is carried out by heating it to a temperature of 80…90° C, at which protein is boiled.

Additional heat evolution, associated with biochemical processes in materials and tissues with living protein, leads to a slight increase in the temperature of the working sensor. Due to the good thermal contact of sensors 1 and 2, the temperatures of the working and reference sensors are equalized. In the same way, the inconstancy of the external temperature is compensated to the level of thermal radiation of the researchable and simulation samples.

Experimental studies have shown that the aging of food such as hard cheese is accompanied by an increase in emission radiation. In this case,

the emission factor η increases to 0,05...0,1 (5–10 % of the thermal radiation) after 70–80 days of aging. Further aging of cheese may lead to a loss of taste, nutrition and other properties of a product and is accompanied by a decrease in the emission coefficient to 0.01 (less than 1 % of thermal radiation), and subsequently to zero. The latter indicates a decrease in the number of living microorganisms in the product and the end of the aging stage.

3.9 Radiometric system with advanced measuring functions

In some cases, it becomes necessary to record the dependence of the intrinsic electromagnetic radiation intensity of a biological object in the millimeter range on the intensity of external irradiation with a broadband noise signal. In this case, it is possible to determine the absorbing and reflecting properties of the object depending on the intensity of external radiation.

A similar scheme (Fig. 3.13) includes a dual-frequency switching, which expands the number of measured parameters, as well as provides the possibility of their automated processing [46]. The expansion of the RS functionality with two modulation frequencies is achieved by introducing into the circuit a zero modulation radiometer, two directional couplers A1 and A11 with a power divider U5, two additional attenuators A9 and A10, a second noise generator G5 and switch S2. As a result, it becomes possible to simultaneously receive signals due to both the intrinsic electromagnetic radiation of a biological object and the ability of the object to absorb or reflect external radiation in the EHF range.

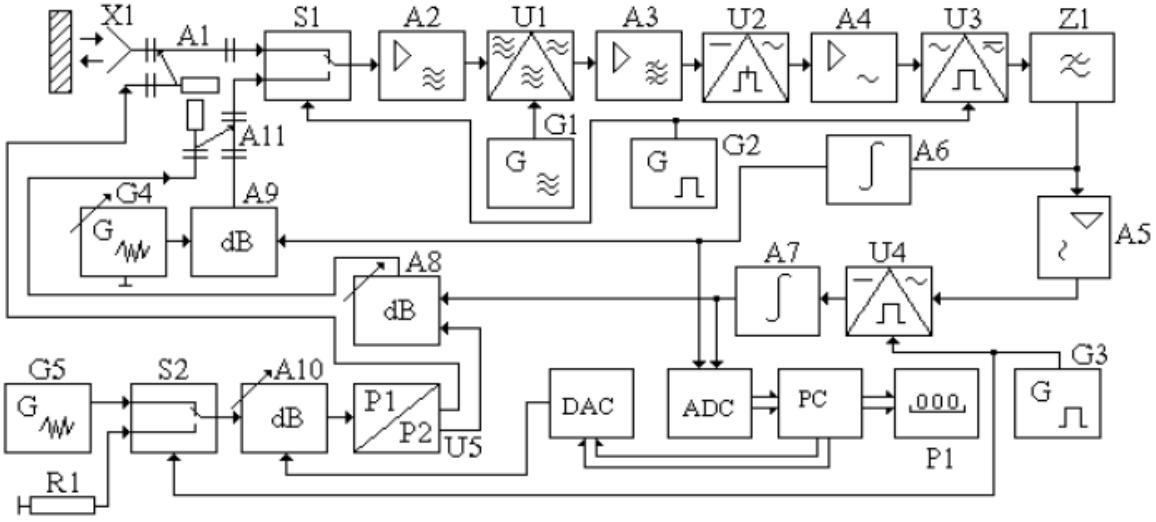

Figure 3.13 – Radiometric system with advanced features

A multifunctional RS works in the following way. The first generator of the reference frequency G2 generates a rectangular low-frequency signal with a frequency f_1, which controls the first switch S1 and the first synchronous detector U3. When the switch S1 is switched, the input of the microwave amplifier A2 is periodically connected to the output of the antenna X1 or to the output of the first noise generator G4 through the second directional coupler A11 and the first controlled attenuator A9. The second generator G3 of the reference frequency also generates a low-frequency square-wave signal with a frequency $f_2 > f_1$.

The duration of the time interval, during which the second noise generator G5 is connected to the directional coupler A1 or A11 through the controlled attenuators A8 and A10, is several times longer than the time interval for the connection of the first noise generator G4 to the microwave amplifier A2.

We will consider the operation of a multifunctional PC with the connection of a second noise generator G5 and the periodic operation of the first switch S1. The researchable object is irradiated in the switching half-time $\Delta t_1 = 1/(2 f_1)$, when the antenna X1 is connected, with the signal of the second noise generator G5, attached to the antenna X1 through the directional coupler A1. The noise signal of the self-radiation of a biological object and the noise signal of the generator G5, reflected from this object, are fed to the input of the microwave amplifier A2. Taking into account of the intrinsic noise of the radiometer, brought to the input of the microwave amplifier A2, the dispersion of the amplified signal is equal to:

$$\overline{U}_{41}^2 = K_1(\overline{U}_1^2 + K_2 K_3 \Gamma \overline{U}_2^2 + \overline{U}_3^2), \qquad (3.135)$$

where K_1 – gain of the microwave amplifier A2 in power; K_2 и K_3 – transmission coefficients of the controlled attenuator A10 and the directional coupler A1 in power; U_1 – object self-radiation signal; U_2 – a signal of the noise generator G5; U_3 – intrinsic noise of the radiometer brought to its input; Γ – the object reflection coefficient.

The signal from the first noise generator G4 passes through the first controlled attenuator A9 into the next switching half-time $\Delta t_2 = \Delta t_1 = 1/(2 f_1)$ to the input of the microwave amplifier A2. The signal of the second noise generator G5 is supplied through a directional coupler A11. The dispersion of the signal at the output of the microwave amplifier A2 is equal to:

$$\overline{U}_{42}^2 = K_1\left(K_2 K_4 K_5 \overline{U}_2^2 + K_6 \overline{U}_5^2 + \overline{U}_3^2\right), \qquad (3.136)$$

where K_4, K_6, K_5 – transmission coefficients of controlled attenuators A8 and A9 and directional coupler A11 in power; U_5 – a signal of the noise generator G4.

The signals with dispersions (3.135) and (3.136) are alternately fed to a mixer U1, to the second input of which a local oscillator signal G1 is supplied. Amplifier A3 isolates the signal from the output spectrum of the mixer in the transition band Δf. The signal is generated at the output of the amplitude detector U2 for several switching periods, the constant component of which is proportional to the total power (3.135) and (3.136). The alternating component of the signal is a periodic function with a frequency f_1, the amplitude of which is determined by the difference in power efficiencies (3.135) and (3.136). This signal is amplified in LFA A4 and fed to the input of the first synchronous detector U3, the second input of which receives the reference signal from the output of the first reference generator G2. As a result, a signal is generated at the output of the first synchronous detector U3:

$$U_6 = \frac{K_0}{2}(\overline{U}_1^2 + K_2 K_3 \Gamma \overline{U}_2^2 - K_2 K_4 K_5 \overline{U}_2^2 - K_6 \overline{U}_5^2), \qquad (3.137)$$

where K_0 – a resulting conversion efficiency of the radiometric channel.

Switching of the second switch S2 occurs after several periods of cross-plugging f_1. In this case, the second noise generator G5 is turned off, and the input of the third controlled attenuator A10 is connected to a load R1 that is equivalent to the output resistance of the generator G5. The signal, the dispersion of which has the following form, is formed during the periodic operation of the first switch S1 with a frequency f_1 in one half-switching period at the output of the microwave amplifier A2:

$$\overline{U}_{71}^2 = K_1\left(\overline{U}_1^2 + \overline{U}_3^2\right), \qquad (3.138)$$

A dispersion signal is generated in the second switching half-cycle:

$$\overline{U}_{72}^2 = K_1\left(K_6 \overline{U}_5^2 + \overline{U}_3^2\right). \qquad (3.139)$$

The following signal is generated in several switching half-periods at the output of the first synchronous detector U3:

$$U_8 = \frac{K_0}{2}\left(\overline{U}_1^2 - K_6 \overline{U}_5^2\right). \qquad (3.140)$$

The signal (3.137) is replaced by the signal (3.140) as a result of periodic switching of the generator G5 with a frequency $f_1 < f_2$. The constant

component of the voltage, proportional to the sum of the signals (3.140) and (3.137), is formed at the output of the low-pass filter Z1:

$$U_9 = \frac{K_0 K_7}{2}[2\overline{U}_1^2 + K_2(K_3\Gamma - K_4K_5)\overline{U}_2^2 - 2K_6\overline{U}_5^2], \qquad (3.141)$$

where K_7 – a coefficient of the filter Z1.

The alternating component of the voltage frequency f_2, proportional to the difference of the signals (3.140) and (3.137), has the following form:

$$U_{10} = \frac{K_0 K_7}{2} K_2(K_3\Gamma - K_4K_5)\overline{U}_2^2. \qquad (3.142)$$

An alternating voltage U_{10} of frequency f_2 with amplitude (3.142) is amplified by the second amplifier A5 and rectified by a second synchronous detector U4, the second input of which receives a reference signal from the generator G3.

The rectified voltage charges the second integrator A7, the output voltage of which controls the operation of the second attenuator A8. The attenuation coefficient A8 is regulated until the power of the signal reflected from the object at one input of the switch S1 becomes equal to the compensating power at the second input of the switch. If the directional couplers A1 and A11 are identical, then their transmission coefficients K_3=K_4 will be equal to each other, and if the compared powers are equal, we have:

$$K_5 = \Gamma. \qquad (3.143)$$

Thus, it is possible to determine the reflection coefficient of the researchable object, regardless of the value of the power emitted by it, according to the value of the attenuator transfer coefficient A8. According to (3.141), a constant voltage (U_9) charges the first integrator A6, the output voltage of which controls the operation of the first attenuator A9. The regulation process occurs until the constant component of the voltage becomes equal to zero (U_9 = 0) at the output of the first synchronous detector U3. Taking into the account the equation (3.143), we have:

$$\overline{U}_1^2 = K_6\overline{U}_5^2. \qquad (3.144)$$

Due to the fact that the power of a noise generator G4 is a constant quantity $\left(\overline{U}_5^2 = const\right)$, the transmission coefficient of the first attenuator A9 is set proportional to the self-radiation power of the researchable object:

$$K_6 = \frac{\overline{U}_1^2}{\overline{U}_5^2} = \frac{\overline{U}_1^2}{P_{01}}, \qquad (3.145)$$

where P_{01} – power of the noise generator G4.

Dual-channel AD converters and computers are used to register the reflection coefficient Γ and the intrinsic radiation of biological objects. In this case, a digital code is generated in parallel with the registration of computer parameters, which is fed to the DA converter. The output voltage of the DA converter contributes to an increase in the gain of the attenuator A10 and a proportional increase in the level of radiated power of the antenna X1.

The reflection coefficient Γ of the researchable object and the sum signal, received by the antenna X1, nonlinearly change in the process of increasing the power that irradiates the object through the antenna. The level of the object self- radiation (U_1) is determined predominately by its internal temperature:

$$\overline{U}_1^2 = ST \,, \tag{3.146}$$

where S – the antenna sensitivity; T – a temperature of the researchable object.

Electrical signals that change the transmission coefficients of the controlled attenuators A9 and A8 are recorded by a computer in the form of the reflection coefficient of the object Γ and the level of intrinsic radiation ($\overline{U}_1^2$) depending on the intensity of the external radiation of the object.

At the same time, the measurement result is not affected by irregularity of the radiation power ($\overline{U}_2^2$), inconstancy of the intrinsic radiation ($\overline{U}_1^2$), inconsistency of the intrinsic noise level of the radiometer ($\overline{U}_3^2$), as well as the instability of the resulting conversion coefficient of the radiometer (K_o) and the parameters of additional elements and units (K_3, K_4, K_7) of RS.

Experimental studies of human intrinsic radiation showed that the spectral density of the radiation noise power is $P_H \sim 10^{-21}...10^{-22}$ W/Hz·cm^2 [56] at normal temperature (T=293 K) in the EHF range (53…78 GHz). Irradiation of a person with a power close to the P_H of the indicated frequency range determines its intensive absorption ($\Gamma \approx 0$). The value of the absorption coefficient remains constant with its further increase (~ in 10 times).A significant increase in the power of the irradiating signal (> 10 times) leads to a spur increase in the reflection coefficient Γ, which indicates the nonlinear properties of the absorption capacity of human skin. Thus, the considered multifunctional modulation RS can be used in microwave medicine technologies for measuring the EHF characteristics of biological objects as a diagnostic system.

3.10 A radiometric system for measuring phase shift of reflected microwave oscillations

Exploration by electromagnetic oscillations of extremely high frequencies (EHF) is used to diagnose biological objects, which allows the use of a number of specific electro physical reactions that are characteristic for living organisms.

There are experimental data that indicate the possibility of diagnosing a number of diseases by changes in the phase of reflected oscillations of the EHF range from biologically active points of human and animal skin [57]. However, these changes are small, do not exceed 1 and even fractions of a degree, and their measurement is associated with a number of difficulties.

Phase shift meters in reflected EHF oscillations usually have a dual-channel structure [5], which includes elements for separating incident and reflected oscillations, two mixers, a common local oscillator, two intermediate-frequency amplifiers, a phase detector, a low-frequency amplifier, and an indicator.

EHF local oscillator signals have equal amplitudes and phases at the inputs of the mixers. Signals with a difference (intermediate) frequency that are proportional to the phase difference of the input EHF signals, are amplified by narrow-band amplifiers of an intermediate frequency. Their low-frequency phase difference is converted to a proportional voltage by a phase detector, which is measured by the output indicator.

However, the accuracy of the measurement of phase shifts by the known device is small due to the influence of the following factors:

- inevitable detuning of narrow-band amplifiers of intermediate frequency with a large mutual conductance of the phase-frequency characteristics;
- amplitude-phase distortions in EHF mixers due to the inequality of the power of incident and reflected EHF oscillations;
- additional phase shifts of the compared signals due to inter-channel connections along the local oscillator chains.

Thereunder, we consider RS (Fig. 3.14.), which provides alternating mixing of EHF oscillations with EHF signals that are displaced in frequency in opposite directions. It allows excluding frequency-phase and amplitude-phase distortions in the channels of the RS, as well as weakening the inter-channel communications. It will make it possible to significantly increase the accuracy of measuring the reflection phase of EHF oscillations [58].

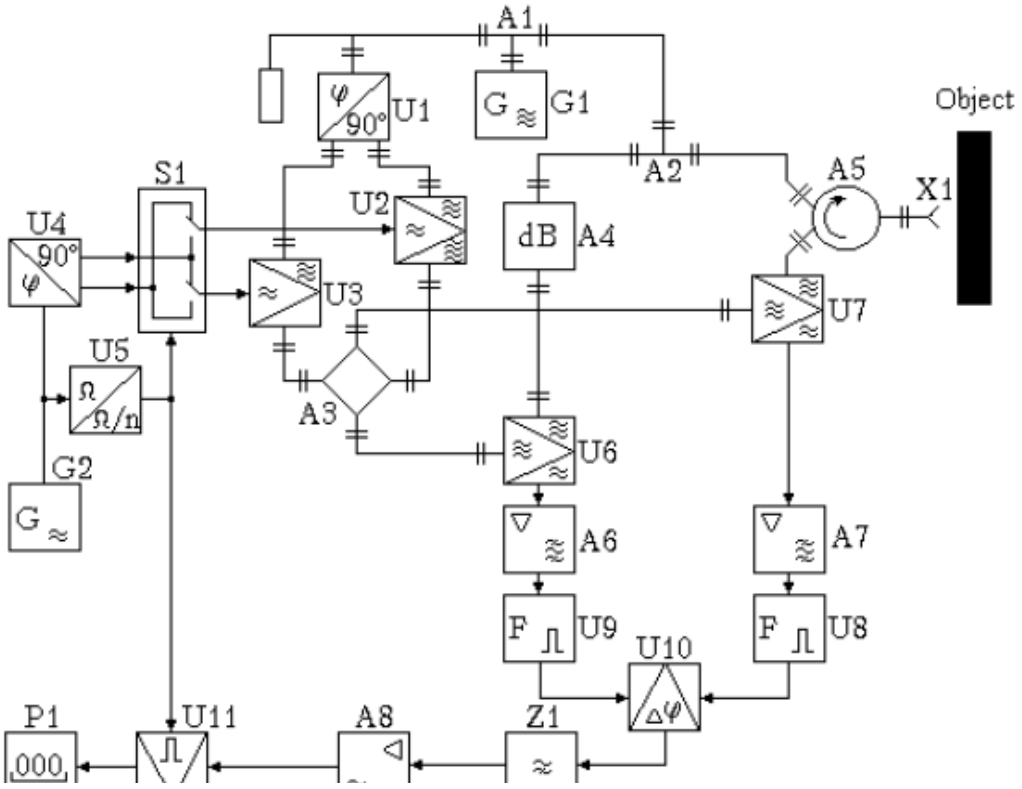

Figure 3.14 – RS for measuring the phase shift of reflected EHF oscillations

The RS includes generator G1 of harmonic oscillations of the EHF range, power dividers A1 and A2 (connected to the generator); a circulator A5 with a receiving and emitting antenna X1 (aimed at the controlled object); a matching attenuator A4 (connected to the second output of the power divider A2); EHF balanced mixers U6 and U7, to the outputs of which serially connected amplifiers of intermediate frequency A6 and A7 are connected; shapers of short pulses U9 and U8 and a trigger phase detector U10.

An EHF quadrature phase splitter U1 is connected to the second output of the first power divider. A hybrid tee A3 is connected through EHF balanced modulators U2 and U3 to the outputs of a phase splitter. The outputs of hybrid tee are connected to the second inputs of the EHF balanced mixers U6 and U7. The low-frequency local oscillator G2 is connected to a low-frequency quadrature phase coupler U4, the outputs of which are connected via the bipolar switch S1 to the modulating inputs of the EHF balanced modulators.

The frequency divider U5 connects the control input of the bipolar switch S1 and the output of the low-frequency local oscillator G2. A high-

pass filter Z1, a low-frequency amplifier A8, a synchronous detector U11 and an indicator P1 are connected to the output of the trigger phase detector U10. The control input of the synchronous detector U11 is connected to the control input of the bipolar switch.

The output harmonic oscillations of the generator G1 of the EHF-frequency range ω,

$$U_1(t) = U_{m1} \cos(\omega t + \varphi_1), \tag{3.147}$$

are divided equally by power dividers A1 and A2.

A part of the oscillation power from the divider A2 through the circulator A5 enters the transceiver antenna X1 and is radiated in the direction of the controlled object. A part of the oscillation power from the divider A2 is supplied to the adjusting attenuator A4. Oscillations reflected from the object can be represented as follows:

$$U_2(t) = U_{m2} \cos(\omega t + \varphi_2) = 0{,}5\ \Gamma U_{m1} \cos(\omega t + \varphi_1 + \Delta\varphi), \tag{3.148}$$

where Γ – the reflection coefficient; $\Delta\varphi$ – an informational phase shift.

The signal $U_2(t)$ is received by the antenna X1 and fed to the input of the EHF balanced mixer U7 of the measuring channel PC through the output of the circulator A5. The oscillations suppressed by the A4 attenuator

$$U_3(t) = U_{m3} \cos(\omega t + \varphi_1), \tag{3.149}$$

are fed to the input of the EHF balanced mixer U6 of the reference channel.

The electric lengths of the EHF of the measuring and reference channels are chosen identical.

A part of the oscillation power from the divider A1 is supplied to the EHF phase splitter U1, for example, a hybrid junction, where it is divided into two equal quadrature oscillations:

$$U_4(t) = U_{m4} \cos(\omega t + \varphi_1) \text{ and } U_5(t) = U_{m5} \sin(\omega t + \varphi_1), \tag{3.150}$$

What is more, $U_{m4} = U_{m5}$. The oscillations $U_4(t)$ and $U_5(t)$ arrive at the signal inputs of the EHF balanced modulators U2 and U3, to the heterodyne inputs of which low-frequency quadrature signals are applied:

$$U_6(t) = U_{m6} \cos(\Omega t + \varphi_3) \text{ and } U_7(t) = U_{m7} \sin(\Omega t + \varphi_3), \tag{3.151}$$

with equal amplitudes ($U_{m6} = U_{m7}$) and initial phase φ_3. The source of low-frequency signals is the local oscillator G2 of the sound frequency Ω, with initial phase φ_3 and low-frequency quadrature phase splitter U4, the output signals $U_6(t)$ and $U_7(t)$ of which are supplied to the modulating inputs of the EHF balanced modulators through an automatic bipolar switch S1.

As a result of the conversion, dual-frequency EHF signals of the summation and difference frequencies are generated at the outputs of the EHF modulators U2 and U3:

$$U_8(t) = 0,5S_1U_{m4}U_{m6}\{\cos[(\omega-\Omega)t+\phi_1-\phi_3]+\cos[(\omega+\Omega)t+\phi_1+\phi_3]\}, \quad (3.152)$$

$$U_9(t) = 0,5S_1U_{m5}U_{m7}\{\cos[(\omega-\Omega)t+\phi_1-\phi_3]-\cos[(\omega+\Omega)t+\phi_1+\phi_3]\}, \quad (3.153)$$

where S_1 – the mutual conductance of balanced modulators.

Since $U_{m4}U_{m6} = U_{m5}U_{m7}$, then the dual-frequency signals $U_8(t)$ and $U_9(t)$ have the same amplitudes, and the component of the shifted frequencies has opposite signs.

Dual-frequency signals are fed to the inputs of the hybrid tee A3, where they are summed and subtracted at the arms of the tee. As a result of the summation of the signals at one output of the tee A3, oscillations of the difference frequency are formed:

$$U'_{10}(t) = S_1K_1U_{m4}U_{m6}\cos[(\omega-\Omega)t+\phi_1-\phi_3], \quad (3.154)$$

and as a result of subtraction, the oscillations of the sum frequency are formed at the other output of the tee.

$$U'_{11}(t) = S_1K_1U_{m4}U_{m6}\cos[(\omega+\Omega)t+\phi_1+\phi_3], \quad (3.155)$$

where K_1 – the transfer constant of the tee junction.

The oscillations of the difference frequency are fed to the second input of the balanced mixer U7, and the oscillations of the sum frequency are fed to the second input of the balanced mixer U6. As a result of balanced mixing of EHF oscillations of the difference frequency $U'_{10}(t)$ with the EHF oscillations $U_2(t)$ of the measuring channel, low-frequency difference oscillations are formed:

$$U'_{12}(t) = K_1S_1S_2U_{m2}U_{m4}U_{m6}\cos(\Omega t+\phi_2-\phi_1+\phi_3+\phi_4), \quad (3.156)$$

where S_2 – steepness of the balanced mixer; φ_4 – a phase shift introduced bythe U7 mixer.

Low-frequency difference oscillations are also formed in the process of balanced compounding of the EHF oscillations of the sum frequency $U'_{11}(t)$ with EHF oscillations $U_3(t)$:

$$U'_{13}(t) = K_1 S_1 S_2 U_{m3} U_{m4} U_{m6} \cos(\Omega t + \phi_3 + \phi_5), \qquad (3.157)$$

where φ_5 – a phase shift, introduced by the mixer U6.

Since the oscillation amplitudes U_{m2} and U_{m3} are not equal generally due to the inconstancy of the reflection coefficient Γ from the controlled object, then $\varphi_4 \neq \varphi_5$.

Low frequency signals $U'_{12}(t)$ and $U'_{13}(t)$ are extracted and amplified by narrow-band selective amplifiers A6 and A7 that are tuned to the frequency Ω of the low-frequency local oscillator G2. However, the output amplified signals are shifted by different phase angles due to the inevitable detuning of selective amplifiers during the device operation:

$$U'_{14}(t) = K_1 K_2 S_1 S_2 U_{m2} U_{m4} U_{m6} \cos(\Omega t + \phi_2 - \phi_1 + \phi_3 + \phi_4 + \phi_6), \qquad (3.158)$$

$$U'_{15}(t) = K_1 K_3 S_1 S_2 U_{m3} U_{m4} U_{m6} \cos(\Omega t + \phi_3 + \phi_5 + \phi_7), \qquad (3.159)$$

where φ_6 and φ_7 – phase shifts introduced by detuned selective amplifiers A6 and A7, respectively ($\varphi_6 \neq \varphi_7$); K_2 and K_3 – gains of amplifiers A6 and A7.

Short pulses are generated by means of the formers U8 and U9 at the moments when zero crossing of voltage curves, which arrive at the linear phase detector U10, that is made, for example, according to the bipolar triggered circuit.

The output voltage of the phase detector is proportional to the phase difference of the input signals:

$$U'_{16}(t) = S_3(\arg U'_{14} - \arg U'_{15}) = S_3(\phi_2 - \phi_1 + \phi_4 + \phi_6 - \phi_5 - \phi_7), \qquad (3.160)$$

where S_3 – the phase detector sensitivity.

The bipolar switch S1 is controlled by the rectangular voltage of the frequency divider U5, which is excited by the low-frequency voltage of the local oscillator G2. A change in the position of the switch S1 contacts occurs at a division ratio n of the frequency divider U5 at time intervals $2\pi n / \Omega$.

At the same time, low-frequency modulating signals shifted by 90° are mutually replaced. As a result, the interchange of the cumulative and difference oscillations of the EHF range occurs at the outputs of the hybrid tee A3:

$$U''_{10}(t) = S_1 K_1 U_{m4} U_{m6} \cos[(\omega + \Omega)t + \varphi_1 + \varphi_3], \quad (3.161)$$

$$U''_{11}(t) = S_1 K_1 U_{m4} U_{m6} \cos[(\omega - \Omega)t + \varphi_1 - \varphi_3]. \quad (3.162)$$

Then, the EHF oscillations $U_2(t)$ of the measuring channel are mixed with the EHF oscillations of the summation frequency $U''_{10}(t)$, which forms difference oscillations of the low frequency of the following form with an alternating sign of the phase difference ($\varphi_2 - \varphi_1$ for $\varphi_1 - \varphi_2$):

$$U''_{12}(t) = K_1 S_1 S_2 U_{m2} U_{m4} U_{m6} \cos(\Omega t + \phi_1 - \phi_2 + \phi_3 + \phi_4). \quad (3.163)$$

EHF oscillations $U_3(t)$ of the reference channel are mixed with EHF oscillations of the difference frequency $U''_{11}(t)$. As a result of the conversion, we get a difference low-frequency oscillation:

$$U''_{13}(t) = K_1 S_1 S_2 U_{m3} U_{m4} U_{m6} \cos(\Omega t + \varphi_3 + \varphi_5). \quad (3.164)$$

Since selective amplifiers introduce the same phase shifts into aggravated voltages, then:

$$U''_{14}(t) = K_1 K_2 S_1 S_2 U_{m2} U_{m4} U_{m6} \cos(\Omega t + \phi_1 - \phi_2 + \phi_3 + \phi_4 + \phi_6), \quad (3.165)$$

$$U''_{15}(t) = K_1 K_2 S_1 S_2 U_{m3} U_{m4} U_{m6} \cos(\Omega t + \varphi_3 + \varphi_5 + \varphi_7). \quad (3.166)$$

Taking into account the changed values of arguments of the compared voltages, the output voltage of the phase detector takes the form:

$$U''_{16} = S_3(\arg U''_{14} - \arg U''_{15}) = S_3(\phi_1 - \phi_2 + \phi_4 + \phi_6 - \phi_5 - \phi_7). \quad (3.167)$$

It can be seen from the voltage comparisons U'_{16} и U''_{16} that when the switch S1 changes its position, the sign of the measured phase difference changes too ($\varphi_2 - \varphi_1$ for $\varphi_1 - \varphi_2$), and the remaining components of the phase difference remain unchanged. Therefore, during the periodic

operation of a switch S1, an alternating voltage component arises in the output voltage of a phase detector U10 and is proportional only to the measured phase difference:

$$U_{17} = 0,5(U'_{16} - U''_{16}) = 0,5S_3(\phi_2 - \phi_1). \qquad (3.168)$$

The alternating component U_{17} is isolated by a high-pass filter Z1, intensified by a switching frequency amplifier A8 and rectified by a synchronous detector U11. The rectified voltage is measured by the indicator P1:

$$U_{18} = S_0(\varphi_2 - \varphi_1), \qquad (3.169)$$

where S_0 – the resulting sensitivity of the conversion of the phase difference to direct-current voltage.

It can be seen from the following expression that the result of the switching and modulation conversion does not depend on amplitude-phase distortions in the mixers (φ_4 and φ_5), as well as the frequency-phase distortions in the selective amplifiers (φ_6 and φ_7).

Since the heterodyne inputs of EHF mixers are decoupled from each other by a hybrid tee, there is practically no phase distortion from spurious interchannel coupling.

Thus, the considered RS of the phase shift conversion of reflected EHF oscillations is invariant to phase distortions in the conversion channels, which ensures an increase in the measurement accuracy.

Experimental studies of RS prototype in the 5-mm range of EHF frequencies (55…65 GHz) confirmed the possibility of measuring small phase changes of the reflected signal within 5…20° with an imprecision of no more than ±0,1° at a frequency of bias of EHF oscillations by 10 kHz and the reflection coefficient of the object Γ=0,8...0,3.

3.11 RS for detection and registration of natural resonant frequencies of BAP bioobjects

Methods and means of mm-therapy have become widespread recently. They are based on the targeted exposure of millimeter-wave electromagnetic radiation on biologically active (acupuncture) points (BAP) of the skin. A reflex reaction of an organism to a local millimeter effect is aimed at normalizing available or artificially induced deviations.

In the mode of the continuous wave generation of millimeter radiation, a reflex reaction appears when the frequency of monochromatic radiation coincides with one of the resonant therapeutic frequencies of a body [9].

In the proposed method for determination of therapeutic EHF frequencies [59], a biological object is irradiated by an amplitude-modulate EHF signal, the side frequencies of which are shifted relative to the frequency of the carrier vibrations by half of the resonance absorption band of BAP.

Then the levels of reflected signals are compared at two side frequencies. The carrier frequency of a modulation signal is changed until the levels of reflected signals are equal. Hence, the carrier frequency is measured, the value of which determines the resonant frequency of an object.

The second amplitude-modulate EHF signal is generated to increase the accuracy, the carrier oscillations and the envelope of which are 90° phase-shifted in the case of the first modulated signal. Modulated signals are added and subtracted simultaneously. First, an object is irradiated with the sum signal, and the reflected signal is mixed with the difference signal.

Every time a low-frequency signal of doubled modulation frequency is extracted from the mixed signals. The carrier frequency of modulated signals is changed until the amplitudes of low-frequency signals are equal. Introduction to a device structure of two balanced EHF modulators and a hybrid tee as an adder and subtractor of EHF signals allows generating modulating signals with only one side frequency. Using an automatic changeover switch controlled by a frequency divider in a control circuit allows mutual substitution of low-frequency modulating signals with a frequency that is lower than the modulation frequency of EHF signals.

Isolation of a difference signal by an amplitude detector from a low-frequency signal of doubled modulation frequency in the form of an alternating voltage of the switching frequency and its control of the EHF generator frequency eliminates the effect of non-identity and instability of parameters of device elements. All this increases the accuracy of determining therapeutic EHF frequencies. Fig. 3.15 depicts RS system structure that is developed by authors [59] for determining therapeutic frequencies.

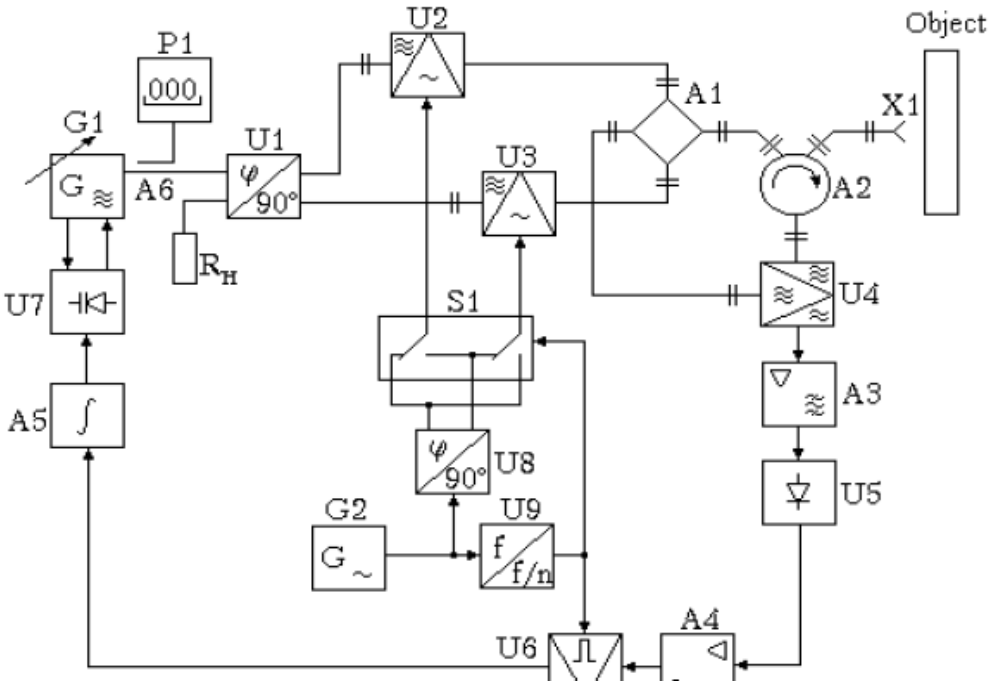

Figure 3.15 – RS for detection and registration
of natural resonant frequencies of BAP of bioobjects

The circuit includes a frequency tunable EHF generator G1 with a frequency adjustment unit U7.Amplitude modulators U2 and U3 are connected to its output through the 90°-hybrid connection.

The outputs of modulators are connected to arms of a hybrid tee A1, to one of the outputs of which a transceiver antenna X1, an irradiated biological object and a balanced mixer U4 are connected through a circulator A2. The second input of a mixer is connected to the second output of a hybrid tee A1.

The output of a balanced mixer U4 is connected in series to a selective amplifier A3, an amplitude detector U5, a low-frequency amplifier A4, a phase-sensitive rectifier U6 and an integrator A5, the output of which is connected to a frequency adjustment unit U7.

The low-frequency generator G2 through 90°-phase splitter U8 is connected to a bipolar automatic switch S1, the control input of which is connected to the output of a low-frequency generator G2 through a frequency divider U9.

The outputs of an automatic switch S1 are connected to the control inputs of amplitude modulators U2 and U3, and the control input of a

phase-sensitive rectifier U6 is also connected to the output of a frequency divider U9.

The EHF frequency meter P1 is connected to the output of the EHF generator G1 through a directional coupler A6.

Monochromatic signal generator G1 is modulated

$$U_1(t) = U_{m1}\cos(\omega_1 t + \varphi_1) \tag{3.170}$$

in an amplitude by a low-frequency signal of a generator G2

$$U_2(t) = U_{m2}\cos(\Omega t + \Phi)\,. \tag{3.171}$$

At the same time, the EHF signal is phase shifted by 90° by a phase splitter U1

$$U_3(t) = U_{m1}\sin(\omega_1 t + \varphi_1) \tag{3.172}$$

At the same time, the EHF signal is phase shifted by 90° by a phase splitter U1:

$$U_4(t) = U_{m2}\sin(\Omega t + \Phi)\,. \tag{3.173}$$

The low frequency value Ω is chosen equal to half the resonance absorption band $\Delta\omega$ of an irradiated biological object, i.e. modulation frequency $\Omega = \Delta\omega/2$.

Two amplitude-modulated signals are formed in a result of modulation:

$$\begin{aligned} U_5(t) = U_H\ \{&\cos\ (\omega_1 t + \varphi_1) + \frac{m}{2}\cos\ \left[(\omega_1 - \Omega)t + \varphi_1 - \Phi\right] + \\ &+\ \frac{m}{2}\ \cos\ \left[(\omega_1 + \Omega)t + \varphi_1 + \Phi\right]\}\ , \end{aligned} \tag{3.174}$$

$$\begin{aligned} U_6(t) = U_H\ \{&\sin\ (\omega_1 t + \varphi_1) + \frac{m}{2}\cos\ \left[(\omega_1 - \Omega)t + \varphi_1 - \Phi\right] - \\ &-\ \frac{m}{2}\ \cos\ \left[(\omega_1 + \Omega)t + \varphi_1 + \Phi\right]\}\ , \end{aligned} \tag{3.175}$$

where $U_{н}$ – a carrier voltage; m – EHF signal amplitude modulation depth coefficient $m < 1$.

The difference frequency component $\omega_2 = \omega_1 - \Omega$ with a phase $\varphi_2 = \varphi_1 - \Phi$ is a signal of the lower side frequency relative to the carrier frequency ω_1 of the radiation, and the component of the sum frequency $\omega_3 = \omega_1 + \Omega$ and phase $\varphi_3 = \varphi_1 + \Phi$ is a signal of the upper side frequency.

Modulation signals (3.174) and (3.175) sum and subtract in a hybrid tee A1, resulting in the formation of signals with suppressed one of the side frequencies:

$$U_7(t) = U'_H\ [\cos\ (\omega_1 t + \varphi_1 + \frac{\pi}{4}) + \frac{m}{2}\ \cos\ (\omega_2 t + \varphi_2)]\,, \qquad 3.176)$$

$$U_8(t) = U''_H\ [\cos\ (\omega_1 t + \varphi_1 - \frac{\pi}{4}) + \frac{m}{2}\ \cos\ (\omega_3 t + \varphi_3)]\,, \qquad (3.176)$$

where U'_H and U''_H – amplitudes of the carrier vibrations.

The modulation depth of microwave oscillations is chosen small within 5...10 % ($m = 0{,}1...0{,}05$). Therefore, the power of the EHF signal is mainly concentrated in carrier oscillations of the frequency ω_1.

First, a biological object with a resonant frequency ω_0 is excited with a sum signal (3.176) with a lower side frequency $\omega_2 = \omega_1 - \Omega$ and a signal reflected from the BAP is extracted.

$$U_9 = U'_H\ [\Gamma_1 \cos\ (\omega_1 t + \varphi_1 + \frac{\pi}{4} + \Delta\varphi'_1) + \Gamma_2 \frac{m}{2}\ \cos\ (\omega_2 t + \varphi_2 + \Delta\varphi_2)]\ , (3.178)$$

where Γ_1 and Γ_2 – the reflection coefficient of an object at a frequency ω_1 and ω_2; $\Delta\varphi'_1$ and $\Delta\varphi_2$ – additional phase shifts of signals when they are reflected, respectively, at frequencies ω_1 and ω_2.

Depending on the frequency mismatch with an object, the reflection coefficient module has the form:

$$\Gamma_1 = \frac{\sqrt{4\Gamma_0^2 + (1+\Gamma_0)^2 d_1^2}}{\sqrt{4 + (1+\Gamma_0)^2 d_1^2}}\,, \qquad (3.179)$$

$$\Gamma_2 = \frac{\sqrt{4\Gamma_0^2 + (1+\Gamma_0)^2 d_2^2}}{\sqrt{4 + (1+\Gamma_0)^2 d_2^2}}\,, \qquad (3.180)$$

where Γ_0 – a resonance reflection coefficient ($\omega_1 = \omega_0$); $d_1 = 2Q\frac{\Delta\omega_1}{\omega_0}$ – a generalized mismatch of a signal relative to an object; Q – an equivalent Q factor of BAP in an absorption band; $\Delta\omega_1 = \omega_1 - \omega_0$ – frequency mismatch ω_1; $d_2 = 2Q\frac{\Delta\omega_2}{\omega_0}$ – generalized signal mismatch relative to a BAP

resonator at the lower side frequency ω_2; $\Delta\omega_2 = \omega_2 - \omega_0$ – frequency mismatch ω_2.

The EHF signal (3.178) reflected from an object is mixed with the difference EHF signal (3.177) in a mixer U4. Low-frequency oscillations with doubled modulation frequency are isolated from the resulting signal:

$$U_{10} = \frac{S_1}{4}\Gamma_2 K_1 m U'_H U''_H \cos[(\omega_3 - \omega_2)t + \varphi_3 - \varphi_2 - \Delta\varphi_2] = \\ = \frac{S_1}{4}\Gamma_2 K_1 m U'_H U''_H \cos(2\Omega t + \varphi_4)\ , \tag{3.181}$$

where S_1 – a differential trans conductance (steepness of the characteristics) of mixing microwave oscillations; K_1 – a filtration coefficient of low-frequency oscillations; $\varphi_4 = \varphi_3 - \varphi_2 - \Delta\varphi_2$ – the resulting phase of a low-frequency signal.

A low-frequency signal (3.181) is rectified in amplitude by a detector U5 and the voltage is measured:

$$U_{11} = \frac{S_1 S_2}{4}\Gamma_2 K_1 m U'_H U''_H\,, \tag{3.182}$$

where S_2 – the steepness of the conversion of an amplitude detector.

Then an object is irradiated with a difference signal (3.177) with an upper side frequency $\omega_3 = \omega_1 + \Omega$ and the reflected signal is isolated:

$$U_{12} = U''_H[\Gamma_1 \cos\ (\omega_1 t + \phi_1 - \frac{\pi}{4} + \Delta\phi''_1) + \\ + \Gamma_3 \frac{m}{2}\ \cos\ (\omega_3 t + \phi_3 + \Delta\phi_3)]\ , \tag{3.183}$$

where Γ_1 and Γ_3 – a modulus of reflection coefficient respectively, at a frequency ω_1 and ω_3; $\Delta\varphi''_1$ and $\Delta\varphi_3$ – additional phase shifts under reflection, respectively, at a frequency ω_1 and ω_3.

The frequency ω_3 reflection coefficient has the form:

$$\Gamma_3 = \frac{\sqrt{4\Gamma_0^2 + (1+\Gamma_0)^2 d_3^2}}{\sqrt{4 + (1+\Gamma_0)^2 d_3^2}}\,, \tag{3.184}$$

where $d_3 = 2Q\frac{\Delta\omega_3}{\omega_0}$ – generalized detuning of the signal reflected from the BAP at the upper side frequency ω_3; $\Delta\omega_3 = \omega_3 - \omega_0$ – detuning on a frequency of ω_3.

The EHF signal (3.183) reflected from BAP is mixed with a sum EHF signal (3.176). Low-frequency oscillations with a doubled modulation frequency are isolated from the resulting signal:

$$U_{13} = \frac{S_1}{4}\Gamma_3 K_1 m U'_H U''_H \cos[(\omega_3 - \omega_2)t + \varphi_3 - \varphi_2 + \Delta\varphi_3] = \\ = \frac{S_1}{4}\Gamma_3 K_1 m U'_H U''_H \cos(2\Omega t + \varphi_5), \tag{3.185}$$

where $\varphi_5 = \varphi_3 - \varphi_2 + \Delta\varphi_3$ – a resulting phase of a low-frequency signal.

A low-frequency signal (5.65) is detected and its voltage is measured:

$$U_{14} = \frac{S_1 S_2}{4}\Gamma_3 K_1 m U'_H U''_H. \tag{3.186}$$

The voltage low-frequency signals (3.182) and (3.186) are compared and a difference signal is generated:

$$U_{15} = U_{11} - U_{14} = \frac{S_1 S_2}{4} K_1 K_2 m U'_H U''_H (\Gamma_2 - \Gamma_3), \tag{3.187}$$

where K_2 – conversion gain ratio of a difference signal.

The carrier frequency ω_1 of an irradiating signal is changed to obtain a zero value of a difference signal (3.187). Upon reaching a zero difference signal, we have:

$$\Gamma_2 = \Gamma_3. \tag{3.188}$$

We get the following, taking into account values of BAP reflection coefficients at lower and upper side frequencies:

$$\frac{4\Gamma_0^2 + (1+\Gamma_0)^2 d_2^2}{4 + (1+\Gamma_0)^2 d_2^2} = \frac{4\Gamma_0^2 + (1+\Gamma_0)^2 d_3^2}{4 + (1+\Gamma_0)^2 d_3^2}. \tag{3.189}$$

It follows from equality (3.189) that the absolute values of generalized detunings of an object are equal:

$$|d_2| = |d_3| \text{ or } |\omega_2 - \omega_0| = |\omega_3 - \omega_0|. \tag{3.190}$$

Since the side frequencies synchronously change with changes in a carrier frequency ω_1, equality (5.70) is satisfied upon condition:

$$|\omega_1 - \Omega - \omega_0| = |\omega_1 + \Omega - \omega_0| \qquad (3.191)$$

Then a carrier frequency of an irradiating signal necessarily coincides with a tuned frequency of BAP,

$$\omega_1 = \omega_0 = \frac{1}{\sqrt{LC}}, \qquad (3.192)$$

where – L and C are equivalent inductance and capacitance of the BAP molecular resonator.

Thus, the frequency of EHF oscillations is precisely tuned to the resonant frequency of an object by the equality of products of two EHF signals of side frequencies, in which one of the signals is reflected from an object by a signal of one side frequency. The other one is symmetrical relative to the carrier frequency of the other side frequency.

Moreover, the inconstancy of absolute values of object reflection coefficients in the vicinity of the resonance Γ_2 and Γ_3, as well as the inequality of amplitudes of mixed signals U'_H and U''_H, the instability of mixing characteristics (S_1), detection (S_2) and filtering coefficient (K_1) due to its inevitable frequency detuning do not affect the alignment accuracy of the irradiating signal frequency with the resonant frequency of an object. The resonant frequency of the object $\omega_0 = \omega_1$ is measured by an EHF frequency meter.

A radiometric system operates in the following sequence. The injected signal of a frequency tunable EHF generator G1 is separated with the help of EHF hybrid connection U1 into two quadrature signals. A low-frequency signal of a generator G2 is similarly divided by a phase splitter U8 into two quadrature signals. Amplitude modulation of EHF signals, phase-shifted by 90°, is carried out in modulators U2 and U3 by low-frequency signals, also shifted by 90°. EHF signals with suppressed one of the side frequencies are formed as a result of summing and subtracting the modulated EHF signals in a hybrid tee A1.

In this case, a sum signal with a lower side frequency is formed at one output of a tee A1. A difference signal with the upper side frequency is formed at the other output. BAT of an object are irradiated with an EHF signal with suppressed side frequency through a transmit-receive antenna X1. The reflected EHF signal extracted by circulator A2 is mixed in a

balanced mixer U4 with an EHF signal in which the second side frequency signal is suppressed.

A mutual substitution of low-frequency modulating signals shifted by 90° occurs at inputs of modulators U2 and U3 with the help of an automatic switch S1 periodically with a switching frequency that is equal to the frequency of an output voltage of a frequency divider U9. In this case, the sum and difference EHF signals are mutually replaced at outputs of a hybrid tee A1. As a result, packets of low-frequency oscillations with a double modulation frequency are formed at an output of a balanced mixer U4, amplitudes of which are proportional to reflection coefficients of an object at symmetric side frequencies.

Packets of low-frequency oscillations are allocated and amplified by a selective amplifier A3 that is tuned to a double modulation frequency. The sequence of oscillation packets with different amplitudes is essentially one amplitude-modulated voltage, which is detected by an amplitude detector U5.

The resulting alternating voltage with a switching frequency of a switch S1 is amplified by a low-frequency amplifier A4 and rectified by a phase-sensitive rectifier U6, the reference voltage of which is supplied from an output of a frequency divider U9. The envelope phase of a modulated signal emitted by a selective amplifier A3 varies in dependence to a sign of the signal detuning regarding BAP resonant frequency. Therefore, the polarity of an output voltage of a phase-sensitive rectifier U6 charging the integrator A5 is determined by a sign of the detuning of the BAP resonator with respect to carrier oscillations of an irradiating signal.

An output voltage of an integrator A5 has an effect on a block U7 and thereby adjusts the frequency ω_1 of the EHF generator G1 to the value of a resonant frequency of BAP ω_0. When the frequency of a generator G1 coincides with a resonant frequency BAT ($\omega_1 = \omega_0$), an amplitude modulation in an output voltage of a selective amplifier A3 disappears and an integrator A5 stops charging with voltage of one or another polarity.

Accurate determination of a resonant frequency by a P1 frequency meter is ensured by means of the frequency alignment of the EHF generator G1 with the BAP resonant frequency. When tuning the frequency of the EHF generator G1, the search and determination of other resonant frequencies occur in a similar way.

The considered RS allows an automatically search for resonant frequencies of the BAP object on side frequencies ω_2 and ω_3 with high accuracy.

Time for determining the therapeutic frequencies of biological objects is significantly reduced at the same time and the efficiency of treating patients is increased by affecting their reflex zones with electromagnetic radiation of a frequency ω_1 that coincides with one of the therapeutic frequencies.

It is possible to change the ratio of powers at the resonant and side frequencies by changing the modulation depth m, providing an additional therapeutic effect.

3.12 Radiometric system for measuring reflective and absorbing properties of bio objects

In recent years, EHF therapy at biologically active points (BAP) has become widespread, in which BAP are irradiated with a noise signal in the millimeter wave range. To increase the effectiveness of treatment, pulse noise generators are used, in which the pulse repetition rate is selected in the low-frequency range of the manifestation of human biorhythms (1...100 Hz). A wide spectrum of a pulse-modulated signal contains spectral components that coincide with therapeutic frequencies and provide a simultaneous reflex effect on most of them. The duration of the procedure is reduced and the total absorbed dose is also reduced due to the operational search for individual resonant therapeutic frequencies.

RS, which allows to evaluate objectively the therapeutic effect in the process of patient irradiation by the magnitude of the reflected signal, regardless on the patient's own radiation level, due to which the treatment efficiency is increased, is shown on Fig. 3.16.

The RS contains a power supply unit (PSU), a cascade of pulse voltage generation U1, a noise pulse generator G1, a high-pass filter Z1, a directional reflected wave splitter A1, to the first output of which a broadband antenna X1 is connected, a mixer U2, a heterodyne G2, an intermediate-frequency band amplifier A2, a quadratic detector U3, a low-frequency amplifier A3, a synchronous detector U4, a low-pass filter Z2 and an indicator PA1. The position O denotes the surface of the irradiated object.

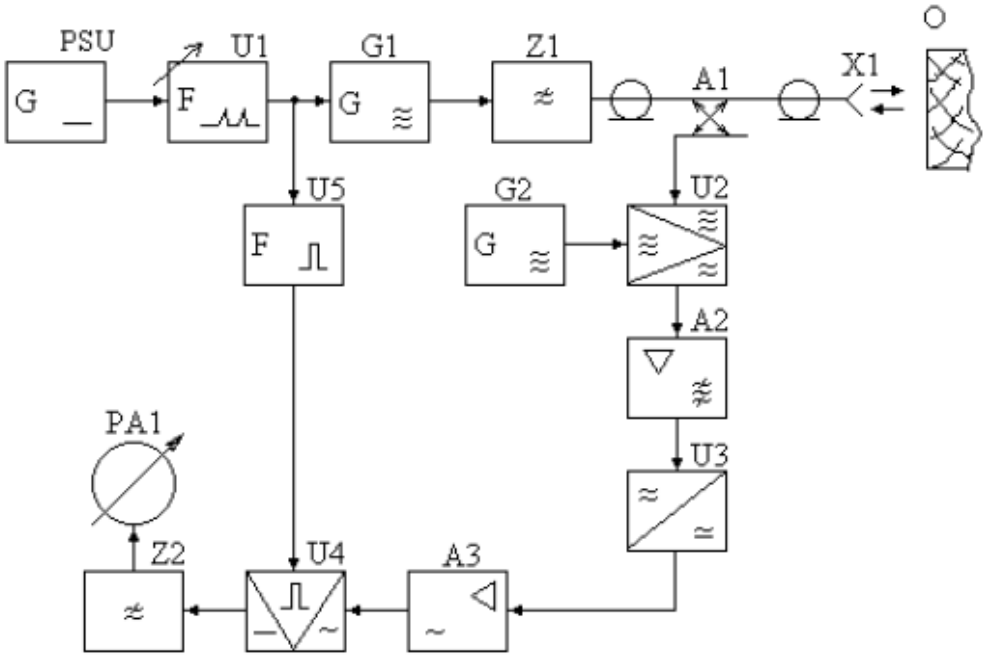

Figure 3.16 – RS for optimization of the frequency of the modulating signal

The supply voltage from the PSU is supplied to the cascade U1 of the pulse voltage generation, in which the low pulse repetition rate of the noise radiation characteristic of the range of human biorhythms is set. From the output of cascade U1, high voltage pulses are fed to the input of the gas-discharge noise generator G1. Electromagnetic noise radiation generated at the output of a pulse generator passes through a high-pass filter Z1, which limits the spectrum of noise radiation at a given cutoff frequency and corresponds to the lower boundary of the mm range of the electromagnetic spectrum of the noise signal. The impact of low frequencies in the radiation spectrum, which are harmful to the human body, is suppressed by the filter Z1.

The noise radiation formed in this way with a spectrum limited from below and a predetermined distribution of power spectral density through a directional splitter A1 arrives at an antenna X1 representing a transmitting and receiving device (for example, a log-periodic micro-band structure). The emitting signal acts on the selected BAP on the skin surface O, determining the therapeutic effect. The part of the noise radiation reflected from the surface O, together with the BAP's own radiation, enters the antenna X1 and, through the other output of the directional splitter A1, is fed to the input of the mixer U2, to another input of which the local heterodyne G2 is supplied. Including the intrinsic noise of the mixer $\overline{U}_{11}^2$, the variance of the input signal of the mixer can be represented as:

$$\overline{U}_{11}^2 = \overline{U}_2^2 + \overline{U}_3^2 + \overline{U}_4^2, \quad (3.193)$$

where $\overline{U}_2^2$ – is the dispersion of the reflected signal; $\overline{U}_3^2$ – dispersion of the BAP signal; $\overline{U}_4^2$ – dispersion of the noise of the mixer taking into account the noise of the heterodyne.

As a result of mixing the input noise signal with the monochromatic signal of the heterodyne, a spectrum of difference frequencies is created, part of which falls into the passband of the intermediate frequency amplifier A2. The part of the frequency spectrum allocated and amplified by amplifier A2 creates a narrow-band noise signal and its dispersion is proportional to the power of the reflected broadband signal $\overline{U}_{11}^2$.

In the pauses between the action of irradiating pulses on the BAP of the skin surface O by the antenna X1, only the object's own radiation is received, which, through the directional splitter A1, enters the input of the mixer U2. The dispersion of the input signal of the mixer U2 in pauses $\overline{U}_{12}^2$ can be expressed as:

$$\overline{U}_{12}^2 = \overline{U}_3^2 + \overline{U}_4^2. \quad (3.194)$$

As a result of mixing the input signal with the heterodyne G2 signal and amplifying the intermediate frequency amplifier A2, a narrow-band noise signal with a dispersion proportional to the power of the BAP natural radiation and natural noise $\overline{U}_{12}^2$ will appear. The intermediate frequency signals are detected by a quadratic detector U3. As a result of detection, a sequence of video pulses is formed with amplitudes proportional to $\overline{U}_{11}^2$ and $\overline{U}_{12}^2$, and a pulse repetition rate set by cascade U1. An alternating voltage component of the video pulses is extracted and amplified by a low frequency amplifier A3. The amplified voltage is rectified by a synchronous detector U4. The output voltage of the synchronous detector is smoothed out by a low-pass filter Z2 and is measured by the indicator PA1. Since the variable component of the voltage is proportional to the difference between the dispersions of the noise signals $\overline{U}_{11}^2$ and $\overline{U}_{12}^2$, the measured voltage is determined only by the power of electromagnetic radiation $\overline{U}_2^2$ reflected from the BAP on the surface of the skin. The measurement result is not affected by the level of the object's own

radiation and the level of noise of the measuring part of the device circuit. For the minimum readings of the indicator PA1, which correspond to the maximum absorption, the repetition rate of the radiation pulses is set, and the exposure time is controlled by the moment of a sharp increase in the readings of the indicator. Since the level of the reflected signal of the EH frequencies characterizes the physiological state of the body, the considered device can be used for diagnosis and treatment.

The research has shown that the state of the body largely depends on its bioenergy information potential. In the presence of pathology in the body (the presence of a disease), a strong absorption of the emitting signal occurs through the BAP, which means that the minimum value of the reflected signal is displayed. In the absence of pathology, the reflected signal remains constant in this therapeutic wavelength range.

Thus, modulating RS allows to determine the presence of pathology and exert a therapeutic effect by the EHF radiation, contributing to the restoration of the patient's electromagnetic framework.

The values of biologically active (therapeutic) frequencies, allowing to restore partially or fully different functional disturbances in the life of biological objects, should be determined on the background of measuring low levels of absorbed power. The measurement in the frequency band of small (at the noise level) values of the absorbed power, as well as the assessment of the absorption capacity of biological objects, are complicated by some difficulties, in particular, by the dependence of the measurement result of the reflected signal not only on the absorption capacity of the BAP, but also on the level of radiation.

In addition, at non-thermal intensities of external EMI due to the absence of thermal effects in the irradiated medium, it is impossible to use the most sensitive and accurate calorimeters of absorbed power. For the same reason, thermo resistive, thermoelectric, bolometric and other types of thermal power meters cannot be used.

Fig. 3.17 shows the functional diagram of RS for assessing the absorbency of biological tissues, regardless of the level of the irradiating signal.

The device contains: 1 – generator of the EHF range; 2 and 5 – amplitude modulators; 3 – attenuator; 4 – circulator; 6 – antenna; 7 – amplitude detector; 8 and 11 – selective amplifiers; 9 and 12 – synchronous detectors; 10 and 13 – low-pass filters; 14 – measuring device; 15 – radio

frequency generator; 16 – frequency divider; 17 – diode-capacitor circuit; 18 – differential amplifier; 19 is a voltage reference source; 20 – integrator; 21 – tested biological tissue.

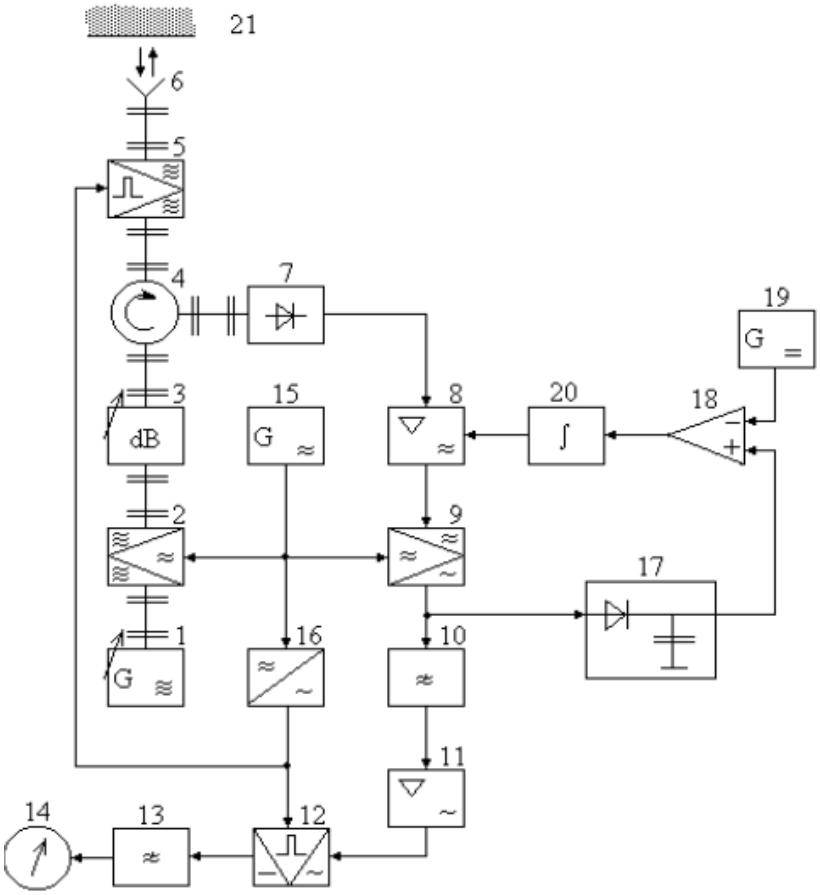

Figure 3.17 – RS for assessing the absorbency of biological tissues

The device operates as follows.

The oscillations of the generator 1 of the EHF range are supplied to the amplitude modulator 2, controlled by a radio frequency generator. In this case, the oscillations of the EHF range are modulated in amplitude with a given modulation depth. Attenuator 3 sets the low intensity of the probing oscillations. The intensity-normalized oscillations pass through the circulator 4 and are fed to the amplitude modulator 5, controlled by a rectangular low-frequency voltage. Modulator 5 provides a modulation depth of m_2 up to 100 %, i. e. it operates in an interrupt mode with a simultaneous reflection of these oscillations.

When the modulator 5 is open, packets of the passed EHF oscillations arrive at the antenna 6 and are emitted as a probe signal to the biological tissue under study. If the oscillation frequency does not coincide with the

therapeutic frequency of the biological tissue, then a weak absorption of the probe signal occurs, and the rest of it is reflected. The reflected signal is received by the antenna and through the open modulator 5 and the circulator 4 is sent to the amplitude detector 7. At the same time, the antenna receives its own EHF radiation, which is also fed to the amplitude detector.

When the modulator 5 is closed, the EHF oscillations of the generator 1 are reflected from it and also sent to the amplitude detector 7 through the circulator 4.

The intensity of the incident and reflected EHF oscillations is comparable to or even less than the intensity of instrumental noise and obstacles. As a result of detecting packages of EHF oscillations, a mixture of high-frequency oscillations of the frequency of the modulation generator 15 and broadband noise is formed. Selective amplifier 8, tuned to the frequency of the radio frequency generator 15, allocates and amplifies packages of high-frequency modulating oscillations. The amplified radio frequency voltage is detected by a synchronous detector 9, which is controlled directly by the voltage of the modulating generator 15.

After synchronous detection of high-frequency voltage packets, video pulses are formed. Their amplitudes can be calculated as:

$$U_1 = k_1^2 k_2^2 m_1^2 S_1 k_3 P_1, \tag{3.195}$$

$$U_2 = k_1^2 k_2^2 m_1^2 S_1 k_3 P_2, \tag{3.196}$$

where k_1, k_2, k_3 – respectively, the transmission coefficients of the attenuator 3, circulator 4 and the gain of the selective amplifier 8; S_1 – the steepness of the conversion of the amplitude detector 7; P_1, P_2 – power probing and reflected oscillations.

From the sequence of video pulses with amplitudes U_1 and U_2 a low-pass filter 10 selects the low-frequency component of the voltage of the interrupt frequency with the amplitude:

$$U_3 = \frac{U_1 - U_2}{2} = k_1^2 k_2^2 m_1^2 S_1 k_3 \frac{P_1 - P_2}{2}. \tag{3.197}$$

where k_4 – is the gain of the selective amplifier 11.

The video pulses U_1 and U_2 from the output of the synchronous detector 9 also arrive at the diode-capacitor circuit 17. Due to the fast charge and slow discharge of the capacitor in the circuit, the amplitude of the larger sequence of video pulses is stored. Since the power of incident oscillations is always greater than the power of reflected oscillations, it always exceeds the power of reflected oscillations. Therefore, the output voltage of the circuit is set at the level U_1. As a result, at the output of the diode-capacitor circuit 17, a constant voltage is formed:

$$U_5 = U_1 = k_1^2 k_2^2 m_1^2 S_1 k_3 \frac{P_1}{2}. \quad (3.198)$$

The voltage U_5 and stable voltage $U_6 = const$ from the reference voltage source 19 are supplied to the inputs of the differential amplifier 18, from the output of which the amplified differential voltage is taken:

$$U_7 = k_5 (U_5 - U_6), \quad (3.199)$$

where k_2 –is the gain of the differential amplifier.

The voltage U_7 charges the integrator 20, which controls the gain of the selective amplifier 8. The process of automatic gain control lasts until the integrator reaches zero input voltage. In this case, the steady-state value of the gain of the selective amplifier 8 will be equal to:

$$k_3 = \frac{2U_6}{k_1^2 k_2^2 m_1^2 S_1 P_1}. \quad (3.200)$$

With this in mind, the voltage supplied to the measuring device 14 has the form:

$$U_4 = k_4 U_6 \frac{P_1 - P_2}{P_1}. \quad (3.201)$$

It can be seen from the obtained expression that the measured voltage is proportional to the relative value of the absorbed power, which excludes the influence of the inconstancy of the power of the microwave radiation on the assessment of the absorption capacity of biological tissues. The measurement result is also not affected by the level of intrinsic electromagnetic radiation of the studied tissue, instrumental noise and interference of the RS conversion path.

The sensitivity of the RS to the level of absorbed power is easily controled by changing the gain of the low-frequency selective amplifier 11.

By changing the frequency of the mm wavelength range generator 1, the absorption capacity of biological tissues is evaluated depending on the values of biological active frequencies. So, when the frequency of the generator coincides with the biologically active (therapeutic) frequency, the absorption increases sharply and the coefficient of relative absorption capacity approaches one:

$$k_n = \frac{P_1 - P_2}{P_1} \to 1. \qquad (3.202)$$

Thus, the biologically active tissue frequencies can be determined from the maximum values of the absorption coefficient k_n, and the absorption band of biological tissue at these frequencies can be determined from a change in the value of k_n with frequency deviations.

When tuning the frequency of the EHF generator in a wide frequency band, it is possible to register the absorption spectrum of the tissue under study at various given levels of external electromagnetic mm radiation.

The developed RS allows us to study, in particular, the absorption capacity of human skin, for example, in the frequency range 50...80 GHz with an irradiation level of $P_1 \le 10^{-6}$ W/cm^2. At a modulation frequency of 100 kHz and a switching frequency of 1 kHz, it is possible to determine the absorption capacity by the value of the absorption coefficient in the range from 0.001 to 0.998 with a relative error of not more than 0.5 %.

When receiving electromagnetic radiation from a biological object, information about both thermal and bioinformation radiation is simultaneously received. It is very difficult to separate this information and isolate a signal that would be determined only by the bioinformation component of radiation.

A method for detecting and measuring electromagnetic radiation from biological objects, based on the effect of a probing monochromatic signal on biologically active points (BAP) on the skin of humans and animals, on the reception of the reflected signal, and the extraction of the signal from the secondary radiation of the object from one of the combination frequencies that arise from mixing the irradiating signal and harmonics of the biorhythm signal of the irradiated biological object. A part of the spread spectrum signal reflected from the biological object is fed back to the monochromatic radiation source, where it is mixed with the initial radiation at a nonlinear object. As a result, a polyfrequency effect on a biological

object is generated, and the harmonic components of it are synchronized with the biorhythms of the studied man or animal.

The system receives the secondary radiation, which is a consequence of the interaction of the probing signal with the bioinformation radiation signals of the object, and a part of the broadband radio thermal radiation inside the reception band of the combinational components of the reflected signal. Therefore, this method does not provide information on the intensity of bioinformation radiation of a biological object separately.

A functional diagram of a radiometric system for detecting and measuring of electromagnetic radiation of biological objects is presented in Fig. 3.18.

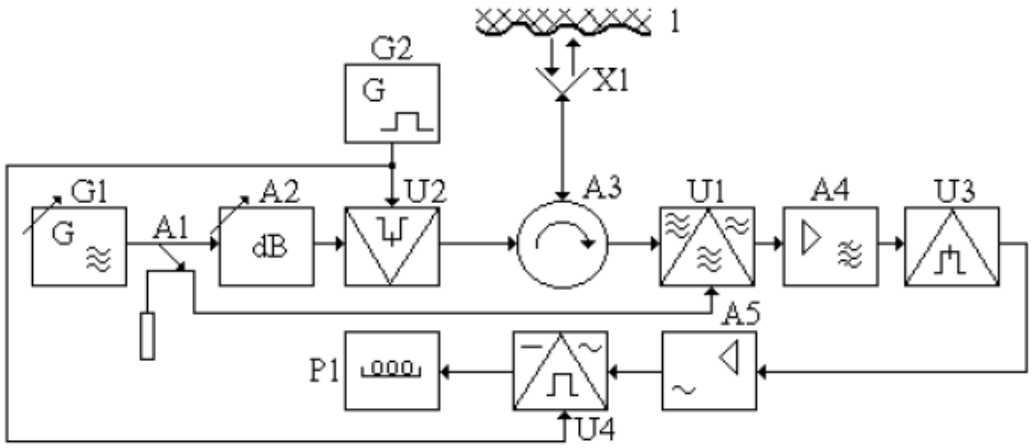

Figure 3.18 – RS for measuring bio-informational component of a living object signal

The system includes a series-tunable EHF generator G1, a directional splitter A1, an adjustable attenuator A2, a pulse modulator U2, the output of which is connected to the first input of the circulator A3, an EHF mixer U1, an intermediate-frequency amplifier (IFA) A4, amplitude quadratic detector U3, low frequency power amplifier A5, synchronous detector U4, digital voltmeter P1. The transmitting-receiving antenna X1, located near the biological object is connected to the second input of the circulator A3. The output of the directional splitter A1 is connected to the second input of the mixer U1. The outputs of the reference low frequency generator G2 are connected to the control inputs of the pulse modulator U2 and the synchronous detector U4.

The principle of operation of the radiometric system for the detection and measurement of electromagnetic radiation of biological objects is as follows.

Bio-active points on the skin of humans and animals have nonlinear (in the electrical sense) properties. Therefore, when probing the BAP of an object with electromagnetic waves (EMW) of the EHF range (millimeter waves) in the absorption zones of the BAP, the EMW interacts with the bioinformation radiation from the body cells. If the frequency ω_1 of the probing monochromatic signal coincides or is close to one of the characteristic frequencies ω_0 of the biological object, then the probing oscillations are mixed with its own coherent electromagnetic oscillations, which are generated by cells and subcellular structures.

Therapeutic (resonant) frequencies, as shown by experiments, are equal to the biorhythms of the body or are the multiple of them. As a result of mixing the oscillations of the probe ω_1 frequency signal with the harmonics of the oscillations of the dominant Ω frequency biorhythm in the nonlinear element of the BAP, the oscillations of combinational frequencies are formed ($\omega_1 \pm n\Omega$, where n – the number of harmonic). As a result of this, secondary electromagnetic radiation at combinational frequencies occurs at the biological object, the intensity of which is determined by the level of the physiological state of the organism.

The probe signal reflected from a biological object with an extended spectrum (due to the secondary radiation ω_1, $\omega_1 \pm n\Omega$) and intrinsic electromagnetic radiation is mixed with a part of the initial monochromatic oscillations of frequency ω_1. The result of mixing the components of the received signal is in forming of oscillations of the intermediate subtraction frequency ($\omega_p = n\Omega$) and the spectrum of nearby oscillations falling into the passband $\Delta\omega$ of the intermediate frequency path. The intensity of the total signal in the passband $\Delta\omega$ is determined by the expression:

$$P' = S\left(P + \overline{U}_1^2 + \overline{U}_2^2 + \overline{U}_3^2\right), \qquad (3.203)$$

where S –is the steepness of the conversion of the signal receiver; P –is the power of the secondary bioinformation radiation of the object at the combination frequency; $\overline{U}_1^2$ – is the dispersion of a part of the spectrum of the thermal radiation of an object in the $\Delta\omega$ band; $\overline{U}_2^2$ – is the dispersion of a part of the spectrum of the primary bioinformation radiation of an object in the $\Delta\omega$ band; $\overline{U}_3^2$ – is the dispersion of the intrinsic noise of the receiving equipment in the $\Delta\omega$ band.

In practice, the power of intrinsic noise exceeds the power of the received radio thermal and bioinformation radiation ($\overline{U}_3^2 > \overline{U}_1^2 + \overline{U}_2^2 + P$). To detect and measure the secondary radiation, the probing object is subjected to pulse amplitude modulation. Therefore, irradiation of a biological object is carried out periodically by pulses with a low repetition rate. In the pauses between the pulses of the probe signal, the own electromagnetic radiation of the biological object is received, the intensity of which in the reception band equals to:

$$P'' = S\left(\overline{U}_1^2 + \overline{U}_2^2 + \overline{U}_3^2\right). \quad (3.204)$$

The intensities of the received signals P' and P'' are compared. To this purpose, the system detects pulses of an intermediate frequency and extracts an alternating voltage component with a pulse repetition rate from the sequence of video pulses. The amplitude of the alternating voltage is:

$$U_{\sim} = SK\frac{P' - P''}{2} = S_o P, \quad (3.205)$$

where K – is the conversion coefficient of the elements of the RS channels; S_o=KS is the resulting steepness of a single-channel conversion of bioinformation radiation intensity into voltage.

From the obtained expression, we can see that the amplitude of the low-frequency subtraction signal is proportional to the power of the secondary bioinformation electromagnetic radiation of the biological object and does not depend on the radiothermal component of the radiation, as well as on the level of intrinsic noise of the measuring equipment.

Studies have shown that the intensity of bioinformation radiation is reduced in a sick body compared to that in a healthy one. Therefore, by the level of secondary radiation, which is proportional to the intensity of bioinformation radiation, it is possible to control the level of the physiological state of a person and other bioobjects with high accuracy.

In a radiometric system (Fig. 3.18), a millimeter-wave monochromatic signal is generated by an EHF generator G1. The controlled attenuator A2 sets the required level of exposure for the biological object (not more than 10^{-12} W/cm^2). The probe signal is periodically interrupted by the pulse modulator U2, which is controlled by the low-frequency voltage from the generator G2. The pulses of the probe signal pass through the circulator A3 and are emitted by the antenna X1 in the direction of the studied biological

object 1. The pulses reflected from the biological object are received by the antenna X1 and through the circulator A3 they enter the input of the microwave mixer U1, to the second input of which the part of the power of the initial sounding oscillations is supplied through directional splitter A1. As a result of mixing, oscillations of the subtractive frequency are formed, in the spectrum of which there are also oscillations of the combinational frequencies of the secondary radiation of the biological object.

Amplifier A4 has a predetermined pass band with a central band tuned to one of the combinational frequencies of the secondary radiation spectrum. The amplified intermediate frequency signal is extracted by a detector U3 with a quadratic characteristic. The video pulses resulting from the detection have an amplitude proportional to the power of the high-frequency signal.

The values of the amplitudes are also affected by the thermal radiation of the biological object and the level of the noise of the mixer U1 and the elements of the EHF pathway (circulator A3 and antenna X1).

In the pauses between the probe pulses, EHF pulses of the self-radiation of the biological object 1 are received from the antenna X1 through the circulator A3 together with the noise of the receiving path. As a result of mixing the received pulses and input noise with the signal of the generator G1, a spectrum of oscillations of subtractive frequencies arises from the interaction between the spectral components of the EHF radiation of the biological object and noise with oscillations of the generator G1.

A part of the components of the spectrum of subtractive frequencies hits the pass band of the APA A4. The amplified signal is detected by a quadratic detector U3. The amplitude of the generated video pulses is proportional to the intensity of the natural radiation of the biological object and the noise power of the receiving unit of the device that hits the passband of the filter Z1.

The low power amplifier A5 isolates and amplifies the variable component of the sequence of video pulses, which is proportional only to the secondary radiation of the biological object.

The amplified voltage is rectified by a synchronous detector U4, which is controlled by the low-frequency voltage of the generator G2. The rectified voltage is measured with a digital voltmeter P1, the readings of which are proportional to the level of secondary radiation of a probed

biological object, determined by the intensity of coherent radiation of cells of a living organism.

So the influence of the intrinsic noise of measuring equipment and the level of radio thermal radiation of a biological object determined only by its temperature on the result of measuring are excluded due to the single-channel conversion of reflected pulses and pulses of the self-radiation of a biological object.

3.13 Feedback radiometric system using the object own radiation level

Another application in millimeter resonance therapy has the impact on bioactive points by continuous electromagnetic radiation of the noise-like spectrum of the mm range.

As an acting factor, it uses the spectrum components of a broadband signal having the nature of white noise with a uniform spectral density in the entire range of radiation frequencies. In this case, the patient's body itself absorbs the oscillation energy of those frequencies that coincide with its own resonant (therapeutic) frequencies. However, the continuity of the emission of a noise-like signal limits its spectrum that reduces the body reflex response.

In microwave resonance therapy (MRT) , the patient's selected BAPs are exposed with both noise signals and pulses of noise-like electromagnetic radiation of non-thermal intensity with a spectrum in the millimeter wavelength range that follow with a low frequency of biorhythms of the patient's body. To increase the effectiveness of this therapy, electromagnetic radiation is used with a spectrum having the nature of flicker noise in the frequency range from the left border of the millimeter region to the right border of its visible region. Amplitude modulation of microwave radiation is carried out by a low-frequency signal in the range from 0,1 Hz to 100 Hz and is affected by modulated radiation with an average value of the noise power spectral density not exceeding 10^{-18} W/Hz·cm^2.

The choice of a specific modulation frequency and the average spectral density is carried out according to the subjective feelings of the patient, which does not allow optimizing objectively the parameters of electromagnetic radiation and reducing the time of treatment sessions.

We developed RS, which in the process of patient treating provides objective information about his state of health according to the level of his

own electromagnetic radiation in the millimeter range. That allows to set the modulation frequency, stimulating an increase in the level of intrinsic electromagnetic radiation and to adjust the level of external radiation depending on the emissivity of the patient.

This circuit algorithm of the RS operation is constructed by receiving the patient's own electromagnetic radiation of BAPs in pauses between the irradiating pulses using, for example, a broadband directional coupler connected at the output of the irradiating channel. Processing of received and part of the emitted pulses of electromagnetic radiation can be performed in one receiving radiometric channel consisting of an EHF mixer, an intermediate frequency amplifier, a quadratic detector, a synchronous detector and a low-pass filter, which is connected to the output of a broadband directional coupler.

The goal is to obtain the maximum value of the received object's own electromagnetic radiation by changing the frequency of the audio power generator and regulation of the repetition rate of the irradiating pulses. The audio power generator simultaneously controls its voltage with an amplitude modulator and a synchronous detector. An increase in the intensity of irradiating pulses to the level of each patient's own radiation and determining the exposure time until a steady-state value of the increased intensity of the patient's own electromagnetic radiation is reached increases the effectiveness of the treatment and reduces the time of the procedure.

Fig. 3.19 presents a functional diagram of a broadband irradiation MRT system, which contains a mm-wave (EHF) noise generator G2, the output of which is connected in series to an adjustable attenuator A4, a valve A3, an amplitude modulator U1, a broadband directional coupler A1 and a broadband antenna X1.

The output of the broadband directional coupler A1 is connected in series to an EHF mixer U2 with an EHF heterodyne of monochromatic oscillations G1, an intermediate frequency amplifier A2, a quadratic detector U3, a low frequency power amplifier A5, a synchronous detector U4, a low-pass filter Z1, and an indicator P1. The audio power generator G3 is connected to the control inputs of the amplitude modulator U1 and the synchronous detector U4. The position «Object» indicates the patient's body.

The broadband noise signal of the millimeter-wave generator G2 through the adjustable attenuator A4 and the valve A3 is fed to the amplitude modulator U1, which is designed on *pin*-diodes and operates by the principle of signal reflection from a closed modulator. When the modulator is open, the noise signal through the directional coupler A1 enters the broadband antenna X1 and is emitted towards the patient. The intensity of electromagnetic radiation is pre-set to minimum using an adjustable A4 attenuator (at the level of the patient's minimum possible radiation).

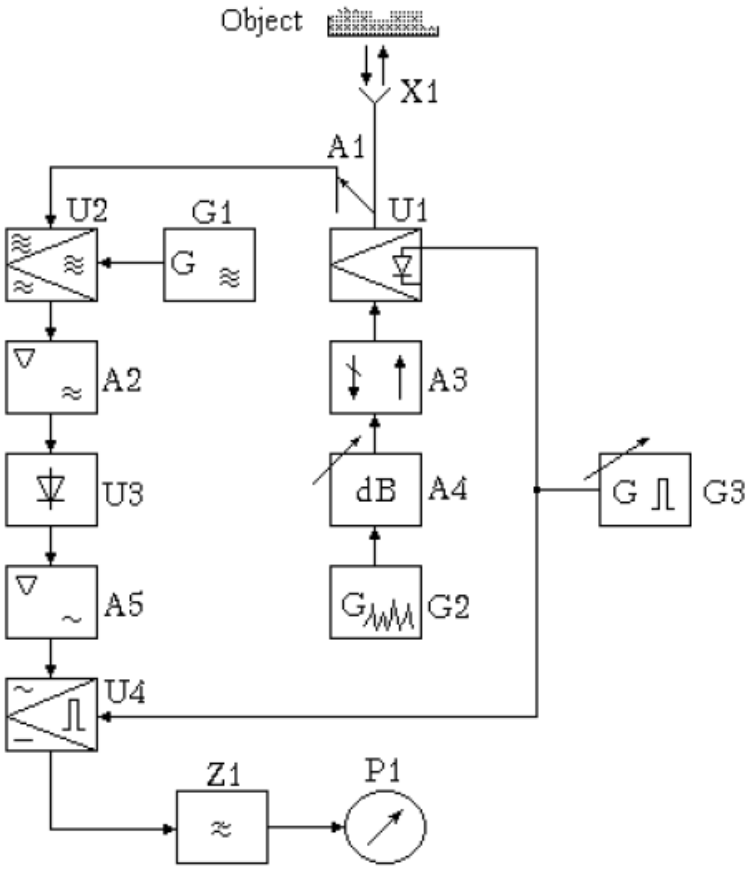

Figure 3.19 – RS for optimization of the exposure parameters by the patient's own radiation

Part of the emitted signal through a broadband directional coupler A1 is fed to the input of the EHF mixer U2, and the signal from the EHF local oscillator G1 comes to its second input. As a result of the signal mixing, subtractive intermediate frequency oscillations are generated, amplified by the intermediate frequency amplifier A2. The wide passband of amplifier A2 allows the transfer of a significant part of the spectrum of the emitted signal to an intermediate frequency. A signal amplified at an intermediate frequency is detected by a quadratic detector U3.

The patient's own millimeter radiation is received by the broadband antenna X1 and then through the open modulator U1 it enters the valve A3, in which it is absorbed. Received radiation does not enter the directional coupler A1.

The rectangular voltage of the audio power generator G3 controls the amplitude modulator U1. When the amplitude modulator U1 is closed, the noise signal of the generator G2 is reflected from the modulator and absorbed in the valve A3. The noise signal received by the broadband antenna X1 from the BAP of the patient is reflected from the closed modulator U1 and through the directional coupler, A1 enters the input of the EHF mixer U2.

The dispersion of the noise signal received by the broadband antenna is determined by the expression

$$\overline{U}_1^2 = S_1 T_E \ , \tag{3.206}$$

where S_1 – is the sensitivity of the antenna; T_E is the effective temperature of the irradiated BAP on patient's skin.

If the gain coefficient of the directional coupler A1 is designated K_1, then the dispersion of the input signal of the EHF mixer U2, taking into account its own noise, has the form:

$$\overline{U}_{21}^2 = K_1 \overline{U}_1^2 + \overline{U}_3^2 , \tag{3.207}$$

where $\overline{U}_3^2$ – is the dispersion of the intrinsic noise of the EHF mixer U2 reduced to its input, taking into account the noise of the heterodyne G1 and amplifier A2.

With the modulator U1 open, the dispersion of the input signal of the EHF mixer U2 will be:

$$\overline{U}_{22}^2 = K_1 K_2 \overline{U}_0^2 + \overline{U}_3^2 , \tag{3.208}$$

where K_2 – is the gain of the attenuator A1; $\overline{U}_0^2$ is the dispersion (power) of the noise signal of the generator G2.

Thus, as a result of switching the modulator U1 with a low frequency, electromagnetic radiation pulses impact on the patient being irradiated with a repetition rate set by the generator G3 and pulse duty cycle that equals 2. At the same time, part of the energy of these pulses also goes to the input of the EHF mixer U2. In the pauses between the irradiating pulses, electromagnetic energy pulses with the same frequency from the patient's BAP with a temperature T_E comes up at the input of the EHF mixer U2. So

after combining these pulses at the input of the EHF mixer U2, at its output an EHF signal is formed modulated in amplitude with a modulation depth:

$$m = \frac{K_1(K_2\overline{U}_0^2 - \overline{U}_1^2)}{K_1(K_2\overline{U}_0^2 + \overline{U}_1^2) + 2\overline{U}_3^2}. \quad (3.209)$$

Given that the power of the intrinsic noise of the EHF mixer is much higher than the power of millimeter radiation during resonant therapy ($\overline{U}_3^2 >> K\overline{U}_0^2$), we obtain:

$$m = \frac{K_1(K_2\overline{U}_0^2 - \overline{U}_1^2)}{2\overline{U}_3^2} << 1. \quad (3.210)$$

Pulses of the modulated signal transferred to the intermediate frequency are alternately detected by the quadratic detector A2, forming video pulses with amplitudes at the output:

$$U_4 = S_1K_3S_2(K_1\overline{U}_1^2 + \overline{U}_3^2), \quad (3.211)$$

$$U_5 = S_1K_3S_2(K_1K_2\overline{U}_0^2 + \overline{U}_3^2), \quad (3.212)$$

where S_1- is the steepness of the conversion of the mixer U2; K_3- is the gain of the amplifier A2 of intermediate frequency; S_2- is the steepness of the transformation of the quadratic detector G1.

The low frequency power amplifier A5 amplifies the variable component of the sequence of video pulses with amplitude:

$$U_6 = K_4\frac{U_4 - U_5}{2} = K_1S_1K_3S_2K_4\frac{\overline{U}_1^2 - K_2\overline{U}_0^2}{2}, \quad (3.213)$$

where K_4- is the gain of the low frequency power amplifier A5.

The amplified alternating voltage is rectified by a synchronous detector U4, which is controlled by the low-frequency voltage of the generator G3. The rectified voltage is smoothed by the low-pass filter Z1 and fixed by the indicator P1. It is possible to provide the maximum indexes on indicator P1 by changing the pulse repetition rate of electromagnetic energy pulses using the generator G3. That means that when $K_2\overline{U}_0^2 = const$ the difference in the intensities of the radiated and received energy increases:

$$\Delta U = U_1^2 - K_2U_0^2 > 0. \quad (3.214)$$

That indicates an increase in the intensity of the patient's own radiation. It means the activation of energy resources of the irradiated biological object.

Then, by adjusting the gain of the attenuator A4, the P1 indicator reads comes to zero when

$$K_2 \overline{U_0^2} = \overline{U_1^2}. \quad (3.215)$$

From here, the gain coefficient of the attenuator A4 is:

$$K_2 = \frac{\overline{U_1^2}}{\overline{U_0^2}}. \quad (3.216)$$

Conditions (3.215) and (3.216) mean that the intensities of the millimeter effect and the intrinsic millimeter radiation of the object are equal, so it allows us to choose the optimal MRT conditions.

We can see from the condition (3.215) that its implementation is not affected by the instability and inconstancy of the parameters of the units of the measuring pathway of the circuit (K_1, S_1, K_3, S_2, K_4). Thus, using the considered method, we can optimize the repetition rate and intensity of millimeter-wave pulses and thereby increase the effectiveness of treatment and shorten its time.

The sequence of the RS operation is as follows. First, the attenuator A4 provides the maximum attenuation ($K_2 \approx 0$). In this case, the patient is practically not irradiated with anything, and the antenna X1 receives only its own millimeter radiation from the BAP. The modulation depth of the EHF signal (3.210) is set to maximum, and the audio power amplifier U3 amplifies a relatively large alternating voltage with amplitude:

$$U_6' = 0{,}5 K_1 S_1 K_3 S_2 K_4 \overline{U_1^2}. \quad (3.217)$$

This voltage is rectified by a synchronous detector U4 and is measured by indicator P1.

Then, the attenuation of the attenuator A4 is reduced ($K_2 > 0$), and the process of irradiating the patient with millimeter radiation begins. The radiation intensity increases to obtain a zero reading of the indicator P1. This means a preliminary equalization of the radiated and received electromagnetic energy.

After reaching zero indications, the frequency of the audio power generator G3 changes to obtain the maximum indications on P1 that means an increase in the intensity of the body's own radiation under the influence of stimulating pulse irradiation. Then, the irradiation intensity of the attenuator A4 is increased again until the indicator P1 reaches zero, i.e. until the equality of the irradiated and increased received energies is established, and so on.

The frequency tuning of the generator G3 and attenuator A4 is repeated 3-4 times during the MRT process to obtain optimal millimeter-wave radiation parameters. The cessation of changes in the indicator P1 indicates the object saturation with electromagnetic energy, after which the MRT session ends. The procedure repeats in the next treatment session.

The treatment process is considered complete when a stable and sufficiently high level of intrinsic millimeter radiation (approximately 10^{-12} W/cm^2) is observed during regular MRI sessions.

The considered RS can be used for human and animal diagnostics by the level of their own electromagnetic radiation with the noise generator G2 turned off. Studies have shown that the spectral density of the intrinsic radiation of a healthy person in the millimeter range is $10^{-21}...10^{-22}$ W/Hz·cm^2. A decrease in the level of intrinsic radiation of less than 10^{-22} W/Hz·cm^2 may indicate serious disorders, in particular disorders of the immune system.

The use of the considered RS in clinical practice allows to expand the list of diseases, which treatment is advisable connected with the use of noise resonance therapy, as well as to reduce treatment time by optimizing the exposure parameters and their relationship with the level of the own radiation of a biological object (human, animal or plant).

3.14 Radiometric system with automatic regulation of irradiation power

The generating and measuring equipment of ultra-weak microwave signals, in particular millimeter wavelengths, has been recently developed and used. The use of such techniques in physics, biophysics, medical physics for research purposes, in quantum medicine as a practical application of the fundamentals of the physics of living necessitated the development of systems for diagnostics, treatment and metrological support for equipment of low-intensity mm-range signals. One of the most interesting for researchers is the absorption parameter of physical and biological objects. Particular attention is paid to the study of absorption characteristics in the interaction of electromagnetic fields with human skin, since the value of the skin absorption capacity is directly related to the biological effect, and the correct choice of the frequency and power of exposure is the basis for increasing the efficiency of the use of quantum medicine technologies.

Experimental studies have shown a resonant reaction of the human body to the influence of certain frequencies of the mm range, and the

dynamic range of the intensities of the irradiating signal can vary over a fairly wide range (up to 10-30 times).

The study of the impact of electromagnetic radiation (EMR) of the mm range on a human determined the strong effect of its intensity and spectral composition on the therapeutic effect. Depending on the temperature T_G of the radiating body of the thermal noise generator relative to the human body temperature ($T_o \approx 310$ K), there are positive ($T_G > 310$ K) and negative ($T_G < 310$ K) electromagnetic energy fluxes. After the interaction with a heat generator, the patient's skin area may emit more electromagnetic energy than it absorbs, so this case is equivalent to radiation with a negative flux. Such situation occurs when the temperature of the radiating body of the generator is lower than the temperature of the irradiating area of the skin ($T_G < T_o$). With the inverse temperature ratio ($T_G > T_o$), the positive energy fluxes arise.

In some cases, especially at the treatment of patients with inflammatory diseases that are accompanied by pain syndromes, the best therapeutic effect is observed with the combined use of negative and positive fluxes of electromagnetic energy. However, the choice of a specific temperature of the radiating body of the heat generator, depending on the patient's state of health and its individual characteristics, has not yet been determined.

Human skin does not possess the properties of a blackbody and therefore it is not a coordinated load in the circuit of the radiation receiver. Studies have shown that this load is non-linear and has distinct frequency and dispersion properties. Recorded biological effects that demonstrate a resonant character with high equivalent Q factor confirm that. The dependence of biological effects on the intensity of irradiation has a clearly threshold form.

At the resonant absorption frequencies, the human skin becomes radio-transparent, which ensures a traveling wave mode from the irradiation source to the irradiating area of the skin at these frequencies. The more frequencies in the noise EMR spectrum coincide with the natural (therapeutic) absorption frequencies of a person, the more electromagnetic energy is transmitted from the generator to the patient. In this case, the intensity of the patient's exposure should not exceed the threshold, above which the skin cells are closed like with an electrically conductive curtain and begin to reflect EMR. Since the radiation intensity and its spectral composition depend on the temperature of the radiating load of the generator, for each patient there is an optimal temperature for generating

EMR, which ensures the best coordination of the radiation source with the patient's skin. Quantitatively, the degree of agreement is estimated by the traveling wave coefficient.

To ensure the measurement of the absorption capacity of human skin, depending on the intensity (temperature) of the irradiating signal, a radiometric system is developed. Its structure diagram is shown in Fig. 3.20.

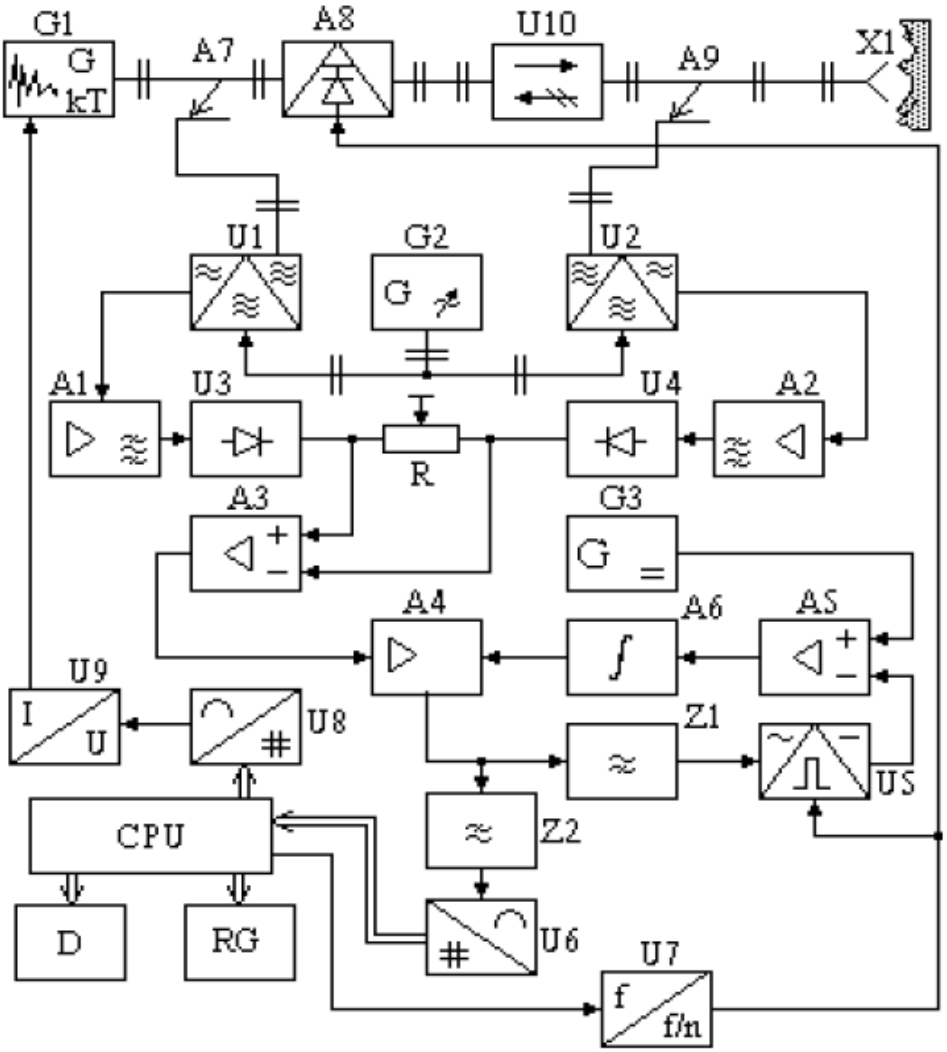

Figure 3.20 – RS for assessing the response of a biological object to the temperature of the microwave signal

A matched load is installed into the waveguide of generator G1, which is heated or cooled by a semiconductor thermopile. Depending on the temperature of the thermopile, the waveguide load generates mm-range electromagnetic energy fluxes, the intensity and spectrum of which is

determined by the degree of heating of the emitting body. Directed electromagnetic radiation (EMR) through a switching modulating flux distributor (SMFD) EMR in the first half-cycle of the voltage of the switching frequency Ω coming from the frequency divider U7, is fed to the antenna X1 and irradiates the patient's skin area. SMFD contains directional couplers A7 and A9, a modulator U10, controlled by the voltage of the frequency divider U7, and valve A8. The skin absorbs part of the EMR, and part is reflected and received by the antenna X1. The received EMR through the SMFD, mixer U2 and amplifier A2 affects the quadratic detector U4. In second half-period of the switching frequency voltage, the incident EMR of the generator G1 is reflected from the closed modulator of the SMFD and through the directional coupler, mixer U1, and amplifier A1 goes to the quadratic detector U3.

The reflected EMR passing through the coupler is absorbed by the load of the generator G1.

The output voltages of the quadratic detectors U3 and U4 affect the inputs of the differential amplifier A3. During the calibration of the device, the movable contact of the rheochord R is set in such way that the intrinsic noise of the detectors U3 and U4 and other microwave elements of the RS are mutually compensated. At the same time, the EMR reflected from the SMFD modulator and from the patient's skin, arriving at the inputs of quadratic detectors at different half-periods of the modulating (control) voltage, would be amplified with a differential amplifier A3 without attenuation. At the same time, video pulses of opposite polarity appear at the output of the differential amplifier, and their amplitudes are proportional to the powers of the input signals:

$$U_1 = +SK_1K_2P_i, \tag{3.218}$$

$$U_2 = -SK_1K_3P_n, \tag{3.219}$$

where S –is the sensitivity of the detectors U3 and U4; K_1– is a gain coefficient of directional couplers of the SMFD; K_2– is a gain coefficient of the valve of the SMFD; K_3– is a gain coefficient of the regulating attenuator of the incident wave of the SMFD; P_i and P_n are the powers of reflected (informational) and incident EMR.

Video pulses with amplitudes U_1 and U_2 are alternately amplified by an operational amplifier A4 with an automatic gain control system (units

A5, A6 and G3). A high-pass filter Z1 separates the alternating component of voltage from the amplified bipolar video pulses. The amplitude of this voltage is:

$$U_3 = K_4 \frac{U_1 - U_2}{2} = SK_1 K_4 \frac{K_2 P_i + K_3 P_n}{2}, \tag{3.220}$$

where K_4 – is the gain of the operational amplifier A4.

The alternating voltage is rectified by the synchronous detector U5 and affects one input of the differential amplifier A5. The constant voltage of the reference voltage source G3 affects the other input of the amplifier A5. It amplifies the subtractive voltage:

$$U_5 = K_5(U_3 - U_4) = K_5\left(SK_1 K_4 \frac{K_2 P_i + K_3 P_n}{2} - U_4 \right), \tag{3.221}$$

where K_5 – is the gain of the differential amplifier A5.

The differential voltage (3.221) charges the integrator A6, and its output voltage changes the gain of the operational amplifier A4. The process of gain automatic l adjusting lasts until the input voltages of the differential amplifier A5 are equalized. Equating the differential voltage (3.221) to zero, we obtain:

$$U_4 = SK_1 K_4 \frac{K_2 P_i + K_3 P_n}{2}. \tag{3.222}$$

Let us determine the set value of the gain of the operational amplifier A4 from the previous expression:

$$K_4 = \frac{2U_4}{SK_1(K_2 P_i + K_3 P_n)}. \tag{3.223}$$

A low-pass filter Z2 separates the constant voltage component from the amplified bipolar video pulses with amplitudes (3.218) and (3.219):

$$U_6 = K_4 \frac{U_1 + U_2}{2} = SK_1 K_4 \frac{K_2 P_i - K_3 P_n}{2}. \tag{3.224}$$

Substituting the value of the gain from (3.224) to the expression (3.223), we obtain the value of the DC component of the voltage:

$$U_6 = U_4 \frac{K_2 P_i - K_3 P_n}{K_2 P_i + K_3 P_n}. \tag{3.225}$$

The constant voltage (3.225) is supplied through the ADC U6 to the input of the CPU, and its value is measured and fixed on the recorder RG and display D.

In the process of calibrating the device, the antenna X1 is closed with a metal screen, so it ensures almost complete reflection of the EMR $(P_n \approx P_i)$. The SMFD attenuator is adjusted until the potentiometer reads zero, and the equality is established:

$$K_3 = K_2 . \tag{3.226}$$

Taking into account condition (3.226), the measured voltage (3.225) can be represented as:

$$U_6 = U_4 \frac{P_i - P_n}{P_i + P_n} = U_4 K_{TW} , \tag{3.227}$$

where $K_{TW} = \frac{P_i - P_n}{P_i + P_n}$ –is a coefficient of the traveling wave.

Thus, in the case of a constant reference voltage ($U_4 = const$), the readings on the computer recording device are proportional to the coefficient of the traveling wave K_{TW} .

The start of registration corresponds to the extreme maximum value of the output voltage of the DAC U8 and the output current of the converter U9, as well as the temperature of the noise generator G1. The positive polarity and voltage value are set by the converter U9 using the DAC codes U8. The actual value of the K_{TW} is measured and recorded by the computer. During the registration process the voltage at the output of the DAC U8 is proportionally regulated using the microcomputer program. The electric current through the thermopile begins to decrease, which means that the heating of the load decreases. The electric power dissipated in the thermopile is determined by the expression:

$$P_b = K_p I_b , \tag{3.228}$$

where K_p – is the Peltier coefficient, depending on the material of the electrodes of the thermopile; I_b –is a current through thermopile.

Since the temperature of the thermopile is proportional to the dissipated electric power, the load temperature of the generator G1 changes in proportion to the change in the voltage at the output of the DAC U8 until

the other extreme value of the voltage of DAC U8 is reached. In this DAC position, the temperature of the load reaches a minimum value. The values of the K_{TW} coefficient are recorded on the paper printer RG, and are also indicated on the display D.

The traveling wave coefficient depends on the intensity of the electromagnetic radiation and characterizes the absorption capacity of the irradiated skin area. With K_{TW}=1, all the EMR of the generator is absorbed by the object. If K_{TW}<1 it indicates the appearance of reflection of EMR and poor matching of the emitter of the heat generator and the patient's skin. Therefore, the highest values of K_{TW} recorded on RG allow us to determine the temperature or several temperatures at which the absorption of EMR will reach the maximum. These temperatures are individual for each patient; the effect of treatment depends on the accuracy of their use.

Potentiometer R is set when the source supplying the thermopile of generator G1 is turned off. In this case, the load of the generator G1 is almost in thermodynamic equilibrium with the patient's skin, and only the microwave noise of the device affects the differential amplifier A3. By adjusting the slider of the potentiometer R, we achieve a zero reading of the RG recorder. When the thermopile is turned on, the generation of EMR fluxes begins and the RG readings become proportional to the traveling wave coefficient, regardless of the level of intrinsic noise.

Thus, the described device allows determining the optimal parameters of the emitted signals depending on the temperature characteristics of the irradiated skin surface of the patient. It contributes to a significant increase in the effectiveness of treatment.

3.15 Measurement assurance of high-sensitivity microwave radiometric systems

Modulation meters of parameters of low-intensity signals belong to a complex class of measuring devices for their metrological evaluation and maintenance. Metrological evaluation of such devices is much more complicated with the extension of the operating frequency range into the zone of mm waves (λ=1…10 mm). However, the demand for radiometers, especially for scientific research in the fields of physics, biology and medicine, is increasing. Frequency range extension, sensitivity enhancement and precision of measurements requires detailed scientific

research in the field of electromagnetic fields and radiation, their interaction with physical agents and biological objects.

The mm-gamut modulation meters provide metrological monitoring of an equipment [43], the output signal capacity of which can reach $10^{-10}...10^{-13}$ W [60]. A number of works by the author are devoted to solving the problems of validation of such highly sensitive systems [61, 62].

The main metrological parameters of high-sensitivity RS, which must be measured first of all, include:

- estimation of an error appraisal of power measurement;
- determination of fluctuation sensitivity;
- estimation of a range of operational frequencies and bandpass flatness.

Signal elements (amplitude, phase, and frequency) that pass through the radiometer channel are subject to various influences. As a result, primary information about the most common measurement errors, multiplicative and additive ones, is accumulated.

The use of modulation single channel schemes of periodic comparison in a variant, for example, shown in Fig. 3.2 and high switching frequency allows reducement of multiplicative and additive measurement errors [63]. However, modulation meters of a microwave range have their peculiarities because of the presence of peculiar elements of this range – antennas, transmission lines, and electronic components with distributed parameters. It does not always make it possible to use the classical approaches of low-frequency range to analyze circuits and processes of error generation.

According to [6], the main part of the error of power measurement (90…95 %) corresponds to microwave converters and units, which, in fact, determine the level of accuracy of measuring means. Thus, the error of a microwave converter is 9…14 % with the main measurement error of the microwave power (10…15 %), and the low-frequency channel (a direct-current voltmeter) is about 1 %.

The analysis of main errors of high-sensitivity RS of a microwave range was carried out by the author [64], the results of which are as follows.

The main sources of the most common errors of a radiometer with input frequency conversion (Fig. 3.21) are the mismatch of a device input with the microwave signal source, the input modulator and the switching modulator S1.

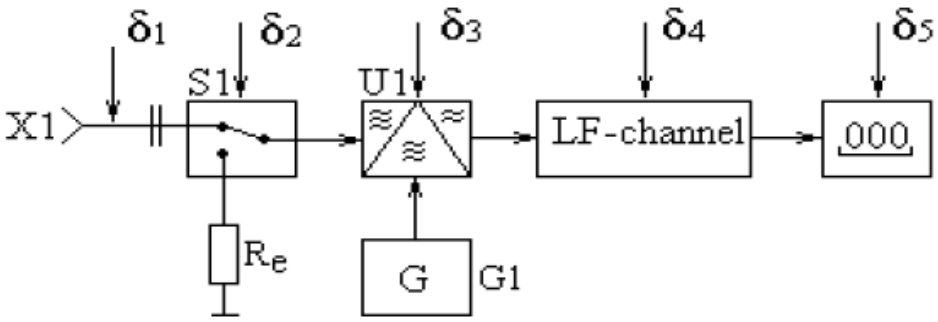

Figure 3.21 – The scheme of errors distribution in a radiometer path

Containing an intermediate frequency amplifier, a quadratic detector, an amplifier and a filter of a switching frequency, a synchronous detector, a low-pass filter and an indicator, a low-frequency conversion channel has less influence on the main measurement error. It is because the amplification, filtering and conversion operations are performed where accurate processing of informative signal parameters is possible.

The total error of the radiometer (Fig. 3.21) can be shown as follows:

$$\delta_{RS} = \delta_1 + \delta_2 + \delta_3 + \delta_4 + \delta_5, \qquad (3.229)$$

where δ_1 – an error from a mismatch of a meter input with the wave resistance of the microwave signal source; $\delta_2, \delta_3, \delta_4, \delta_5$ – the errors of corresponding units of a modulator, a frequency converter, a low-frequency channel and an indicator.

The use of RS in measurement schemes is possible in several ways:

- a connection to a signal source through a waveguide line (Fig. 3.22);
- a direct connection of RS and a generator (Fig. 3.22);
- the introduction of an attenuator to extend the dynamic range of measurement between the RS and a generator.

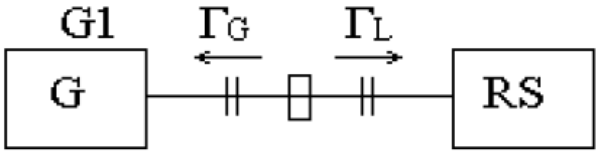

Figure 3.22 – A scheme for measuring the power source (a generator) of RS microwave signal

In Fig. 3.22, Γ_G, Γ_L are modules of a reflection coefficient at the generator and RS input. The sum error from the mismatch is $\delta_H < 2{,}5\,\%$ with small coefficient values $|\Gamma_G| = |\Gamma_L| \leq 0{,}15$ and an initial loss of 0 dB.

The application of an attenuator at the input of a measuring system extends a dynamic range of a device. However, it is necessary to coordinate the microwave units in order to reduce errors, as well as to ensure the minimum suppression of an attenuator in its initial state. With the agreed inputs $|\Gamma_G|=|\Gamma_L|\leq 0{,}15$ and a transfer factor of an attenuator $K_A=1$, the error of this measurement scheme increases and can be ≈ 8.1 %.

Studies [61, 64] have proved that the intrinsic noises of microwave units lead to reflection from closed *p-i-n*-keys when using switching measurement inverters in the mode of a circuit-breaking push or a contractor and cause an interference error, which at the nominal value of a switching parameter (Γ_s = 0,35) and $P_п/P_s=1$ reaches 8.2 %. Reduction of the interference error is possible by choosing a mixer and heterodyne circuit with minimal noise characteristics and introducing noise suppression by means of a release valve. As a result, due to the inclusion of a valve of PVV1-46 type in the waveguide path between a modulator and a mixer, a suppression factor $K_П \geq 20$dB is provided in the opposite direction that is sufficient to reduce the level of interference error at values of $0{,}2<\Gamma_s<0{,}42$, $\delta_м \leq 1{,}0$ %.

The use of standardized error estimation methods (a substitution method) and non-standardized noise generators, certified by indirect parameters (temperature and standing wave ratio), in the mm frequency range in the absence of a standard reference base are one of the possible ways to solve the problems of metrological provision of highly sensitive RS.

By using the offset method for determining the main error of the measured power, it is replaced by a known value of the calibration generator using a reference attenuator.

When using the bias method, the determination of a main error of the power, measured as P_X, is carried out by replacing with the known value of the calibration generator P_c with a help of a standard attenuator. The scheme of measuring power by the method of «replacement» is shown in Fig. 3.23.

The measurement block diagram has been optimized taking into account the maximum reduction in the influence of the component errors discussed above. The impact of a system mismatch with a generator module, an attenuator and a modulator input was got through the use of A3 matching transformer and A1 and A4 valves.

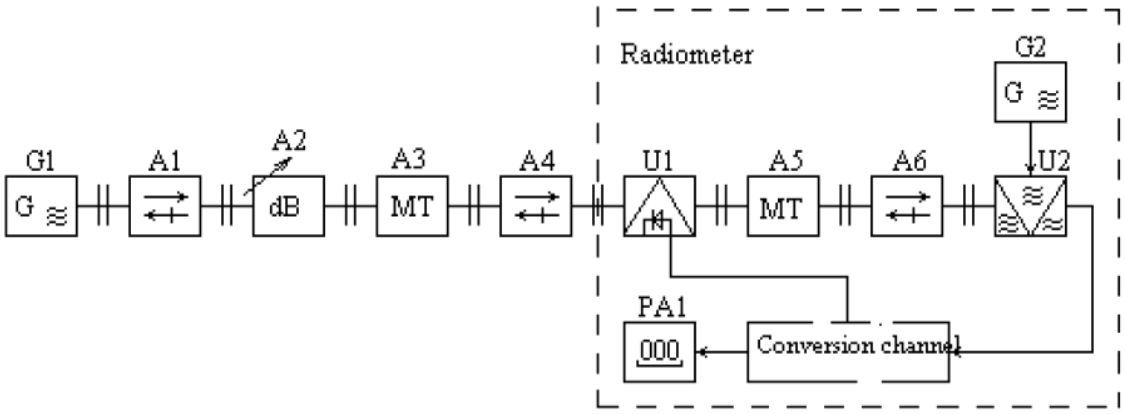

Figure 3.23 – A diagram of the power measurement
of a generator modulewith a radiometer

The influence of a modulator mismatch at the output and noises of a microwave path and the local oscillator on the measurement results was reduced by using a matching transformer A5 and a valve A6.

Figure 3.24 – A workstation for checking a high-sensitivity radiometric system
for 37…53 GHz frequency range using a standard noise oscillator G_n (right)

The process of measuring the power of monochromatic signals was carried out in two stages. Initially, preliminary operational run-up of a radiometer was performed for the measurement procedure.

The generator module was connected to its input, whose power had to be measured. The value of the measured signal power P_X on PA1 indicator was fixed, and if the dynamic range of an indicator was insufficient, then the input standard attenuator A2 was additionally used. The attenuator and indicator testimony was recorded and a generator

module was disconnected. Then the calibration power value P_K was established and measured using standard measuring means of a monochromatic signal gauge generator at the same frequency.

When the calibration generator is connected to the input of a measuring circuit by means of an attenuator, the indicator constant $N_2 = N_1$ is set and an attenuator constant A_K is fixed. The value of the integral power of a monochromatic signal of a generator module can be determined by the following formula [64]:

$$P_X = P_c\left(A_X / A_c\right), \tag{3.230}$$

where A_X, A_c – the values of an attenuator when measuring respectively unknown calibration power.

The appraisal of highly sensitive radiometric systems NU-1, NU-2 using the «substitution method» has provided a relative error within $38{,}0\,\% > \delta P > 29{,}0\,\%$ [65, 66].

The analysis of calculations shows that a considerable part of the error (50 %) corresponds to M3-22A power meter with M5-50 thermal converter and D3-38 attenuator, with the maximum suppression of a signal. Commonly, the achieved level of accuracy will generally be insufficient with accurate power measurements.

An advanced technique of estimating systems accuracy at levels $10^{-13}…10^{-14}$ W is the use of thermal generators of a standard noise (a standard noise oscillator) [7, 67]. Taking into account the high sensitivity of developed RS ($10^{-13}...10^{-14}$W), the author [64] has proposed a thermal generator of the standard noise of mm-range with a low temperature of a working medium (20-50°C). It is because the output power in the band conditions is RC $\Delta f = 10^8$Hz is $P_{\min}$ = 4,04·10^{-13}Вт, $P_{\max}$ = 4,45·10^{-13}W, which is greater than RS sensitivity.

The output power level of a standard noise oscillator can vary by 5…10 times and be (1…5)·10^{-13} W due to the high sensitivity of developed modulation meters. This level provides an insignificant gradient of a temperature of a standard noise oscillator relative to the environment. The development of such a generator is somewhat simplified and opens the possibility of providing high metrological characteristics.

The distribution of the output power of a certified thermal generator of a standard noise for testing high-sensitivity RS is shown in the line graph 3.25.

The distribution of output power has a linear character, allowing the scale of the generator to be accurately calibrated. The dashed line shows the variation of temperature and its corresponding power.

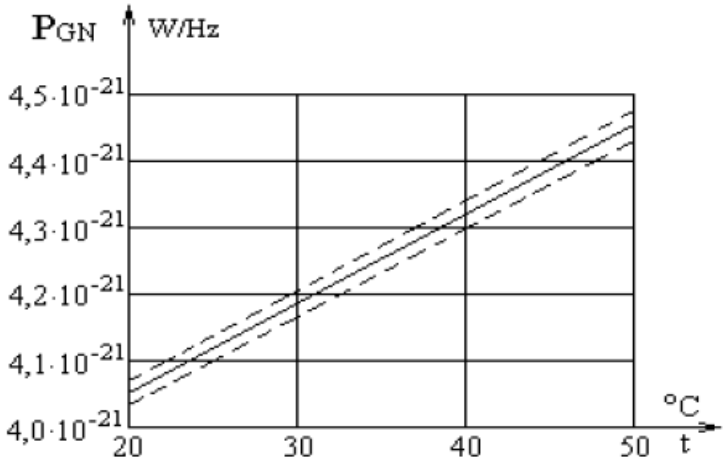

Figure 3.25 – The distribution of output power within temperatures regulation of a standard noise oscillator G_n

Since the band of a real radiometer $\Delta f \approx 1 \cdot 10^8$ Hz [7, 39] and the temperature limits of a standard noise oscillator G_n change from 20°C to 50°C, the limits of power regulation at the output of the generator will be:

$$P_{G_n \min} = kT_1\Delta f = 4{,}045 \cdot 10^{-13}\text{Wt}; \quad P_{G_n \max} = kT_2\Delta f = 4{,}39 \cdot 10^{-13}\ \text{Wt}.$$

The accuracy of setting the power at the output of of a standard noise oscillator G_n is determined by the accuracy of installation and maintaining the temperature inside the thermostat. In this case, the output power of a standard noise oscillator is determined from the expression:

$$P_{Gn} = \Delta f\left(T \pm \Delta T\right), \tag{3.231}$$

where $\pm\Delta T = \pm 0{,}5^0\text{C}$ – maximum temperature fluctuations inside a thermostat.

The error of forming the power of the standard noise is within $\delta P = \pm 0{,}16\,\%$.

The sum error of power formation of the standard noise and the use of a standard noise oscillator G_n in the consistent mode is δP_Σ=0,26 %, which makes it possible to attribute oscillator to measuring means that are suitable for the estimation of parameters of highly sensitive radiometers.

Fig. 3.26 shows the amplitude-frequency response of RS on the frequency range 37…53 GHz. The characteristics are taken at different temperatures (scale divisions) of noise oscillator G_n.

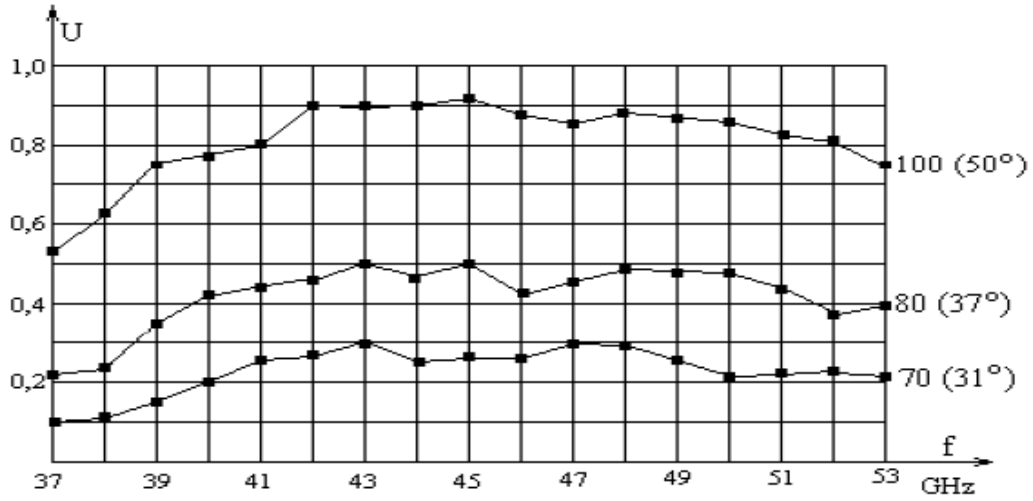

Figure 3.26 – Amplitude-frequency response of RV NU-1 № 01

Using the obtained graphs, it is possible to determine the range of RS operating frequencies, the sensitivity, and the uneven frequency response [7, 64, 68].

Additional verification of developed high-sensitivity radiometric systems NU-1, NU-2 recorded the value of relative measurement error within $10,0\% > \delta P > 15,0\%$ with the help of a certified standard noise oscillator G_n [69].

To conclude the section, we would like to state the following:

- radiometric methods and means with switching-modulation conversion are extensively used in various fields of science and technology, where it is necessary to measure parameters of low-intensity signals. Radiometry facilities are characterized with high accuracy when measuring various physical quantities, implementation simplicity, and high sensitivity;

- developed by the authors and presented in this section structural diagrams of radiometric systems have confirmed the high functionality of the developed equipment and the switching-modulation method by information signal conversion;

- the described examples of radiometric system operation in the reception mode and the radar (irradiation) mode at signal levels of 10^{-13} ... 10^{-14} W can be used to solve practical problems of studying and diagnosing low-intensity microwave fields and radiation of physical bodies and biological objects. At the same time, area of such systems is determined only by the type of information signals and input converters of physical quantities.

SECTION 4 DEVICES FOR THE FORMATION, RECEPTION AND PROCESSING OF LOW-INTENSITY SIGNALS BASED ON JOSEPHSON JUNCTIONS

Introduction to section 4

This section is devoted to the use of superconductors and the Josephson junction, which is based on them, for building devices for generating, receiving, and processing low-intensity electromagnetic signals.

The main characteristic of the superconductors is the complete absence of resistance at a temperature lower than the phase transition temperature T_K. The absence of resistance means that it is possible to «excite» the supercurrent in the superconducting loop at a temperature below the phase transition temperature T_K. Such current will circulate indefinitely, without changing. Supercurrents are a quantum phenomenon, which has at its core the formation of loosely coupled electron pairs (Cooper pairs) that move around the substance without colliding with a crystal lattice. The forces binding electrons to a Cooper pair are very weak, so the superconductivity occurs at low temperatures when the thermal energy of an electron is less than the energy gap width that is the energy required to separate the pair. This binding can be broken if a significant current is run through or a strong magnetic field is applied.

The second important characteristic of the superconductors that differentiate them from «perfect conductors» is that they are perfect diamagnets. That is, if there is an external magnetic field inside the superconductor, the magnetic field is equal to zero. This means that, when cooling a superconductor located in a magnetic field, the induction field lines are excluded from the material as soon as the temperature is decreased to the critical T_K.

In 1963, an English scientist Josephson found that tunneling of Cooper pairs could take place through the contact of two superconductors separated by a thin dielectric, that is, the insulating layer between the two superconductors acts as a superconductor. It is established that the supercurrent vanishes easier in the presence of an insulating layer compared to a solid superconductor.

When a current crosses a contact, there are two fundamentally different types of its behavior, known as DC and AC Josephson effects. In the case

of the DC Josephson effect, the direct supercurrent can reach some critical value I_0 and there is no voltage drop on the contact. The value of the critical current I_0 for the contact is much smaller than the maximum current crossing the superconductor in the absence of an insulating layer.

The AC Josephson effect occurs when a fixed voltage is applied to the contact, and in this case the supercurrent of the Cooper pairs oscillates with frequency [70]

$$f_0 = \frac{2gU}{h}, \tag{4.1}$$

where g – the electron charge; h – the Planck constant; f_0 – Josephson or plasma frequency. It follows from the aforementioned expression that the Josephson contact can be used as a generator of harmonic signals; or vice versa, as a very accurate voltage standard. It should be noted that the frequency generation is high, and is tens – hundreds of GHz, even at very low voltages.

The Josephson junction (JJ) in the resistive state is a natural source of low-intensity signals in millimeter and submillimeter waveband, which can be tuned in frequency by changing the voltage. The use of the JJ for the construction of digital radio-technical and measuring devices makes it possible to significantly reduce the energy consumed by switching, since its limit value for semiconductor electronics is 10^{-13} J/bit and for superconductor electronics, 10^{-19} J/bit [71, 72].

The high sensitivity to the change of the magnetic field at the level of the magnetic flux quantum (Φ_0=2,07·10^{-15} T) makes it possible to use such devices for the measurement of low-intensity electromagnetic fields. Such devices are widely used in the medical field. The sensitivity threshold outside the current can be units or even tenths of an A, which makes it possible to construct ultrasensitive devices for receiving and processing low-intensity electromagnetic signals [73, 74].

Modern standards of voltage unit, volt, are made based on the Josephson effect. The standard includes the Josephson junction, driven with microwave radiation at a frequency of 8…10 GHz. The value of the quantum voltage is 4…10 mV. The high sensitivity of the method based on Josephson junctions and superconducting quantum interference devices (SQUID), which are based on them, makes it possible to detect small changes in magnetization compared to a large static value. This is because the sensitivity of the method does not depend on the signal level [6].

This method has great potential for studying the magnetic characteristics of a substance containing a small number of magnetic impurities, as well as microgram samples. As a result, the high sensitivity of the method allows conducting measurements in very weak fields of less than 10 Gs, in some cases; this fact is of fundamental importance.

The possibility of registering magnetic fields with such a device is based on the fact that the current flowing in the loop depends on the magnetic current flowing through this closed circuit. The first superconducting magnetometers were created just a few years after the discovery of the Josephson effect, and currently, the sensitivity limit of modern SQUIDs exceeds 10^{-14} T/Hz$^{1/2}$ [75].

The necessity to keep the operability of SQUID at the helium temperature restrained the wide use of SQUID, microscopes. Users of such microscopes experienced significant difficulties in positioning the SQUID against the sample, as well as loading and changing the samples. The replacement of a low-temperature SQUID with sensors based on high-temperature superconductors made it possible to operate the device at nitrogen temperatures, which significantly expanded the scope of research and stimulated commercial use of the SQUID.

The application of the quantization effect of the magnetic flux in the loop of Josephson junctions, through which the current flows, makes it possible to move from an analog way of presenting information to a discrete one. Based on these effects, elements of fast one-quantum logic are built, where the unit of information is magnetic flux quantum. This allows processing signals with frequencies above 100 GHz at extremely low energy dissipation. It is particularly valuable that such a structure is both a logical element and a memory element [72]. As the amount of data transmitted on the Internet doubles every three-four months, even the best of the semiconductor devices, which are currently being developed, will not be able to transmit such large streams of information in the nearest future. Three-dimensional structures, consisting of Josephson electronic circuits in an array, appear to be the only alternative to planar semiconductor microcircuits.

4.1 Mathematical model of Josephson transition

The progress of modern digital technologies is largely due to the development of superconducting digital devices based on rapid single-quantum logic, for which the phenomenon of superconductivity and

Josephson transitions are used. The extremely low magnitude of the switching power of the Josephson elements and their high speed makes it possible to use the clock frequencies for low temperature superconductors up to 100 GHz, and for high-temperature superconductors – to units of THz, which allows simultaneously increasing both the speed and the degree of integration of superconducting digital devices [77].

The application of macroscopic quantum effects in semiconductors allows you to create highly sensitive high-performance ADCs (Analog-to-Digital Converter) and DACs (Digital-to-Analog Converter). This enables the development of full digital devices that receive process and transmit signals for modern telecommunication systems in the gigahertz and terahertz frequency ranges [73].

The use of Josephson transition in parametric amplifier schemes allows us to obtain the sensitivity of devices close to the quantum limit at frequencies from units to hundreds of GHz. Frequency mixers based on tunnel Josephson junctions have no equal in the noise temperature in the frequency range up to 1 Threshold and such mixers are already in use [78].

Therefore, the development of mathematical models of Josephson transitions, which are an elemental basis for the construction of such devices, is an urgent task.

The calculation of devices based on Josephson transitions is based on the use of mathematical models that describe the dependence of currents and voltages on the parameters of the superconductor materials and the dielectric layers that divide them.

Questions of the construction of mathematical models of Josephson transitions are devoted to works [79, 80]. In known works, more attention is paid to the calculation of the volt-ampere characteristics of such transitions and does not take into account the dependence of the phase of the wave function and the output voltage on the electrostatic transfer capacitance, or numerical methods for solving the differential equation that describe the change of current when changing the voltage and parameters of the equivalent circuit are used. Therefore, the task of this work is to develop a model that would give an opportunity to obtain the analytic dependence of the phase of the wave function and the output voltage on the Josephson transition from the current, the transfer capacitance and the active resistance.

An equivalent scheme of the Josephson transition is shown in Fig. 4.1.

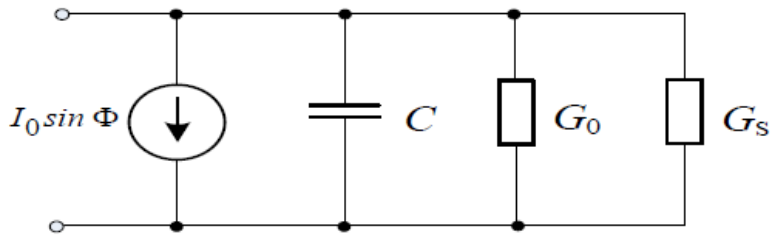

Figure 4.1 – Amplitude-frequency response of RV NU-1 № 01

Equivalent Josephson transition scheme.

The current flowing through the Josephson transition is defined as follows [79].

$$I = I_0 sin\,\Phi + (G_0 + G_S)U + C\frac{dU}{dt}, \tag{4.2}$$

where I_0 is the Josephson Critical current; C is electrostatic capacity of two superconductors; G_0 is the nonlinear conductance of the Josephson transition; G_S is Shunt conductivity of the outer circle; Φ is the phase difference of wave functions in superconductors.

Because

$$\frac{d\Phi}{dt} = \frac{2q}{\hbar}U, \tag{4.3}$$

Then

$$\frac{dU}{dt} = \frac{\hbar}{2q}\cdot\frac{d^2\Phi}{dt^2}.$$

From expression (4.3) determine the phase dependence of the applied voltage

$$\Phi = \frac{2qU}{\hbar}\cdot t + const.$$

In view of the above relations, the expression (4.2) should are rewritten as follows

$$I = I_0 sin\Phi + \frac{(G+G_S)\hbar}{2q}\cdot\frac{d\Phi}{dt} + \frac{C\hbar}{2q}\cdot\frac{d^2\Phi}{dt^2}.$$

Divide the right and left sides to I_0:

$$\frac{I}{I_0} = sin\Phi + \frac{G\hbar}{2qI_0}\cdot\frac{d\Phi}{dt} + \frac{C\hbar}{2qI_0}\cdot\frac{d^2\Phi}{dt^2}. \tag{4.4}$$

Let us introduce a replacement

$$x = \frac{2qI_0 t}{\hbar G} = \omega_0 t, \tag{4.5}$$

$$\beta = \frac{2q}{\hbar} \cdot \frac{I_0}{G} \cdot \frac{C}{G} = \omega_0 \frac{C}{G} \text{ (McCumbers factor)} \quad (4.6)$$

where $\omega_0 = \frac{2q}{\hbar} \cdot \frac{I_0}{G}$ is the rotational frequency of the Josephson junction, which corresponds to the frequency of voltage generation when leaked through a resistor with conductivity of G of maximum current.

Given the above changes, the expression (4.4) can are rewritten in the form

$$\frac{I}{I_0} = sin\Phi + \frac{d\Phi}{dx} + \beta \frac{d^2\Phi}{dx^2}$$

Dividing the right and left parts into an β, we get

$$\frac{d^2\Phi}{dx^2} + \frac{1}{\beta} \cdot \frac{d\Phi}{dx} + \left(\frac{sin\Phi}{\beta} - \frac{I}{I_0\beta} \right) = 0. \quad (4.7)$$

Taking into account expressions (4.5) and (4.6), we define β through x

$$\beta = \frac{x}{t} \cdot \frac{C}{G}.$$

Given this, the expression (4.7) can are rewritten as follows

$$\frac{d^2\Phi}{dx^2} + \frac{a}{x} \cdot \frac{d\Phi}{dx} + \frac{a}{x} \left(sin\Phi - \frac{I}{I_0} \right) = 0, \quad (4.8)$$

where $a = \frac{tG}{C}$.

This differential equation in form has the form similar to the Bessel equation [81]. With $x = 0$, the coefficient for the first derivative and for a nonlinear term goes to infinity, that is, there is a gap. In this case, it is impossible to say in advance whether there is a solution to the equation with $x = 0$. That is, the theorem on the existence of a unified solution cannot are used here. Equation (4.8) does not belong to any of the types of equations of the second order and therefore, when solving it we will consider two cases:

- the first case corresponds to the condition when Φ takes small values and $sin\Phi \approx \Phi$;

- the second case corresponds to the condition when Φ takes large values and $sin\Phi$ needs are taken into account.

In this paper, we consider only the first case. For the first case, the equation (4.8) can are rewritten as follows

$$\frac{d^2\Phi}{dx^2}+\frac{a}{x}\cdot\frac{d\Phi}{dx}+\frac{a}{x}\left(\Phi-\frac{I}{I_0}\right)=0.$$

We seek the solution of this equation in a numerical series

$$\Phi=C_0+C_1x+C_2x^2+C_3x^3+\ldots+C_nx^n+\ldots. \qquad (4.9)$$

Having differentiated this series twice and substituting these values in the differential equation (4.7), we obtain

$$\begin{aligned}&2C_2+3\cdot2C_3x+4\cdot3C_4x^2+\ldots+n(n-1)C_4x^{n-2}+\\&+\frac{a}{x}\left(C_1+2C_2x+3C_3x^2+\ldots+nC_nx^{n-1}+\ldots\right)+\\&+\frac{a}{x}\left(C_0+C_1x+C_2x^2+C_3x^3+\ldots+C_nx^n-\frac{I}{I_0}\right)\end{aligned}. \qquad (4.10)$$

This equation can are rewritten in the form

$$\sum_{n=2}^{\infty}n(n-1)C_nx^{n-2}+\frac{a}{x}\sum_{n=1}^{\infty}nC_nx^{n-1}+\frac{a}{x}\sum_{n=0}^{\infty}C_nx^n-\frac{a}{x}\cdot\frac{I}{I_0}=0.$$

Equating to zero the coefficients for all degrees x, we obtain a system of equations for determining the coefficients $C_0, C_1, C_2, \ldots$

If we assume that $C_0=0$, then the expression to determine the coefficients can be written as follows

$$C_n=(-1)^{n-1}\frac{a^{n-1}C_1}{n!\prod_{n=1}^{n-1}\left[a+(n-1)\right]}. \qquad (4.11)$$

Substituting the values of the coefficients (4.11) in expression (4.9), we obtain

$$\begin{aligned}&\Phi=C_1\left[x-\frac{ax^2}{2(1+\alpha)}+\frac{\alpha^2x^3}{3!(1+\alpha)(2+\alpha)}-\frac{\alpha^3x^4}{4!(1+\alpha)(2+\alpha)(3+\alpha)}+\ldots\right.\\&\left.\ldots+(-1)^{n-1}\frac{a^{n-1}x^n}{n!\prod_{n=1}^{n-1}\left[a+(n-1)\right]}\right]=C_1(-1)^{n-1}\frac{a^{n-1}x^n}{n!\prod_{n=2}^{n-1}\left[a+(n-1)\right]}\end{aligned} \qquad (4.12)$$

Since the solution of the differential equation is obtained in the form of a series, it is necessary to investigate it on convergence. To do this, we will

use the sign of Dalamer. We define the ratio of the absolute values of two successive members of the series, as is done in [81]

$$\frac{C_1\alpha^{n+1-1}x^{n+1}}{(n+1)!\prod\limits_{n=2}^{n+1-1}\left[a+(n+1-1)\right]}:\frac{C_1\alpha^{n-1}x^{n}}{n!\prod\limits_{n=2}^{n-1}\left[a+(n-1)\right]}=\frac{\alpha x}{n\left[a+(n-1)\right]}.$$

From the last expression it follows that for any value of x the ratio of two consecutive members of a series goes to zero, if $n\to\infty$, which proves the absolute convergence of the series.

Thus, the expression for the phase of the wave function of the Josephson transition can are written as follows

$$\Phi(x)=C_1\sum_{n=\varphi}^{\infty}(-1)^{n-1}\frac{a^{n-1}x^{n}}{n!\prod\limits_{n=2}^{n-1}\left[a+(n-1)\right]}. \qquad (4.13)$$

Taking into account (4.12), the expression for determining the voltage at the Josephson transition has the form

$$U(x)=\frac{\hbar}{2gt}\cdot\frac{I}{I_0}\sum_{n=1}^{\infty}(-1)^{n-1}\frac{a^{n-1}x^{n}}{n!\prod\limits_{n=2}^{n-1}\left[a+(n-1)\right]}. \qquad (4.14)$$

It should be noted that at $n<2$ the product $n!\prod\limits_{n=2}^{n-1}\left[a+(n-1)\right]$ an are considered equal to 1.

If you take a for a symbol of the sum and substitute its value in (4.14), we get

$$U(x)=\frac{I}{\omega_0 C}\sum_{n=1}^{\infty}(-1)^{n-1}\frac{a^{n-2}x^{n}}{n!\prod\limits_{n=2}^{n-1}\left[a+(n-1)\right]}.$$

Using expression (4.13), the dependence of the phase of the wave function on the parameters of the equivalent scheme of the Josephson transition (electrostatic capacitance, nonlinear and shunt resistance and current) is calculated. Output data for calculation were selected in this way $I_0=10^{-5}$ A, $G=10^{-2}$ cm, $C=10^{-15}\div10^{-16}F$, $I=5\cdot10^{-6}$ A. The graph of the dependence of the reduced value of the phase difference of the wave

function on the Josephson transition capacity for various values of the currents is given in Fig.4. 2.

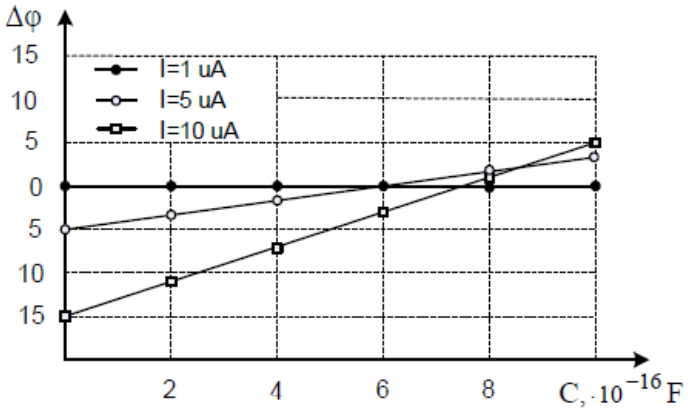

Figure 4.2 – Dependence of the phase difference of wave functions on capacitance

Josephson's transition.

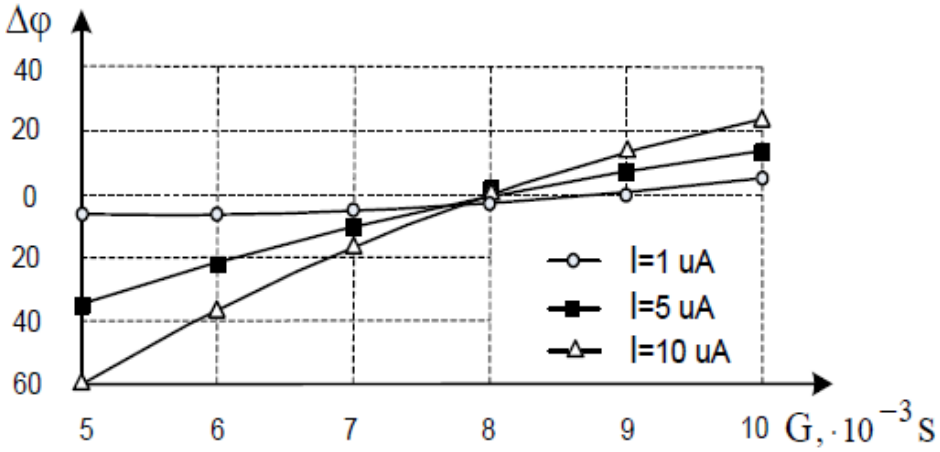

Figure 4.3 – Dependence of the phase difference of wave functions on the conductance of the Josephson transition

As can be seen from the graph, the phase difference of the wave function changes by at least 20 in order of order, and therefore in this range of capacitance changes it is possible to suppose that $sin\Phi \approx \Phi$ and use the expression (4.13) for calculating devices on the Josephson transitions. The increase in the current flowing through the transition leads to an increase in the phase difference of the wave functions. Figure 4.3 shows the dependence of the phase difference of wave functions on the conductance of the Josephson transition for different values of currents flowing through the transition.

As it can be seen from the graphs, the phase difference of wave functions increases with decreasing conductivity and with increasing current. At a current value of more than 5 μA, the phase difference of wave functions increases significantly and the resulting expression for the calculation of devices based on Josephson transitions is not useful. For conductors less than 10^{-2} cm, the model developed above should also are used inappropriately.

Using the proposed model, calculations of the dependence of the alternating voltage on the transition from the parameters of the equivalent Josephson transition scheme have being carried out, which showed that its value is of the same order as the experimental results given in the famous works of domestic and foreign authors.

4.2 A Josephson junction-based superconducting quantum interferometers

Let us review the magnetic field effect on the current that flows across the Josephson junction in parallel to the field lines. Assuming that the transition dimensions in the perpendicular direction to the applied field are smaller than the current penetration depth λ, the effect of the Josephson current self-shielding will not be taken into account. In this case, the magnetic field will penetrate evenly into the dielectric layer between the superconductors, and the Josephson current density expression takes the form [74].

$$j(x) = j_e \sin(\varphi_0 + Kx), \tag{4.15}$$

where $K = \frac{d\varphi_0}{dx} = \frac{2e}{\hbar c} H_0 \left[\lambda_{L1} th\frac{d_1}{2\lambda_{L1}} + \lambda_{L2} th\frac{d_2}{2\lambda_{L2}}\right]$; d_1, d_2 – the superconductor films thickness; H_0 – the external magnetic field strength; λ_{L1}, λ_{L2} – the current penetration depth into the superconductor; φ_0 – the initial phase of the wave function; j_e – the density of the tunneling current whose value can be calculated using the expression [5]

$$j_c = \frac{e\mu^2}{8\pi U}\frac{\Delta_0^2}{Tc}$$

where $\mu = \frac{mv_0^2}{2}$ – the chemical potential; Δ_0 – the order parameter module; U – the potential barrier height; T_K – the critical temperature, v_0 – the Fermat's speed.

The total current flowing through the Josephson junction can be calculated by integrating the expression 4.15.

$$I = \int_0^L J(x)dx = \frac{2I_c}{K}\sin\frac{KL}{2}\sin\frac{KL}{2}\sin\left(\varphi_0 + \frac{KL}{2}\right). \quad (4.16)$$

The value $\psi_0 = \varphi_0 + \frac{KL}{2}$ acts as the arbitrary phase, which is determined (with the corresponding value of the magnetic field H_0) by the value of the current flowing through the junction.

The maximum value of the Josephson current flowing in the absence of the resistance can be determined from ratio (4.16)

$$I_M = I_C\left[\frac{\sin{}^{\pi\phi}/_{\phi_0}}{\pi\phi/_{\phi_0}}\right], \quad (4.17)$$

where $\phi_0 = \frac{h}{2q}$ is a quantum of the magnetic field, and the value ϕ is determined by the expression [74]

$$\phi = H_0 L\left(\lambda_{L1} th\frac{d_1}{2\tau\lambda_{L1}} + \lambda_{L2} th\frac{d_2}{2\lambda_{L2}}\right). \quad (4.18)$$

As follows from (4.17), the critical current of the Josephson junction is an oscillatory function of the external magnetic field. The oscillation period depends on the thickness of the superconductor films and the depth of the magnetic field penetration into the superconductor.

If the film thickness is much greater than the penetration depth, the oscillation period is determined by the expression

$$\Delta H_0 = \frac{\phi_0}{L\Delta}.$$

If the thickness of the superconductor films is much smaller than the penetration depth, then the oscillation period is determined by the expression

$$\Delta H_0 = \frac{2\phi_0}{L(d_1+d_2)}. \quad (4.19)$$

The analysis of the expressions (4.18, 4.19) shows that the measurement of the oscillation period makes it possible to directly determine the depth of the magnetic field penetration into a superconductor. And if the thickness of the superconductor films is much smaller than the penetration depth, the oscillation period depends on the temperature, since Δ depends on the temperature.

We determine how the energy of two superconductors, that are separated by a dielectric film, forming a tunnel junction, changes with the change of the external magnetic field.

The connection between the energy and the critical current can be calculated with the following expression.

$$E(x) = \frac{\hbar I_c}{2g}[1 - \cos\varphi(x)].$$

If we integrate this expression over x and take into account (4.17), then the expression for a complete energy change under the effect of a magnetic field can be written in the following way:

$$\Delta E = \int_0^L E(x)dx = \frac{\hbar I_c}{2g}\left[1 - \frac{\sin {}^{\pi\phi}/_{\phi_0}}{{}^{\pi\phi}/_{\phi_0}}\cos(\varphi_0 + {}^{\pi\phi}/_{\phi_0})\right].$$

Thus, the value of the energy change is determined by the magnetic field and the value of the current which flows through the contact, which means that the energy oscillates with the change H_0. There is a phase transition at points $\phi = n\phi_0$, n=1,2,3… when an integer number of quanta of the magnetic field ϕ_0 enters the junction. This transition is connected with the discontinuous change of the junction characteristics. Due to the sensitivity of the Josephson current to the phase change of the wave function, the interference of the superconducting current occurs. It can occur in one as well as in two or more Josephson junctions, that are included in one superconducting array.

Based on this effect, direct current superconducting quantum interference devices (DC SQUID) are built. They are extremely sensitive converters of the magnetic signal to the voltage.

The scheme of such DC SQUID is shown in Fig. 4.4 a. In Fig. 4.4 b, there is a diagram of the radio frequency SQUID (RF SQUID), which has one Josephson junction in a superconducting loop, inductively coupled to a resonant circuit. A resonant current is induced in a resonant circuit of such amplitude so that the maximum value of the current induced in the SQUID loop exceeds the critical current of the Josephson junction. The output signal is the voltage on the resonant circuit, which is represented by a periodic function of the magnetic flux threading the superconducting loop area with a period of ϕ_0.

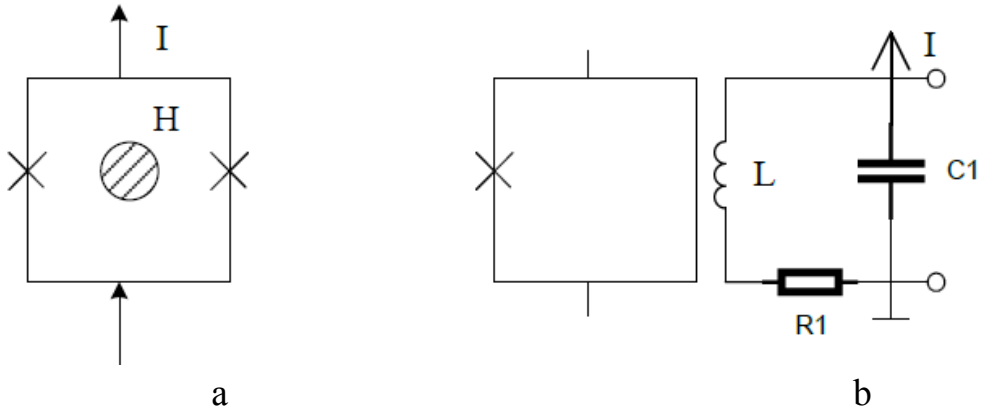

Figure 4.4 – Direct current superconducting quantum interferometer (DC SQUID) (a), radio frequency superconducting quantum interferometer (RF SQUID) (b)

The total current flowing through DC SQUID can be calculated by the expression

$$I = I_{C1} \sin\varphi_1 + I_{C2}\varphi_2, \tag{4.20}$$

where φ_1 i φ_2 –the phase jumps of the wave function at the corresponding transitions.

Given that in the system shown in Fig. 4.4 the condition of phase coherence is fulfilled since this is a general property of superconductors regardless of their specific structure, the wave functions must be unambiguous. This means that the phase change at the loop tracing must be divisible by 2π. Based on this, we can write down

$$\varphi_1 + \varphi_2 + 2\pi\frac{\varphi}{\varphi_0} = 2\pi n, \tag{4.21}$$

Introducing a new variable $\psi = \varphi_1 + \frac{\pi\varphi}{\varphi_0}$, the expression for the current (4.21) will take the form [74]

$$I = I_{C1} \sin(\psi - \frac{\pi\varphi}{\varphi_0} + I_{C2}\, sin(\psi + \frac{\pi\varphi}{\varphi_0}) . \tag{4.22}$$

Using simple trigonometric transformations, the expression (4.22) can be written in the following way

$$I = I_m \sin(\psi - \alpha), \tag{4.23}$$

where $I_m = \sqrt{(I_{C1} - I_{C2})^2 + 4I_{C1}I_{C2}\, cos^{\;2}\frac{\pi\varphi}{\varphi_0}}$, $\alpha = arctg\left[\frac{I_{C1} - I_{C2}}{I_{C1} + I_{C2}} tg\frac{\pi\varphi}{\varphi_0}\right]$. (4.24)

If the interferometer consists of two identical Josephson junctions, then $I_{C1} = I_{C2}$, the expression for maximum critical current $I_m$takes the form

$$I_m = 2I_C \left|\cos\frac{\pi\varphi}{\varphi_0}\right|. \quad (4.25)$$

An analysis of this expression shows that the critical current of the SQUID takes the value zero whenever the flux φ is equal to the half of the flux quantum value $\Phi = (n+\frac{1}{2})\Phi_0$. (Fig. 4.5).

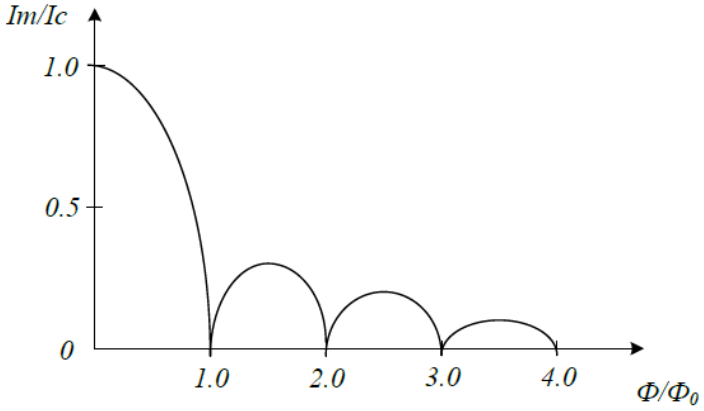

Figure 4.5 – Dependence of the maximum value of the steady Josephson current on the magnetic field

The value of the phase in the expression (4.23) is determined by the amount of current flowing through the interferometer. The expressions (4.23) shows that the maximum current oscillates in the flow function with a period equal to the flux quantum Φ_0. As $\Phi_0 = \frac{h}{2g} \approx 210^{-15}$ T is a very small value, such an interferometer can be used to record very small magnetic fields.

In case different Josephson junctions are used, i.e. $I_{C1} \neq I_{C2}$, the critical current does not turn to zero, but fluctuates between the minimum $|I_{C1} - I_{C2}|$and maximum $|I_{C1} + I_{C2}|$ values. The DC SQUIDs, which are a superconducting loop containing two Josephson junctions, are widely used for the construction of highly sensitive galvanometers, magnetometers, and converters of the magnetic signal to voltage. However, such devices are characterized by very limited linearity and small dynamic range. High-linearity and high-dynamic range in the low-frequency range in the SQUID-based devices are achieved through the use of external feedback. Such external feedback is not possible in the devices, which are used to receive and amplify millimeter and submillimeter waveband.

Multi-element Josephson structures can be used to construct wide-band, high-linear, and highly sensitive millimeter-wave devices[82], that provide an increase in the dynamic range due to the use of loops with many interferometers. When using this method, the dynamic range increases $\sqrt{N}$ times, where N is the number of Josephson structures. The high response linearity of the magnetic signal to voltage conversion function can be achieved by using specially designed elements with high-linear voltage reproduction. Such an element can be represented as the scheme shown in Fig. 4.6 [83]

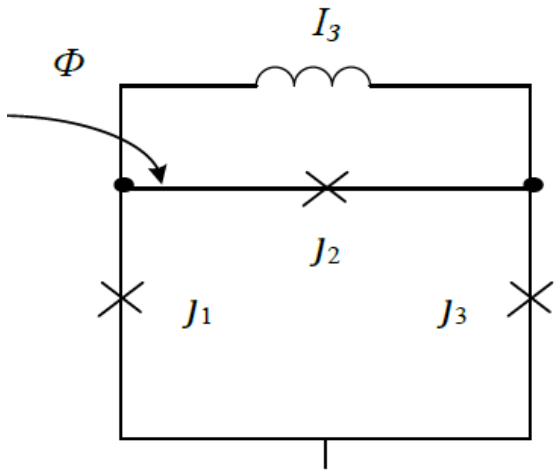

Figure 4.6 – Superconducting quantum DC interferometer sensor with high response linearity conversion of magnetic field to voltage (Bi-SQUID)

To ensure a linear dependence of the voltage on the magnetic flux, a double-contact SQUID is used, where an additional Josephson junction is introduced in parallel with the main inductance, which provides additional nonlinear signal transformation in the SQUID input circuit. Such Josephson junction is always in the superconducting state and plays the role of nonlinear inductance. This transition and the inductance of the superconducting loop form a single-contact SQUID, which performs a nonlinear transformation of the magnetic flux Φ of the input signal into the phase difference of the Josephson junctions $\Delta\varphi = \varphi_1 - \varphi_2$ of the double-contact SQUID. This conversion can be reversed for the subsequent nonlinear transformation of the phase difference into a constant component of the voltage. Thus, we obtain the resulting linear transformation of the input signal into the voltage.

4.3 Microwave low-intensity signal generators based on Josephson junctions

While developing low-intensity signal processing devices, the generators, the frequency of which can several times exceed the frequency of information signals, are widely used. This is especially evident in frequency-pulse information coding, where the generators of auxiliary signals are widely used [84, 85].

Since the benefits of the method of pulse-frequency information processing are manifested in the ultra-high frequency (UHF) band, such generators should provide generation in this range.

Recently, the most common transmitters in the frequency range of more than 100 GHz are generators based on the backward-wave oscillators [86]. Such generators provide a monochromatic mode of operation with a range of electronic settings up to 30 % of the central frequency, with output power up to hundreds of milliwatt at frequencies about one terahertz. However, the maintenance of high operating frequencies requires the use of high-voltage power supplies due to the need for a large accelerating voltage. Major drawbacks include the need for large permanent magnetic fields, which leads to a significant increase in size and mass. In addition, large difficulties arise when adjusting and configuring such generators.

Multi-stage semiconductor multipliers based on quantum semiconductor superlattice, which are layers of semiconductors with varying sizes of band gap, are used to construct millimeter generators. However, the output power of such generators is much smaller than that of generators based on BWO and it decreases with increasing the number of multiplicative stages, as well as decreases the range of electronic resetting [86–91].

In addition, quantum cascade lasers may be used to design millimeter-range generators, which can provide generation at frequencies from tens of terahertz to 100 THz, as well as generators based on resonant-tunneling diodes that represent an epitaxial heterostructure in which the tunnel-thin layer of a semiconductor with a smaller band gap is placed between layers with a larger band gap.

However, such devices are characterized by a number of disadvantages, which include, first of all, an extremely small range of frequency adjustment and low output power. Therefore, such generators are

not suitable for industrial use. It should also be noted that the designs of all generators mentioned above do not allow them to be used in integral devices [90, 92].

To eliminate some of the disadvantages listed above the generators based on Josephson junctions are used. They use the AC Josephson effect and can be tuned over a wide range of frequencies by changing the voltage.

Design and study of these generators are considered in the works [97, 98, 93]. The authors discuss multielement Josephson structures, the conditions for the mutual synchronization of Josephson junctions and the application of distributed tunneling junctions in order to reduce the width of the line of electromagnetic oscillations generation and to increase the power.

However, the known papers do not contain the study of the dependence between the alternating voltage amplitude, the Josephson oscillations period and the parameters of the equivalent circuit of the resistively shunted Josephson junction. That is why the purpose of this section is to develop the analytical dependence of the wave function phase difference in superconductors at the Josephson junction from the parameters of the equivalent circuit of the resistively shunted tunnel junction. These equations make it possible to calculate the dependence of the period and the amplitude of the electromagnetic oscillations as well as the time dependence of the super high frequency voltage while comprising several junctions into the electric circuit.

Let's consider a single resistively shunted Josephson junction.

From the fundamental correlation for AC Josephson effect, it follows that the frequency with which the supercurrent of Cooper pairs changes is determined by the equation 4.1.

Frequency f_0 is called Josephson frequency. We should note that even with very small voltages applied to the junction, the frequency is quite high and at U_0=10 μV it is about 4.83 GHz.

The voltage variable in time at such junction we can show as [79]

$$U(t) = \frac{\hbar}{2q} \cdot \frac{d\Phi}{dt} = R\left(I - I_0 \cdot \sin\Phi\right), \tag{4.26}$$

where Φ – wave function phase difference in superconductors, I_0 – critical current, R – shunting resistance.

After simple transformations we get

$$\int \frac{d\Phi}{I/I_0 - \sin\Phi} = \frac{2qRI_0}{\hbar}(t - t_0).$$

Left part of the expression can be easily calculated using a known method of substitution $y = tg(\Phi/2)$. As a result of integration we get

$$\frac{2}{\sqrt{(I/I_0)^2 - 1}} \cdot arctg \frac{2tg(\Phi/2) - 1}{\sqrt{(I/I_0)^2 - 1}} + C = \frac{2qRI_0}{\hbar}(t - t_0).$$

If $C = 0$ then

$$\Phi = 2arctg\left\langle \alpha^{-1}\left\{\sqrt{\alpha^2 - 1} \cdot tg\left[\frac{qRI_0}{\hbar}(t - t_0)\sqrt{\alpha^2 - 1}\right] + 1\right\}\right\rangle. \qquad (4.27)$$

This equation allows us to calculate the dependence of the wave function phase when the current flows through a Josephson contact from the magnitude of this current and the shunting resistor *R*.

The analysis of the last expression shows that the internal tangent goes to infinity, provided that

$$\frac{qRI_0}{\hbar}(t - t_0)\sqrt{\alpha^2 - 1} = n\pi.$$

Herewith $I = I_0$, $\Phi = 2arctg1$.

At the same time, the derivative of the wave function phase $d\Phi/dt$ is continuous in time and is a periodic function with period [70]

$$T = \frac{\pi\hbar}{qRI_0\sqrt{\alpha^2 - 1}} = \frac{\pi\hbar}{qR\sqrt{I^2 - I_0^2}},$$

which depends on the shunting resistance and the current flowing through the Josephson junction. The dependence of the oscillation period on the shunting resistance is shown in Fig. 4.7.

As we can see from the given graphs, the period of microwave oscillations decreases with the growth of shunting resistance, which is connected with the decreasing of the current flowing through this resistance, and, consequently, the current flowing through the Josephson junction nonlinear resistance grows up, and the frequency of oscillations increases. Fig. 4.8. shows the dependence of the period of microwave oscillations on the I/I_0 ratio.

As the graphs show us, increasing this ratio results a decrease in the period due to the grow of the voltage at Josephson junction.

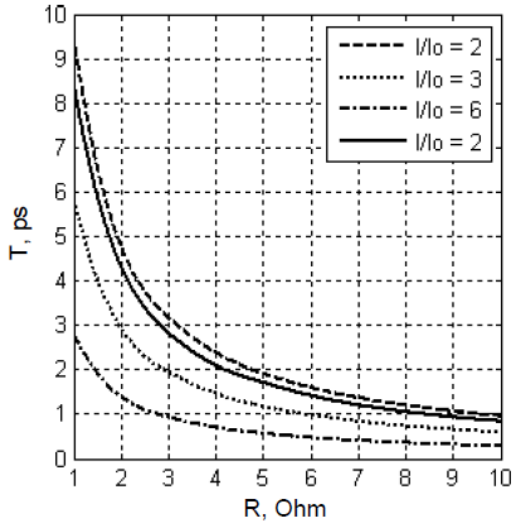

Figure 4.7 – Dependence of the period of microwave oscillations on the shunting resistance

To verify the reliability of the obtained analytical dependence of the wave function phase difference and instantaneous voltage from the parameters of the equivalent circuit of the resistively shunted junction, a calculation of the time dependence of the oscillation period from the shunting resistance R and the I/I_0 ratio for the structure of the three Josephson junctions was performed (Fig. 4.9). The calculation was held using the superconductor schematic editor and «WinS» simulator, which is used for design and analysis of analog and digital signals of superconductor electronic circuits [94].

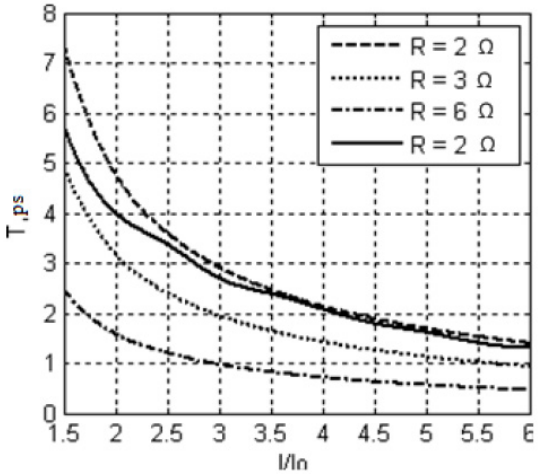

Figure 4.8 – Dependence of the period of microwave oscillations on the I/I_0 ratio

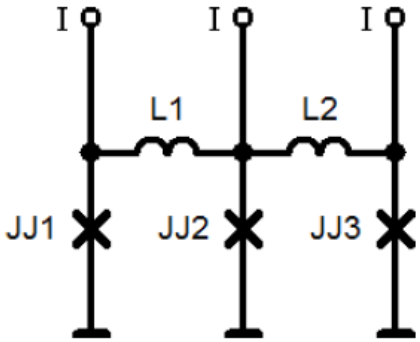

Figure 4.9 – Scheme of the generator with three Josephson junctions

The results of calculations of the dependence of the oscillation period on the shunting resistance for three Josephson junctions and the I/I_0 ratios are shown in Fig. 4.7 and Fig. 4.8 by solid lines. Comparison of the results obtained with two methods shows that the difference for the case of dependence $T = f(I/I_0)$ is in the range from 3 % to 25 %. Moreover, when increasing the I/I_0 ratio the deviation reduces (Fig. 4.10, *a*). In the case of dependence $T = f(R)$ deviation lies within the range from 10 % to 13 % (Fig. 4.10, *b*). This suggests that the given analytical expressions can be used for approximate calculations.

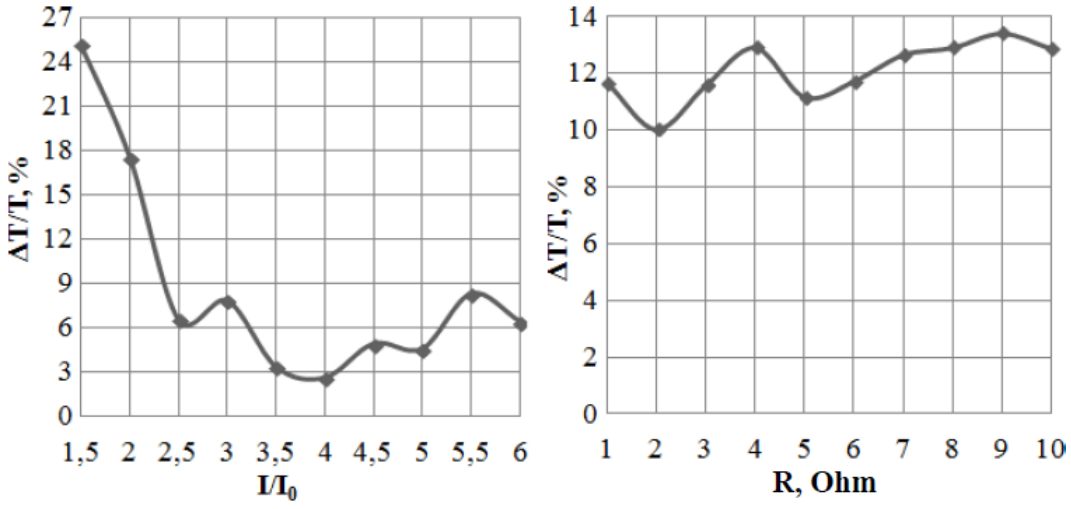

Figure 4.10 – Dependence of deviations of the period of electromagnetic oscillations on the ratio of currents I/I_0 (*a*) and on shunting resistance (*b*), in accordance with the WinS program for the analysis of devices at Josephson junctions

To determine the time dependence of the voltage of the super high frequency oscillations in accordance with (4.26), it is necessary to calculate the derivative $d\Phi/dt$ taking into account (4.27).

Let $\frac{qRI_0}{\hbar} = \eta$. Given that $\frac{d\Phi}{dt} = \frac{d\Phi}{dx} \cdot \frac{dx}{dt}$, we get

$$\frac{d\Phi}{\mathrm{dt}} = \frac{2\alpha^{-1}\left(\alpha^2 - 1\right)\eta \cos^{-2}\left[\sqrt{\left(\alpha^2 - 1\right)\eta(t - t_0)}\right]}{1 + \left\langle \alpha^{-1}\left\{\sqrt{\left(\alpha^2 - 1\right)}tg\left[\sqrt{\left(\alpha^2 - 1\right)\eta(t - t_0)}\right] + 1\right\}\right\rangle}.$$

Performing a few simple transformations, we obtain an expression for determining the junction voltage variable in time:

$$U = \frac{\alpha^{-1}\left(\alpha^2 - 1\right)RI_0}{1 + \alpha^{-2}\cos\left[2\sqrt{\left(\alpha^2 - 1\right)\eta(t - t_0)}\right] + \alpha^{-2}\sqrt{\left(\alpha^2 - 1\right)}\sin\left[2\sqrt{\left(\alpha^2 - 1\right)\eta(t - t_0)}\right]}. \quad (4.28)$$

The obtained expression enables us to calculate the instantaneous value of the voltage generated at the Josephson junction and the dependence of the oscillations amplitude on the parameters of the equivalent circuit for the Josephson junction. The result of calculation is shown in Fig. 4.11.

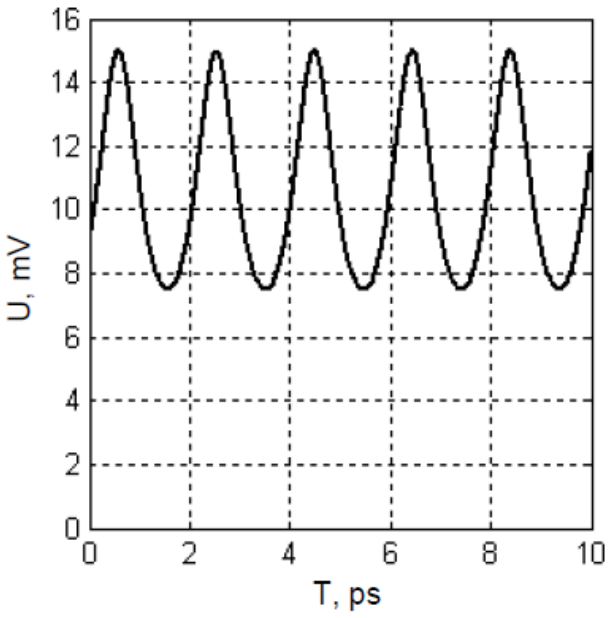

Figure 4.11 – The instantaneous value
of the voltage generated at the Josephson junction

We can see on the graph that the output signal is periodic and has a sinusoidal-like shape. Simple calculations and comparison of results (Figs. 4.7 and 4.11) show that the period of oscillations is the same and equals about 2 ps, which indicates the presence of synchronization of Josephson junctions. Minor deviations may occur in a reason of the capacity of Josephson junction that was not taken into account when calculating the wave function phase difference and instantaneous voltage.

Comparing the results obtained in theoretical calculations, based on the equivalent junction circuit and using computer simulation, by solving non-linear differential equations, shows that the differences do not exceed 25 %, and can therefore be used for approximate calculations.

The advantages of generators based on Josephson junctions include the following:

- low power consumption gives the opportunity to increase the integration degree of devices on their base significantly;
- a wide frequency resetting range, which is limited only by the possibilities of harmonization of the generator and load;
- small dimensions and weight.

However, generators based on a single Josephson junction are characterized by a number of disadvantages.

First, the small value of the output power, which cannot exceed 100 nW.

Secondly, the output resistance of the Josephson transition is very low, and therefore it is difficult to reconcile it with the load. The typical values are 50 or 75 Ohms. Due to this, the reflection coefficient of a load increases.

Thirdly, the width of the generation line for a single junction can be hundreds of megahertz, which leads to significant frequency instability.

In our case, given that the auxiliary signals generators will be loaded on other devices that are also implemented on the Josephson junctions, so the coordination disadvantage is not significant here.

In order to increase the output power and reduce the width of the generation line, it is advisable to use methods based on the sequential and parallel connecting of several Josephson junctions.

If all the junctions of the circuit are synchronized, then the output power increases in proportion to the number of junctions, and the radiation line width decreases. An analysis of different types of multielement

Josephson structures has been carried out for the design of auxiliary signal generators. To construct generators single lumped Josephson junctions, multielement synchronous Josephson structures, distributed Josephson junctions and multilayer structures based on high-temperature superconductivity, or bicrystal Josephson junctions can be used.

The main obstacles that arise in creating multi-element synchronous Josephson structures are the technological deviations of their parameters from the nominal values. This refers to the critical current, the deviation of which is particularly important for high-temperature Josephson junctions, electrostatic capacity, non-linear conductivity, tunneling of quasiparticles, energy gap width, the density of Cooper pairs in superconductors, the thickness of the dielectric, etc.

Despite the fact that a lot of works are devoted to multielement synchronous Josephson structures [79, 82, 95, 96] till now there are clearly no criteria for choosing electrodynamic coupling circuits that would provide the strongest interaction of Josephson elements that is necessary for providing a synchronous generation mode, their optimal location on MSSL, maximum resistance to deviation of parameters and matching the load circuits. In addition, the problem of a substantial narrowing of the synchronous generation line and increasing the frequency stability by increasing the number of Josephson junctions in the multielement structure and the ways of their connection remain open.

A large number of publications that are devoted to the theoretical and experimental study of various multi-element structures, distributed Josephson junctions based on the low-temperature superconductors, to the questions of the synchronization of the Josephson generation, and matching such structures to external load, indicates the relevance of this research direction.

Let us consider a generator based on a multielement Josephson structure with distributed electromagnetic coupling circuits, in which the Josephson junctions interact with a standing wave of current. The scheme is depicted in Fig. 4.12.

Fig. 4.12. Generator based on distributed two-element Josephson structure (a) an its equivalent scheme (b) for the case of using 20 links of LC elements and four-element Josephson structure (c) and its equivalent scheme (d).

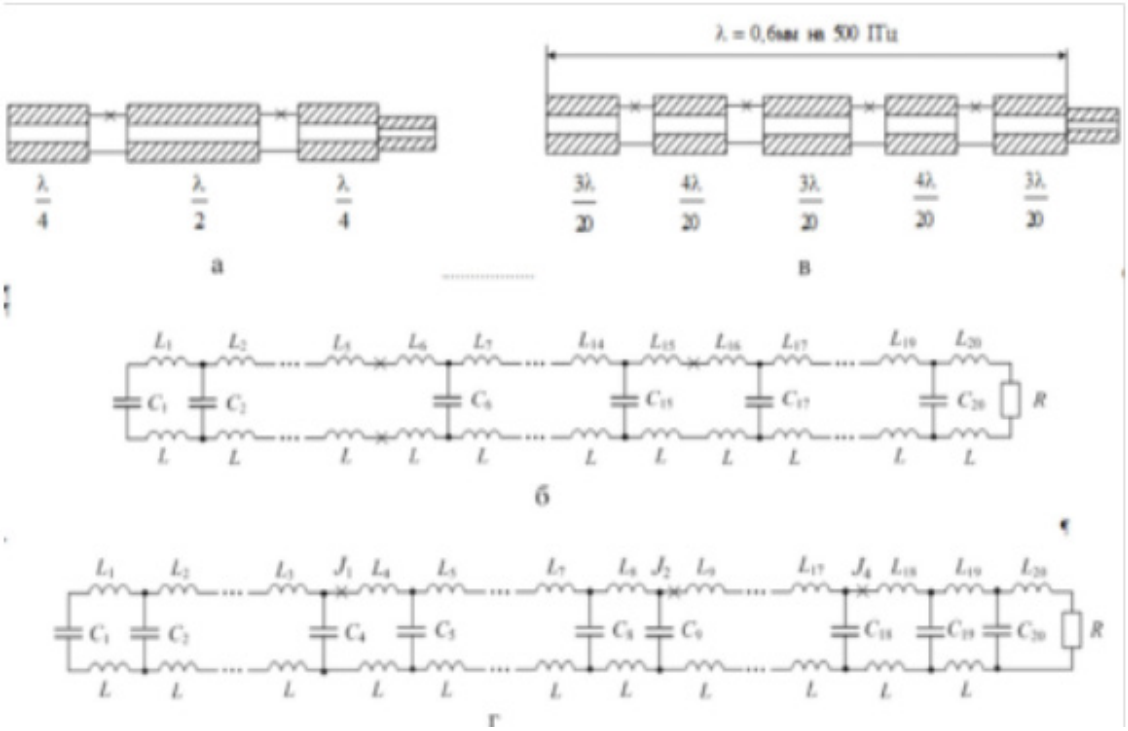

Figure 4.12. Generator based on distributed two-element Josephson structure (a) an its equivalent scheme (b) for the case of using 20 links of LC elements and four-element Josephson structure (c) and its equivalent scheme (d)

We will simulate the distributed structure with *LC* circuits. Such structure can be implemented on Josephson junctions technology using high-temperature superconductor microstrip lines. Junctions interact with a standing wave of current, since they are included into the superconductor circuits, and the standing wave, exciting here, provides the common mode of the Josephson generation. Generation frequency is determined by the full length of the distributed microstrip line. It is shown in [82] that the smallest generation line width occurs in the case of a weak reflection of waves from the Josephson junction. In our case, when the Josephson junction interacts with a standing wave of current, this condition fulfills when the junction impedance is smaller than the wave impedance of MSSL.

The use of the case when the junctions interact with the standing wave of current, but not the voltage, is connected with the fact that when using the second case, increasing the number of junctions to three or more does not lead to a decrease of the generation line width, only the power increases [82].

We used software complex PSCAN to simulate the structure shown in Fig. 4.12. This program was developed in the laboratory of cryogenic electronics on the physical faculty at Lomonosov Moscow State University and it is one of the most effective automated Windows-compatible software

packages for numerical analysis of superconductor electric circuits with an arbitrary number of Josephson junctions [97]. The complex finds a solution of the differential equations system using an automatically variable integration step over time. The system of equations is automatically generated inside the software package on the basis of the structure of the investigated circuit. Unlike the semiconductor circuits, the analysis of superconductor schemes is based on equations of the Josephson phase balance for superconductor circuits, i.e. the node-phase analysis is used. In this case, the non-linear differential equation describing the current flowing through the Josephson junction for the simplest resistive model looks like

$$A\ddot{\varphi} + B\dot{\varphi} + sin\varphi + C\varphi + I_{jk} = \bar{I}_k + \tilde{I}_{k3},$$

where A, B, C – some coefficients that take into account the parameters of the resistive model of the Josephson junction. They can be calculated in accordance with (4.8); I_{jk} – fluctuation current; $\bar{I}_k$ – direct current; $\tilde{I}_{k3}$ – current flowing through the coupling circuit.

The difference of this equation from the analogous given in [82] is that here the junction inductance is taken into account and an additional term $C\varphi$ appears.

For modeling of the generator, which structure is shown in Fig. 4.12, we used MSSL with the length of λ. It played the role of a resonator. The Josephson junctions were located at different distances between themselves and at each end of the MSSL. While simulating, the distributed structure consisted of 20 *LC*-circuits. The results of simulation are shown in Fig. 4.13a, b.

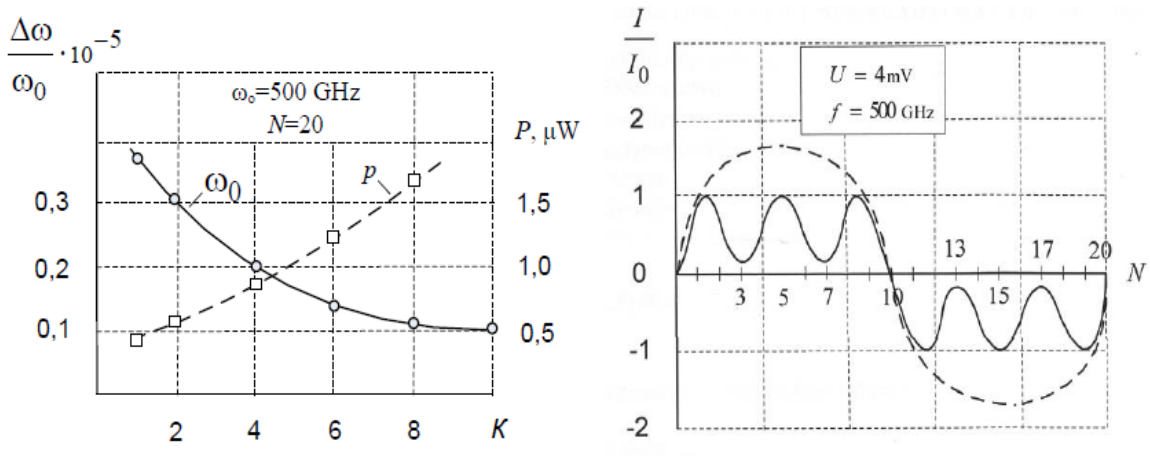

a b

Figure 4.13 – The dependence of the generation line width and output power on the number of Josephson junctions connected in MSSL

As we can see from Fig. 4.13 increasing the number of junctions connected in MSSL leads to a decrease in the width of the generation line. The simulation showed that the width of the generation line and the output power are influenced by the location of Josephson junctions in a microstrip superconductor resonator. Thus, if there are four Josephson junctions connected to the resonator, the minimum generation line width and the highest power is observed when the placement of Josephson junctions in the structure corresponds to $N_1 = 3, N_2 = 7, N_3 = 13, N_4 = 17$ for the case of 20 LC circuits, i.e. at the points where the maximum interaction of Josephson junctions with a standing wave of current takes place.

The study of the dependence of the generation line width on the location of the Josephson junction in the distributed structure showed that, in the case of a single-element structure, the minimum line of synchronous generation occurs when the junction is placed in the nodes of the standing wave, in condition of small losses. With an increase in losses occurring while using HTSC, the junction is to be placed in the nodes of the standing wave of current. In the case of two Josephson junctions, it is expedient to place them symmetrically relative to the center of the resonator, at a distance $\frac{\lambda}{4}$ from its ends. In the case of four Josephson junctions, they should also be located symmetrically relative to the center of the resonator, at a distance $\frac{\lambda}{5}$ from each end and $\frac{3}{10}\lambda$, i.e. closer to the node of the standing wave of current. This arrangement provides the maximum interaction of the Josephson junction with a standing wave of current and therefore provides a minimum generation line width and maximum power. Choosing the optimal location for Josephson junctions in the resonator based on MSSL gives an opportunity to provide optimal generator parameters.

4.4 The estimation of the oscillator frequency instability of low-intensity signals based on Josephson junction

According to Josephson junction theory, it is known that the electromagnetic field, which is generated by Josephson current density, is monochromatic, despite the existence of separate mechanisms that lead to frequency instability.

In the general case, the oscillation of an electromagnetic field takes place at a fixed frequency, determined by the expression (4.1).

Taking into account the structure of a field at Josephson junction shows that the oscillations take place on the harmonics of the basic frequency $\omega_n = n\omega$, where $n = 2,3,\ldots$. As theoretical calculations show, each of the harmonics is characterized by high stability. However, as experimental studies show, there are some deviations from the ideal case, that is: the width of the oscillation line is characterized by a small but finite value.

The stability of radiation is influenced predominantly by the temperature and concentration dependence of the critical current density and the temperature instability of the voltage at Josephson junction. Voltage fluctuations will be converted to frequency fluctuations leading to noise frequency modulation of the signal being emitted. The effect of thermal voltage fluctuations at Josephson junction on the frequency instability of the electromagnetic field, generated by this junction, was analyzed in the research [74].

The conducted theoretical analysis showed that the shape of the generation line is Lorentzian one in the case when the width of the generation line is much less than the time constant for a resistively-shunted junction. It can be written as follows:

$$J(\omega) = \frac{1}{\pi} \frac{\Delta\omega_1}{\pi(\omega - {}_0) + \Delta\omega_1^2}.$$

The line width can be calculated with this approximate expression in this case:

$$\Delta\omega_1 = \frac{4Ke^2}{\hbar} R^* T^*.$$

In the second last case when $\Delta\omega >> \frac{1}{R^* C^*}$ the shape of the generation line is Gaussian, and the expression that describes it has the following form:

$$J(\omega) = \frac{1}{\Delta\omega_2 \sqrt{\pi}} exp \frac{(\omega - \omega_0)^2}{\Delta\omega_2}.$$

The width of the line is determined by the expression in this case:

$$\Delta\omega_2 = \frac{2e}{\hbar} \sqrt{\frac{2T}{C}}.$$

The simple calculations made by the above expressions show that they are unsuitable for use because the results obtained are several orders of magnitude different from the real values resulting from the experiments [98, 99, 100, 101]. Therefore, an approach is proposed in this section, which is to estimate the influence of the spectral density of low-frequency and high-frequency fluctuations of the current of ordinary electrons and Cooper pairs on the width of the generation line. Let us consider how the width of the generation line changes when various types of Josephson structures are applied.

It is known that the width of the generation line for a single element Josephson structure is determined by the expression [82]:

$$\Delta f = \frac{1}{2}\left(\frac{2e}{\hbar}\right)^2 S_{\mathrm{V}}(0).$$

The spectral density of low-frequency voltage fluctuations $S_{\mathrm{V}}(0)$ is determined by the product of the differential resistance of Josephson junction at the operating point and the effective spectral density of low-frequency current fluctuations:

$$S_{\mathrm{V}}(0) = R_d^2 S_I^*(0),$$

where R_d is differential resistance at the operating point, the value of which can be calculated, taken into consideration the expression for the voltage at the junction.

Using the expression (4.28) for the current-voltage characteristic of Josephson shunt junction, the differential resistance can be calculated by the expression:

$$R_d = \frac{R_{Ш} \cdot R_{П}}{R_{Ш} + R_{П}} \cdot \frac{I}{\sqrt{I^2 + I_0^2}},$$

where $R_{П}$; $R_{Ш}$ are differential junction resistance and shunt resistance.

The effective spectral density of low-frequency current fluctuations for the case of a resistive Josephson junction model is determined by the expression [95]:

$$S_I^*(0) = S_I(0) + \left(\frac{I_C^2}{2I^2}\right) S_I(\omega), \qquad (4.29)$$

where $S_I(0)$ and $S_I(\omega)$ are respectively low-frequency and high-frequency spectral densities of current fluctuations. Let us determine the high-frequency spectral density of current fluctuations.

Since currents of both ordinary electrons and Cooper pairs flow through Jepherson junction, the fluctuation spectral density of these currents can be calculated by the following expressions:

$$S_{in}(\omega) = 2q(I_{n1} + I_{n2}),$$
$$S_{ip}(\omega) = 4q(I_{p1} + I_{p2}),$$

where I_{n1}, I_{n2} – currents of ordinary electrons; I_{p1}, I_{p2} – currents of Cooper pairs.

It is assumed here that both currents can flow through Josephson junction in both directions. Taking into account the probability of charged current carriers passing through Josephson junction, the magnitude of currents can be calculated by the expression [70]:

$$I_{n1} + I_{n2} = I_n cth\left(\frac{2qU}{2KT}\right); \qquad I_{p1} + I_{p2} = I_p cth\left(\frac{2qU}{2KT}\right), \tag{4.30}$$

where U – voltage at Josephson junction; T – absolute temperature; K – Boltzmann's constant.

Taking into account (4.30), the total current spectral density can be calculated by the expression:

$$\overline{S_I(\omega)} = \overline{S_{I_n}(\omega)} + \overline{S_{I_p}(\omega)} = 2qI_n cth\left(\frac{qU}{2KT}\right) + 4qI_p cth\left(\frac{2qU}{2KT}\right). \tag{4.31}$$

In the case when Josephson junctions are formed on the basis of low-temperature superconductors, we can assume that the condition $qU >> KT$ is met, then the function *cth* tends to 1 and the expression for the total current spectral density has the following form:

$$\overline{S_I(\omega)} = 2qI_n + 4qI_p = 2q(I_n + 2I_p). \tag{4.32}$$

In the case of usage of high-temperature superconductors, the condition $qU << KT$ is met, and therefore the function *cth* is approximated by the function of the inverse of its argument, and the total current spectral density is determined by the expression:

$$\overline{S_I(\omega)} = 4KT\frac{I}{U} \tag{4.33}$$

To calculate the low-frequency spectral density of current fluctuations $S_\tau(0)$, we will use the expression given in [95]:

$$S_I(0) = \frac{1}{\pi U}\left[KTI_n + \frac{hf}{2} cth\frac{eU}{KT}\right], \qquad (4.34)$$

where K – Boltzmann's constant; f – frequency; I_n, I_p – normal and superconducting current components.

Substituting (4.34) and (4.32) into (4.29), we obtain an expression for the width of the generation line in the following form for the case of low-temperature superconductors:

$$\Delta f = \frac{1}{2}\left(\frac{2e}{\hbar}\right)_2^2 R_\partial^2 \left\{\frac{1}{\pi U}\left[KTI_n + \frac{hf}{2} cth\frac{eU}{KT} I_p\right] + \left(\frac{I_0^2}{2I^2}\right) 2q\left(I_n + 2I_p\right)\right\}. \qquad (4.35)$$

If $qU << KT$, then $S_I = 4KT\frac{I}{U}$.

It is necessary to consider (4.33) in the case of high-temperature superconductors. Then the expression for the width of the generation line can be written as:

$$\Delta f = \frac{1}{2}\left(\frac{2e}{\hbar}\right)_2^2 R_\partial^2 \left\{\frac{1}{\pi U}\left[KTI_n + \frac{hf}{2}\frac{KTI_S}{eU} I_p\right] + \left(\frac{I_0^2}{2I^2}\right)\frac{4KT\left(I_n + 2I_p\right)}{U}\right\}, \qquad (4.36)$$

where $R_\partial = \frac{dU}{dI} = \frac{d}{dI}\left(\frac{RI_0 a^{-1}в}{(a^{-2}+1)\cos^2 A + a^{-2}в\sin^2 A + 2a^{-2}в^{1/2}\sin A\cos A}\right)$.

Using expressions (4.35) and (4.36), the dependence of the generation line width on the current flowing through Josephson junction, the load resistance and the shunt resistance have been calculated. The results of the calculations are shown in Fig.4.14.

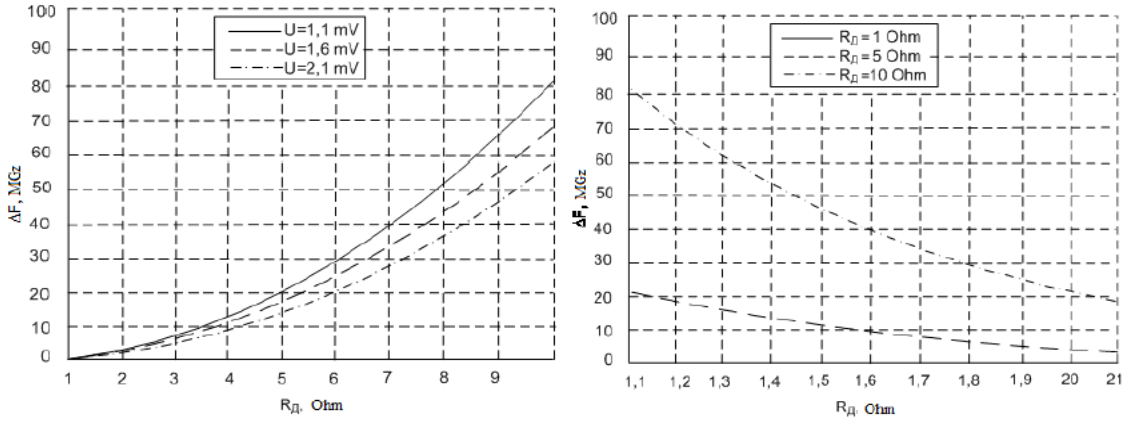

(a) (b)

Figure 4.14 Dependence of generation line width on dynamic resistance (a) and the voltage at Josephson junction (b)

An analysis of the results shows that the generation line width is tens or even hundreds of MHz, so there is a need to reduce its width.

It is due to the fact that the frequencies must be significantly spaced to increase the noise immunity in the construction of digital radio technical devices with frequency encoding information. The auxiliary signal generators are used, the frequency of which is twice and sometimes three times bigger than the frequency of information signals, then there are difficulties associated with the need to match in a wide range of frequencies. It is also necessary to increase the signal strength, since they are widely used in such devices, which reduce the signal level and complicate its processing.

In order to reduce the generation line width and to increase the output power, it is suggested to use multi-element synchronous Josephson structures.

Different types of such structures are considered in [87, 95, 101, 102]. The analysis of different types of one- and two-dimensional multi-element Josephson structures have been analysed in the papers [6,103], in which the strongest interaction between Josephson junctions takes place.

An inductive electromagnetic coupling is used to ensure the in-phase mode of Josephson generation. It is shown that the maximum range of stable coherent radiation occurs at some values of the impedance of the circuit which are approximately equal to the impedances of Josephson junction, that is, when

$$r = \frac{R}{R_N} \cong 1,\ l = \frac{L}{L_I} \cong 1,$$

where R_N – Josephson junction resistance; $L_I = \dfrac{\hbar}{2eI_0}$ – the characteristic inductance of Josephson junctions and at the value of the McCumber Parameter $\beta \cong 1$.

When applying a two-contact Josephson structure with an *LR* – coupling circle, with optimal circuit parameters, a coherent generation mode occurs when the critical current changes within 20 %. It occurs in the case of the individual parameters of the coupling circle described above and in the frequency range $\omega = \dfrac{\omega_0}{2}$.

The synchronization range ΔI_0 at $\beta << 1$ decreases with increasing frequency of generation rateably $\frac{1}{\omega}$ because the imaginary conduction frequency of the coupling circle reduces. As the frequency decreases, the synchronization range narrows due to a decrease in the interaction of Josephson elements because of the energy transfer from the first harmonic to the higher harmonics [6].

However, the influence of electromagnetic coupling circles on the generation line width is not considered in known works when using a two-contact structure with *LR* – a coupling circle (Fig. 4.15).

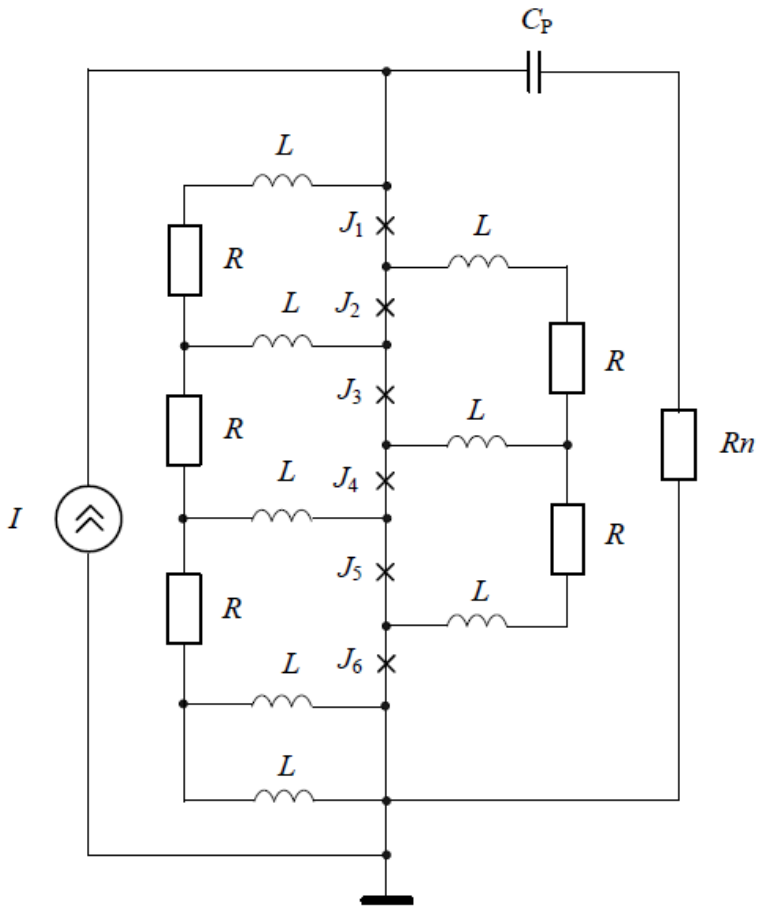

Figure 4.15 – A generator based on two-contact Josephson structure

To study such a generator, we will use the resistive model of Josephson junction. Considering this, we construct an equivalent generator circuit, which is shown in Fig. 4.16.

The parameters of the equivalent circuit elements have been selected as follows:

$$L_{\Pi} = \frac{h}{2eI},\ L \approx L_{\Pi},\ R_{\Pi} = \frac{dU}{dI},\ R \approx R_{\Pi},\ C = \frac{\beta G}{\omega_0},\ \omega_0 = \frac{2g}{\hbar}\frac{I_0}{G},$$

$$\beta = \frac{\omega_0 C}{G} = 1.$$

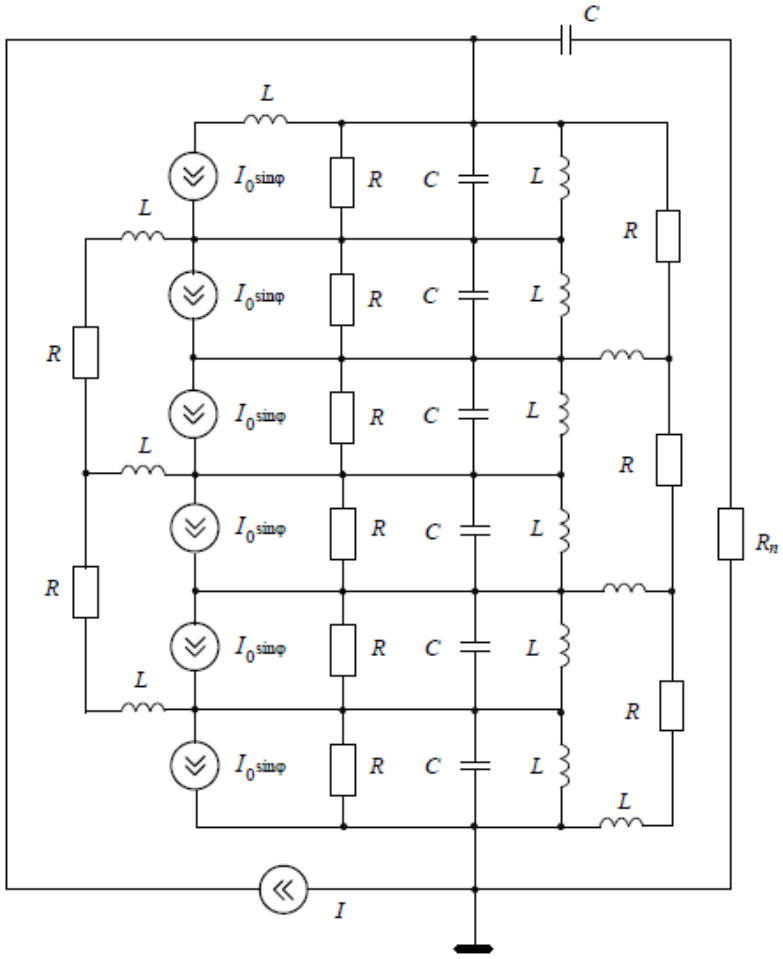

Figure 4.16 – The equivalent generator circuit based
on two-contact Josephson structure

The difference of the suggested equivalent generator circuit is that the inductance is taken into account in order to increase the convergence of the obtained results with the experimental data in Josephson junction model. This inductance occurs when the current passes through Josephson junction, the magnitude of which is determined by the critical current I_0 and the phase difference of the waves functions. The studies were conducted using PASCN software package and the superconducting circuit editor and WinS simulator.

During it, the effect of electrodynamic coupling circuits on the magnitude of the output power and the generation line width was

evaluated. In this case, it was assumed that all Josephson junctions were characterized by exactly the same parameters. The parameters of the electrodynamic coupling circuits were chosen under the condition that $R_1 = R_2$, $R_3 = R_4 = R_5$, $L_1 = L_2 = L_3$, $L_4 = L_5 = L_6 = L_7$. The results of the studies are shown in Figures 4.17, 4.18, 4.19, 4.20, 4.21.

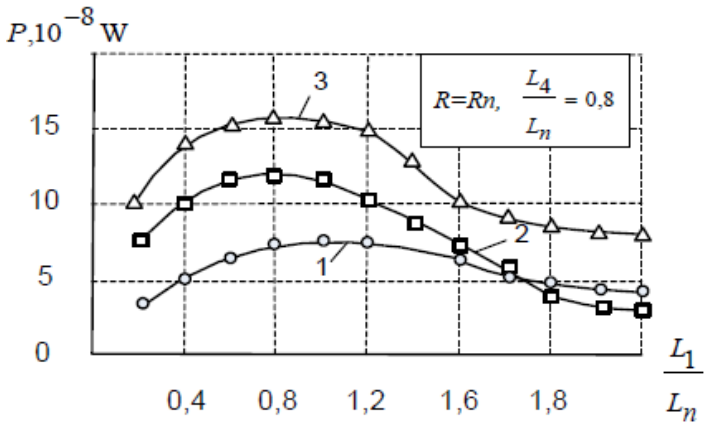

Figure 4.17 – The dependence of the output power on the value of the inductance of the circuits of electrodynamic coupling

$$1 - \frac{L_4}{L_n} = 0{,}8\,;\; 2 - \frac{L_4}{L_n} = 1{,}0\,,\; 3 - \frac{L_4}{L_n} = 1{,}2$$

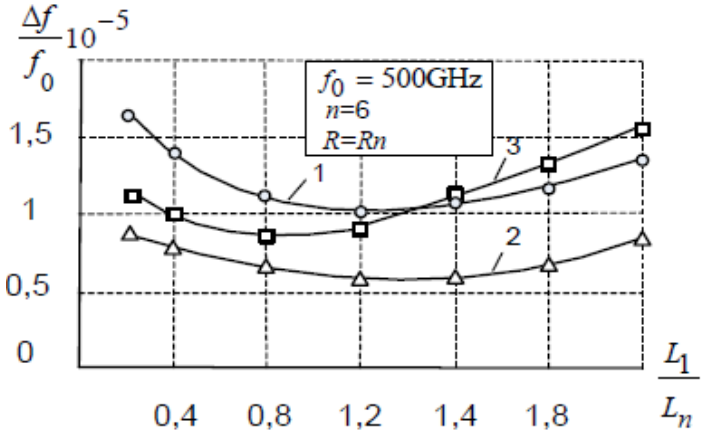

Figure 4.18 – The dependence of the given generation line width from inductances of coupling circuits

$$1 - \frac{L_4}{L_n} = 0{,}8\,;\; 2 - \frac{L_4}{L_n} = 1{,}0\,;\; 3 - \frac{L_4}{L_n} = 1{,}2$$

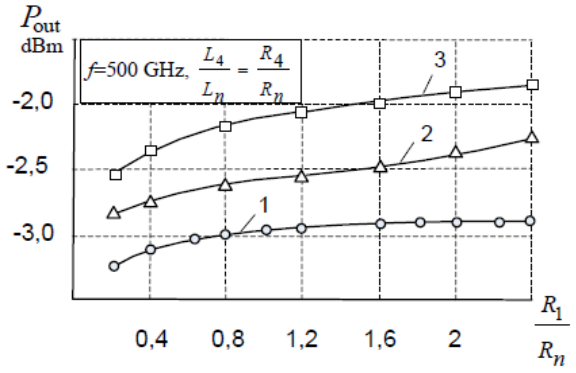

Figure 4.19 – The dependence of the output power on the active resistance of the electrodynamic coupling circuit

$$1-\frac{L_1}{L_n}=0{,}8\,;\ 2-\frac{L_1}{L_p}=1{,}0\,;\ 3-\frac{L_1}{L_n}=1{,}2$$

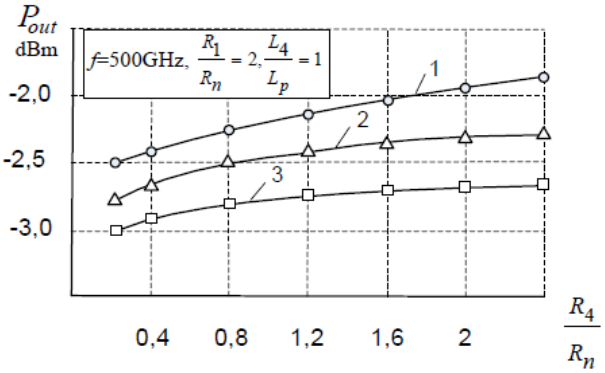

Figure 4.20 – The dependence of the output power on the active resistance of the electrodynamic coupling circuit

$$1-\frac{L_1}{L_n}=1{,}2\,;\ 2-\frac{L_1}{L_p}=1{,}0\,;\ 3-\frac{L_1}{L_n}=0{,}8$$

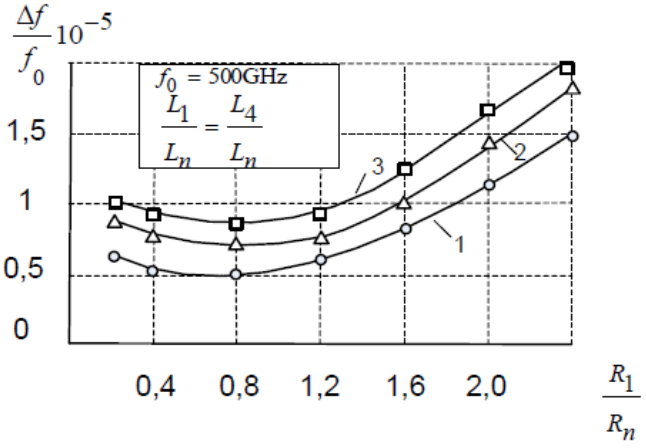

Figure 4.21 – The dependence of the generation line width on the active resistance of electrodynamic coupling circuit

$$1-\frac{R_4}{R_n}=1{,}0;\ 2-\frac{R_4}{R_n}=1{,}6;\ 3-\frac{R_4}{R_n}=2.$$

The analysis of the obtained results shows that the maximum value of power can be obtained with inductances of the coupling circuit $L \div L_4$, equal to the Josephson inductance (Fig. 4.17) and inductances $L_4 \div L_7$, equal to approximately 1.2LP (Fig. 4.17, 4.19). An increase in the active resistances of the electrodynamic circles leads to an increase in the output power, which is released on the load resistance (Fig. 4.19, 4.20). This is because the amount of current flowing in the coupling circuits decreases with increasing resistance. Therefore, the current flowing through the load circuit increases, as well as the reflection coefficient decreases, which is caused by the better matching of the output of the generator with the wave resistance of MSSL.

The generation line width is minimal when the inductances of the electrodynamic coupling circuits are in the range of 0.5 $L_П$ to 1.2 $L_П$. The width of the generation line increases with the increase of the active resistances of the circles of electrodynamic coupling (Figs. 4.18, 4.21).

The generation line width increases as the active resistances of the electrodynamic coupling circuits increase (Figs. 4.18, 4.21).

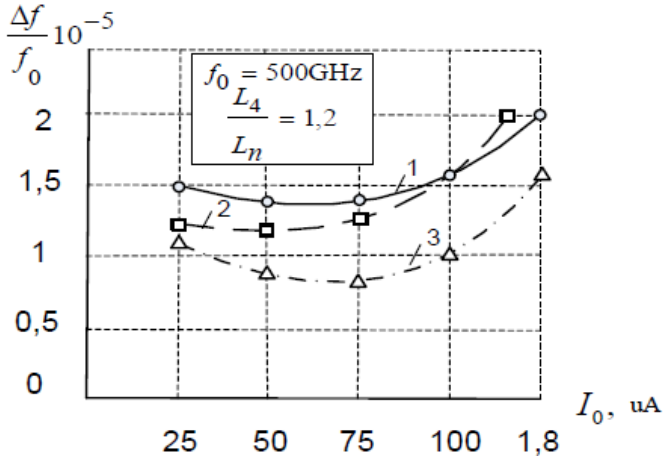

Figure 4.22 – The dependence of the generation line width on the critical current $1-\frac{L_1}{L_n}=0{,}8;\ 2-\frac{L_1}{L_n}=1{,}0;\ 3-\frac{L_1}{L_p}=1{,}8$.

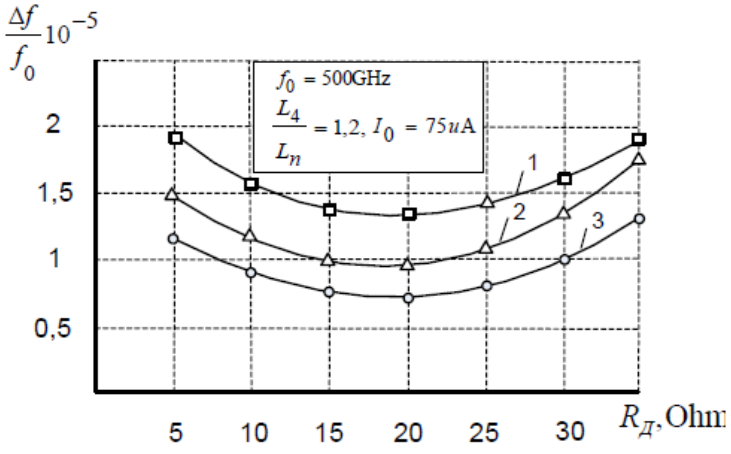

Figure 4.23 – The generation line dependence on the dynamic resistance

$$1-\frac{L_1}{L_n}=0{,}8\,;\ 2-\frac{L_1}{L_n}=1{,}0\,;\ 3-\frac{L_1}{L_n}=1{,}2\,.$$

The comparison of the obtained results with those shown in Fig. 4.14 indicates that increasing the number of junctions to 6 leads to a decrease in the generation line width by about 5-6 times. The study of the dependence of the generation line width and output power on the critical current and dynamic resistance shows that a change in the critical current and dynamic resistance within 20 % does not lead to a significant change in the generation line width (Fig. 4.24, 4.25) when changing the circuits inductance of electrodynamic coupling in the range of 0.8 $L_П$ to 1.2 $L_П$.

4.5 Frequency converters for the processing of low-intensity signals

Specific nonlinear properties of Josephson contacts can be used to construct logical frequency mixers. In [85], an analysis of the technical level of basic circuits used for the construction of digital radio engineering devices with frequency-pulse encoding of information is presented and showed that it is advisable to use double-ended field-effect transistors for the construction of logic frequency mixers, which allow to realize equivalent inputs and can be used in the frequency range up to several tens of Gigahertz [104].

Significantly expand the range of operating frequencies and, accordingly, increase the speed, possibly by using for the construction of logic mixers of the frequency of transitions of Josephson [105–108], the characteristics of which differ significantly from the characteristics of mixers based on semiconductor devices.

It is known that under the action of a high-frequency field on the Josephson contact on the voltage-ampere characteristic, vertical ladder sections are observed at displacements that satisfy the expression [74]

$$2eU_0 = n\hbar\omega, \quad n = 1,2,3\ldots,$$

where U_0 – bias voltage; ω – frequency of the ultra-high frequency field.

The height of the steps depends periodically on the applied field.
If a high-frequency electromagnetic field with frequency Ω is fed to the Josephson junction, then there is a frequency modulation of the Josephsonian current at a voltage at the junction that equal to ω_0 [74],

$$\omega = \frac{2e}{\hbar}\left[U_0 + U\cos(\Omega t + \theta)\right], \tag{4.37}$$

where U – is a variable voltage that is proportional to the high-frequency field strength.

In this case, the Josephson current can be calculated by the expression

$$I = I_0 \sin\int_0^t \omega dt \ . \tag{4.38}$$

In order to calculate the current flowing through the Josephson junction, it is necessary to substitute (4.37) into (4.38)

$$I = I_0 \sin\int_0^t \frac{2e}{\hbar}\left[U_0 + U\cos(\Omega t + \theta)\right]dt \ . \tag{4.39}$$

The direct calculation of the integral (4.39) gives such a dependence of the current on the time and voltage on the Josephson junction

$$I(t,U) = I_0 \sin\left[\frac{2e}{\hbar}U_0 t - \frac{eU}{2\pi f\hbar}\cos(2\pi f t + \theta) - \frac{eU}{2\pi f\hbar}\cos\theta\right]. \tag{4.40}$$

If we put it in series (4.40), the expression for determining the dependence of the superconducting tunneling current on the applied voltage and time can be written in the form [74]

$$I(U,t) = I_0 J_n\left(\frac{2eU}{\hbar 2\pi f}\right)\sin\left[(2\pi f_0 t + \varphi_0) + n(2\pi f t + \theta)\right], \tag{4.41}$$

where J_n – nth order Bessel function; $f_0 = \frac{2eU_0}{\hbar}$ – Josephson frequency, which, using elements of the equivalent Josephson junction scheme, can be calculated by the expression

$$f_0 = \frac{2e}{\hbar}\frac{I_0}{G}.$$

That is, it corresponds to the frequency of generation of the voltage by the Josephson junction when flowing through a resistor with a conductivity G of the maximum direct current of the Josephson effect. G is the magnitude of the nonlinear conductivity of the tunneling of quasiparticles (Cooper pairs).

Let us consider in more detail the processes of interaction of the high-frequency field with the Josephson junction.

Consider the case when a high frequency radio pulse with a frequency of filling is fed to the Josephson junction. The radio pulse voltage varies by law

$$U = U_1 cos(\omega_I t + \theta),$$

and a constant voltage is applied U_0.

In the absence of an external variable field, the wave function of a Cooper pair with energy E is given the form

$$\psi = f(x,y,z)exp\left(-i\frac{Et}{\hbar}\right), \tag{4.42}$$

where $f(x,y,z)$ – some coordinate function; t – time; $\hbar = \frac{h}{2\pi}$ – Planck's constant.

This wave function is peculiar to the Hamiltonian of the non-excited system H_0. When applying an external high-frequency voltage pulse to the Josephson junction, the Hamiltonian of an excited Cooper pair system can be written as

$$H = H_0 + eU_1 cos(\omega_1 t + \theta). \tag{4.43}$$

Then the wave function can be rewritten as

$$\psi = f(x,y,z)exp\left(-i\frac{Et}{\hbar}\right)\left[\sum_n A_n exp(-in\omega_1 t + \theta\right], \tag{4.44}$$

where A_n – unknown function.

Substituting (4.43) and (4.44) into the Schrödinger equation, we obtain

$$i\hbar\frac{d\left[f(x,y,z)exp\left(-\frac{iEt}{\hbar}\right)\sum_n\left[A_n exp(-in\omega_1 t+\theta)\right]\right]}{dt}= \tag{4.45}$$
$$=\left[H_0+eU_1(cos\omega_1 t+\theta\right]\cdot\left[f(x,y,z)exp\left(-\frac{iEt}{\hbar}\right)\right]\sum_n A_n exp\left(-in\omega_1 t+\theta\right).$$

After differentiation and simple transformations we obtain the equation

$$2nA_n=\frac{eU_1}{\hbar\omega_1}\left(A_{n+1}+A_{n-1}\right),$$

the solution of which is represented by the Bessel function of order n:

$$A_n=J\left(\frac{eU_1}{\hbar\omega_1}\right). \tag{4.46}$$

Substituting (4.42) into (4.40), we obtain the solution of the Schrödinger equation as a wave function

$$\psi=f(x,y,z)exp\left(-i\frac{Et}{\hbar}\right)\sum_n J_n\left(\frac{eU_1}{\hbar\omega_1}\right)exp\left(-in\omega_1\right). \tag{4.47}$$

From the last expression we can conclude that the energy levels of Cooper pairs, under the action of high-frequency radio pulses, are split into levels that are described by wave functions ψ_n with energies $E+n\hbar\omega_1$, and the probability of completing these levels is proportional $J_n\left(\frac{eU_{\omega_1}}{\hbar\omega_1}\right)$.

When absorbing a quantum of radiation, the Cooper pair increases its energy by $\hbar\omega$, which is equivalent to applying to the Josephson voltage transition $\frac{\hbar\omega}{e}$, and the tunneling current, in this case, is determined by the function $J\left(U_0+\frac{\hbar\omega}{e}\right)$.

To determine the full current, it is necessary to consider the likelihood of the transition of Cooper pairs from one state ψ_n to another ψ_e. With this in mind, the total current through the Josephson junction can be calculated by expression [78]

$$I(U,t)=\sum_n\sum_e J_n\left(\frac{eU_1}{\hbar\omega_1}\right)J\left(\frac{eU_1}{\hbar\omega_1}\right)exp\left[-i(n-e)\omega_1\right]J\left(U_0+\frac{n\hbar\omega_1}{e}\right). \tag{4.48}$$

Expression (4.44) can be rewritten as

$$I(U,t)=\alpha_0+\sum_{e=0}^{\infty}(2\alpha_e cose\omega_1 t+2b_e sin\omega_1 t),$$

where

$$\alpha_e(U)=\sum_n J_n\left(\frac{eU_1}{\hbar\omega_1}\right)\cdot\left[J_{n+1}\left(\frac{eU_1}{\hbar\omega_1}\right)I_{n-1}\left(\frac{eU_1}{\hbar\omega_1}\right)\right]\cdot\frac{\pi\Delta_1\Delta_2}{eR}\cdot\frac{1}{\left(U+\frac{n\hbar\omega_1}{e}\right)};$$

$$b_e(U)=\sum_n J_n\left(\frac{eU_1}{\hbar\omega_1}\right)\cdot\left[J_{n+1}\left(\frac{eU_1}{\hbar\omega_1}\right)-J_{n-1}\left(\frac{eU_1}{\hbar\omega_1}\right)\right]\cdot\frac{2\Delta_1\Delta_2}{eR}\cdot\frac{1}{\left(U_0+\frac{n\hbar\omega_1}{e}\right)}ln\frac{e\left(U_0+\frac{n\hbar\omega_1}{e}\right)}{\sqrt{\Delta_1\Delta_2}}\cdot$$

Then the current amplitude at the frequency ω_1 can be calculated by the expression

$$I_0=\sqrt{\alpha_e^2-b_e^2}\ .$$

Consider now the case where two high-frequency signals of different frequency are fed to the Josephson junction. The Josephson junction, in this case, acts as a frequency mixer whose characteristics are significantly different from those of semiconductor mixers. In the presence of two high frequency signals of different frequencies ω_1 i ω_2 and the voltage at the contact can be written in the form

$$U=U_0+U_1cos(\omega_1 t+\theta_1)+U_2cos(\omega_2+\theta_2),\qquad(4.49)$$

where θ_1,θ_2 – initial phases.

In the general case, the expression for the phase difference of the wave functions can be written as follows

$$\Phi(t)=\Phi_0+\frac{2e}{\hbar}\int U(t)dt\,.\qquad(4.50)$$

Substituting (4.49) into (4.50), we obtain an expression for the phase difference of the wave functions for the case when two microwave signals of different frequency are fed to the transition

$$\Phi(t)=\phi_0+\frac{2eUt}{\hbar}+\frac{2eU_1}{\hbar\omega_1}sin\omega_1 t+\frac{2eU_2}{\hbar\omega_2}sin\omega_2 t\,.\qquad(4.51)$$

Then the expression for the current can be calculated by substituting (4.51) into the expression for the Josephson current

$$I(U,t) = I_0\left[sin\left(\Phi_0 + \frac{2eU_0 t}{\hbar} + \frac{2eU_1}{\hbar\omega_1} sin\omega_1 + \frac{2eU_2}{\hbar\omega_2} sin\omega_2 \right)\right].$$

Taking into account that $U_1 << U_0$ i $U_2 << U_0$, we will calculate the amplitude of the output current for the total $(\omega_1 + \omega_2)$ and the difference $(\omega_1 - \omega_2)$ components of the spectrum of the output signal. In this case, let us assume that for small Δx $sin(x + \Delta x) \approx \sin x + \Delta x \cos x$.

For our case $x = \Phi_0 \frac{2eU_0 t}{\hbar}$,

$$\Delta x_1 = \frac{2eU_1}{\hbar\omega_1} sin\omega_1 t, \quad \Delta x_2 = \frac{2eU_2}{\hbar\omega_2} sin\omega_2 t .$$

Having made simple transformations, taking into account the assumptions made, we obtain an expression for the calculation of the Josephson current

$$I(U,t) = I_0\left[\begin{array}{l} sin\left(\Phi_0 + \frac{2eU_0 t}{\hbar} \right) + \frac{2eU_1 t}{\hbar\omega_1} sin\omega_1 t \cdot cos\left(\Phi_0 + \frac{2eU_0 t}{\hbar} \right) + \\ + \frac{2eU_2}{\hbar\omega_2} cos\left(\Phi_0 + \frac{2eU_0 t}{\hbar} \right) sin\omega_2 t + \\ + \frac{4e^2 U_1 U_2}{\hbar_2 \omega_1 \omega_2} \cdot sin\left(\Phi_0 + \frac{2eU_1 U_2}{\hbar} \right) sin\omega_1 t \cdot sin\omega_2 t \end{array}\right]. \quad (4.52)$$

From the last expression we can calculate the dependence of the output current of the difference and total frequencies on the constant voltage at the junction and the amplitudes of the high-frequency signals

$$I'(U,t) = I_0 \frac{2e^2 U_1 U_2}{\hbar^2 \omega_1 \omega_2} \left[cos(\omega_1 - \omega_2)t - cos(\omega_1 + \omega_2)t \right]. \quad (4.53)$$

An analysis of this expression shows that the current amplitude at the intermediate frequency is proportional to the voltage amplitudes at each of the mixer inputs, and as the frequency increases, the current amplitude decreases.

If we consider the relation for the Josephson current through the transition and substitute (4.49) into the expression for the phase difference of the wave functions (4.50), then the Josephson current can be expressed through Bessel functions of the nth order [74]. With this in mind, the current dependence on the applied voltage can be written as follows

$$I(U,t) = I_k \sum_{k=\infty}^{\infty} \sum_{e=\infty}^{\infty} j_k\left(\frac{2eU_1}{k\omega_1}\right) j_e\left(\frac{2eU_2}{k\omega_2}\right) \times \sin\left[\omega_0 t + \varphi_0 + k(\omega_1 t + \theta_1) + e(\omega_2 t + \theta_2)\right], \quad (4.54)$$

where $\omega_0 = \frac{2eU_0}{\hbar}$ – takes into account the influence of the constant bias voltage.

It should be noted that expression (4.54) takes into account the dependence of the Josephson junction current only on the constant and alternating voltage and does not take into account the dependence of the elements of the equivalent junction scheme. The expression for the Bessel function of any integer order, in our case, can be written in the form [81]

$$j_k\left(\frac{zeU}{\hbar\omega}\right) = \sum_{n=0}^{\infty}(-1)^n \frac{\left(\frac{2eU}{\hbar\omega}\right)^{n+k}}{z^{zn+1} - n!(n+k)!}.$$

As can be seen from this expression, the Bessel function also does not take into account the influence of the parameters of elements of the equivalent Josephson transition scheme on the magnitude of the current. This dependence makes it possible to expression (4.13) given in partition 4.1.

The block diagram of the frequency mixer based on the Josephson junction is shown in Fig. 4.24.

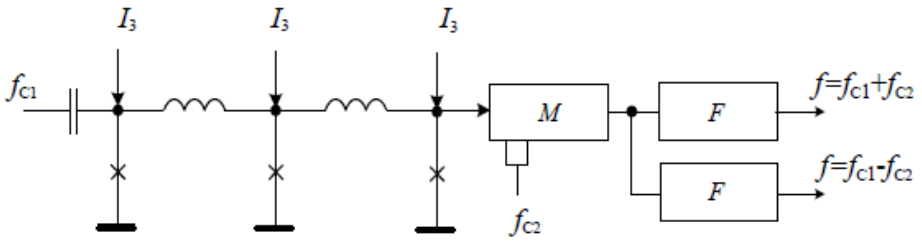

Figure 4.24 – Flowchart of logic frequency mixer

Let's now calculate the mixer parameters based on quantum theory. This involves the use of high-temperature superconductors of the type $YBa_2Cn_3O_{7-x}$. Consider a system consisting of two high-temperature superconductors, separated by a dielectric, which is fed by a constant bias voltage and operates two periodic electric fields of different frequency. In doing so, we will use the tunnel Hamiltonian method to analyze such a system [74].

The wave function of quasiparticles with energy E, in the absence of an alternating electric field, is described by equation (4.42).

If two periodic signals are applied to the NDH electrodes, the transition voltage will be determined by the expression (4.49).

In this case, the Hamiltonian of the quasiparticle system can be written as follows

$$H = H_0 + eU_1 cos\omega_1 t + eU_2 cos\omega_2 t\,.$$

In view of the above, we will search for the wave function of the excited quasiparticle system in the form

$$\psi = f(x,y,z)exp\left(-\frac{iEt}{\hbar}\right)\left[\sum_n A_n exp(-in\omega_1 t)\right]\times\left[\sum_m B_m exp(-im\omega_2 t)\right],$$

where A_n i B_m – unknown functions.

Substituting the wave function into the Schrödinger equation, we obtain

$$i\hbar\frac{d}{dt}\left\{f(x.e,z)exp-\frac{iEt}{\hbar}\left[\sum_n A_n exp(-in\omega_1 t)\right]\times\left[\sum_n B_m exp(-im\omega_2 t)\right]\right\}=$$

$$=\left(H_0 + eU_1 cos\omega_1 t + eU_2 cos\omega_2 t\right)\times f(x.y,z)exp\left(-\frac{iEt}{\hbar}\right)\left[\sum_n A_n exp(-in\omega_1 t\right]\times$$

$$\times\left[\sum_m B_m \exp(-im\omega_2 t)\right].$$

After calculating the derivative and simple transformations, we obtain an equation to determine unknown functions A_n and B_m

$$2nA_n = \frac{eU_1}{\hbar\omega_1}\left(A_{n+1} + A_{n-1}\right),$$

$$2mB_m = \frac{eU_2}{\hbar\omega_2}\left(B_{m+1} + B_{m-1}\right).$$

Let us write the solution of these equations in the form of Bessel functions of order i

$$A_n = J_n\left(\frac{eU_1}{\hbar\omega_1}\right),\quad B_m = J_m\left(\frac{eU_2}{\hbar\omega_2}\right).$$

Given (4.13), we will represent these expressions in the form

$$A_n = \frac{I_1}{I_0}\sum_{n=0}^{\infty}(-1)^{n-1}\left(\frac{tG}{C}\right)^{n-1}\left(\frac{eU_1}{\hbar\omega_1}\right)^{n-1}\Bigg/ n!\prod_{n=2}^{n-1}\left[\frac{tG}{C}+(n-1)\right],$$

$$B_m = \frac{I_1}{I_0}\sum_{m=0}^{\infty}(-1)^{m-1}\left(\frac{tG}{C}\right)^{m-1}\left(\frac{eU_2}{\hbar\omega_2}\right)^{m-1}\Bigg/ m!\prod_{m=2}^{m-1}\left[\frac{tG}{C}+(m-1)\right].$$

With this in mind, the solution of the Schrödinger equation is the wave function of the form

$$\psi = f(x)exp\left(-\frac{iEt}{\hbar}\right)\left\{\sum_n\sum_m J_n\left(\frac{eU_{\omega_1}}{\hbar\omega_1}\right)J_m\left(\frac{eU_2\omega_2}{\hbar\omega_2}\right)\times exp\left[-i\left(n\omega_1+m\omega_2\right)t\right]\right\}.$$

Analysis of the latter expression shows that the energy levels of quasiparticles are split into levels that are described by wave functions ψ_{nm} with energies $E+n\hbar\omega_1+m\hbar\omega_2$ and the probabilities of completing these levels are proportional $J_n\left(\frac{eU_{\omega_1}}{\hbar\omega_1}\right)J_m\left(\frac{eU\omega_2}{\hbar\omega_2}\right)$.

When exposed to a high-frequency electric field, quasiparticles absorb radiation quanta and increase their energy by $\hbar\omega$, which is equivalent to applying to a voltage junction $\frac{\hbar\omega}{e}$. n this case, under the action of constant voltage and absorption of the quantum of radiation, the tunneling current is determined by the function $J\left(U_0+\frac{\hbar\omega}{e}\right)$. When exposed to two electric fields of different frequencies, the quasiparticle will absorb several quanta of energy $\hbar\omega_1$ and $\hbar\omega_2$, the tunneling current will be determined by the expression

$$J_{nm} = J\left(U+\frac{n\hbar\omega_1}{e}+\frac{m\hbar\omega_2}{e}\right). \qquad (4.55)$$

To calculate the total current flowing through the junction, it is necessary to consider the probability of quasiparticle tunneling. It is known that the probability of a quasiparticle transition from a state ψ_{nm} into the state ψ_{ek} is determined by the matrix element $\frac{\psi_{nm}}{\psi_{ek}}$, which according to [78] can be written as follows

$$\left(\psi_{nm}\right) = f(x)exp\left(-\frac{iEt}{\hbar}\right)\times\left\{J_n\left(\frac{eU_{\omega_1}}{\hbar\omega_1}\right)J_m\left(\frac{eU_{\omega_2}}{\hbar\omega_2}\right)exp\left[-i(n\omega_1+m\omega_2\right]t\right\},$$

$$\left(\psi_{pk}\right)= q(x)exp\left(\frac{iEt}{\hbar}\right)\left\{ j_e\left(\frac{eU_{\omega 1}}{\hbar\omega_1}\right)j_k\left(\frac{eU_{\omega 2}}{\hbar\omega_2}\right)\times exp\left[i\left(p\omega_1 + k\omega_2\right)t\right]\right\}.$$

To determine the dependence of full current on voltage and time, it is necessary to sum the matrix elements by different values of n, m, p, k and multiply by the function of current response (4.51). With this in mind, the total current can be calculated by expression

$$I(U,t)= I_m\sum_n\sum_m\sum_p\sum_k j_n\left(\frac{eU_{\omega 1}}{\hbar\omega_1}\right)j_p\left(\frac{eU_{\omega 1}}{\hbar\omega_1}\right)j_m\left(\frac{eU_{\omega 2}}{\hbar\omega_2}\right)\times$$
$$\times\, j_k\left(\frac{eU_{\omega 2}}{\hbar\omega_2}\right)exp\left\{\left[-i\left(m-e\right)\omega_1 + \left(m - k\omega_2\right)\right]t\right\}j\left(U + \frac{n\hbar\omega_1}{e} + \frac{n\hbar\omega_2}{e}\right) \quad (4.56)$$

The last expression makes it possible to calculate the dependence of the current on the applied high-frequency voltages and the time of their action. Taking into account expression (4.13) makes it possible to obtain the dependence of currents on the parameters of the equivalent Josephson junction scheme.

Using Euler's formula, expression (4.46) can be rewritten as

$$I(U,t)= A_0 + \sum_{p=0}^{\infty}\sum_{k=0}^{\infty}\left[2A_{pk}cos(p\omega_1 + k\omega_2)t + 2B_{pk}sin(p\omega_1 + k\omega_2)t\right]. \quad (4.57)$$

Here A_0 is determined from expression (4.56) when $p=0$ and $k=0$.

As is evident from expression (4.57), when acting on the Josephson transition of two high-frequency signals, the output can receive signals at all frequencies that can be written by the expression $p\omega_1 + k\omega_2$. We will be interested in the case when $p=1$, $k=-1$.

For this case, provided that $eU >> \Delta$, current amplitude at intermediate frequency $f_{\text{пч}} = f_1 - f_2$ can be defined by expression

$$I_{\text{пч}} = \sqrt{A_1^2 + B_1^2}\,,$$

$$A_1(U)=\sum_{nm}J_n(a_1)J_m(a_2)\left[\begin{array}{l}J_{n+1}(a_1)J_{m+1}(a_2)+J_{n-1}(a_1)J_{m-1}(a_2)\times\\ \times\dfrac{\pi\Delta_1\Delta_2}{eR}\left(\dfrac{1}{U+\dfrac{n\hbar\omega_1}{e}+\dfrac{n\hbar\omega_2}{e}}\right)\end{array}\right], \quad (4.58)$$

$$B_1(U)=\sum_{nm}J_n(a_1)J_m(a_2)\left[J_{n+1}(a_1)+J_{m+1}(a_2)-J_{n-1}(a_1)J_{m-1}(a_2)\right]\times$$

$$\times\frac{2\Delta_1\Delta_2}{eR}\left(\frac{1}{U+\dfrac{n\hbar\omega_1}{e}+\dfrac{n\hbar\omega_2}{e}}\right)\cdot ln\frac{e\left(U_0+\dfrac{n\hbar\omega_1}{e}+\dfrac{n\hbar\omega_2}{e}\right)}{\sqrt{\Delta_1\Delta_2}},$$

where $a_1=\dfrac{eU_1}{\hbar\omega_1}$, $a_2=\dfrac{eU_1}{\hbar\omega_2}$.

The last expression makes it possible to calculate the dependence of the current amplitude on the difference frequency from the frequency and power of the input information signals, which, as a rule, correspond to logical «0» and logical «1». Since F-elements (frequency mixers) are often used to transmit to high frequencies, it is advisable to calculate current amplitudes *I* at the total frequency when constructing digital radio devices with frequency-pulse encoding of information.

In this case $p=1$ i $k=1$, and for the case where the CILF is ambiguously dependent, then the addition takes place, given that the indices k are equal to 2.

For the case where $p=1$ and $k=1$ expressions for $A_2(U)$ and $B_2(U)$ take the form

$$A_2(U)=\sum_{n,m}J_n\left(\frac{eU_1}{\hbar\omega_1}\right)J_m\left(\frac{eU_2}{\hbar\omega_2}\right)\left[J_{n+1}\left(\frac{eU_1}{\hbar\omega_1}\right)J_{m-1}\left(\frac{eU_2}{\hbar\omega_2}\right)+J_{n-1}\left(\frac{eU_1}{\hbar\omega_2}\right)J_{m+1}\left(\frac{eU_2}{\hbar\omega_2}\right)\right]\times$$

$$\times\frac{\pi\Delta_1\Delta_2}{eR}\left(\frac{1}{U+\dfrac{n\hbar\omega_1}{e}+\dfrac{m\hbar\omega_2}{e}}\right);$$

(4.59)

$$B_2(U)=\sum_{n,m} J_n\left(\frac{eU_1}{\hbar\omega_1}\right)J_m\left(\frac{eU_1}{\hbar\omega_2}\right)\begin{bmatrix} J_{n+1}\left(\frac{eU_1}{\hbar\omega_1}\right)\cdot J_{m-1}\left(\frac{eU_2}{\hbar\omega_2}\right)- \\ -J_{n-1}\left(\frac{eU_1}{\hbar\omega_2}\right)J_{m+1}\left(\frac{eU_2}{\hbar\omega_2}\right)\end{bmatrix}\cdot\frac{2\Delta_1\Delta_2}{eR}\cdot\left(\frac{1}{U_0+\frac{n\hbar\omega_1}{e}+\frac{m\hbar\omega_2}{e}}\right)\times$$

$$\times ln\frac{e\left(U_0+\frac{n\hbar\omega_1}{e}+\frac{m\hbar\omega_2}{e}\right)}{\sqrt{\Delta_1\Delta_2}}\,.$$

Similarly, you can write expressions for the case where $k=2$.

For calculations according to (4.58) the following initial data were used: $U_0=1\div10mV$, $U_1=U_2=0{,}1\text{mV}$, $\Delta_1=\Delta_2=3{,}7\text{meV}$, $R=20\Omega$, ω_1 and ω_2, which were determined according to the Josephson ratio according to the values U_0 and U_1,U_2. The results of the calculations are shown in Fig. 4.25 and 4.26.

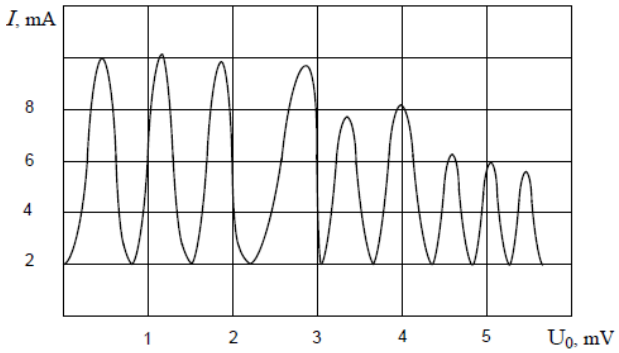

Figure 4.25 – The dependence of the intermediate frequency current on the DC voltage $U_{C1}=U_{C2}=0{,}4$ мВ

The analysis of the results shown in Fig. 4.25 shows that the current-voltage characteristic of the PD is stepped, and therefore the dependence $J_{nm}=f(U_0)$ is characterized by a series of peaks that decrease with voltage.

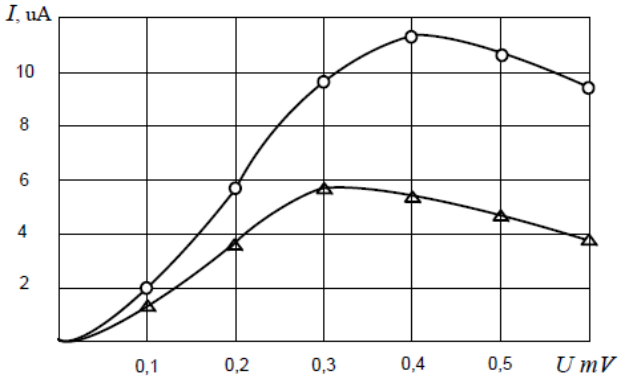

Figure 4.26 – The dependence of the intermediate frequency current on the RF signal voltage

From Fig. 4.26 it can be concluded that the maximum value of the intermediate frequency current occurs at the same voltages of microwave signals at both inputs of the mixer. At the same time, as the signal voltage increases, the current $I_{\text{ПЧ}}$ increases.

4.6 Superconducting digital radio engineering devices for processing low-intensity signals

The main factor that hampering the increase in the clock frequency of modern semiconductor processors is the amount of energy consumed by one logical operation, which is 10^{-13} J / bits for semiconductor devices. As has been shown in [73], the minimum threshold value of the switching energy, for the case of the technology application of digital devices based on superconductors, is 10^{-18} J / bits, that is five orders of magnitude smaller. This makes it possible to increase the clock frequency to 100 GHz and above.

The minimum value of the duration of single-quantum voltage pulses can be about 0.1 ps, when are using high-temperature superconductors that store superconductivity at liquid nitrogen temperature. This makes it possible to increase the clock frequency of digital devices up to 1 THz [73, 109].

In this regard, it is expedient to consider the possibility of constructing digital devices based on superconductors and Josephson junctions, which work is based on the application of single magnetic flux quanta.

In the works [72, 79], the structural schemes of logic devices using resistive-shuffled Josephson junctions are shown, which are represented in Fig. 4.27, 4.28, 4.29.

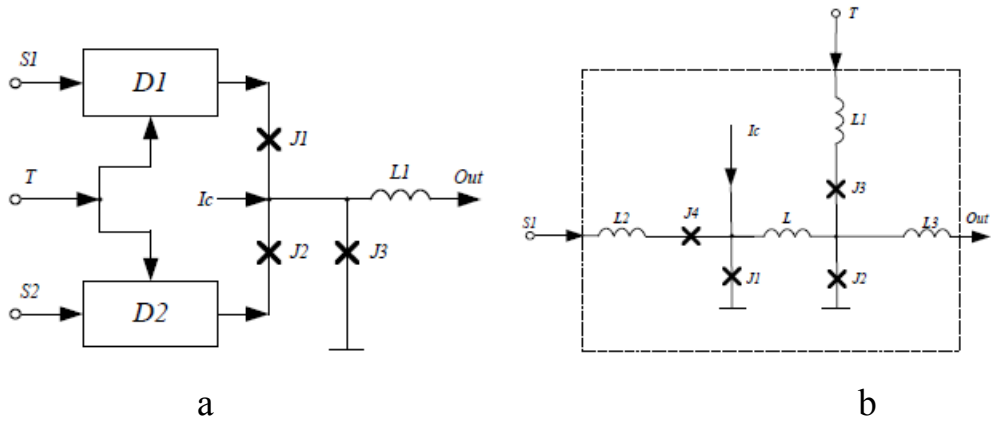

a b

Figure 4.27 – Functional scheme of «AND» logical element (a), element D(b)

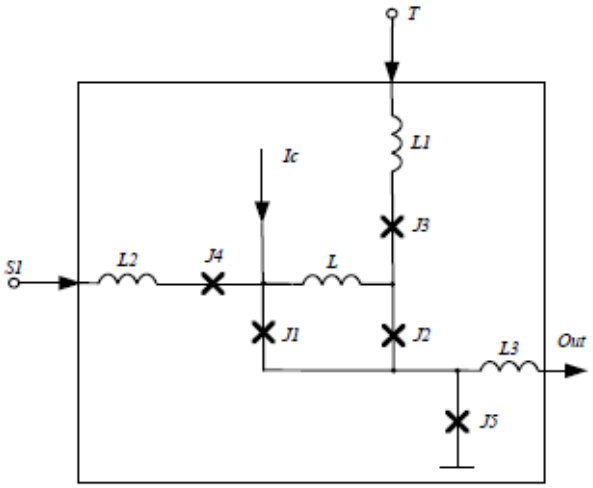

Figure 4.28 – Functional scheme of «NOT» logical element

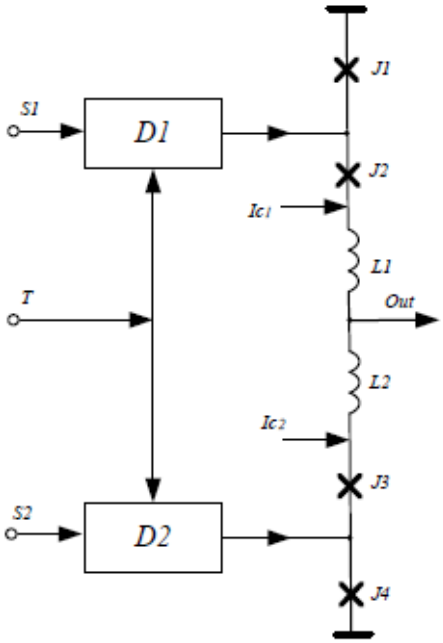

Figure 4.29 – Functional scheme of «OR» logical element

As can be seen from the figures, such schemes are quite complicated. So, for the implementation of an element that performs the function of disjunction, it is necessary 12 Josephson junctions, conjunction – 11 Josephson junctions, inverter – 5 junctions. And this leads to a decrease in the degree of integration and increasing the power that is consumed. Therefore, it is advisable to consider the possibility of simplifying the functional schemes of logic elements which are components of digital radio engineering devices[110].

In [71], the current-voltage characteristics of Josephson junctions are investigated. This work shows that, at present, developing new technology of digital devices based on superconductivity and Josephson junctions, called fast single-quantum logic (FSQL). In such devices, the carrier of information is the single quanta of the magnetic flux Φ_0 and, corresponding to them, the single-quantum voltage pulses generated by the Josephson elements when magnetic fields quanta pass through them.

However, in existing works about FSQL elements, equivalent circuits of logic devices not has been developed and the analysis of their capacity using modern technology and high-temperature superconductivity not has been done.

In [79], functional circuits of logic elements with current injection power are given, but they are quite complex due to the fact that they use a large number of inductive elements.

In this section functional circuits of the basic logic elements with the use of magnetic control are offered.

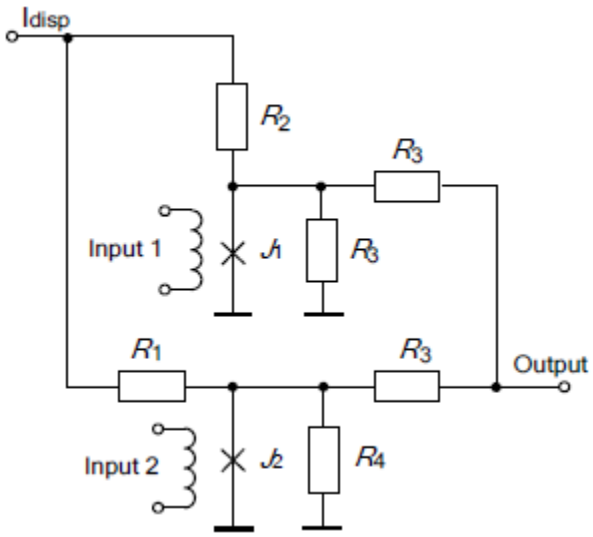

Figure 4.30 – Functional scheme of «OR» logical element

The functional diagram of the logical element «OR» is given in fig. 4.30. The principle of its work as follows. In the absence of signals at the inputs, each of the junctions is in a state of superconductivity, and through them flows a current whose value is determined by the bias current and does not exceed the critical current. In this case, the output voltage is absent, which corresponds to the value of the logical «0». When the signal has been sent to the first input J_1, the first junction passes to the state under voltage, and signal corresponding to the logical «1» has been formed at the output. A similar situation occurs when the input signal arrives at the second input. In this case, the junction J_2 passes to the state under voltage and signal corresponding to the logical «1» has been formed at the output. If each of the inputs receives signals, then both junctions pass into a state under voltage and a logical «1» has been formed at the output. Thus, the given scheme performs the function «OR». Functional circuits of the logical elements «AND», «NOT» are shown in Fig. 4.31, 4.32. The principles of their work are similar to the above.

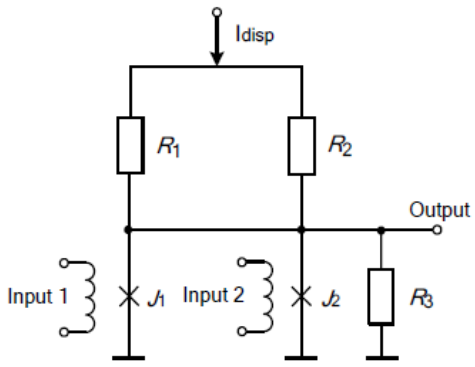

Figure 4.31 – Functional scheme of «AND» logical element

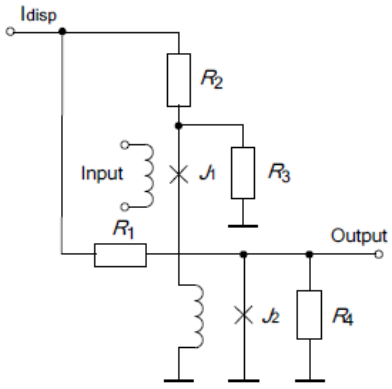

Figure 4.32 – Functional scheme of «NOT» logical element

To calculate the parameters of the logic elements, it is necessary to develop their equivalent schemes, taking into account the equivalent scheme of the Josephson junction. This schemes are subject to magnetic flux due to the passage of electric current through the inductive element. The equivalent scheme of the logical element «OR» is shown in fig.4.33.

In the equivalent scheme, current sources take into account the influence of the magnetic flux on the currents value, which are determined by expression [4.60]

$$I_1 = I_{01}\sin\left(\frac{\pi\Phi_1}{\Phi_0} + Q_{01}\right), \qquad I_2 = I_{02}\sin\left(\frac{\pi\Phi_2}{\Phi_0} + Q_{02}\right). \tag{4.60}$$

Dependence of supercurrent I_{01}, I_{02} on the magnitude of the magnetic flux can be calculated by expression

$$I_0' = I_0 \frac{sin\pi\Phi/\Phi_0}{\pi\Phi/\Phi_0}, \tag{4.61}$$

where $\Phi_0 = 2{,}07 \cdot 10^{-15}$ Wb; R_2, R_5, R_7 – resistances of Josephson junctions tunneling, the magnitudes of which can be calculated by expression $R = K\frac{2\pi^2 U^2}{e\mu}$,

where U – is the voltage at the junction; φ – chemical potential; K – coefficient, which account the dimension.

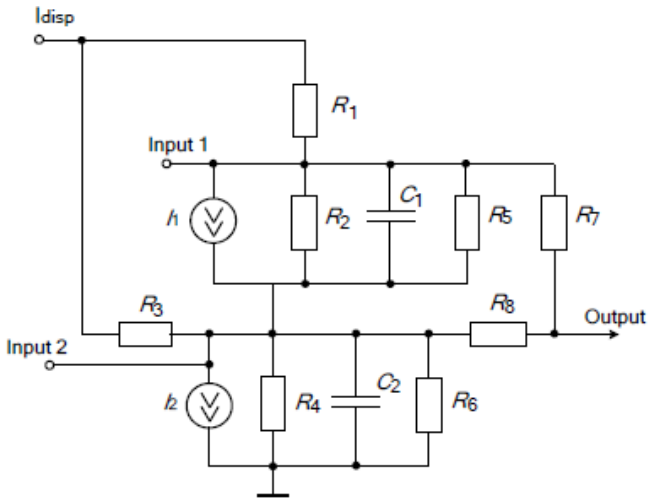

Figure 4.33 – Equivalent circuit of «OR» logical element

Similarly, it is possible to construct equivalent circuits for the logical elements given in Fig. 4.31, 4.32.

Using the proposed equivalent scheme, the calculation of the magnetic flux influence on the magnitude of output current has been represented, with its effect on various elements of the scheme.

Because quantum of magnetic field act the Josephson junction, which leads to the Josephson current decreases, when the logic element is switched, then its speed is determined by the characteristic time of the extinction of the Josephson current, whose magnitude is determined by expression [74]

$$\tau = R_T C,$$

where C – is the capacity of junction, R_T – is the resistance for current quasiparticle per unit area of the junction surface, which depends on the temperature.

Applying the initial data, given in [77], the time of fading Josephson current has been calculated. It is 0,0116 ps. Values of shunt resistors are taken at the same order as the resistance of the junctions. Values of resistors R_7 and R_8 are much less shunt resistances and their impact were not taken into account. It should be noted that the extinction time of current depends on the shunt resistance R_5, R_6 and the resistance R_T, whose magnitude depends on the temperature. It increases to infinity when $T \to 0$. At the temperature corresponding to the state of superconductivity, the value of this resistance may be units kOhm. The calculations carried out

confirm that the speed of logic elements based on Josephson junctions is significantly increasing.

To calculate the energy required to switch the logical element from the state of the logical «1» to the logical «0», we will use the dependence of the supercurrent on the magnetic flux (4.61). It is known that under the influence of a magnetic flux there is a quantization of the super current. At the action of a magnetic flux Φ_0 the magnitude of the current reaches practically zero value, so it is necessary to calculate the amount of energy required to obtain a quantum of magnetic flux. Assuming that the bias current is equal to 1mA, then the energy lost for switching is $2.07 \cdot 10^{-18}$ J.

Simple calculations has shown that the value of the inductance, which is necessary to obtain a flow with magnitude Φ_0, is 2.07 pGn. With an increase of the displacement current, the magnitude of the inductance required to obtain a quantum of the magnetic flux Φ_0 decreases.

4.7 Development of a device for converting a pulse-potential code into frequency-pulse code using Josephson junctions

The use of frequency-pulse encoding of information for the construction of digital radio devices provides increased noises immunity and speed of information conversion through the junction to a range of ultrahigh frequencies and the coding of logical states by different frequency values.

However, as shown in [85], the implementation of such devices requires sources of auxiliary signals, the frequency of which must much exceed several times the frequency of information signals, which complicates their implementation in millimeter and sub-millimeter wavelength bands using modern semiconductor technologies. In addition, since modern computer technology is focused primarily on the use of pulse-potential representation of information, the use of frequency-pulse coding in some cases requires the development of devices that provide the transformation of the pulse-potential code into frequency-pulse.

Josephson elements open the great prospects for the development of digital radio-frequency devices with frequency-pulse representation of information and the use of polysemy, because they are characterized by high speed, high sensitivity and extremely low switching power of 10^{-18} J / bits, which is five orders of magnitude lower than the marginal switching energy for elements based on semiconductors, which is 10^{-13} J / bits [73]. The characteristic frequency of Josephson elements based on low-

temperature superconductors is in the range of hundreds gigahertz, and for high-temperature superconductors can reach units and even dozens of terahertz.

The block diagram of a device that transforms a binary pulse-potential code into a frequency-pulse binary code based on two Josephson junctions is shown in Fig. 4.34 [111].

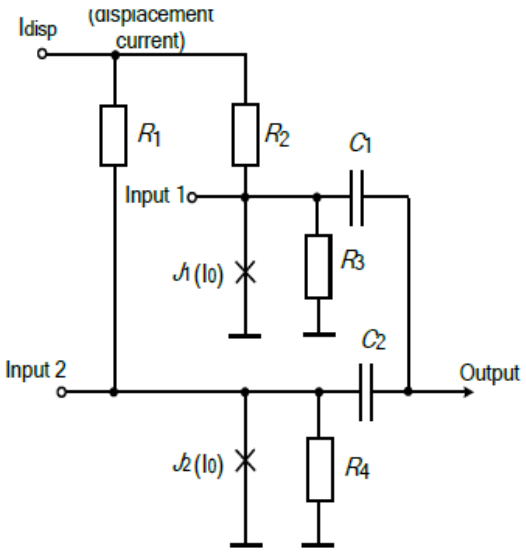

Figure 4.34 – Functional scheme of the transformation device

In the absence of input signals, both junctions are in a state of superconductivity and the currents flowing through the Josephson junctions below the critical ones. When the voltage pulse is applied, which corresponds to the logic «1»' at input 1, there is a generation of ultrahigh-frequency oscillations, the frequency of which is determined by expression

$$\omega = \frac{2 \cdot q}{\hbar} \cdot U_0.$$

If a pulse at the second input are absented, the signal at the output corresponds to the logic «1» and represents a radio pulse with a certain frequency of filling ω_1. When the voltage pulse is applied to the second input and the signal is absent at the first input, the second junction enters the oscillation generation mode and at the output there is a radio pulse, the frequency of which corresponds to the logic «1». When the voltage pulses are applied to each of the inputs, the junctions enter the mode of non-stationary Josephson effect and at the output there is a radio pulse, the filling frequency of which corresponds to the logical «1».

If signals are absented at the inputs, the signal at the output is also absent, that corresponding to the logical «0». That is, in this case, the binary impulse-potential code into a binary frequency-pulse code transformation takes place, provided that the logical «1» are corresponded the radio pulse with a certain filling frequency, and the logical «0» is the absence of a signal. In this case, the presented scheme performs the function «OR» and transforms the pulse-potential signal into a radio-impulse signal.

In the case that the logical «0» and «1» are corresponded to radio pulses of different frequencies, impulses with different voltage values should be applied to Josephson junctions.

Let's consider how the current of Josephson junctions changes with changing the voltage on them. In general, the current's value is determined from the Josephson equation

$$I = I_0 \cdot \sin \Phi(t), \tag{4.62}$$

where I_0 – the current of superconductivity, or critical current, which value, in general, is determined from the solution of the Schredinger equation. As is known, the phase difference of wave functions can be written as

$$\Phi(t) = \Phi_0 + \frac{2e}{\hbar}\int U(t)dt\,. \tag{4.63}$$

Let the voltage, which is applied to the junction, consist of a constant component and a high frequency component

$$U(t) = U_0 + v\cos\omega t\,.$$

Then the expression (4.63) can be rewritten as follows

$$\Phi(t) = \Phi_0 + \frac{2eU_0 t}{\hbar} + \frac{2ev}{\hbar\omega}\sin\omega t\,. \tag{4.64}$$

Substituting (4.64) in (4.62), we received an expression for calculating the current flowing through Josephson junction

$$I = I_0 \sin\left(\Phi_0 + \frac{2eU_0 t}{\hbar}\right) + \frac{2eU}{\hbar\omega}\sin\omega t\cos\left(\Phi_0 + \frac{2eU_0}{\hbar}t\right). \tag{4.65}$$

It was taken into account that the amplitude of the voltage variable U is much smaller than the constant, as well as the fact that sinus of angle with small values approximately equal to the angle value.

In the general case, a tunnel element in a real Josephson contact is shunted by a capacity that results in a hysteresis current-voltage characteristic. This phenomenon is undesirable and it can be removed using resistance which shunts the contact [71]. In our case, this role is performed by resistors R_5, R_6. Given this, the equivalent circuit of the device for converting binary pulse-potential code into frequency-pulse code is shown in Fig. 4.16. In this scheme, C_1, C_2 are the electrostatic capacities of Josephson tunnel junctions, R_3, R_4 are nonlinear resistance of Josephson junctions; R_5, R_6 are shunt resistance.

To calculate the voltage at the output when the pulse-potential signals action at the input, we determine the voltage separately for each of the circuit sections in Fig. 4.35. Using an equivalent scheme, we determine the currents flowing through the Josephson junctions.

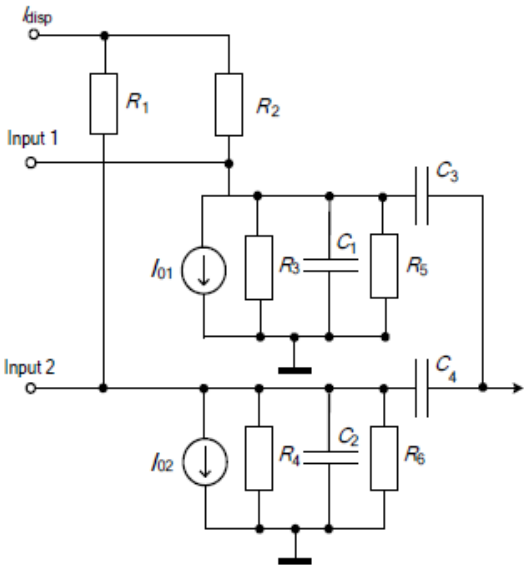

Figure 4.35 – Equivalent circuit of a device for converting a pulse-potential code into a frequency-pulse code

Given that $R_3 << R_5$, and $R_4 << R_6$, the expression for the current can be written as follows

$$I = I_0 \cdot \sin \Phi + \frac{U}{R_3} + C \cdot \frac{dU}{dt}. \qquad (4.66)$$

Since $\frac{d\Phi}{dt} = \frac{2 \cdot q}{\hbar} \cdot U$, then the expression (4.65) can be rewritten in the form

$$\frac{I}{I_0} = \sin\Phi + \frac{d\Phi}{dx} + \beta \cdot \frac{d^2\Phi}{dx^2}, \tag{4.67}$$

where $x = \frac{2 \cdot q \cdot I_0 \cdot R_3}{\hbar} \cdot t$, $\Phi = \frac{2 \cdot q \cdot U \cdot t}{\hbar}$, $\beta = \frac{x}{t} \cdot R_3 \cdot C$,

For the case when voltage is applied to the Josephson junction and $I > I_0$, the value of the resistance R_3 can be calculated from the expression [74]:

$$R = \frac{2 \cdot \pi^2 \cdot U^2}{q^2 \cdot \mu}.$$

Solve (4.67) by numerical methods, we can calculate the dependence of the output variable voltage on the constant voltage on the Josephson junction, as well as the switching time and the energy used for switching. The analytical dependence of the variable voltage on the constant voltage on the junction can be obtained by simplifying the equation (4.65). If we assume that the capacity of the junction is very small and neglected, then the expression for the current will look like

$$\frac{I}{I_0} = \sin\Phi + \frac{d\Phi}{dx}. \tag{4.68}$$

The equation (4.68) can be rewritten in the form

$$\frac{d\Phi}{I/I_0 - \sin\Phi} = dx. \tag{4.69}$$

The solution of this equation shows that the derivative $d\Phi/dt$ is a continuous and periodic function with a period [70]

$$T = \frac{\pi \cdot \hbar}{q \cdot R \cdot I_0 \cdot \left[\left(I/I_0\right)^2 - 1\right]^{1/2}}. \tag{4.70}$$

Taking into account this, the average value of voltage over a period can be calculated as an expression

$$U_{cep} = I_0 \cdot R_3 \cdot \left[\left(I/I_0\right)^2 - 1\right]^{1/2}.$$

The dependence of the oscillation period from the applied constant voltage to the Josephson junction can be calculated by substituting (4.66) into (4.70)

$$T = \frac{\pi \cdot \hbar}{q \cdot R \cdot I_0 \cdot \left[\left(\frac{I_0 \cdot \sin\left(\frac{2 \cdot q \cdot U \cdot t}{\hbar} \right) + \frac{U}{R}}{I_0} \right)^2 - 1 \right]^{1/2}}. \qquad (4.71)$$

Computer simulation of the dependence of the microwave oscillations period from the constant voltage, which applied to the Josephson junction, and from the nonlinear junction resistance in accordance to the expression (4.71), assuming the value of the critical junction current I_0 is 1 mA, was carried out and shown in Fig. 4.36. This diagram represented the dependence of the oscillation period from the constant voltage which applied to Josephson junction, at different values of the junction nonlinear resistance.

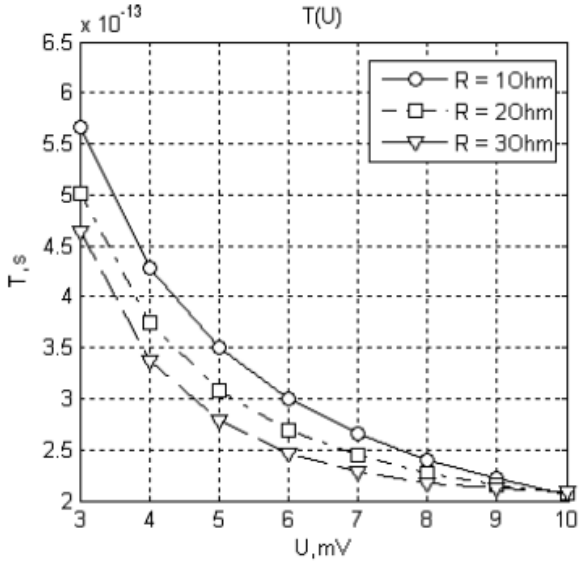

Figure 4.36 – Dependence of the oscillation period from the applied DC voltage to the Josephson junction

Analyzing this graphic dependence, we can conclude that an increase in the constant voltage value applied to the Josephson junction leads to a decrease in the period of microwave oscillations, that is, an increase in their frequency. Similarly, the dependence of the oscillation period on the nonlinear resistance of the Josephson junction at different values of the applied constant voltage is show in Fig. 4.37.

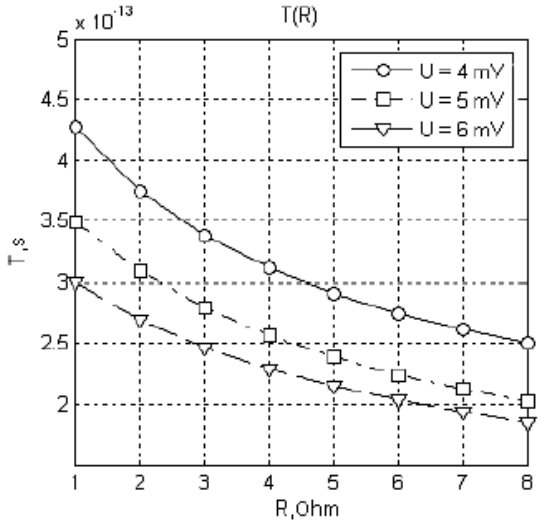

Figure 4.37 – Dependence of the oscillation period on the nonlinear resistance of the Josephson junction

From this graph, it can be seen that the nonlinear resistance of the Josephson junction is inversely proportional to the oscillation period, and therefore is directly proportional to the frequency of oscillations. These studies reflect the possibility of increasing the frequency of Josephson junctions generation to dozens of terahertz.

4.8 Generator of tactical impulses on Josephson junction

Traditional technologies with carriers of the 2…5 GHz range hardly satisfy continuously increasing needs of bandwidth extension and speed raise for wireless information transmission systems and of sensitivity increase for devices of radio-frequency signal reception and processing. This contributes to research and development of devices for wireless transmission, reception and signal processing in the terahertz range [93, 112, 113]. The most effective technology nowadays employed for solving these problems is application of macroscopic quantum effects in superconducting structures and the Josephson effect, this allows to create high-sensitivity, high-speed digital devices of radio-frequency signal transmission and processing for modern millimeter systems of the millimeter and sub millimeter wave ranges.

Such devices are characterized not only by high sensitivity caused by low operating temperatures, but also by high speed and extremely low switch energy of 10^{-18}J/bit, while for semiconductor devices its minimum value is 10^{-13}J/bit).

The clock rates are about hundreds of GHz in devices based on low-temperature superconductivity and equal 1 THz and more in case of high-temperature superconductivity (HTSC) [78].

Nowadays, many suggested options of logical elements on Josephson junctions support execution of fast computer calculations using fast single-quantum circuits. The principle of information processing using these circuits is as follows [73]:

- single-step pulses are used, which divide the entire operation time of the circuit by steps;

- appearance of a single-step pulse at the input or output of the circuit during the cycle is considered as «logical 1», its absence is considered as «logical 0»;

- the single-step pulse at the circuit output at the beginning of the previous step is a logical function of the single-step pulse that had acted at the circuit input at the previous step.

Thus, fast single-step logic is clocked, that is why the clock pulse generator is an important element of such computing circuits.

Such clock pulse generators are widely used when constructing analog-to-digital and digital-to-analog signal converters and in many other systems.

Application of high-temperature superconductors (HTSC) enables to form Josephson junctions with higher values of the characteristic frequency, which is important for creation of Josephson generators in the terahertz range. However, production of the high-quality Josephson junctions with reproduction parameters based on HTSC cause many problems that do not allow applying traditional technologies, which are used in the case of low-temperature Josephson junctions. One of the main methods for forming the Josephson junctions with sufficiently high parameter reproduction is application of the HTSC films grown on bicrystalline substrates [92, 114]. However, traditional concentrated models cannot be employed here because such bicrystalline boundary has a heterogeneous structure.

Therefore, a physical model of the clock pulse generator on the basis of Josephson junctions using high-temperature superconductivity should be built and its parameters and characteristics should be studied.

The YBa_2CuO_{7-x} compound is the most promising and widespread HTSC material. The HTSC epitaxial film grown on the bicrystalline

substrate is also bicrystalline with the same crystallographic orientation, and its bicrystalline boundary is characterized by weak Josephson bonds.

The paper [82] shows that the physical model of the JJ formed on the bicrystalline boundary of two HTSC can be represented as two inductively coupled Josephson elements, their equivalent circuit can be represented as the simple resistive model (Fig. 4,38).

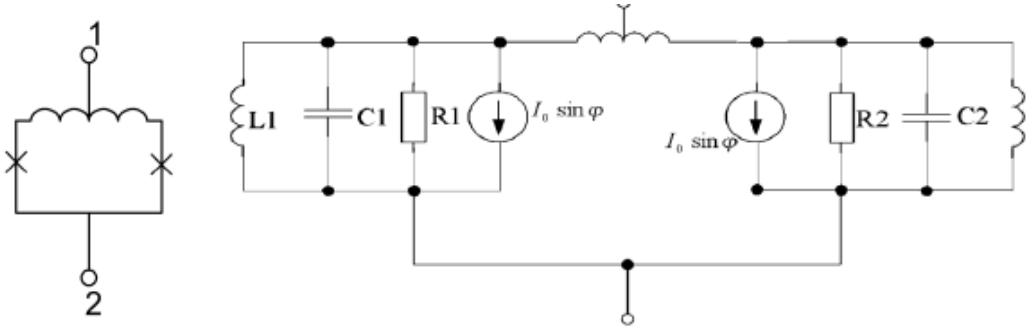

a) b)

Figure 4.38 – Physical model of the bicrystalline JJ (a) and its equivalent circuit (b)

I_0 is the critical current of the JJ; R is the dynamic tunneling resistance of quasiparticles; C is the electrostatic capacitance of the JJ; L is the inductance of the JJ; ¬ is the phase difference of wave functions.

The critical current value depends on the type of the superconductor, its value can be calculated by the expression

$$I_0 = \frac{\Delta}{2_g R_n},$$

where R_n is the junction resistance in normal non-superconducting state; 2 is the energy band gap of the superconductor.

The equivalent JJ circuit differs by taking into account the inductance, its value can be calculated by the expression [82]

$$L = \frac{h}{2qI_0 \cos\Psi} \cdot \qquad (4.72)$$

Provided that nanoscale HTSC-based junctions do not require external shunting for damping, the electric circuit of the clock pulse generator is shown in Fig. 4.39 [72].

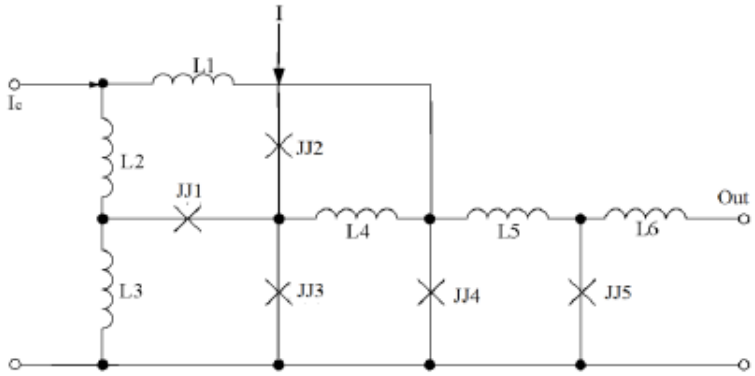

Figure 4.39 – Electric circuit of the clock pulse generator

The physical equivalent circuit of the generator, considering above mentioned, is shown in Fig. 4.39.

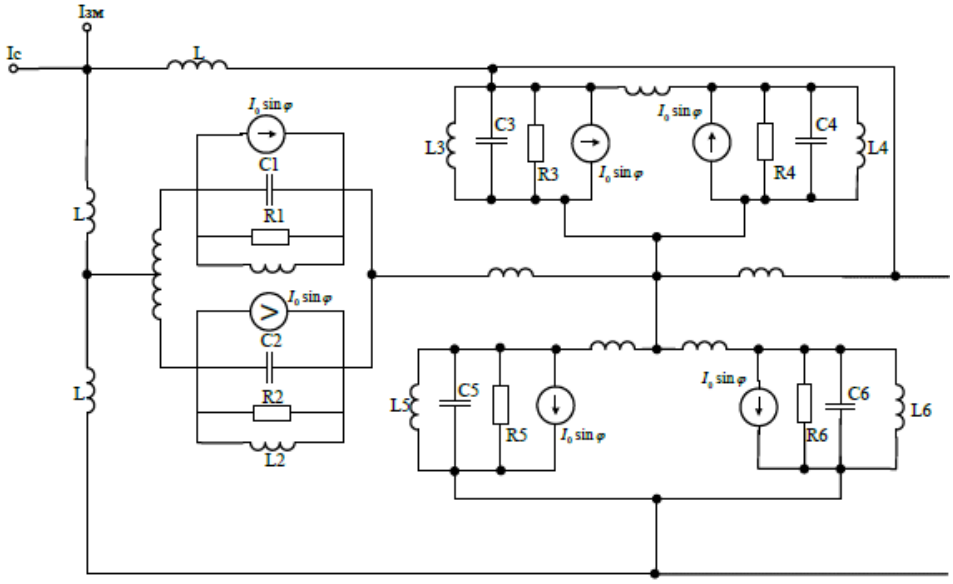

Figure 4.40 – Equivalent circuit of the clock pulse generator on the JJ

The clock pulse generator consists of the superconducting quantum interferometer (SQI) (L3, JJ1, JJ3) and the pulse generator (L4, JJ4, L5, JJ5). The SQI transmits the direct current, which is a little less than the critical current, and the synchronization current I_c, which determines frequency and phase of the clock signal sequence. When clock signals are transmitted over superconducting buses, the pulse amplitude decreases and the pulse expands over time. To preserve the pulse shape, the pulse shaper is applied, to which the bias current with a value slightly low than the critical current is supplied. Therefore, if a «blurry» clock pulse arrives at

the input of the pulse shaper, then a short one-quantum voltage pulse occurs at the output. In some cases, there is a need to extend the single-quantum voltage pulses.

To solve this problem the methods proposed in [83] may be applied. It should be mentioned that direct current superconducting quantum interference sensors (SQIS), which are the superconducting ring with two JJs (L3, JJ1, JJ3), are well known and widely used as highly sensitive transducers of a magnetic signal into voltage. However, they are characterized by a very limited linearity of the reproduced voltage.

In case of the low-frequency SQIS-based devices, high linearity and high dynamic range are achieved by implementing a feedback loop. In case of the millimeter wavelength, such external feedback cannot be implemented, therefore, we suggest for the circuit shown in Fig. 4.39 to use the bi-SQIS proposed in [83] in order to implement pulse shapers.

In order to linearize the voltage response function of the two-contact SQIS, the third JJ is connected in parallel to the main inductance, which is always in the superconducting state and acts as the nonlinear inductance. The additionally added JJ and the main inductance form a single-contact SQIS, which performs nonlinear transformation of the magnetic flux Φ_X into the phase difference of the JJ wave functions $\Delta\Psi = \Psi_1 - \Psi_2$ of the two-contact SQIS.

This nonlinear transformation can also be done as reversed to the subsequent nonlinear transformation of the phase difference $\Delta\prod$ into a voltage constant component, thus we obtain the resulting linear transformation of the input signal into voltage.

The value of voltage on the JJ can be calculated according to the expression

$$U = \frac{\hbar}{2q} \cdot \frac{d\psi(t)}{dt}, \tag{4.73}$$

where $\psi(t)$ is the phase difference of wave functions on the JJ, which can be determined using the equation for the current flowing through the JJ in case of a resistive model (Fig. 4.38b)

$$i(t) = I_0 \sin\psi(t) + c\frac{dU(t)}{dt} + GU(t) + L\int_0^t U(t)dt \ . \tag{4.74}$$

Given (4.72) and (4.73), expression (4.74) can be rewritten as follows

$$\frac{I}{I_0} = \sin\psi(t) + \frac{c\hbar}{I_0 2q}\frac{d^2\psi(t)}{dt} + \frac{G\hbar}{I_0 2q}\frac{dt(t)}{dt} + \frac{\hbar^2}{4q^2 I_0^2 \cos\psi(t)}\psi(t). \qquad (4.75)$$

To solve equation (4.75) we will use the Runge-Kutta method and approximation of the seventh-order polynomial. The polynomial series for calculating the phase difference of wave functions has such form

$$\varphi(t) = P_0 t^0 + P_1 t^1 + P_2 t^2 + P_3 t^3 + P_4 t^4 + P_5 t^5 + P_6 t^6 + P_7 t^7.$$

The following initial data were used when solving this equation: $C = 0.01 \cdot 10^{-12}$ F, G=5/7 S, $I = 2 \cdot 10^{-3}$ A, $I_0 = 1 \cdot 10^{-3}$ A, $t = 2 \cdot 10^{-12}$, the initial phase is $\varphi = 90^\circ$.

The equation solution is:

$$\varphi(t) = -0,007911 + 0,008742 \cdot t + 0,053569 \cdot t^2 + (-0,013860) \cdot t^3 +$$
$$+(-0,199074) \cdot t^4 + (-0,606032) \cdot t^5 + (-0,010983) \cdot t^6 + 2,323014 \cdot t^7.$$

Dependence of the phase difference of wave functions on parameters of the equivalent Josephson junction circuit was investigated using this representation of the differential equation solution. The study results are shown in Figs. 4.41, 4.42, 4.43.

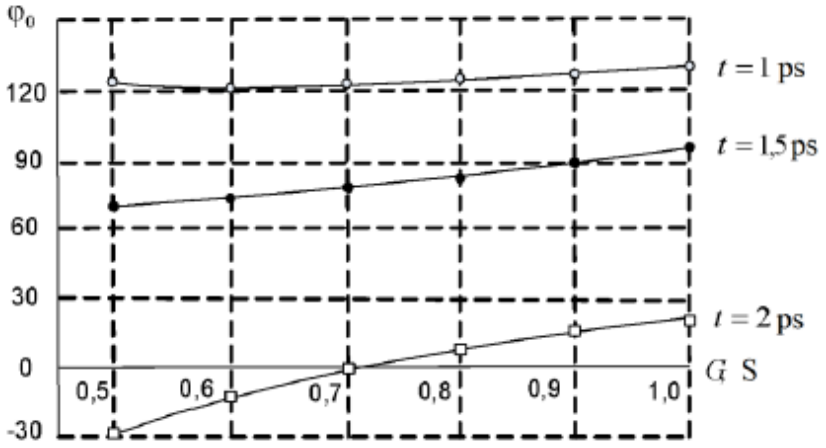

Figure 4.41 – Dependence of the junction voltage on dynamic resistance of the Josephson junction

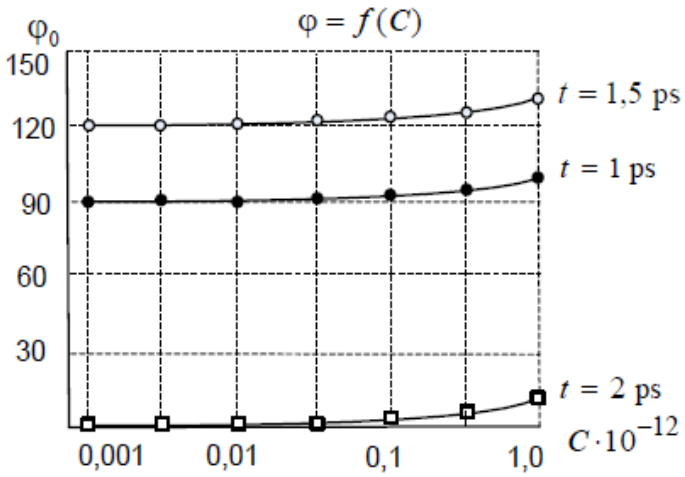

Figure 4.42 – Dependence of the phase difference of wave functions on electrostatic capacitance

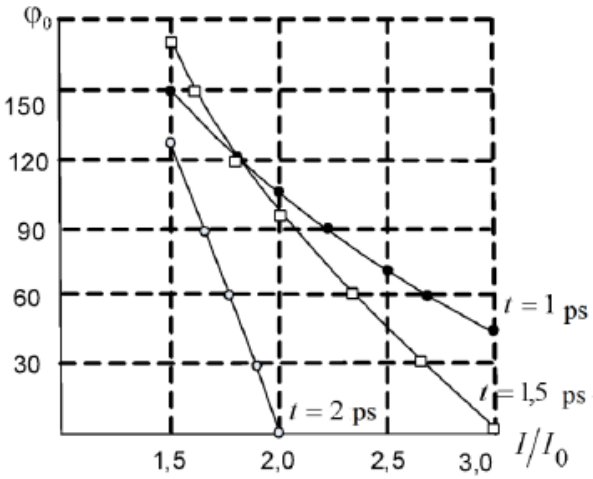

Figure 4.43 – Dependence of the phase difference of wave functions on the critical current

Analysis of the results shows that the change in the junction capacitance to 0.1 pF has almost no effect on the phase difference of wave functions, while the change in the dynamic resistance leads to a significant change in the phase difference of wave functions. The change in the critical current also leads to a significant change in the phase difference of wave functions, which confirms the need to consider the junction inductance when calculating devices based on Josephson junction circuits.

Using the proposed model, we calculated dependence of the AC voltage in the junction on parameters of the equivalent Josephson junction circuit, which showed that its value was of the same order as the experimental results were, this had been given in the known studies of

national and foreign authors. Figure 4.44 shows dependence of the junction voltage on the nonlinear conductivity for different values of junction capacitance. As can be seen from the graphs, decrease of the junction capacitance leads to increase of the junction voltage. This is because decrease of the capacitance leads to increase of the current and, consequently, of the voltage.

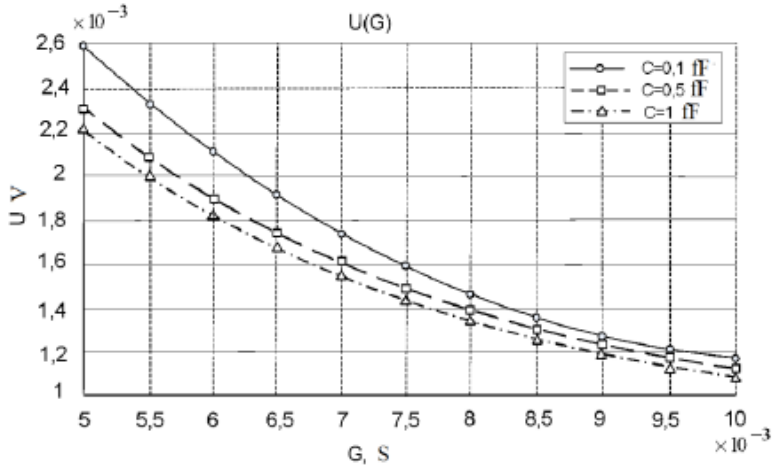

Figure 4.44 – Dependence of the junction voltage on the nonlinear conductivity at different capacitance values

Figure 4.45 shows dependence of the Josephson junction voltage on capacitance for different values of the differential conductivity.

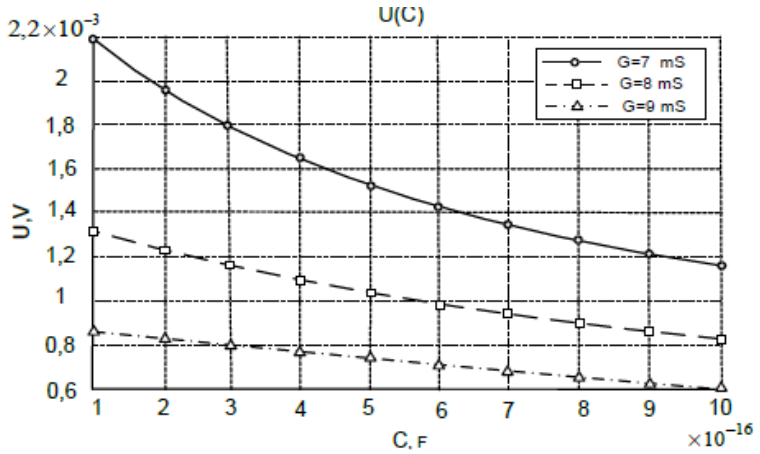

Figure 4.45 – Dependence of the junction voltage on the junction capacitance

As can be seen from the graphs, the voltage decreases with the capacitance increasing, that is why dielectrics with much smaller value ε should be applied to increase the voltage when producing Josephson junctions.

4.9 Pulse-code modulator for processing of low-intensity signals in the terahertz frequency range

One of the most important devices that are widely used in telecommunication systems are pulse code modulators. The use of superconductive technology for their construction will enable the development of high-sensitivity, high-speed, fully digital devices that receive, process and transmit signals in modern telecommunication, radio engineering and information measuring systems in millimeter and sub-millimeter frequency bands.

In the development of high-speed PCMs on the basis of semiconductor technology schemes of parallel type are used most often [115, 116].

For the construction of superconducting PCMs a parallel circuit with the implementation of comparators based on superconducting quantum interferometers (SQUID) is proposed, which makes it possible to simplify the scheme substantially and at the same time provides fast performance. In a conventional parallel PCM a line of comparators working simultaneously digitizes the analog input signal into a $n-$digit digital word. In this type of PCM both quantization and sampling occur simultaneously. The main advantage of the parallel Nyquist PCM is the high conversion rate and therefore it is ideal for digitizing broadband and fleeting signals with low intensity. However, the number of required comparators is $2^n - 1$, one for each quantization level and increases exponentially with the number of output bits n, which makes integration of a large number of bits complex. It is possible to reduce the number of comparators required by using more advanced architectures of parallel Nyquist PCMs [117].

A parallel PCM conductor based on SQUID comparators allows to simplify the scheme significantly and at the same time provides faster sampling. Using the periodicity of the transfer characteristics of the SQUIDs in units of quanta of the magnetic field F_0, the $n-$bit superconducting parallel PCM makes it possible to use only n clocked comparators. To estimate the frequency, let's consider the SQUID on one Josephson junction (Fig. 4.46a), consisting of inductance coil L_3 and junction J_0. The current through the junction is a periodic function (Fig. 4.46b) of the applied input current with period F_0/L_3.

The standard comparator consists of a flow quantifier (SQUID on one Josephson junction) and a sampling circle, called a decision pair or a balanced comparator which includes two sequentially connected Josephson

junctions (J_1 and J_2 in Fig. 4.46c). When the clock signal arrives at the sampler, one of these two sampling Josephson junctions switches to a resistive state. If the current I_{cont} is directed clockwise, J_2 switches creating the logical «1» at the output. At the time when the current I_{cont} is directed against the clockwise, then switches J_1 creating the output «0» (Fig. 4.46d).

On fig.4. 47 a parallel PCM scheme that generates n-bit digital Gray code on the output is shown. The input signal I is sequentially divided in half and comes to a line of identical comparators with periodic thresholds.

An output of the first comparator is the least significant bit (LSB) and output of the last comparator is the most significant bit (MSB) encoded in the Gray code. In n-bit PCM the first comparator receives 2^{n-1} times the current applied to the last comparator. When the input signal increases each comparator passes through several thresholds. Unlike the standard binary code in the Gray code only one of the output bits changes between successive digits. Thus, the Gray code is less sensitive to errors that arise due to minor differences in the comparator thresholds. Consequently, using the Gray code reduces the probability of bit errors.

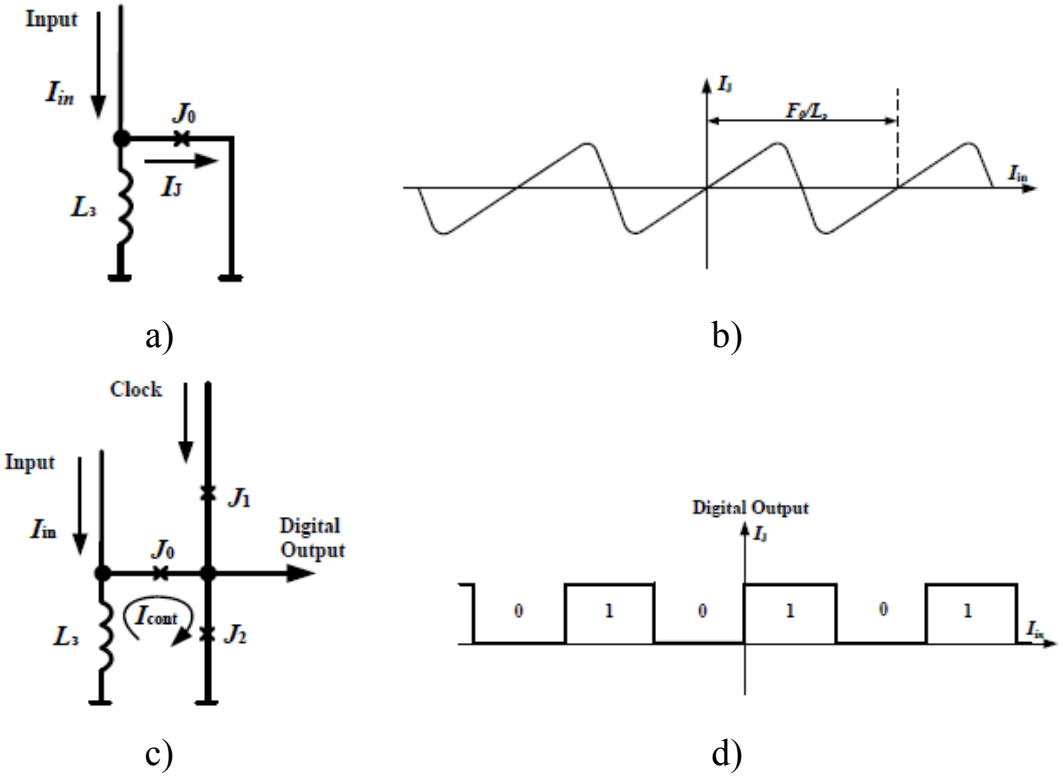

Figure 4.46 – Scheme of SQUID on a single Josephson junction acting as a flow quantifier (a), a periodic transfer characteristic of the SQUID (b), a comparator scheme with a clocked sampling circuit (c), a digital output of the comparator (d)

Like all PCMs with multiple comparators the superconducting parallel PCM is sensitive to the deviation of circuit parameters and other conditions such as resistor matrix, delay in clock, and signal paths, and in this case, differences in the local magnetic medium. The incompatibility of the components depends on the quality of the manufacturing process of integrated circuits.

For correct operation analog and clock sampling signals should be sent simultaneously to each of the comparators which requires precise constructions of the transmission lines along the paths of analog signal and clock sampling, taking into account their propagation from the comparator with the less significant bit to the comparator with the most significant bit. This can limit the number of bits for high-speed parallel PCM [117].

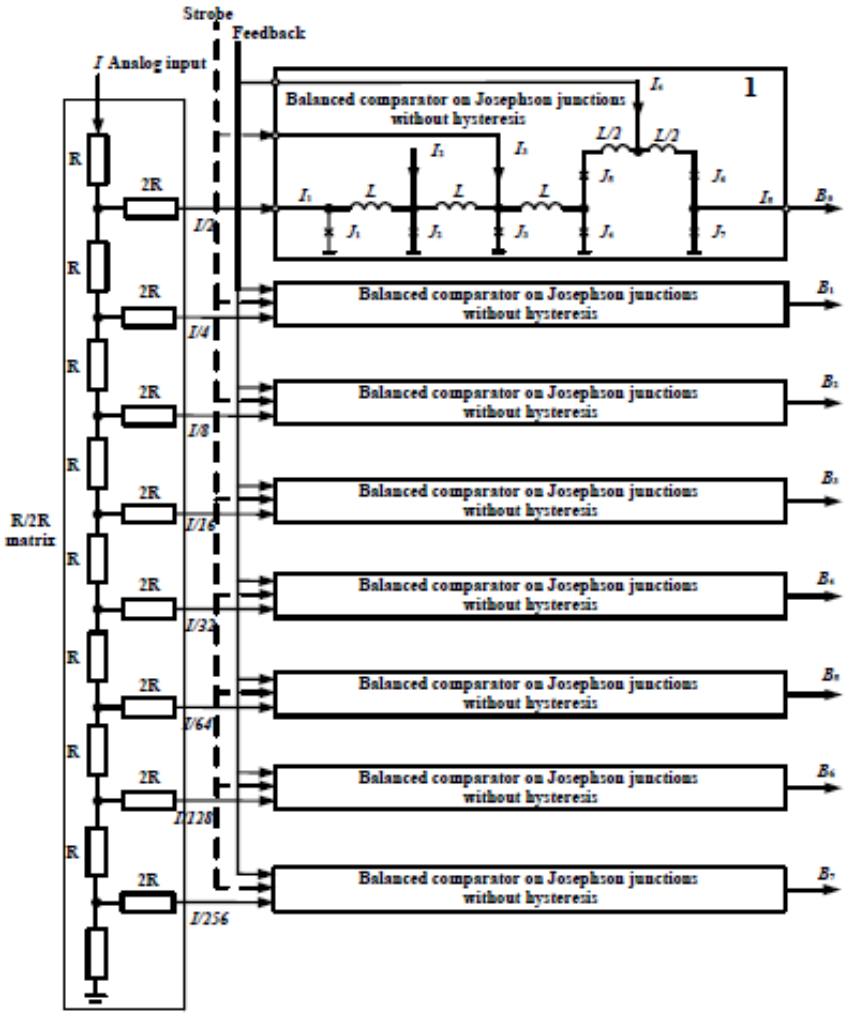

Figure 4.47 – Scheme of superconducting 8-bit parallel PCM with R / 2R matrix and *n* SQUID periodic comparators

Since the PCM based on Josephson junctions provides processing of weakly intense signals, its important parameter is the sensitivity threshold which is largely determined by the influence of thermal and quantum fluctuations on the magnitude of the currents of the comparator junctions.

The sensitivity and threshold of the PCM sensitivity can be determined by the conversion characteristic. In the absence of any fluctuations this characteristic has a threshold character, i.e. the average voltage on the junctions has the form of an ideal step depending on the magnitude of the signal. The influence of fluctuations leads to the blurring of a step which value can be characterized by the parameter of blurring [118].

$$\Delta I_K = \left| dP_2 \Big/ dI_K \right|^{-1},$$

where dP_2 – the probability of switching of Josephson junction.

The calculation of value of the ΔI_C blur parameter gives an opportunity to determine the threshold of the PCM sensitivity. In case of measuring systems this parameter determines the minimum error of measurement.

The sensitivity of the PCM is determined by the width of the blurring of the switching characteristic of the comparator by thermal and quantum fluctuations. Since the PCM will provide processing of weakly intense signals we will use the superconductors with a low critical current density and those that characterized by the HTS to construct it. It is shown in [118] that in case of small critical currents quantum fluctuations can not be taken into account, and therefore in our case the blurring of thresholds of the characteristic will be determined only by thermal fluctuations. In [117] it is shown that when using single-quantum pulses the blurring of the characteristic depends on the current increase rate and the *Stewart-McCumber* parameter β

$$\begin{aligned} \Delta I_K &= 0{,}17\left(\frac{2eKTI_0}{h}\right)^{1/2}\left(\frac{\alpha}{\beta}\right)^{3/8} \qquad \beta >> 1, \\ \Delta I_K &= 0{,}43\left(\frac{2eKTI_0}{h}\right)^{1/2}\alpha^{3/8} \qquad \beta << 1, \end{aligned} \tag{4.76}$$

where α – current increase rate under the action of a strobe pulse.

The analysis of these expressions shows that the magnitude of the blurring of the threshold characteristic increases with the increase of critical currents I_0.

Since in our case the HTS is used on the basis of which the Josephson bicrystal junction is formed, then the value of the critical current can be determined in this way. The bicrystal limit is split into a finite number of sections N, which are called facets. The critical current density within each facet is equal to its constant, i.e. the density of the critical current is depicted by the step function [82].

$$I_C = \sum_{i=1}^{n} I_{CI} \cdot \Delta x_i \frac{\sin\left(\pi\Delta x_i / a\right)}{\pi\Delta x_i / a} \cdot \sin\left[\frac{2\pi\langle x_i\rangle}{a} + C(i)\right],$$

where I_{CI} – critical current density of the facet; $\Delta x_i = \frac{x_i - x_{i+1}}{2}$ – length of the facet; $\langle x_i\rangle = \frac{x_i + x_{i-1}}{2}$ – coordinates of middle of the facet, $i = 1, 2, \ldots n$; $a = \phi / L_\phi$, ϕ – full magnetic flux in the junction; $C(i)$ – some constant value.

This should be taken into account in the expressions (4.76).

Then, the sensitivity of the PCM is determined by the sensitivity of comparator δI_x and it is proportional to the blurring of the threshold characteristic ΔI_x [118].

$$\delta I_x = \frac{\Delta I_x}{\sqrt{N}}, \tag{4.77}$$

where N – the averaging factor associated with the statistical nature of the measurement.

The averaging factor is equal to the number of pulses that used to measure one time point of the output signal and can be calculated from the expression

$$N = \frac{\Delta T}{\delta t} \tau_{max} \cdot f, \tag{4.78}$$

where ΔT – pulse processing time; τ_{max} – maximum length of the processed signal; f – frequency of repetition of pulses; δt – time resolution of comparators; $\tau_{max} \le f$ – the maximum length of the measured signal.

The analysis of the results presented in [118] shows that the time resolution of nonhysteresis comparators can be $(5 \div 10) \cdot t_C$, where $t_C = \frac{1}{f} = \frac{\hbar}{2eU_C}$, i.e. $\delta t = \frac{10\hbar}{2eU_C}$, U_C – the value of the characteristic voltage for the superconductor.

Substituting (4.76) and (4.78) in (4.77) we obtain an expression for calculating the sensitivity of the PCM

$$\delta I_x = 0{,}17(2eKTI_0)^{1/2}\left(\frac{\Delta TeU_C}{5}\tau_{max} \cdot f\right)^{-1/2}\left(\frac{\alpha}{\beta}\right)^{3/8}.$$

The analysis of the last expression shows that the sensitivity of the PCM increases in proportion to $\sqrt{I_0 T}$ and decreases in proportion to $\sqrt{U_C f}$.

The calculations performed using the above expressions show that the sensitivity threshold for PCI based on HTS can be ones of nanoampere (at $\Delta I_K = 32\ mkA, \quad \delta I_K = 1{,}16\ nA$) for nitrogen temperatures, and less than one nanoampere for PCM based on LTS (at $\Delta I_K = 12\ mkA, \quad \delta I_K = 0{,}43\ nA$) for helium temperatures. These indices are more than an order of magnitude higher than those of semiconductor PCM which is very important in processing of weakly intense signals in the terahertz range.

The following data is used for calculations. The variation of the characteristic voltage U_C for different types of superconductors and time resolution is given in table 4.1.

Table 4.1 – Dependence of time resolution on the characteristic voltage of the superconductor

U_C	0,7	1,4	2,8	3,2
δt_{min}	2,62	1,31	0,66	0,52

The dimensionless current increase rate $\alpha = \frac{2}{\pi}$, the ***Stewart-McCumber*** parameter $\beta = 1,\ I_0 = 0{,}20\ mA$ for nitrogen temperatures and $I_0 = 0{,}125\ mA$ for helium temperatures.

PCM structure scheme based on comparators using Josephson transitions and high-temperature superconductivity is proposed.

The analytical dependences of the value of threshold characteristic blurring on the critical current and temperature are obtained. It is established that the magnitude of the blurring increases directly proportional to $\sqrt{I_0 T}$.

The analytical dependences of the PCM sensitivity on the critical current, temperature, and characteristic voltage of the superconductors are obtained. It is shown that the sensitivity increases linearly to $\sqrt{I_0 T}$ and decreases in proportion to $\sqrt{U_C}$.

The research results show that devices with low temperature superconductors are characterized by a lower threshold of sensitivity and are much lower compared to similar devices based on semiconductors, which makes it possible to use such PCMs for the processing of weakly intense signals.

LIST OF REFERENCES

1. Скрипник Ю. А. Микроволновая радиометрия физических и биологических объектов / Ю. А. Скрипник, А. Ф. Яненко, В. Ф. Манойлов, В. П. Куценко, Ю. Б. Гимпилевич. – Житомир : Волынь, 2003. – 408 с.

2. Есепкина Н. А. Радиотелескопы и радиометры / Н. А. Есепкина, Д. В. Корольков, Ю. Н. Парийский. – Г. : Наука, 1972. – 416 с.

3. Николаев А. Г. Радиотеплолокация / А. Г. Николаев, С. В. Перцов. – М. : Сов. Радио, 1964. – 335 с.

4. Куценко В. П. Методы и средства сверхвысокочастотной радиометрии / В. П. Куценко, Ю. О. Скрипник, Н. Ф. Трегубов, К. Л. Шевченко, О. П. Яненко. – Донецьк : Наука і освіта, 2011. – 324 с.

5. Черноушенко П. А. Измерение электронных параметров дециметрового и сантиметрового диапазона волн / П. А. Черноушенко, А. В. Бородин. – Г. : Радио и связь, 1986. – 159 с.

6. Билько М. И. Измерение мощности на СВЧ / М. И. Билько, А. К. Томашевский. – Г. : Радио и связь, 1986. – 167 с.

7. Ситько С. П. Аппаратурное обеспечение современных технологий квантовой медицины / С. П. Ситько, Ю. А. Скрипник, А. Ф. Яненко. – К. : ФАДА, 1999. – 199 с.

8. Yanenko O. P. Microwave radiometry in medico-biologica lapplications / O. P. Yanenko // Visnyk Ternopilskoho natsionalnoho tekhnichnoho universyteta, 2014 p. – № 4 (76). – P. 155–163.

9. Sitko S. P. Vvedenie v kvantovuyu meditsinu [Introduction to quantum medicine] / S. P. Sitko and L. N. Mkrtchyan. – Kiev : Pattern Publ., 1994. – 148 p.

10. Биняшевский Э. В. Сборник методических рекомендаций и нормативных актов микроволновой резонансной терапии / Э. В. Биняшевский, Б. П. Грубник, С. А. Дерендяев и др. – К. : Оберіг, 1997. – 127 с.

11. Yanenko O. P. Eguipmen and technologies of low intensity millimeter therapy / O. P. Yanenko, S. M. Peregudov, I. V. Fedotova, O. D. Golovchanska // Visnyk NTUU «KPI» Seriya : Radiotekhnika. Radioaparatobuduvannya. – 2014. – № 59 – P. 103–110.

12. Evaluation of irradiative abilities of dental materials / A. Janenko, S. Peregudov, A. Politun, O. Golovchanska // Materials of the 9th World Endodontic Congress. Tokio, Japan. – 2013.

13. Николова Л. Специальная физиотерапия с Л. Николова. – София : Медицина и физкультура, 1983. – 433 с.

14. Microwave Evaluation of Electromagnetic Compatibility of Dielectric Remedial and Therapeutic Materialswith Human Body / Oleksiy Yanenko, Kostiantyn Shevchenko,Vladyslav Malanchuk, Oleksandra Golovchanska // International Journal of Materials Besearch. – 2019. – Vol. 7, no. 1. – P. 37–43.

15. Яненко О. П. Особливості мікрохвильових низькоінтенсивних випромінювань матеріалів для фізіотерапевтичних процедур / О. П. Яненко, Б. І. Яворський, Р. А. Ткачук, В. П. Русинчук // Вісник НТУУ «КПІ». Серія Радіотехніка. Радіоапаратобудування. – 2014. – № 60. – С. 114–121.

16. Понежа Г. В. Положительные и отрицательные потоки микроволнового излучения от физических и биологических объектов / Г. В. Понежа, С. П. Ситько, Ю. А. Скрипник, А. Ф. Яненко // Physics of the Alive. – 1998. – Vol. 6, № 1. – С. 11–14.

17. Пат. 59399 Україна. Спосіб мікрохвильової терапії / Бундюк Л. С., Кузьменко О. Р., Понежа Г. В., Сітько С. П., Скрипник Ю. О., Яненко О. П. 2003. Бюл. № 9.

18. Физико-химические свойства элементов // Справочник под редакцией Н. В. Самсонова. – К. : Наукова думка, 1965. – 809 с.

19. Пат. 49357 Україна. Спосіб вимірювання потужності електромагнітного сигнала та ідентифікації стоматологічних матеріалів / Яненко О. П., Перегудов С. М., Головчанська О. Д. 2008. Бюл. № 15.

20. Москвин С. В. Основы лазерной терапии / С. В. Москвин, А. А. Ачилов. – М. : Медицина, 2008. – 255 с.

21. Ремизов А. Н. Медицинская и биологическая физика / А. Н. Ремизов. – М. : Высшая школа, 1996. – 608 с.

22. Rojas J. C. Low-level light therapy of the eye and brain / J. C. Rojas, F. Gonzalez-Lima // Eye and Brain. – 2011. – No. 3. – P. 49–67.

23. Пат. України № 91337. Пристрій для світлотерапії / О. П. Яненко, С. В. Михайленко, опубл. 25.06.2014, Бюл. № 12.

24. Пустова С. В. Дослідження електрофізичних і електромагнітних параметрів біологічно активних точок людського організму /

С. В. Пустова, О. П. Яненко // Вісник НТУУ «КПІ». Серія Радіотехніка. Радіоапаратобудування. – 2007. – № 34. – С. 142–149.

25. Попечителев Е. П. Медицинские приборы, аппараты, системы и комплексы. Ч. 4 / Е. П. Попечителев, Н. А. Кореневский. – Курск, 2006. – 311 с.

26. Терещенко М. Ф Контроль дози лазерного опромінення біологічних тканин температурним методом / М. Ф. Терещенко, І. В. Максимчук, Л. А. Мамедов, С. П. Якубовський // Вісник НТУУ «КПІ», Приладобудування. – 2013. – № 45. – С. 175–180.

27. Adey W. Freguecy and Power Windowindg in Tissue Interaction with Wear Electromagnetc Filds // IEEE. – 1980. – Vol. 68, № 1. – P. 140–147.

28. Основы оптической радиометрии под ред. проф. А. Ф. Котюка. – М. : Физматлит, 2003. – 504 с.

29. Оптические измерения / А. М. Борбат, И. С. Горбань, Б. А. Охрименко и др. – Киев : Техника, 1967. – 245 с.

30. Пат. України № 65746. Фотометр / Овчинніков С. С., Поліщук В. М., Горяшик М. М., опубл. 10.05.2007. Бюл. № 6.

31. Пат. України № 23102. Фотометр / Єсаулов С. М., Осадчий Р. М., Таран О. А., опубл. 15.04. 2004. Бюл. № 4.

32. Пат. України № 90426. Фотометричний вимірювач / Яненко О. П., Михайленко С. В., Ліснічук А. С. Горшков А. В., опубл. 26.05.2014. Бюл. № 10.

33. Зеленков І. А. Фотометрія : навч. посібник / І. А. Зеленков. – Київ : НАУ, 2003. – 180 с.

34. Гуревич М. М. Фотометрия (Теория, методы и приборы) / М. М. Гуревич. – Л-д. : Энергоатомиздат, 1983 – 272 с.

35. А. с. № 1511603 СССР. Полевой спектрофотометр / Кульчицкий А. П., Обринский Л. У., опубл. 30.09.89. Бюл. № 36.

36. Пат. України № 381107. Фотометр / Буняк А. М., Борисенков А. А., опубл. 30.05.2001 р. Бюл. № 4.

37. А. с. № 1511602 СССР. Спектрофотометр / Герасимов С. Ю., опубл. 30.09.1989. Бюл. № 36.

38. Яненко О. П. Радіометричний модуляційний вимірювач інтенсивності оптичного випромінювання / О. П. Яненко, С. В. Михайленко, А. С. Ліснічук // Вісник НТУУ «КПІ» Серія : Радіотехніка. Радіоапаратобудування. – 2013. – № 52. – С. 96–101.

39. Скрипник Ю. А. Модуляційні радіометричні пристрої та системи НВЧ діапазону : навч. посіб. / Ю. О. Скрипник, В. П. Манойлов, О. П. Яненко. – Житомир : ЖІТІ, 2001. – 373 с.

40. Пат. України № 119255. Фотометричний вимірювач поглинальної здатності слабо прозорих матеріалів / Яненко О. П., Шульга В. О., Шевченко К. Л., Головчанська О. Д., опубл. 25.09.2017. Бюл. № 18.

41. Шелухин О. И. Радиосистемы ближнего действия / О. И. Шелухин. – М. : Радио и связь, 1989. – 237 с.

42. Измерение радиотепловых и плазменных излучений / А. Е. Башаринов , Л. Т. Тучков, В. М. Поляков, Н. И. Ананов. – М. : Сов. Радио, 1968. – 390 с.

43. Скрипник Ю. А. Проблемы измерения низкоинтенсивного излучения миллиметрового диапазона / Ю. А. Скрипник, А. Ф. Яненко // Физика живого. – 1998. – Т. 6, № 1. – С. 108–112.

44. Яненко О. П. Основні принципи побудови високочутливих комутаційно-модуляційних радіометрів міліметрового діапазону / О. П. Яненко // Вісник ЖІТІ. – 1998. – № 8. – С. 111–118.

45. Скрипник Ю. А., Модуляційні радіометри: структури, основні співвідношення та особливості / Ю. А. Скрипник, А. Ф. Яненко // Вісник ЖІТІ. – 2001. – № 17. – С. 53–60.

46. Пат. України № 28122. Нульовий модуляційний радіометр / Скрипник Ю. О., Яненко О. П., опубл. 2000. – Бюл. № 5.

47. Пат. України № 27625. Модуляційний радіометр / Скрипник Ю. О., Перегудов С. М., Яненко О. П., опубл. 2000. – Бюл. № 4.

48. Скрипник Ю. А. Радиометрическая система для исследования излучений биологических объектов / Ю. А. Скрипник, А. Ф. Яненко, С. Н. Перегудов // Физика живого. – 1998. – Т. 6, № 1. – С. 19–22.

49. Скрипник Ю. О. Шляхи зниження флуктуаційного порогу чутливості вимірювачів слабких сигналів / Ю. О. Скрипник, О. П. Яненко // Вісник ЛПІ. Автоматика, вимірювання та керування. – № 420. – 2001. – С. 20–26.

50. Пат. України № 57820. Модуляційний радіометр / Скрипник Ю. О., Яненко О. П., Колисниченко М. В., опубл. 2003. – Бюл. № 7.

51. Пат. України № 53790. Двоканальний супергетеродинний радіометр / Казаков М. І., Куценко В. П., Сітько С. П., Скрипник Ю. О., Яненко О. П., опубл. 2003. – Бюл. № 2.

52. Пат. України № 27651. Диференційний радіометр / Скрипник Ю. О., Яненко О. П., опубл. 2000. – Бюл. № 4.

53. Пат. України № 27641. Одноканальний радіометр / Скрипник Ю. О., Яненко О. П., опубл. 2000. – Бюл. № 4.

54. Пат. України № 14887 А. Спосіб вимірювання потужності електромагнітного випромінювання надзвичайно високих частот / Скрипник Ю. О., Яненко О. П., Горбань Є. М., Куценко В. П., опубл. 2006. – Бюл. № 6.

55. Пат. України № 33222 А. Мікрохвильовий пристрій для аналізу ємнісних властивостей живого білка / Скрипник Ю. О., Шевченко К. Л., Цимбалюк В. І., опубл. 2001. – Бюл. № 1.

56. Ситько С. П. Экспериментальное исследование излучения некоторых объектов в мм-диапазоне / С. П. Ситько, Ю. А. Скрипник, А. Ф. Яненко // Физика живого. – 1998. – Т. 6, № 1. – С. 15–18.

57. Чиграй Е. С., Яременко Ю. Г. Динамика коэффициента отражения мм-волн от кожи при КВЧ-воздействии // Миллиметровые волны в медицине и биологии : сб. докл. II Рос. симпозиума. – М. : ИРЭ РАН. – 1997. – С. 192–193.

58. Пат. України № 37273. Пристрій для вимірювання зсуву фаз у відбитих НВЧ-коливаннях / Скрипник Ю. О., Яненко О. П, Іващенко В. О., опубл. – 2001. – Бюл. № 4.

59. Пат. України № 28128. Спосіб виявлення та визначення електромагнітного випромінювання від біологічних об’єктів та пристрій для його здійснення / Скрипник Ю. О., Яненко О. П., опубл. 2000. – Бюл. № 5.

60. Метрологія апаратури квантової медицини / О. П. Яненко // Технічна електродинаміка : тематичний випуск. – К., 2000. – Ч. 1. – С. 108–111.

61. Яненко О. П. Оцінка похибки р-і-п-модуляторного ключа методом еквівалентного чотириполюсника / О. П. Яненко // Вісник ЖІТІ. – 2001. – С. 98–101.

62. Яненко О. П. Методи та засоби калібровки високочутливих радіометричних систем мм-діапазону / О. П. Яненко // Вісник ВПІ. – 1999. – № 6. – С. 93–97.

63. Скрипник Ю. А. Измерительные устройства с коммутационно-модуляционными преобразователями / Ю. А. Скрипник. – Киев : Вища школа, 1975. – 256 с.

64. Яненко О. П. Високочутливі модуляційні структури радіометричної апаратури НВЧ-діапазону : дис. … доктора техн. наук : 05.11.08 / Яненко Олексій Пилипович. – Вінниця, 2003. – 379 с.

65. Український центр стандартизації та метрології. Свідоцтво про державну метрологічну атестацію «Установка для вимірювання малих рівнів потужності міліметрового діапазону хвиль НУ-1 № 1» № 26-007 від 26.12.2000 р.

66. Український центр стандартизації та метрології. Свідоцтво про державну метрологічну атестацію «Установка для вимірювання малих рівнів потужності міліметрового діапазону хвиль НУ-2 № 1» № 26-008 від 26.12.2000 р.

67. Кессель В. Эталоны теплового шума: определения, реализация и методы сравнения / В. Кессель, Д. Джаник // ТИИЭР. – 1986. – Т. 74, № 1. – С. 130–131.

68. Яненко О. П. Оцінка граничної чутливості РС мм діапазону / О. П. Яненко // Вісник ЖІТІ. – 1999. – № 9. – С. 189–192.

69. ХДНДІМ. Свідоцтво про державну метрологічну атестацію «Генератора шуму теплового ГШТ № 01» № 235 від 5.03.2003 року

70. Шумы в электронных приборах и системах / М. Букингем, А. Б. Мещерякова, В. П. Митрофанова, Г. А. Сидоровой. – Пер. с англ. под ред. В. Н. Губанова. – М. : Мир, 1986. – 399 с.

71. Корнев В. К. Эффект Джозефсона и его применение в сверхпроводниковой электронике / В. К. Корнев // Соровский образовательный журнал. – 2001. – Т. 2, № 8. – С. 84–90.

72. Войтович И. Д. Наноэлектронная элементная база информатики / И. Д. Войтович, В. М. Корсунский. – М. : Интернет-Университет Информационных технологий. БИНОМ, 2013. – 643 с.

73. Корнев В. К. Исследование динамических процессов в джозефсоновских устройствах сверхпроводниковой электроники :

автореф. дис. на соискание ученой степени доктора физико-математических наук / В. К. Корнев. – М. : 2007 – 38 с.

74. Кулик И. О. Эффект Джозефсона в сверхпроводящих туннельных структурах / И. О. Кулик, И. К. Янсон. – Москва : Наука, 1970. – 271 с.

75. Боков М. М. Применение методов квантовой метрологии в процессе эксплуатации современных образцов вооружения и военной техники / М. М. Боков, М. Е. Гришоев, М. Б. Мищенко // Журнал фундаментальных исследований. – 2015. – С. 23–31.

76. Головин Ю. Н. Нанотехнологическая революция стартовала. [Електронный ресурс] / Головин Ю. Н. – Режим доступу: http:www. abitura com./ modernphysics/nano/nano2. htm.

77. Тиханский М. В. Моделирование процессов коммутации в джозефсоновских элементах логики «И» и «ИЛИ» / М. В. Тиханский, Р. Р. Крисько // Физика низких температур. – 2013. – Т. 39, № 2. – С. 127–133.

78. Калашников В. К. Гармонический смеситель на туннельном переходе сверхпроводник-изолятор-сверхпроводник / В. К. Калашников, А. В. Худченко, А. Б. Барышев, В. П. Кошелен // Радиотехника и электроника. – 2011. – Т. 56, № 8. – С. 1–9.

79. Сугано Т. Введение в микроэлектронику / Т. Сугано, Т. Икома, Е. Такэиси. – М. : Мир, 1988. – 320 с.

80. Кичак В. М. Математична модель переходу Джозефсона / В. М. Кичак, В. В. Кичак // Вісник ВНТУ. – 2014. – № 3/119. – С. 101–106.

81. Араманович И. Г. Уравнения математической физики / И. Г. Араманович, В. И. Левин. – М. : Наука, 1969. – 288 с.

82. Арзуманов А. В. Многоэлементные синхронные джозефсоновские структуры : дис. ... канд. ф.-м. н. / А. В. Арзуманов. – М. : МГУ, 2007.

83. Корнев В. К. От одно- и двухконтактного сквидов к би-сквиду / В. К. Корнев, И. И. Соловьев, А. В. Шарафиев, Н. В. Кленов // Радиотехника. – 2012. – № 12.

84. Петров Г. В. Нелинейная модель полевого транзистора с двумя затворами Шоттки / Г. В. Петров, А. В. Храмов // Радиотехника. – 1990. – № 2. – С. 43–46.

85. Кичак В. М. Синтез частотно-імпульсних елементів цифрової техніки : монографія / В. М. Кичак. – Вінниця : УНІВЕРСУМ-Вінниця, 2005. – 291 с.

86. Генератори допоміжних сигналів на базі переходів Джозефсона / В. М. Кичак, М. Д. Гузь, В. В. Кичак, А. В. Вергелюк // Вестник национального технического университета Украины «КПІ». Радиотехника и аппаратостроение. – 2014. – № 57. – С. 121–127.

87. Application of a Superlattice Multiplier for High Resolution THz Spectroscopy / C. P. Endres, F. Lewen, T. F. Giesen, S. Schlemmer, B. G. Paveliev // Review of Scientific Instruments. – 2007. – Vol. 78, is. 4. – P. 043106–043106–6.

88. Design and Characterization of a Room Temperature All-Solid-State Electronic Source Tunable From 2.48 to 2.75 THz / A. Maestrini et al. // IEEE Transaction on THz science and Technology. – 2012. – Vol. 2, no. 2.

89. G. Chattopadhyay. Technology, Capabilities and Performance of Low Power Terahetz Sources // IEEE Transaction on THz science and Technology. – 2011. – Vol. 1, no. 1. – P. 33–53.

90. Stability of HEB Receivers at THz Frequencies Proceedings of SPIE / T. Berg et al. // SPIE BellinghamWA. – 2004. – Vol. 5498. – P. 605–615.

91. Еру И. И. Твердотельные источники гетеродинного излучения субмиллиметрового диапазона / И. И. Еру // Радиофизика и радиоастрономия. – 2010. – Т. 15, № 2. – С. 224–233.

92. Торгашин М. Ю. Разработка и исследование джозефсоновских генераторов терагерцового диапазона на основе распределенных туннельных переходов: дис. … канд. техн. наук : 01.04.03 / М. Ю. Торгашин; ИРЕ РАН им. В. М. Котельникова. – М., 2013. – 140 с.

93. Кременецкая Я. А. Резонансно-туннельные диоды при больших напряжениях смещения / Я. А. Кременецкая, В. Е. Чайка, Г. Е. Чайка // Зв’язок. – 2004. – № 1. – С. 60–62.

94. Kaplunenko V. K. Superconducting circuit simulator «WinS». [Електронный ресурс] / V. K. Kaplunenko. – Режим доступу: http:www. kapl. tv/wins_text. htm.

95. Kooi J. W. Performance of the Caltech Sabmillimeter Observatory Dual-Color 180-720 GHz Balanced SIS Receivers / J. W. Kooi, R. A. Chamberlin, R. Monje et al. // IEEE Trans. Terahertz Science and Technology. – 2014. – Vol. 4, no. 2. – P. 149–164.

96. Antenna coupled planar arrays of Josephson junctions / M. Tarasov, E. Stepantsov, T. Lindstrom et al. // Physica C. – 2002. – V. 372–376, pt. 1. – P. 355–9.

97. Корнев В. К. Численное моделирование ширины линии генерации в синхронных многоэлементных джозефсоновских структурах / В. К. Корнев, А. В. Арзуманов // Журнал технической физики. – 1998. – Т. 24, № 15. – С. 52–59.

98. Кичак В. В. Вплив флуктацій струму на параметри надвисокочастотних генераторів / В. В. Кичак, В. М. Кичак, М. Д. Гузь // Контроль і управління в складних системах (КУСС-2014) : матеріали XIII Міжнародної конференції. – Вінниця. – С. 118.

99. Kychak V. M Evaluation on dependence of Josephson Junction Generation Linewidth from Its Geometrical Dimensions and Critical Current / V. M. Kychak, D. S. Hromovyi, M. D. Huz // UkrMiCo'2016, 11–15 September 2016. – Kyiv : National Technical University of Ukraine, 2016. – P. 218–221.

100. Kychak V. M. Influence of Critical Current and Parameters of Josephson Junction on Frequency Stability of Oscillator / V. M. Kychak, D. S. Hromovyi, M. D. Huz // Information and Telecommunication Sciences. – 2016. – V. 7, № 2. – P. 54–61.

101. Кузьмин Л. С. Взаимная синхронизация джозефсоновских контактов / Л. С. Кузьмин, К. К. Лихарев, Г. А. Овсянников // Радиотехника и электроника. – 1981. – № 5. – С. 1067–1076.

102. Овсянников Г. А. Взаимная синхронизация в многоконтактных джозефсоновских структурах / Г. А. Овсянников, Л. С. Кузьмин, К. К. Лихарев // Радиотехника и электроника. – 1982. – Т. 27, вып. 8. – С. 1613–1621.

103. К вопросу о корегентном состоянии цепочки туннельных джозефсоновских переходов / А. В. Арзуманов, В. К. Корнев, Г. А. Овсянников, А. Д. Маштаков // Журнал технической физики. – 1998. – Т. 24, вып. 15. – С. 1–7.

104. Кичак В. М. Радіочастотні та широтно-імпульсні елементи цифрової техніки : монографія / В. М. Кичак, О. О. Семенова. – Вінниця : УНІВЕРСУМ-Вінниця, 2008. – 162 с.

105. Кичак В. В. Застосування переходів Джозефсона для побудови пристроїв перетворення імпульсно-потенціального входу в частотно-імпульсний / В. В. Кичак, М. Д. Гузь // Вимірювальна та обчислювальна техніка в технологічних процесах. – 2013. – № 3. – С. 66–70.

106. Сверхпроводниковый интегральный приемник субмилиметрового диапазона / П. Н. Дмитриев, А. Б. Ермаков, Н. В. Кинев и др. // Успехи современной радиоэлектроники. – 2010. – № 5. – С. 75–81.

107. Шитов С. В. Малошумящий СИС смеситель на частоту 1 ТГц с двойной дипельной антенной / С. В. Шитов, А. В. Марков, Б. Д. Джексон и др. // Журнал технической физики. – 2002. – Т. 72, вып. 9. – С. 87–92.

108. Выставочкин В. И. Преобразователь частоты на SHS переходе / В. И. Выставочкин // Журнал технической физики. – 1985. – Т. 11, вып. 5. – С. 290–295.

109. Вендик О. Г. Приборы криогенной электроники. Высокотемпературные сверхпроводники / О. Г. Вендик, С. Г. Колесов. – М. : Знания, 1990. – 64 с.

110. Кичак В. М. Дослідження радіочастотних операційних елементів десяткової системи числення // Вісник ВПІ. – 1999. – № 4. – С. 77–81.

111. Кичак В. В. Вплив флуктацій струму на параметри надвисокочастотних генераторів / В. В. Кичак, В. М. Кичак, М. Д. Гузь // Контроль і управління в складних системах (КУСС-2014) : матеріали XIII Міжнародної конференції. – Вінниця : ВНТУ, 2014. – С. 118.

112. Кичак В. В. Цифрові радіотехнічні пристрої на базі високотемпературної надпровідності та переходів Джозефсона / В. В. Кичак, Г. Г. Бортник // Вісник Хмельницького національного університету. – 2014. – № 1. – С. 117–120.

113. Ревин Л. С. Быстрые переключения и генерация в джозефсоновских контактах / Л. С. Ревин. – Нижний Новгород : б. из., 2016.

114. Исследование СВЧ-свойств высокотемпературных джозефсоновских контактов на сапфировой бикристалической подложке /

Е. Е. Пестов, Д. В. Мастеров, А. Е. Парафин, С. А. Павлов, А. М. Клушин // Физика твердого тела. – 2017. – Т. 59, вып. 11.

115. Быстродействующие интегральные микросхемы ЦАП и АЦП и измерение их параметров / А. Й. К. Марцинкавичюс, Э. А. К. Багданскис, Р. Л. Пашюнас и др. ; под. ред. А. Й. К. Марцинкавичюс, Э. А. К. Багданскис. – М. : Радио и связь, 1988. – 224 с.

116. Bortnik G. The mathematical model of the analog-digital converter / G. Bortnik, V. Kichak, S. Bortnik // Modern Problems of Radio Engineering, Telecommunications and Computer Science Proceedings of International Conference. – 2006. – P. 564–565.

117. Mukhanov O. A. Superconductor Analog-to-Digital Converters / O. A. Mukhanov, D. Gupta, A. M. Kadin. V. K. Semenov // Proceedingsofthe IEEE. – 2004. – Vol. 92, no. 10. – P. 1564–1584.

118. Аскарзаде И. Н. Динамические свойства балансного компаратора на джозефсоновских переходах с кулоновской блокадой / И. Н. Аскарзаде // Журнал технической физики. – 2016. – Т. 86, вып. 9.

119. Kychak V. M. Pulse-code modulator for processing of weakly intense signals in the terahertz frequency range / V. M. Kychak, M. Vasylkivskyi, V. Kychak, M. D. Huz // UkrMiCo’2018, 10–14 September 2018. – Odessa : Odessa National Academy of Telecommunication (ONAT), 2018.

Яненко, О.

Я60 Методи та засоби формування, оброблення та використання низькоінтенсивних електромагнітних сигналів : монографія / О. П. Яненко, К. Л. Шевченко, В. М. Кичак. – Вінниця : ВНТУ, 2020. – 268 с.

ISBN 978-966-641-811-4

У монографії узагальнено науково-технічний досвід, накопичений авторами у сфері формування, вибору, перетворення та обробки слабких параметрів сигналу. Автори розглядають особливості комутаційних та модуляційних перетворень та ланцюгів високочутливих радіометрів НВЧ та оптичного діапазону, а також методи та засоби формування сигналів низької інтенсивності із застосуванням переходів Джозефсона. Може бути корисною для студентів та аспірантів, а також для фахівців у галузі розробки та використання обладнання низького сигналу в телекомунікаціях та радіозв'язку, фізиці, біології, медицині, матеріалознавстві та інших прикладних галузях науки та техніки, пов'язаних з використанням сигналів низької інтенсивності.

УДК 621.317: 621.371: 615.849

Наукове видання

Яненко Олексій Пилипович
Шевченко Костянтин Леонідович
Кичак Василь Мартинович

МЕТОДИ ТА ЗАСОБИ ФОРМУВАННЯ, ОБРОБЛЕННЯ ТА ВИКОРИСТАННЯ НИЗЬКОІНТЕНСИВНИХ ЕЛЕКТРОМАГНІТНИХ СИГНАЛІВ

Монографія
(*англійською мовою*)

Видання здійснене в авторській редакції
Оригінал-макет підготовлено В. Кичаком

Підписано до друку 5.08.2020 р.
Формат 29,7×42¼. Папір офсетний.
Гарнітура Times New Roman.
Друк різографічний. Ум. др. арк. 15,48
Наклад 300 (1-й запуск 1–75) пр. Зам № В2020-10

Вінницький національний технічний університет,
ІРВЦ ВНТУ,
21021, м. Вінниця, Хмельницьке шосе, 95,
ВНТУ, ГНК, к. 114.
Тел. (0432) 65-18-06.
press.vntu.edu.ua; *email*: kivc.vntu@gmail.com.
Свідоцтво суб'єкта видавничої справи
серія ДК № 3516 від 01.07.2009 р.

Віддруковано ФОП Барановська Т. П.
21021, м. Вінниця, вул. Порика, 7.
Свідоцтво суб'єкта видавничої справи
серія ДК № 4377 від 31.07.2012 р.